NASA CR-
R-9271

COMPREHENSIVE PROGRAM SUMMARY REPORT

NONCIRCULAR ORIFICE HOLES AND ADVANCED FABRICATION TECHNIQUES FOR LIQUID ROCKET INJECTORS (PHASES I, II, III, AND IV)

NAS9-9528

by

R. M. McHale

and

W. H. Nurick

ROCKETDYNE DIVISION/ROCKWELL INTERNATIONAL
6633 CANOGA AVENUE/ CANOGA PARK, CALIFORNIA

prepared for

NASA LYNDON B. JOHNSON SPACE CENTER
Mr. Merlyn F. Lausten: Project Manager

FOREWORD

This report was prepared for the NASA Lyndon B. Johnson Space Center, Houston, Texas, by the Rocketdyne Division of Rockwell International. The study was conducted under Contract NAS9-9528, Mr. M. F. Lausten, Project Manager. A comprehensive summary of the entire four-phase program is presented in this document.

ABSTRACT

This report is a comprehensive summary of the results of a cold-flow and hot-fire experimental study of the mixing and atomization characteristics of injector elements incorporating noncircular orifices. Both liquid/liquid and gas/liquid element types are discussed. Unlike doublet and triplet elements (circular orifices only) were investigated for the liquid/liquid case while concentric tube elements were investigated for the gas/liquid case. It is concluded that noncircular shape can be employed to significant advantage in injector design for liquid rocket engines.

CONTENTS

ILLUSTRATIONS

TABLES

SYMBOLS

A	=	area, $in.^2$
AR	=	orifice aspect ratio, x_1/y_1
B, b	=	larger dimension for noncircular orifice, inches
c*	=	characteristic velocity, ft/sec
CCTE	=	circular concentric tube element
C_D	=	orifice coefficient
C_p	=	specific heat, Btu/lbm-R
D, d	=	diameter or characteristic length, inches
$\overline{D}$	=	mass median diameter, usually microns
D_H	=	hydraulic diameter, inches
E_m	=	mixture ratio uniformity parameter, Eq. B-4
f	=	hydraulic friction factor
f( )	=	function of ( )
GCC	=	gas/liquid circular concentric element code
GCR	=	gas/liquid rectangular concentric element code
G/L	=	gas/liquid
GST	=	gas/liquid multishowerhead triplet element code
h	=	liquid sheet thickness, inch
K	=	general constant, or hydraulic loss factor, or bulb compressibility, $lbm/ft\text{-}sec^2$
L	=	orifice length, or general dimension-length
M	=	momentum flux, ρu^2, or general dimension-mass
mff	=	mass fraction flux
MR	=	mixture ratio, $\dot{w}_o/\dot{w}_f$
P	=	perimeter, inches

P, ΔP = pressure, psia, and delta pressure, psid

P_c/P_j = ratio of momentum on jet centerline to momentum based on average jet velocity, $\rho V_c^2/\rho\bar{V}^2$

P_D = dynamic pressure ratio, $(1/2\rho_1 V_1^2)/(1/2\rho_2 V_2^2)$

$\dot{Q}$ = heat flux, Btu/in.^{2}-sec

R = centerpost recess depth, inches

r = radial distance, inches

Re, Rey = Reynolds number

RCTE = rectangular concentric tube element

STE = showerhead triplet element

T = temperature, R, or general dimension-time

U, u = velocity, ft/sec

U.D. = unlike doublet code

U.T. = unlike triplet code

V, v = velocity, ft/sec

w = smaller dimension for noncircular orifice, inches

$\dot{w}$ = flowrate, lbm/sec

We = Weber number

x = larger dimension for rectangles, inches, also orifice spacing

y = smaller dimension for rectangles, inches

GREEK

δ^* = boundary layer displacement thickness

ε_c = contraction ratio

ε/D = relative surface roughness

η_{c^*} = characteristic velocity efficiency

θ = orifice impingement angle, degrees

μ = viscosity, lbm/ft-sec, or microns

ξ = spray angle, degrees

ρ = density, lbm/ft^3

σ = surface tension, lbf/ft

ϕ = centerline momentum ratio $\rho_1 V_1^2 d_1 / \rho_2 V_2^2 d_2$

SUBSCRIPTS

0 = stagnation properties

1 = liquid orifice dimensions, concentric element - smaller orifice, doublets - outer orifices, triplets

2 = centerpost dimensions, concentric element - larger orifice, doublets - center orifice, triplets

3 = gas port dimensions, concentric element

B,b = back pressurant properties

C = chamber, or cross velocity

C.F. = cold flow

D = based on diameter

E, e = entrance condition

E = environment properties

f = due to friction

f, F = fuel-side properties

g, G = gas-side properties

H.F. = hot fire

i = general index for i^{th} quantity

j = jet properties

L	=	liquid-side properties, or ligament properties
mix	=	mixing process limited
o	=	oxidizer-side properties
opt	=	optimum condition
s	=	static properties
sat	=	saturation properties
T	=	total or stagnation properties, also throat conditions
vap	=	vaporization process limited
v.h.	=	velocity head
x	=	based on length

1.0 SUMMARY

This report contains a comprehensive review of the results of a 4-year applied research program. The objective of the program was to determine the influence of orifice and element shape upon the performance of injector elements for liquid rocket propellant injectors. Investigation of this subject was divided into three major categories: (1) the characterization of single, noncircular orifices; (2) t characterization of unlike-doublet injector elements having rectangular- and triangular-shaped orifices for liquid/liquid propellant applications; and (3) the characterization of concentric tube injector elements of rectangular shape for gas liquid propellant applications.

The primary methods of evaluation were cold-flow mixing and atomization experiment techniques with a limited amount of single-element, hot-fire experimentation for verification purposes.

The program was conducted in four phases. The technology areas investigated under each phase are summarized in Table 1-1.

Before reading this document, the following questions must be foremost in the mind of every individual:

1. Do noncircular orifices offer advantages for injector design that are not available with circular orifices?
2. Should noncircular technology be employed for injector applications at this time?
3. Is further research in the area of noncircular technology warranted in the light of the results of this program?

The answer to all of these questions is an unequivocal yes.

TABLE 1-1. SUMMARY OF THE NONCIRCULAR ORIFICE PROGRAM BY PHASE

Phase

I Liquid/Liquid Applications

1. Cold-flow determination of the effect of shape upon C_D for noncircular orifices
2. Cold-flow evaluation of the atomization and mixing characteristics of unlike doublets with rectangular and triangular orifices with sharp entrances
3. Cold-flow evaluation of the mixing and atomization characteristics of elements formed from commercially available spray nozzles
4. Single-element, hot-fire evaluation of unlike doublets and spray fan elements

II Gas/Liquid Applications

1. Preliminary cold-flow evaluation of the mixing and atomization characteristics of concentric tube injector elements of rectangular shape (measurement of mixing uniformity and dropsize in two-phase flowfields conducted in atmosphere)

III Gas/Liquid Applications

1. Detailed cold-flow mixing and atomization characteristics evaluation of rectangular concentric tube injector elements (measurement of mixing uniformity and dropsize in two-phase flowfields, conducted in pressurized environments)
2. Preliminary cold-flow mixing and atomization evaluation of a multi-showerhead triplet element

IV Gas/Liquid and Liquid/Liquid Applications

1. Single-element, hot-fire evaluation of gas/liquid rectangular concentric tube injector elements (LOX/GH_2 at 800 psia)
2. Detailed additional cold-flow mixing evaluation of a circular concentric tube element (pressurized environment, gas/liquid)
3. Detailed cold-flow mixing evaluation of rectangular unlike doublets with rounded-orifice entrances (liquid/liquid)
4. Cold-flow mixing and atomization evaluation of triplet injector elements with circular orifices having rounded entrances (liquid/liquid)

Notice that the question--"Are noncircular orifices better than circular orifices?"--has not been posed. If one sets out to answer this question, one misses the point of the entire subject. The nature of this question is similar to the questions: "Are big trucks better than small trucks?", or "Is a screwdriver better than a wrench?". The answer is obviously--It depends upon what you want to do with it (or them).

Circles are nothing more than a specific, limiting class of items termed "shapes." As a matter of fact, it is the *only* class of shapes for which the characteristic dimension is uniquely related to the cross-sectional area. Rather than a noncircular orifice investigation, the program that is documented in this report has been a study of the general nature of injector elements with the restriction to circular orifices removed.

Significant results of this program have shown that the maximum high levels of mixture ratio uniformity ($E_m \geq 85$ percent) can be achieved with unlike-doublet elements (for liquid/liquid applications) having rectangular orifices, regardless of propellant density ratio or operational mixture ratio. This is not possible with circular orifices.

It has also been shown that the mixture ratio uniformity, E_m, can be significantly improved with rectangular concentric tube elements for gas/liquid applications for mixture ratios above 4:1 (liquid to gas). This is the operating regime for most gas/liquid rocket injectors except perhaps those for gas generators. Also, in the areas of gas/liquid technology, it has been demonstrated that the spray field produced by rectangular concentric tube elements can be "tailored" to provide improved injector/chamber wall thermal compatibility while maintaining high injector performance.

During the program, a greater insight into the nature of, and a greater appreciation for, the circular orifice has also been realized. Once again, the study of the general has shed light upon the specific. Results presented in this report

include improved methods for estimating the values or orifice coefficients for circular and noncircular orifices, a better physical understanding of the nature of the unlike-doublet mixing process, and an appreciation for the effect of injection parameters upon the mixing and atomization characteristics of gas/liquid concentric tube injector elements.

This technology should be employed in today's rocket engines and further investigation into the *general* nature of liquid propellant injector elements should be pursued.

All of the significant results of the program are reviewed in this report. Details of the individual phases may be found in Ref. 1-1, 1-2, and 1-3.

2.0 INTRODUCTION

2.1 BACKGROUND

Most rocket engine injector designs in existence today employ circular orifices. Historically, circular holes have been incorporated primarily because of manufacturing limitations. With the advent of new fabrication techniques, injector orifices can now be manufactured by means other than twist drilling. As a result, noncircular orifices can now be produced with relative ease. Because of these fabrication advances, it is appropriate to re-evaluate injector design practices to see if noncircular orifice designs can offer superior qualities in terms of greater design flexibility, lower cost, better reproducibility, and/or improved performance and injector-thrust chamber compatibility.

Potential advantages of noncircular orifices can be envisioned from an examination of certain of the limitations associated with circular orifices. One of the greatest limitations of a circular orifice is that its characteristic dimensions, the diameter (d), is functionally related to its cross-sectional area. This seems like a rather trivial shortcoming until one reflects upon the degrees of added flexibility that could be achieved if this limitation were removed.

One of the simplest forms of the noncircular shape is the rectangle. The rectangle has two characteristic dimensions (x and y). As a result, two independent parameters must be specified to describe a given rectangle; the characteristic length, y and the "aspect ratio," x/y. With a circle, only one independent parameter exists, the diameter, d.

One example of exactly how this added degree of freedom available with a rectangle could be advantageous is provided in an examination of the optimum mixing unformity design criterion for unlike-doublet elements.

It is widely known in the rocket industry (Ref. 2-1) that optimum mixture ratio uniformity in the spray formed by an unlike-doublet element is achieved by balancing the momentum of the two opposing propellant jets. The exact design relationship for circular orifices may be expressed in the following form:

$$\frac{\rho_f V_f^2 d_f}{\rho_o V_o^2 d_o} = 1 \tag{2-1}$$

In terms of the properties of the propellant combination selected and the specified operational mixture ratio, the design criterion becomes:

$$\left(\frac{d_f}{d_o}\right)_{opt} = \sqrt[3]{\frac{\rho_o/\rho_f}{MR^2}} \tag{2-2}$$

Thus, for circular orifices, the design requirements specify the diameter ratio of the orifices, as well as the area ratio of the orifices. It has been shown (Ref. 2-1) that the level of mixing for an unlike doublet is a function of the diameter ratio. As a result, although the mixing level provided by an element design based upon Eq. 2-2 is the highest that can be achieved with that propellant combination, the level may not be as high as unlike doublets with other diameter ratios (i.e., other propellant combinations) could achieve.

With the rectangular element, however, there exists the added variable, "aspect ratio." As a result, the characteristic opposing lengths of the two orifices, as well as their area ratio, may be specified independently. The basic question this example raises is: "Can the rectangle, with its extra degree of freedom, be employed in unlike-doublet element design to provide the same high levels of mixture ratio uniformity for all propellant applications?"

It is to this question, as well as many other questions of a similar nature, that this study was dedicated. Application of noncircular technology was investigated for both liquid/liquid and gas/liquid propellant systems.

2.2 TECHNICAL APPROACH

There is an apparent dichotomy that has developed in present-day technology. On the one hand, there is an increasing demand for excellence, while on the other hand, there is a demand to lower costs. This is especially true of the technology associated with the aerospace industry. It is becoming more and more evident that yesterday's techniques and approaches to research and development are not suited to the accomplishment of both of these primary objectives.

In this program, the objective was to evaluate and characterize new and different rocket engine injector elements to broaden the foundation of injector design. The requirements for these new elements include such considerations as ultrahigh performance, reduced fabrication costs, and increased design flexibility. If a development technique based upon cut and try with full-scale hardware had been selected to meet this objective, the time and dollar expenditures required would prove to be astronomical in magnitude.

At Rocketdyne, a new and advanced approach to rocket engine injector characterization has been developed. The major objectives of this new approach are to reduce overall costs and to provide, at the same time, greater insight into the actual mechanisms that influence injector performance.

Rather than attempting to analyze a complete injector on a hot-fire basis, study is initiated with single-injector elements on a cold-flow basis employing nonreactive propellant simulants. Furthermore, the overall performance-limiting processes associated with combustion in a rocket chamber are grouped into two separate classes: (1) mixing processes and (2) atomization processes.

These processes are investigated independently with cold-flow modeling techniques. Mixing characteristics are defined by the direct measurement of mass and mixture ratio distribution profiles employing appropriate propellant simulants to model the injection parameters. These profiles are characterized by a mixing uniformity parameter, E_m, and also by a mixing limited c* efficiency, $\eta_{c^*_{mix}}$, obtained by combustion model analysis of the mass and mixture ratio profile data.

The atomization process is investigated with the "frozen wax" technique. Molten wax is injected through the element and the frozen particles collected to determine the mass median droplet diameter as well as the dropsize distribution about the median size. A vaporization rate-limited combustion model is employed to estimate the contribution of the vaporization process to the overall performance in the form of the vaporization-limited c* efficiency, $\eta_{c^*_{vap}}$.

The two independent performance estimates are then combined to estimate the overall efficiency by the first order approximation of their product, $\eta_{c^*_{pred}} = \eta_{c^*_{mix}} \times \eta_{c^*_{vap}}$. This method produces design and analysis information pertaining to the performance of many different elements, and variations of these elements, at a cost far less than that incurred in hot-fire analysis.

Following single-element, cold-flow analysis, the usual program includes single-element, hot-firing studies of those element configurations that were shown to be of interest by the cold-flow tests.. Single-element, hot-fire tests provide additional information about the mixing and atomization mechanisms at a cost that is also substantially below full-scale injector firings.

The final step in the research investigation is usually the design of a full-scale or multielement injector whose design has been dictated by the information obtained in the single-element, cold-flow and hot-fire programs. The full-scale injector design dictated by this approach is usually quite close to the final configuration and will not require costly major redesign. The overall cost of the development program is well below that of the cut-and-try approach, with the added advantage that detailed information is available concerning the role of operating and design variables in the performance of the injector. In other words, the injector will be high performing and the investigators will know why it is and will be able to extend their knowledge to the design of related hardware without the necessity of starting from scratch.

Information pertaining to chamber compatibility is also made available in the results of a program that contains single-element, cold-flow studies. The mass and mixture ratio profiles offer a direct picture of the flowfield, which can be

expected from a given element. Superimposition of these pictures and the geometry of the chamber wall yields an estimate of the interaction of zones of defined temperature and the wall surface. Without cold-flow results, information of this nature must be obtained through direct hot-fire testing.

The validity of this overall approach has been documented by many programs. Two of particular interest are the space-storable propellant injector study, NAS3-1205 (Ref. 2-2), and the gas-augmented injector study, NAS3-12001 (Ref. 2-3). In these programs, excellent agreement was obtained between hot-fire test results and cold-flow estimates of these results.

The study of noncircular orifices, the results of which are presented in this report, followed the guidelines of this technical approach through the level of single-element, hot-fire analysis. No full-scale or multielement injectors were tested. This remains as the final step in the overall initial evaluation of noncircular orifices. Throughout this program, circular orifices and elements containing circular orifices were included in the various studies to provide a logical basis of comparison with state-of-the-art injector configurations.

3.0 THE GENERAL PROBLEM AND ASPECTS OF THE SELECTION OF SIGNIFICANT VARIABLES

The objective of this program was to determine experimentally the influence of orifice and/or element geometry upon the performance of liquid rocket injectors. To attack this problem from a fundamental standpoint, the concept of performance was subdivided into three major aspects: (1) the characteristics of the individual orifice and its effect upon the jets issuing from the injector, (2) the characteristics of the mixing of two propellant streams, and (3) the characteristics of the atomization of the liquid components and the subsequent vaporization of the droplets produced by the atomization process.

In each of the major sections of this report, some mention is made (in certain cases, detailed discussion is presented) of the methods employed to define the parameters that would be most important to each of the individual aspects of performance. In general, the parameters may be grouped into two basic classes: (1) geometrical parameters and (2) operational parameters. Geometrical parameters are those that describe the shape, size, number, and relative orientation of the injector elements. Operational parameters include such variables as propellant properties (density, viscosity, surface tension, etc.), operating pressures, flowrates, velocities, and mixture ratios. The more important of these classes for this program is the geometrical parameter class.

In the study of single-injector orifices, a theoretical model was employed to show that the hydraulic diameter of the orifice, the Reynolds number, and the term $\sqrt{\frac{L/D}{Re}}$ were most significant in determining the orifice coefficient, C_D, for a particular configuration. On the other hand, analytical and empirical formulations presented for the mixing and atomization characteristics of liquid/liquid and gas/liquid propellants show clearly that the hydraulic diameter is not a significant parameter and that its incorporation in such an analysis could lead to confusion and improper physical interpretation of the results.

In the study of the mixing characteristics of unlike-doublet elements with rectangular orifices, it was found that the parameter, ϕ, the centerline momentum rati

$$\phi = \frac{\rho_f b_f V_f^2}{\rho_o b_o V_o^2} \qquad (3\text{-}1)$$

and the aspect ratio of one of the orifices, b_o/w, were required to specify an optimum design for mixing. Further, it has been demonstrated that Reynolds number has a significant effect upon mixing.

Both the liquid/liquid and gas/liquid studies of atomization suggest strongly that Weber number plays a significant role. Weber number is a measure of the relative strength of dynamic "stripping" forces compared to droplet surface tension stabilizing forces.

It is in the specification of these parameters and the suggestion of their significance that this document is most valuable.

4.0 SINGLE-ORIFICE STUDY

4.1 BACKGROUND

The objective of the single orifice study was the extensive evaluation of the influence of orifice shape as well as operational variables upon the discharge coefficient of small injector orifices.

Model orifices of both circular and noncircular shape were cold-flow tested with water as a propellant simulant under many practical design and operational conditions. The primary results of the program were expressed in terms of the discharge coefficients of the various orifices; however, photographs of the orifice jets were also taken.

Orifice shapes investigated during this program included the circle, square, rectangle, slot, equilateral triangle, isoceles triangle, and diamond. The design variables tested were orifice length-to-hydraulic diameter ratio (L/D), and entrance condition. Nominal values of L/D of 2, 4, 6, and 20 were employed. Orifice entrances were both sharp and well rounded. Operational variables investigated included orifice pressure drop (10 to 70 psid), back pressure (0 to 100 psig), manifold cross velocity (0 to 20 ft/sec), and fluid temperature (45 to 135 F).

The orifices were formed in aluminum plates using the electrical discharge machining (EDM) technique. This process involves the removal of material from the specimen (aluminum plate) by electrical discharge to a brass electrode whose cross section was the desired orifice shape. Specimens were predrilled to allow flushing of waste material through the part. In regular production application, the wastes are flushed through the electrode, which is hollow.

A simplified matrix showing the orifice and operational variables tested during cold-flow experimentation is presented in Table 4-1. Seven orifice shapes were investigated: circle, square, rectangle, equilateral triangle, slot, diamond,

TABLE 4-1. SINGLE ORIFICE TEST MATRIX

Shape	L/D_H 2 4 6 20	P_b, psig 0 50 100	V_c, ft/sec 0 5 10 20	Helium	GN_2	ΔP, psid 20 60	Temperature: Ambient 70	Temperature: Low 45	Temperature: High 130	Sharp	Round
Circle	X	X	X X X X		X	X	X			X	
	X	X	X X X X		X	X	X			X	
	X	X X X	X X X X	X	X	X	X	X	X	X	X
	X	X	X X X X		X	X	X			X	
Square	X	X	X X X X		X	X	X			X	
	X	X	X X X X		X	X	X			X	
	X	X X X	X X X X	X	X	X	X	X	X	X	X
	X	X	X X X X		X	X	X			X	
Rectangle	X	X	X X X X		X	X	X			X	
	X	X	X X X X		X	X	X			X	
	X	X X X	X X X X		X	X	X			X	X
	X	X	X X X X		X	X	X			X	
Equilateral Triangle	X		X X X X		X	X	X			X	
	X		X X X X		X	X	X			X	
	X	X X X	X X X X		X	X	X	X	X	X	X
	X	X	X X X X		X	X	X			X	
Slot	X		X X X X		X	X	X			X	
	X		X X X X		X	X	X			X	
	X	X X X	X X X X		X	X	X				X
	X	X	X X X X		X	X	X			X	
Diamond	X	X X X	X X X X		X	X	X			X	
Isosceles Triangle	X	X X X	X X X X		X	X	X			X	

L/D_H = orifice length to hydraulic diameter ratio
V_c = manifold cross velocity
P_b = chamber back pressure
ΔP = orifice pressure drop

and isosceles triangle. These shapes, along with their nominal dimensions, are shown in Fig. 4-1. All shapes were designed to have an area equal to that of a 0.060-inch-diameter circle. Actual areas, lengths, hydraulic diameters, and nominal and actual length-to-hydraulic diameter ratios for all orifices tested are presented in Table 4-2.

The test program is shown in Fig. 4-2. The testing was conducted in three steps: (1) Initial Characterization and Screening, (2) Design and Operational Sensitivity, and (3) Fluid Properties Study.

For Step 1, seven shapes were fabricated with an L/D_H nominally equal to 6.0. These orifices had sharp entrances. Each orifice was evaluated at 0, 50, and 100 psig back pressure over a pressure drop range from 15 to 60 psid. Gaseous nitrogen was used as a pressurant for most of the testing; however, two of the shapes were tested with helium. (Manifold cross velocity was zero and the water temperature ambient.) Motion pictures and still photographs were taken of the free jets at most flow conditions.

Following Step 1, two of the shapes (isosceles triangle and diamond) were eliminated from further study. This left five orifice shapes. In Step 2, the orifice pressure drop was fixed at 20 psig, the back pressure fixed at 100 psig (GN_2), and ambient temperature water employed. Each orifice shape was tested with L/D_H's of 2, 4, 6, and 20 (sharp entrance) with cross velocities of 0, 5, 10, and 20 ft/sec. The $L/D_H = 6$ configurations were also tested with rounded entrances at cross velocities of 0, 5, 10, and 20 ft/sec. To test the effect of water temperature on orifice coefficient, three of the shapes were selected for additional testing in Step 3 with water temperatures varied from 45 to 130 F. The orifices were run over a pressure drop range from 15 to 60 psid.

In all, 409 individual tests were run during the program. The data and a detailed matrix of test conditions for each run appear in Ref. 4-1.

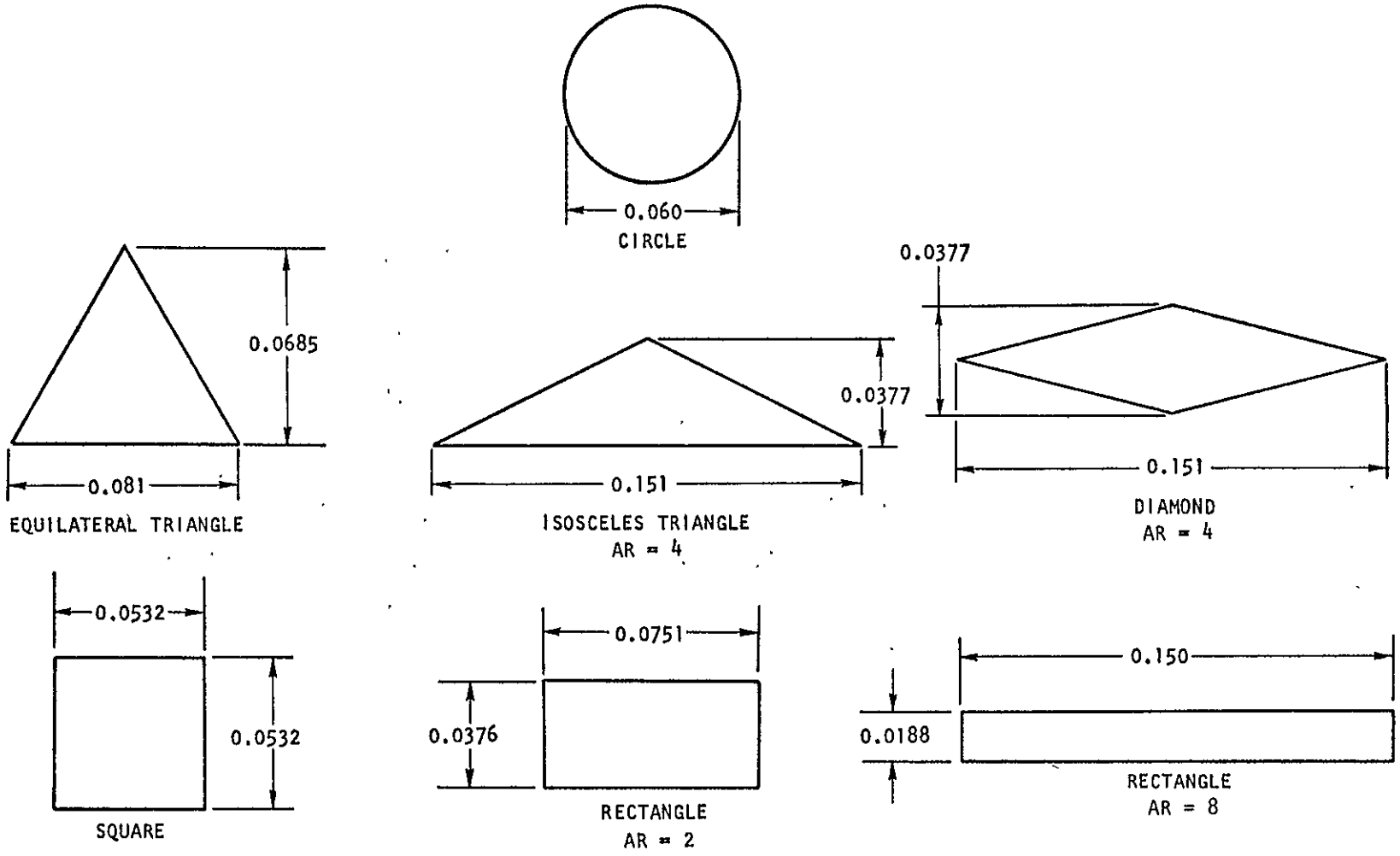

Figure 4-1. Orifices Selected for Single Orifice Cold-Flow Evaluation

TABLE 4-2. MODEL ORIFICE SPECIFICATIONS

Shape	Nominal L/D	Actual L/D	Area, $in.^2$	Length, in.	Hydraulic Diameter, in.
Circle	2	1.97	0.00289	0.120	0.061
	4	3.93	0.00285	0.240	0.061
	*6(1)	5.90	0.00278	0.360	0.061
	6(2)	5.89	0.00317	0.359	0.061
	20	20.73	0.00271	1.20	0.0579
Square	2	1.89	0.00309	0.106	0.0561
	4	3.83	0.00296	0.212	0.0554
	6(1)	5.91	0.00272	0.319	0.0540
	6(2)	6.06	0.00310	0.321	0.0530
	20	20.64	0.00281	1.063	0.0515
Rectangle	2	1.93	0.00286	0.099	0.0512
	4	3.84	0.00286	0.199	0.0518
	6(1)	5.64	0.00286	0.298	0.0528
	6(2)	5.91	0.00352	0.318	0.0538
	20	19.84	0.00289	0.994	0.0501
Slot	2	1.22	0.00382	0.0535	0.0438
	4	2.84	0.00372	0.1205	0.0425
	6(1)	4.69	0.00334	0.1865	0.0398
	6(2)	5.49	0.00445	0.251	0.0457
	20	18.92	0.00313	0.664	0.0351
Equilateral Triangle	2	1.84	0.00334	0.092	0.050
	4	3.60	0.00328	0.185	0.0514
	6(1)	5.22	0.00306	0.277	0.0531
	6(2)	5.99	0.00330	0.278	0.0464
	20	20.26	0.00304	0.924	0.0456
Isosceles Triangle	6(1)	4.88	0.00329	0.210	0.043
Diamond	6(1)	5.14	0.00322	0.216	0.042

*L/D's of 2 and 4 were made from 6(1), 6(2) was made from 20. L/D = 6(2) was rounded.

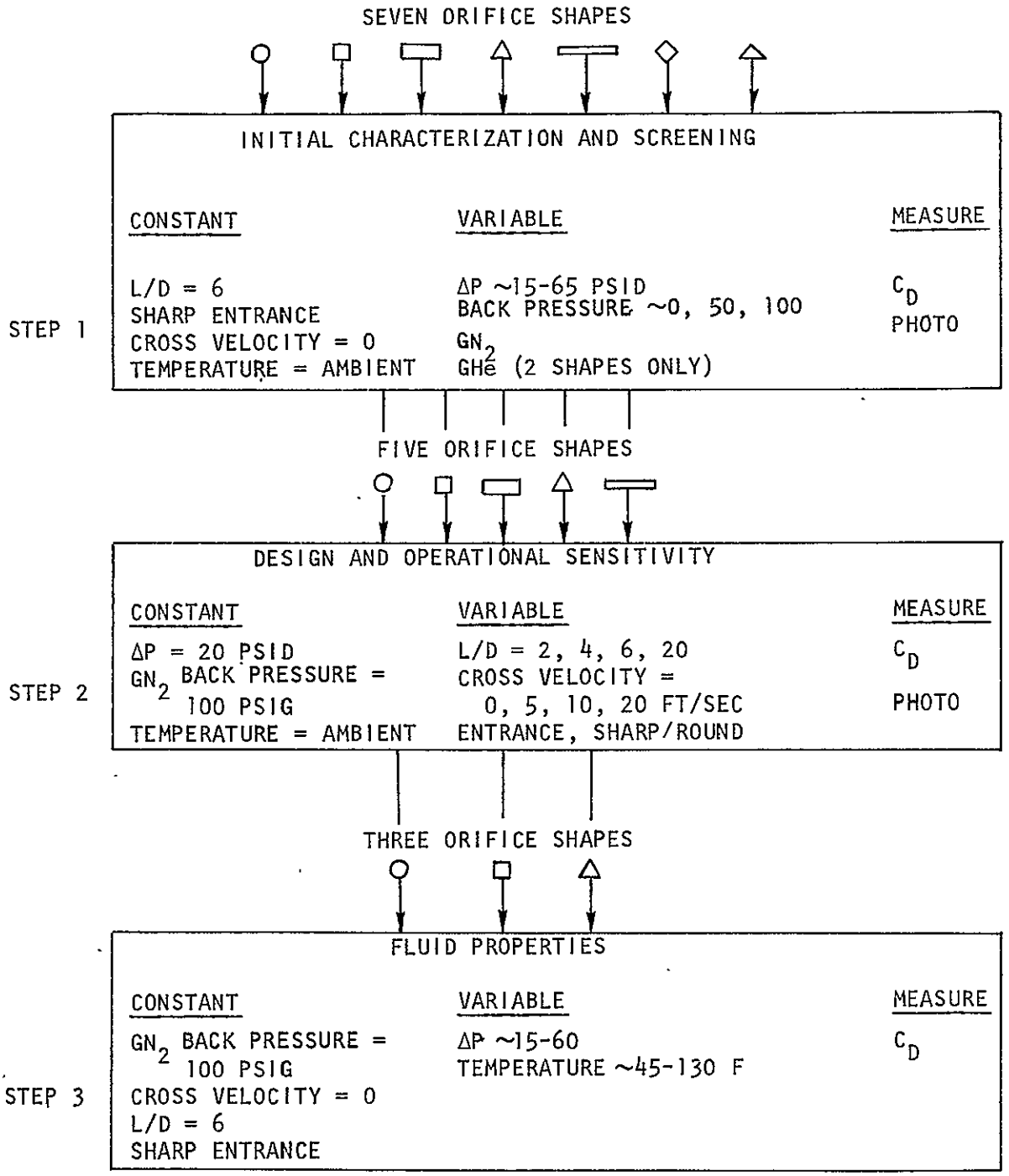

Figure 4-2. Single-Orifice, Cold-Flow Characterization Program

The results are presented in graphical form, with appropriate discussion, in sections that group data according to effect. These sections are: (1) effect of pressure drop and back pressure (with GN_2 and He), (2) effect of cross velocity, (3) effect of entrance condition, (4) effect of orifice shape orientation to cross velocity, and (5) effect of water temperature. The effect of orifice L/D is not treated explicitly until Section 4.3 of the report; however, the data for various L/D's are presented as functions of cross velocity.

4.2 EXPERIMENTAL RESULTS

4.2.1 Effect of Pressure Drop and Back Pressure

4.2.1.1 Gaseous Nitrogen Pressurant. For this study, the length-to-hydraulic diameter ratio for all orifices was 6:1. All orifices had sharp entrances and were tested with ambient temperature water and zero manifold cross velocity. The experimental results for all seven shapes are presented in Fig. 4-3. Orifice coefficient, C_D, is plotted as a function of pressure drop across the orifice, ΔP, for back pressures of 0, 50, and 100 psig. The data were taken with GN_2 as the back pressurant. The data for each shape are presented in two groups (open and closed symbols). Open symbols are used to denote points that are assumed to be "unflipped," while solid points denote "flipped" or separated flow.

It is well known that the tendency for an orifice to flip is affected by the back pressure into which the orifice is flowing. As the back pressure is increased, the pressure drop at which hydraulic flip is first experienced increases. Thus, the higher the back pressure, the less likely an orifice is to flip at a given pressure drop.

It is evident from the data in Fig. 4-3 that the circle was most affected by hydraulic flip (or back pressure). The circle shows the greatest difference in values of C_D for "flipped" and "unflipped" conditions. For the other shapes, the appearance of flip is not clear.

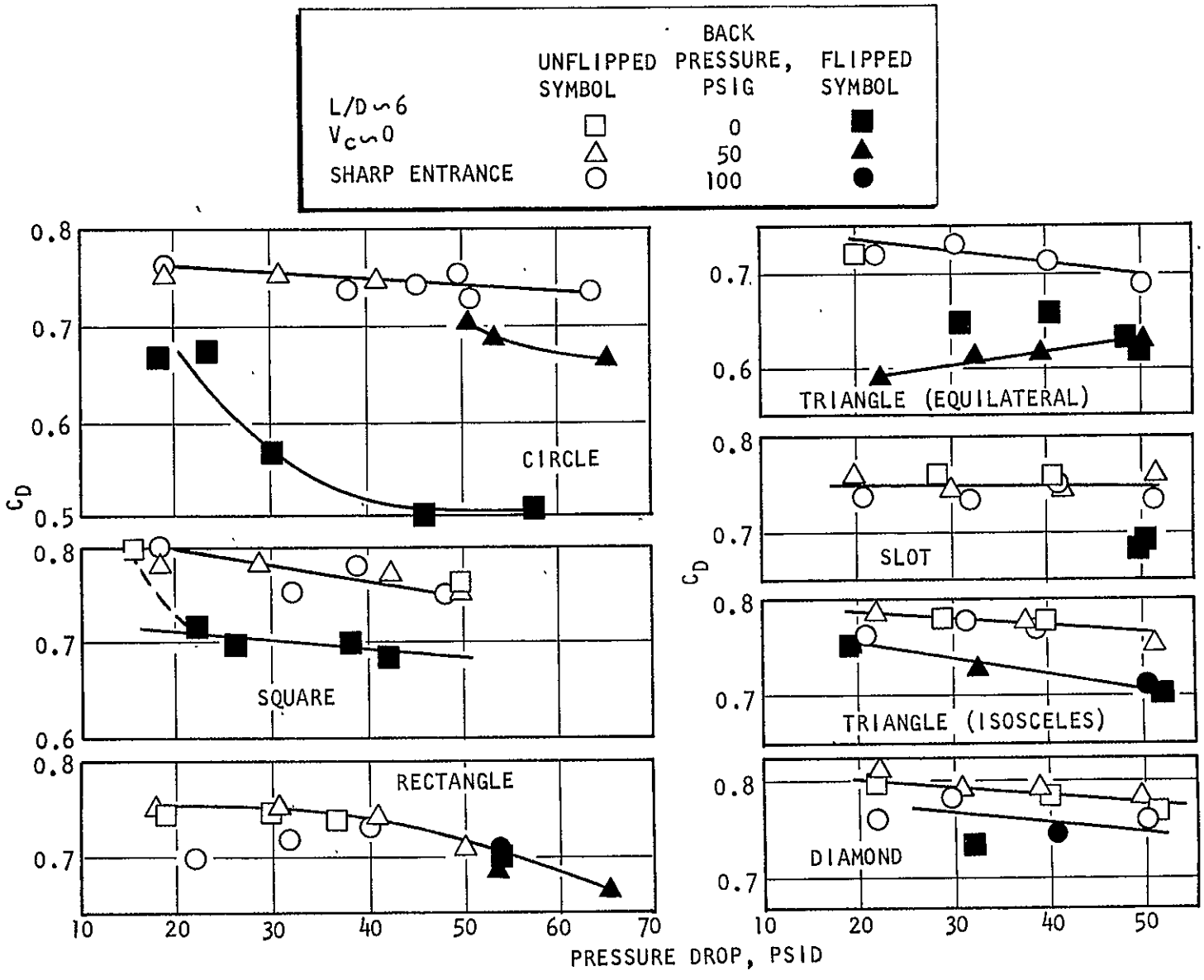

Figure 4-3. Effect of Pressure Drop and Back Pressure

Only two of the shapes (circle and the equilateral triangle) represented in Fig. 4-3 show evidence of true separated flow. The other shapes do produce what appears to be different levels of operation. However, the values of the discharge coefficient at these "other" levels are not indicative of separated flow. This conclusion was substantiated by photographic evidence (Ref. 4-2). It may be that the shapes which did not experience separation could be forced to separate at operating conditions other than those tested under this program (e.g., different Reynolds number or L/D). However, over the range of variables tested, orifices other than the circle and equilateral triangle did resist separation.

It is interesting that an orifice may change from one operating level to another and not experience simple flow separation or reattachment. This is quite significant for injector orifice design, for the change of operating level is still accompanied by changes in the free jet characteristics. This could produce changes in mixing and atomization characteristics of injector elements incorporating these "unstable" types of orifices. These changes in characteristic behavior during operation are, of course, highly undesirable for injector applications.

The important results represented in Fig. 4-3 are summarized below:

1. Only the circle and equilateral triangle show evidence of true hydraulic flip (i.e., separated flow); the other shapes experience transition to various operating levels without flow separation. The circle also changes operating level with attached flow at 50-psig back pressure.
2. All shapes produce values of C_D that are quite similar in magnitude (for attached flow). For example, at 20 psid, the smallest value is found for the equilateral triangle (≈ 0.736), while the largest is found for the square and diamond (≈ 0.80), which is a total spread of only 8.35 percent.
3. The unflipped value of C_D tends to decrease slightly with increasing pressure drop for all shapes. This is more than likely due to a change in the entrance flowfield with Reynolds number.

4.2.1.2 Helium Pressurant. It has long been a question as to whether it is the back pressure that influences orifice flow or the density of the gas used as the back pressurant. Northop (Ref. 4-3) discusses the role of gas density in the hydraulic flip characteristics of circular orifices. It may be concluded from Northop's data that the pressure drop at which an orifice will "flip" is more a function of the density of the environment than of its pressure. Northop determined this by testing orifices at several back pressures with helium and GN_2. (At the same back pressure, these two gases yield densities which differ by a factor of 7.) At each back pressure, he found the ΔP at which hydraulic flip occurred. Northop's results are shown in Fig. 4-4. It can be seen that critical pressure drop would not correlate with back pressure alone.

In the noncircular orifice program, the objective in this portion of the study was to determine the effect of different densities at similar back pressures on the absolute value of orifice coefficient (as contrasted with Northop's objective of "flip" ΔP). To do this, the circular and the square orifices were tested using He and GN_2 as a pressurant. The results are presented in Fig. 4-5. Here C_D is plotted as a function of pressure drop. The solid lines are representative curve fits of the data taken with GN_2. Plotting symbols indicate the helium data. Dashed lines are extrapolations of the solid lines made to point out the similarity of the helium and nitrogen data. It is interesting to note that the density of the back pressurant did not, in general, affect the value of the discharge coefficient. This suggests that the jet shearing interaction with the gaseous environment does not influence the orifice hydraulics. Density is only important when the jet is separated from the walls of the orifice (flipped).

4.2.2 Effect of Cross Velocity and Entrance Condition

A 0.34- by 0.34-inch square passage was provided for the cross flow. Orifices were oriented so that the cross velocity vector was parallel to the largest axis of the orifice and perpendicular to the orifice center line.

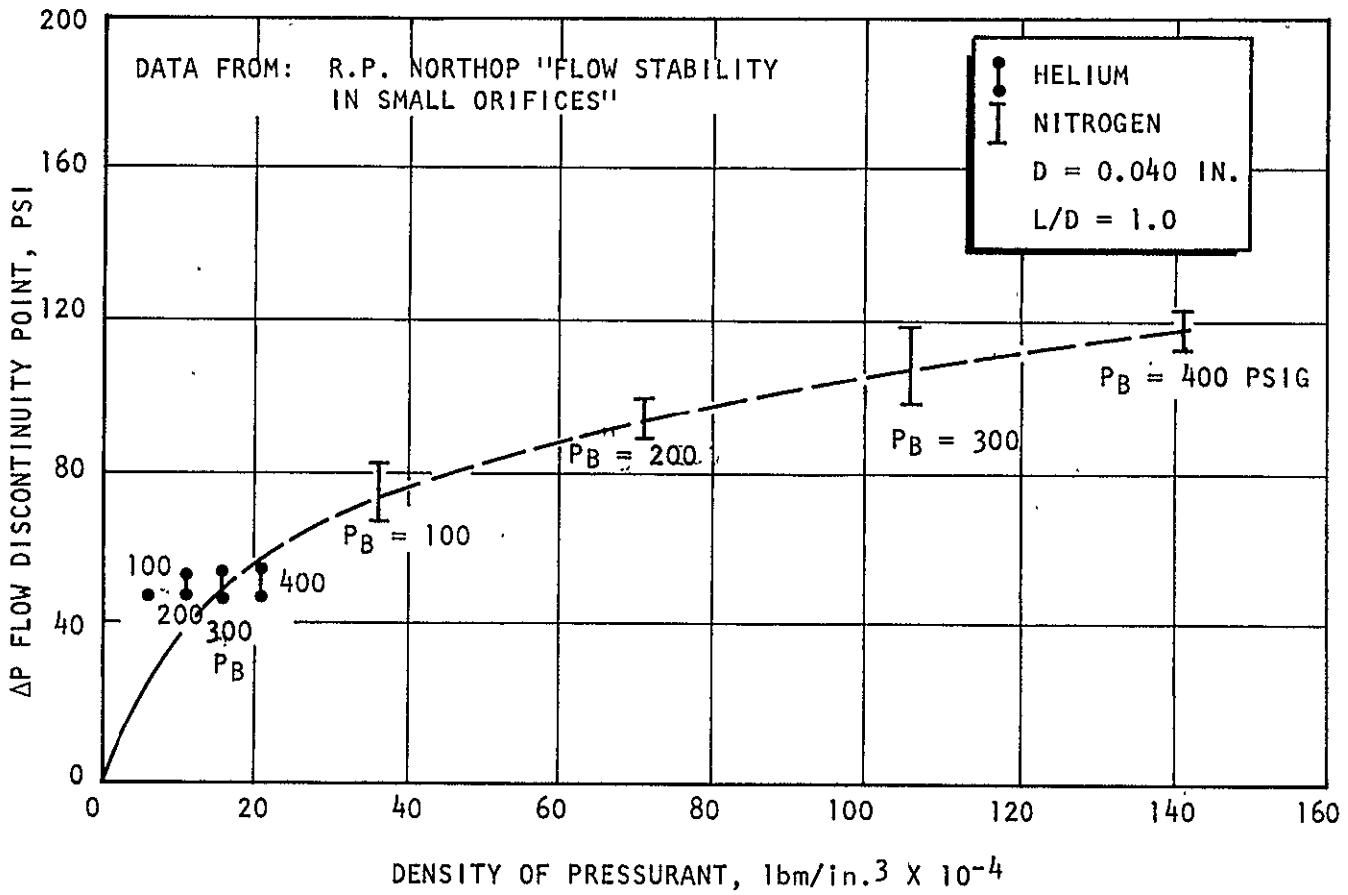

Figure 4-4. Flow Break Point (ΔP) Versus Density of Pressurant for Helium and Nitrogen Gas Atmospheres

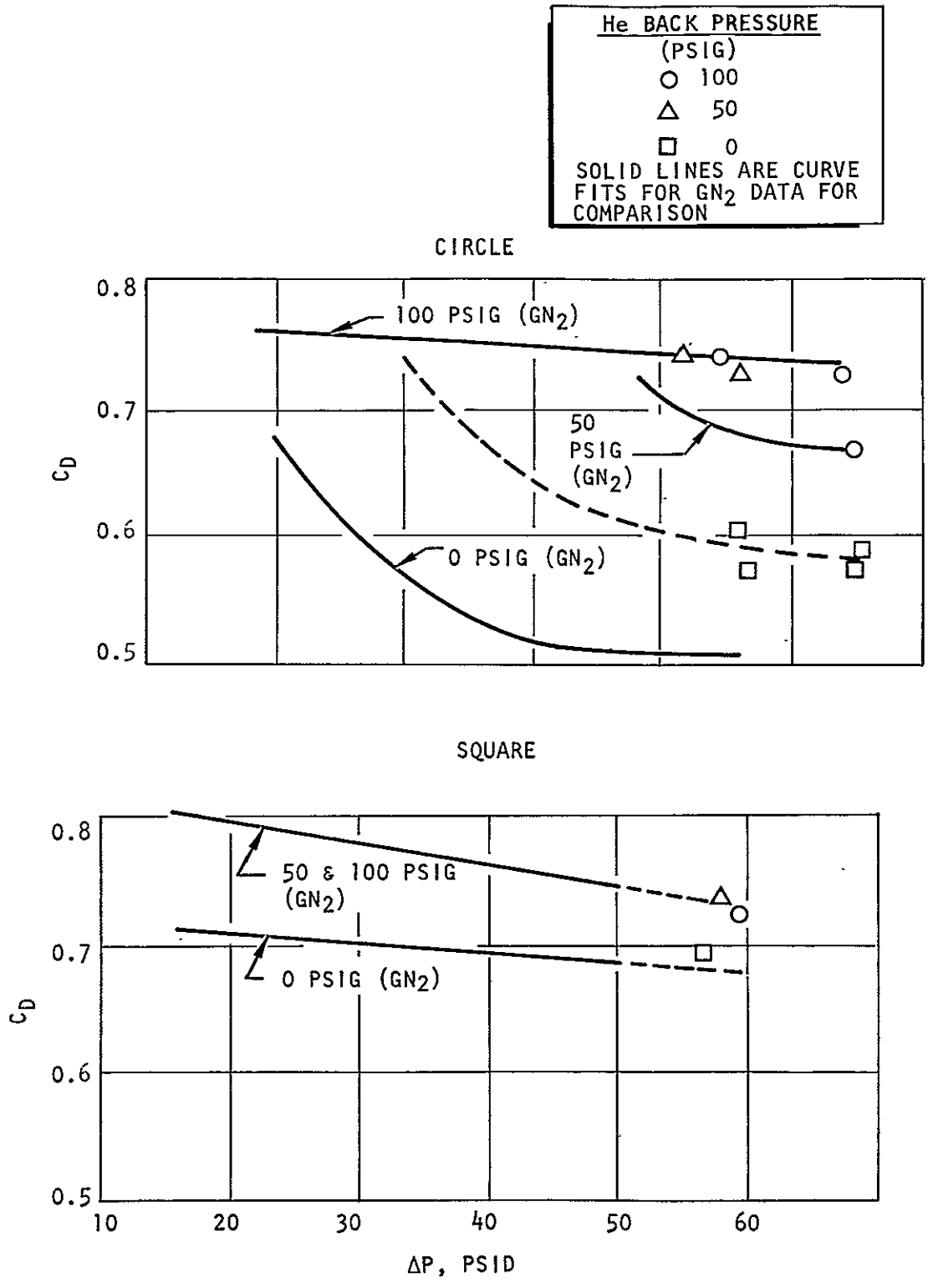

Figure 4-5. The Effect of Helium versus Nitrogen Back Pressure

4.2.2.1 Sharp Entrance Orifices. Data for sharp entrance orifices are presented in Fig. 4-6 in which discharge coefficient is plotted against cross velocity for each of the L/D ratios studied. The values of L/D quoted are nominal. Refer to Table 4-2 for the exact values. All tests were conducted at a nominal pressure drop of 20 psid.

Two conclusions that may be drawn from the cross velocity results are: (1) discharge coefficient decreases with cross velocity for all shapes, and (2) cross velocity causes some of the orifices with small L/D's to both flip and unflip (instability).

Unstable flow (flip and unflip) is found with the circle at L/D = 2, the triangle L/D = 4, the rectangle L/D = 2, and the square L/D = 2. The slot did not show evidence of instability.

For the L/D = 20 orifices, the C_D values are all similar and the response to cross velocity similar for all shapes.

4.2.2.2 Rounded Entrances. Orifices with L/D = 6.0 were also tested with well-rounded entrances. These orifices were tested at 20-psid pressure drop with variable cross velocity. The results of this test series are shown in Fig. 4-7. Solid lines labeled "sharp" are included for each shape to show the average level of the results for orifices of L/D = 6 with sharp entrances. In contrast to the sharp entranced orifices, the C_D values for the rounded entrances increased with cross velocity. (A discussion of these effects is included in Section 4.3.)

4.2.3 Effect of Shape Orientation (With Respect to Cross Velocity Vector)

In the cross velocity testing, which has been presented in the previous sections, the orifices were oriented such that the cross velocity vector was parallel to the longest axis of an orifice. To determine the effect of different orientation, the slot orifice was rotated 90 degrees from its original orientation. The slot

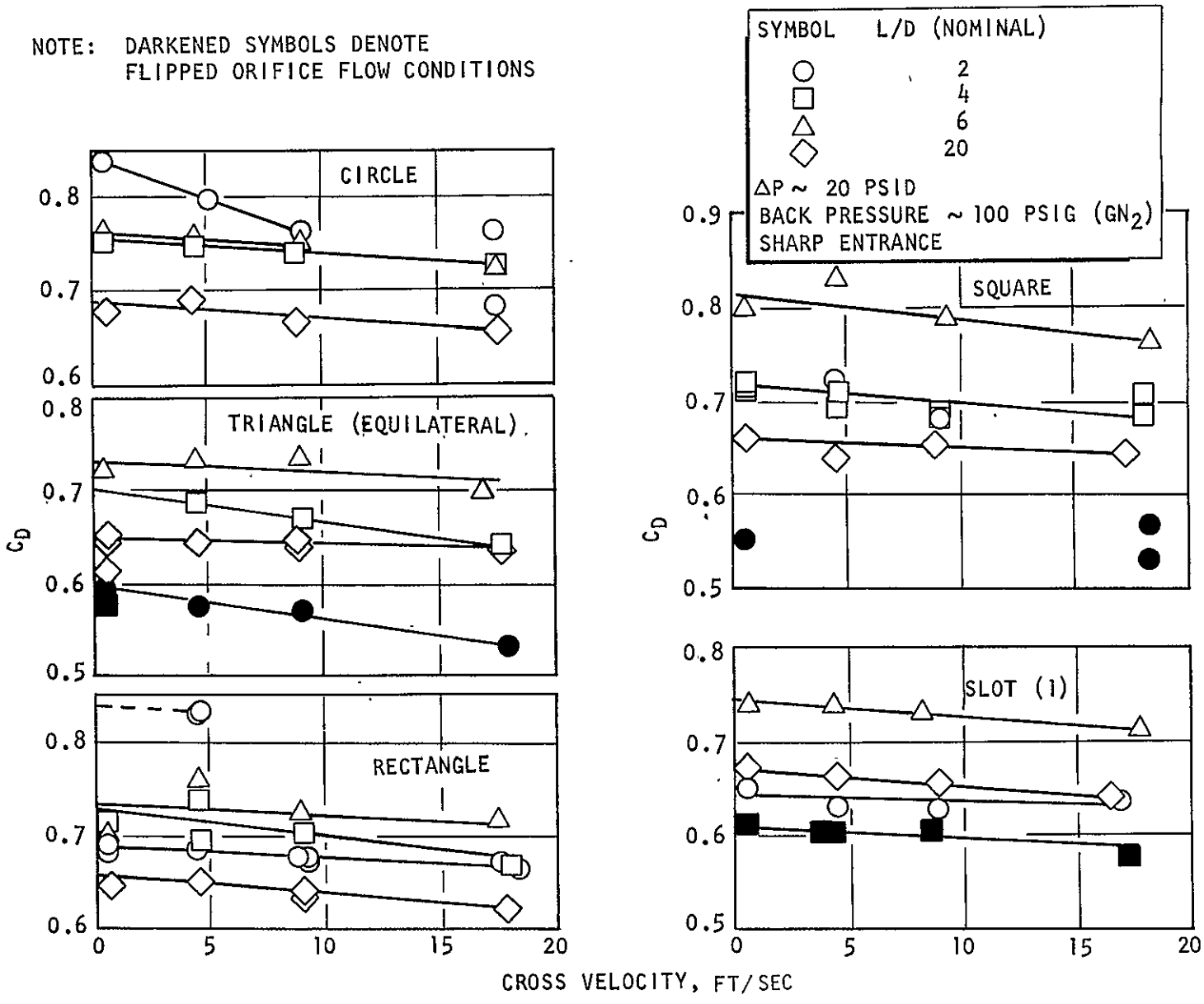

Figure 4-6. Effect of Cross Velocity

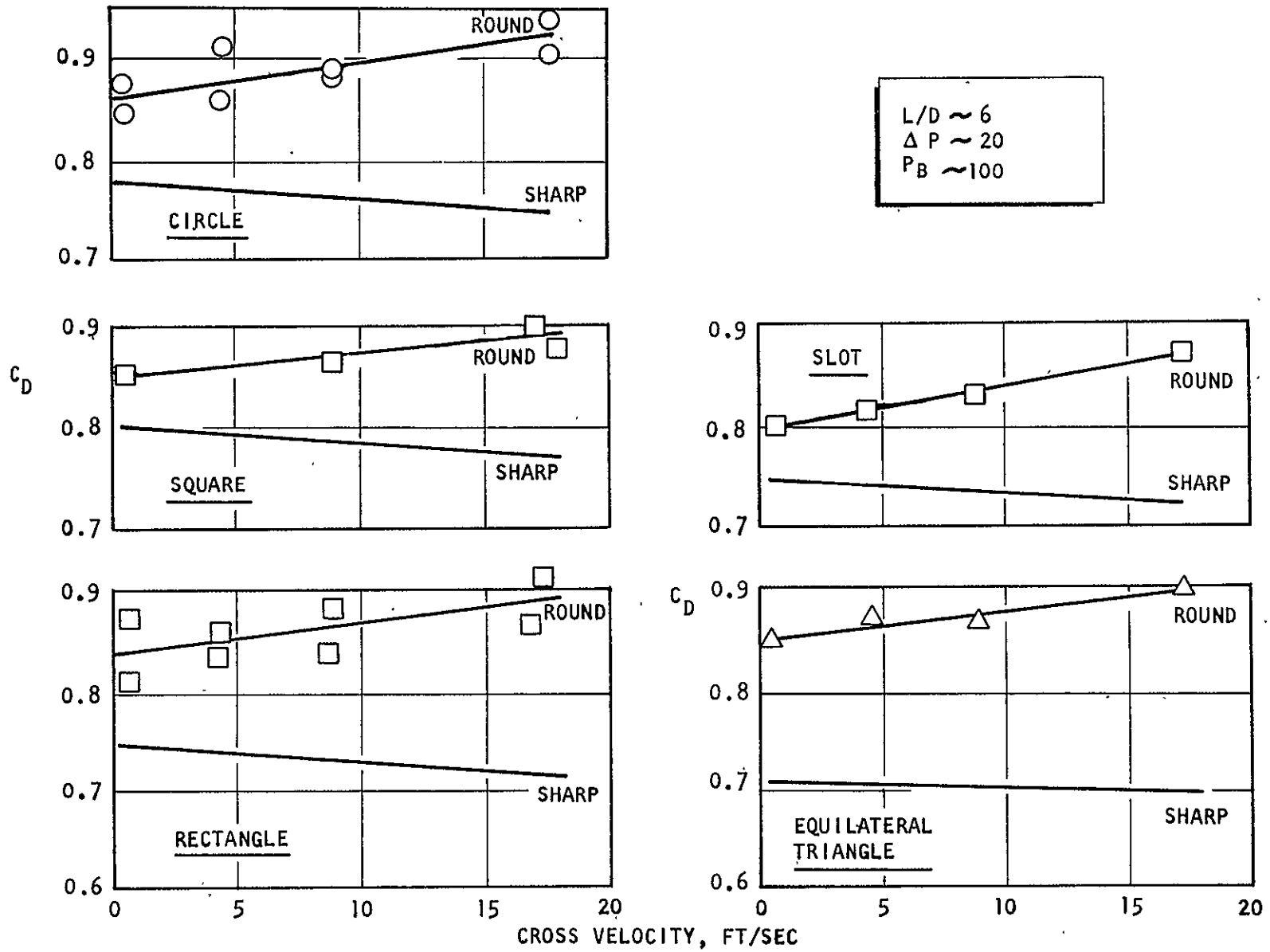

Figure 4-7. Effect of Rounded Entrance

was chosen for this study because it was thought that it would be the most sensitive to orientation. (It would be expected that the differences in C_D produced by orientation would be smaller for the other shapes.) Results from tests with both orientations are presented in Fig. 4-8 for L/D = 2, 6, and 20 for sharp entrance slots and for L/D = 6 round entrance slot. Orientation to cross velocity is depicted by plotting symbol. There is very little difference between the orifice coefficients for the two orientations. The greatest difference is found in the shortest L/D orifices. However, for all sharp L/D's and orientations, the rates of change of C_D with V_c are similar; for both orientations of the rounded slot, the rates of change and coefficient magnitudes are identical.

4.2.4 Effect of Fluid Temperature

To determine the effect of fluid temperature on C_D, the circular, triangular, and square orifices (sharp entrance, L/D = 6) were tested over a significant pressure drop range with water temperatures of 45, 75, and 135 F and back pressure = 100-psig GN_2 (see Fig. 4-9). Within the precision of the experiment, no effect due to temperature could be isolated. No attempt was made to determine the effect of temperature on orifice hydraulic flip characteristics.

4.2.5 Effect of Various Parameters on Jet Appearance

Photographs taken during the program are not presented in this report. However, they appear in Ref. 4-1. Certain of the more important facets of the photographic data are presented here for completeness.

One distinct trend in jet appearance was noted during the program. Increased agitation and early jet breakup were observed as L/D was decreased as well as when cross velocities were imposed on the orifices. The most disturbed jets were observed for short orifices with high cross velocities. Agitation was much reduced at a given set of operating conditions by rounding the entrance of an orifice.

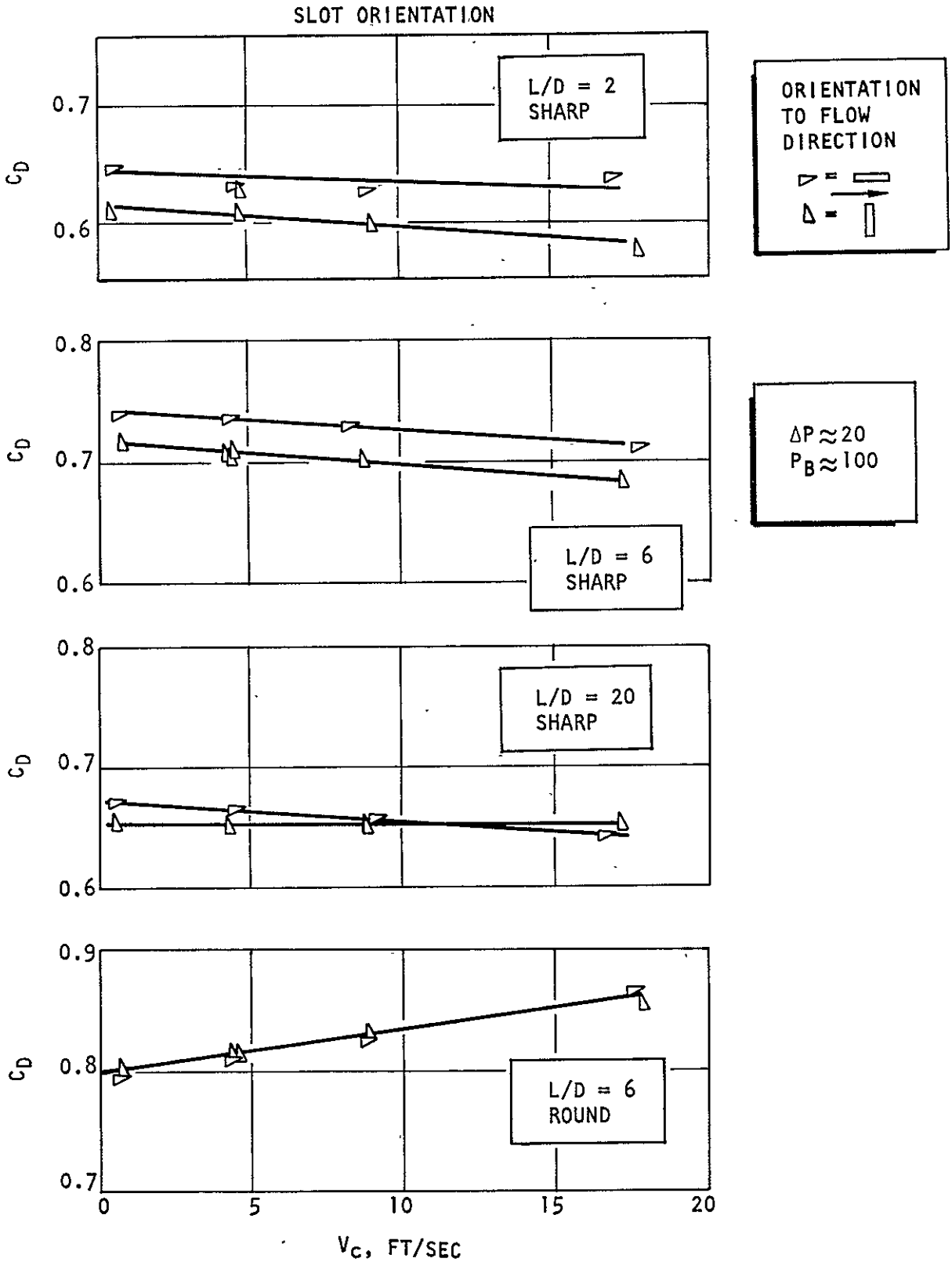

Figure 4-8. Orientation Effects

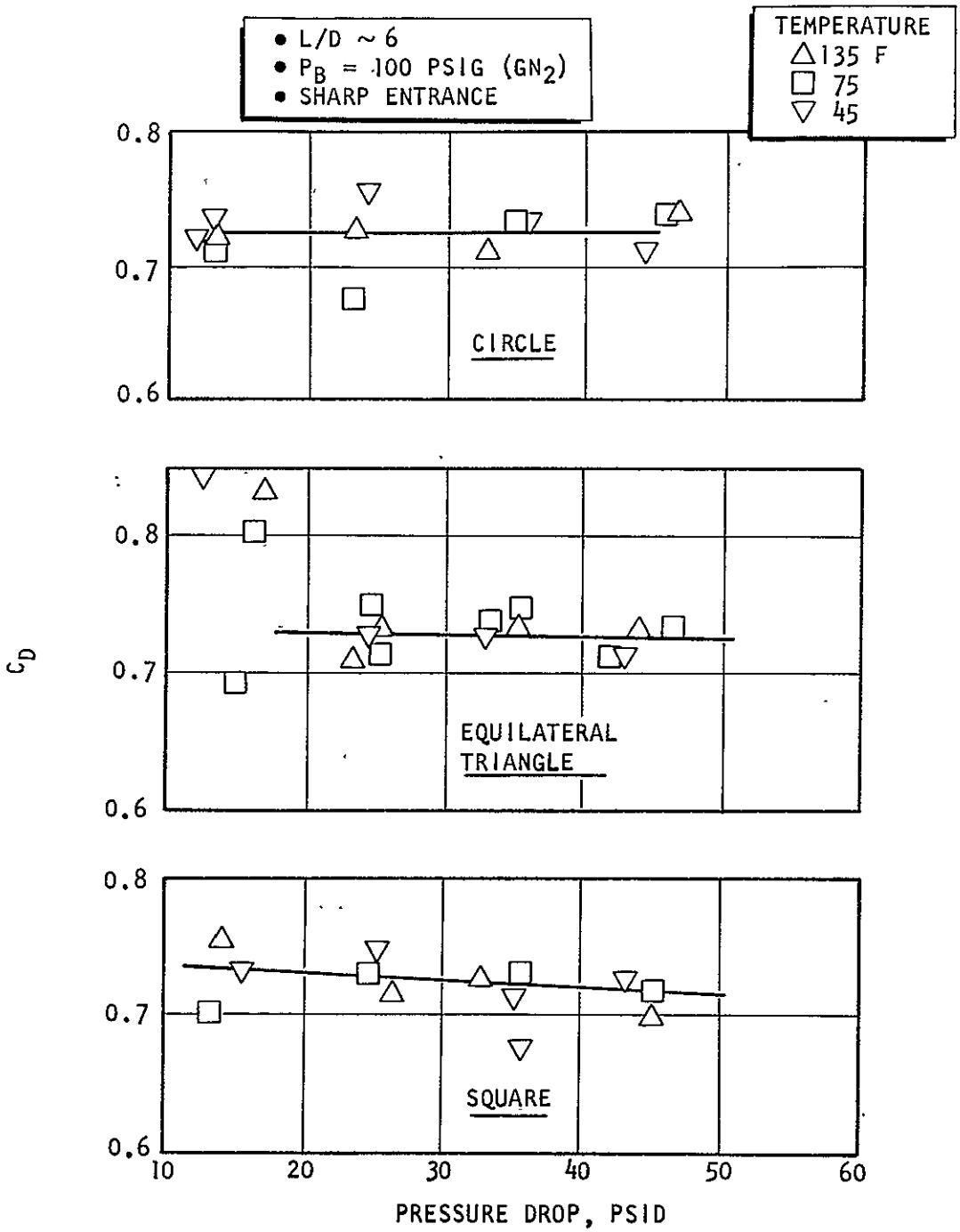

Figure 4-9. Temperature Effects

4.3 DEVELOPMENT OF ANALYTICAL ORIFICE COEFFICIENT MODELS AND CORRELATION OF THE TEST RESULTS

4.3.1 Background

In the literature of fluid mechanics there are many names and many definitions applied to the hydraulic parameter commonly referred to as the orifice coefficient. Other names for this variable include; flow coefficient, discharge coefficient, and flow factor.

Orifice coefficient is defined as the ratio of the actual flow passing through an orifice to the flow that would pass through that orifice at the same pressure drop if the flow were frictionless. Several alternate definitions may be derived from this basic description. For example, the orifice coefficient, when squared, expresses the efficiency of production of average velocity head in the orifice. These definitions are shown below in equation form:

$$C_D = \dot{W}_{actual}/\dot{W}_{ideal} \tag{4-1}$$

$$C_D = \frac{\dot{W}_{actual}}{A\sqrt{2g\rho\Delta P}} \tag{4-2}$$

$$C_D^2 = \frac{1/2\rho U_o^{\,2}}{g\ \Delta P} \tag{4-3}$$

where

C_D = orifice coefficient
$\dot{W}$ = flowrate (lbm/sec)
A = geometric area of the orifice (ft^2)
ρ = density (lbm/ft^3)
ΔP = $p_1 - p_2$ = upstream stagnation pressure minus downstream static pressure (lbf/ft^2)

In predicting pressure drops in a fluid system, loss factors are often used in place of orifice coefficients. This is due to the fact that the loss factor, or coefficient, is a more general parameter that describes losses due to many contributing factors. The "loss factor" expresses the pressure drop in a system in units of the velocity head based upon the square of the average velocity. That is;

$$\Delta P = K\ (1/2\rho\bar{V}^2) \tag{4-4}$$

The loss factor, K, may be written as a sum of individual loss factors:

$$K = \sum_{i=1}^{n} K_i \tag{4-5}$$

where the K_i is the loss factor derived from various contributing factors in a system. In pipe flow, some of the losses considered are entrance loss, frictional loss, and velocity head:

$$\Delta P = \Sigma\ K_i\ (1/2\rho\bar{V}^2) = (K_{vh} + K_f + K_e).\ (1/2\rho\bar{V}^2) \tag{4-6}$$

where

K_{vh} = velocity head factor = 1.0
K_f = loss factor due to fraction = f L/D for fully developed flow
K_e = loss factor due to vena contracta and subsequent diffusion at entrance

Additional K-factors may be added to account for losses due to valves, elbows, sudden expansion in area, etc. For orifices, the K-factor can be related to orifice coefficient by combining Eq. 4-3 and 4-6:

$$K = \Sigma\ K_i = 1/C_D^2 \tag{4-7}$$

Unfortunately, application to orifices is not quite as straightforward as Eq. 4-7 implies. Due to the fact that the flow in short orifices (L/D < 20) is far

from fully developed, the standard concepts of friction factor and entrance loss are not directly applicable. However, the concept of loss factor is useful in the development of an orifice model.

4.3.2 Orifice Coefficient Model

In the following, a model is developed that is intended to predict the discharge coefficient of circular and noncircular orifices (nonseparated jets) as a function of orifice shape, size, length, entrance condition, and the flowrate through the orifice.

The first step in the development of the model is the derivation of a simplified theory for orifices with well-rounded entrances. This theory is then extended to include orifices with sharp entrances.

The theory is intended to describe only the wall frictional aspects of the orifice coefficient and draws upon empirical results to describe losses encountered at the entrance to the orifice. For example, no theoretical development is presented to describe the variation of the entrance "vena contracta" as a function of Reynolds number or entrance manifold-to-orifice diameter ratio.

4.3.2.1 Well-Rounded Entrance Model. A typical orifice with a well-rounded entrance is shown in cross section in Fig. 4-10.

At the entrance to the orifice, the fluid is accelerated to a velocity that is very nearly equal to the average velocity $[\dot{W}/\rho A]$ over the entire cross section of the orifice. Due to nonideal entrance wall contour, there may be losses introduced into the stream as turbulence at the entrance. This would constitute an entrance loss factor, even for well-rounded entrances.

Due to the rapid acceleration of the fluid, the boundary layer that has been developing in the reservoir is thinned down appreciably at the entrance and can be considered to grow anew. Thus, in the entrance section of an orifice, the

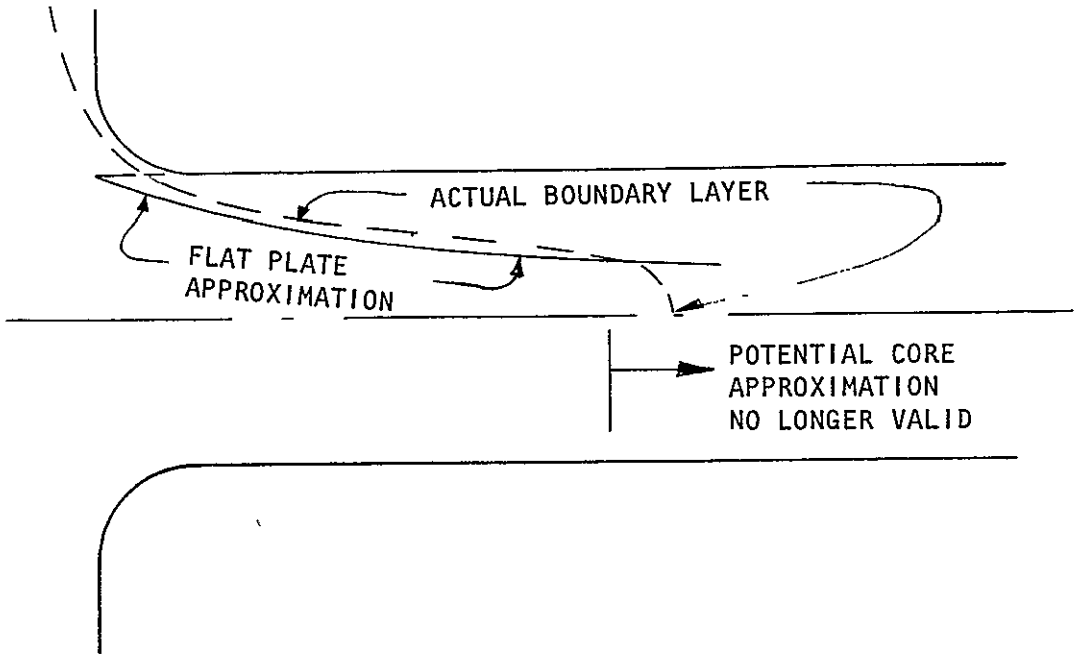

Figure 4-10. Orifice Cross Section

flowfield may be well approximated by a potential core region in the center surrounded by a zone in which the viscous effects are restricted (i.e., the boundary layer). Because the boundary layer thickens as the fluid proceeds downstream, the effective flow area is diminished, requiring the velocity in the potential core to increase to meet continuity requirements. The boundary layer continues to grow downstream until the entire flowfield is subject to viscous forces. At this point, the boundary layer approximation is no longer valid and the equations of motion must be solved over the entire cross section. Although the total area is influenced by viscous forces, the flow is still not yet "fully developed." Fully developed flow is achieved somewhat farther down the orifice length and is distinguished by the fact that the velocity profile at a given cross section is identical to that at subsequent stations downstream.

A simplified model can be postulated for orifices that are short enough so that the boundary layer approximation may be employed to describe the flowfield. A free body of the fluid in a short orifice is shown in Fig. 4-11.

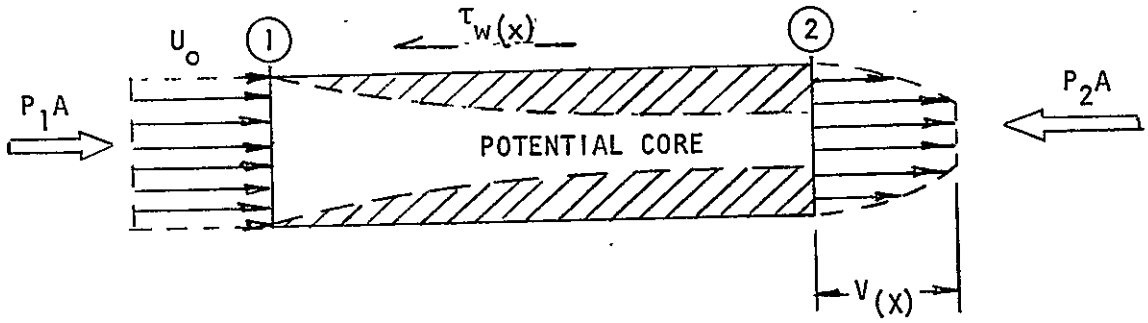

Figure 4-11. Fluid Free Body With Boundary Layer

An integral momentum equation may be written for this control volume.

$$P_1 - P_2 = \frac{1}{A}\int_o^L \tau_{w(x)}\, dA_w + \frac{1}{A}\left\{\int_{A_2} \rho u^2 dA - \rho A\, U_o^2\right\} \tag{4-8}$$

Since it is assumed that viscous effects are limited to the boundary, there exists a potential core through which the pressures and velocities at stations 1 and 2 can be related by Bernoulli's equation:

$$P_1 + \rho \frac{U_o^2}{2} = P_2 + \rho \frac{V_{(x)}^2}{2} = P_{o_1} \tag{4-9}$$

Solving Eq. 4-9 for $P_1 - P_2$, and dividing by $1/2\rho_o U_o^2$, a nondimensional expression for the orifice static pressure change is obtained:

$$\frac{P_1 - P_2}{1/2\rho U_o^2} = \frac{V_{(x)}^2}{U_o^2} - 1 \tag{4-10}$$

The total pressure in the reservoir may be related to the static pressure at the entrance to the orifice by a relationship obtained from Eq. 4-6:

$$\frac{P_{o_1} - P_1}{1/2\rho U_o^2} = 1 + K_E \tag{4-11}$$

Equations 4-10 and 4-11 may be combined to yield an expression for entire pressure drop from reservoir stagnation to exit static:

$$\frac{P_{o_1} - P_2}{1/2\rho U_o^2} = K_E + \frac{V_{(x)}^2}{U_o^2} \tag{4-12}$$

and by the definition of the orifice coefficient, Eq. 4-7:

$$K_o = \frac{1}{C_D^2} = K_E + \frac{V_{(x)}^2}{U_o^2} \tag{4-13}$$

The term $V_{(x)}^2/U_o^2$ can be interpreted, physically, by employing the boundary layer displacement thickness concept (i.e., loss of effective flow area):

$$\frac{V_{(x)}}{U_o} = \frac{A}{A-A_{\delta*}} \tag{4-14}$$

where

A = geometric area of the orifice

$A_{\delta*}$ = area taken up by displacement boundary layer

Substituting for $V_{(x)}/U_o$ in Eq. 4-13:

$$K_o = \frac{1}{C_D^2} = K_E + \left(\frac{A}{A-A_{\delta*}}\right)^2 \tag{4-15}$$

If there were no entrance loss and $K_E = 0$, then:

$$C_D = \frac{A-A_{\delta*}}{A} \tag{4-16}$$

To obtain a first-order approximation to the solution of Eq. 4-16, it could be assumed that the boundary layer develops in a manner similar to that on a flat plate. Further, since the boundary layer is in the early stages of development, a laminar solution may be employed. Under these restrictions, the Blassius solution for δ^* may be used (see Ref. 4-4):

$$\frac{\delta^*}{x} = \frac{1.72}{\sqrt{Re_x}} \tag{4-17}$$

where

x = length of the orifice

Re_x = Reynolds number based on x

The area taken up by boundary layer is approximately equal to the perimeter of the orifice multiplied by the displacement thickness of the boundary layer at the exit:

$$A_{\delta^*} \simeq p\delta^* \tag{4-18}$$

Combining Eq. 4-16, 4-17, and 4-18:

$$C_D = 1 - \frac{(1.72)px}{A\sqrt{Re_x}} \tag{4-19}$$

The area of the orifice is eliminated from Eq. 4-19 through the definition of hydraulic diameter, $D_H \equiv 4A/p$:

$$C_D = 1 - 6.88 \frac{X/D_H}{\sqrt{Re_x}} \tag{4-20}$$

Noting that x is merely the length of the orifice and that Reynolds number based on length can be written in terms of Reynolds number based upon hydraulic diameter

$$Re_x = L/D_H \, Re_{D_H} \tag{4-21}$$

Equation 4-20 may be written:

$$C_D = 1 - 6.88\sqrt{\frac{L/D_H}{Re_{D_H}}} \tag{4-22}$$

and, if there is an entrance loss:

$$C_D = \sqrt{\frac{1}{K_E + \left(\frac{1}{1-6.88\sqrt{\frac{L/D_H}{Re_{D_H}}}}\right)^2}} \tag{4-23}$$

where

K_E = entrance loss coefficient

L/D_H = length over hydraulic diameter

Re_{D_H} = Reynolds number based on hydraulic diameter

The important result of this approximate analysis is the discovery of the parameter:

$$\sqrt{\frac{L/D_H}{Re_{D_H}}} \tag{4-24}$$

This parameter provides a similarity criterion for orifices of different shape, length, and operating Reynolds numbers.

The primary shortcoming of the approximate model (Eq. 4-23) is that the boundary layer development expression is that for a constant freestream, or potential core velocity. Therefore, the predicted boundary layer growth will be more rapid than

that in an actual orifice. In the real flowfield, the freestream velocity is forced to increase as the boundary layer thickness increases, producing a boundary layer in an accelerating flowfield. This layer is thinner at a given station downstream than a layer developing in a constant velocity flowfield. Orifice coefficients predicted by this model should, therefore, be lower than the actual values at given values of $\sqrt{(L/D_H)/Re_D}$. (In addition, the simplified area relation (Eq. 4-18) adds significantly to the inaccuracy of the model.)

In 1956, Rivas and Shapiro (Ref. 4-5) published the results of a theoretical analysis of the discharge coefficients of rounded-entrance flowmeter orifices. Their work was limited to orifices of circular cross section. Their analysis considered the development of a laminar boundary layer at the entrance and along the length of well-rounded orifices. The boundary layer calculation included the effect of an accelerating potential core. Rivas and Shapiro cast their boundary layer results into the form of an effective, entrance friction factor and used this factor to evaluate the orifice coefficient according to the following equation:

$$C_{D_f} = \frac{1}{\sqrt{1 + \bar{f}\, L'/D}} \tag{4-25}$$

where

$\bar{f}$ = effective friction factor, not the same as standard friction factor for fully developed flow

$L'/D = L/D + L_{eq}/D$ = length to diameter ratio for the orifice, length taken at start of cylindrical section plus an effective L_{eq}/D to account for boundary layer losses in the entrance section

C_{D_f} = orifice coefficient due to friction

Nomenclature used by Shapiro and Rivas is explained more fully in Fig. 4-12.

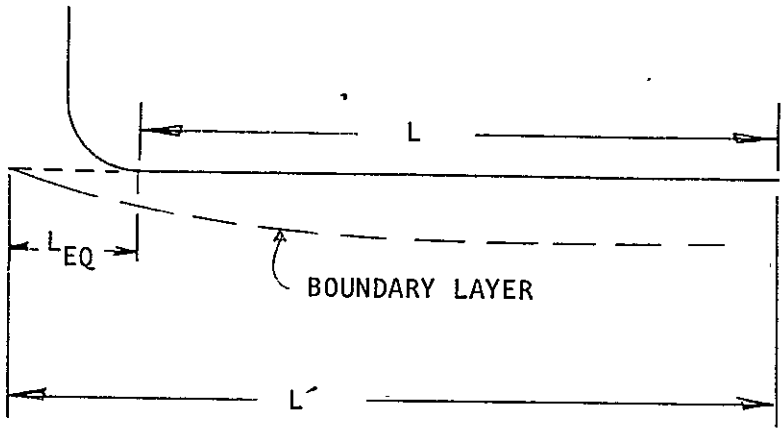

Figure 4-12. Nomenclature of Rivas and Shapiro (Ref. 4-5)

If the contour at the entrance of a given orifice is not ideal and an additional entrance loss is incurred, Rivas' formulation may be modified in the following manner to incorporate this loss:

$$C_D = \frac{1}{K_E + \frac{1}{C_{D_f}^2}} \tag{4-26}$$

where

C_D = total orifice coefficient
K_E = entrance loss factor
C_{D_f} = C_D predicted for wall frictional effects only

Equation 4-26 has the same form as Eq. 4-23. The effective friction factor, $\bar{f}$, as presented by Rivas and Shapiro, is presented in Fig. 4-13.

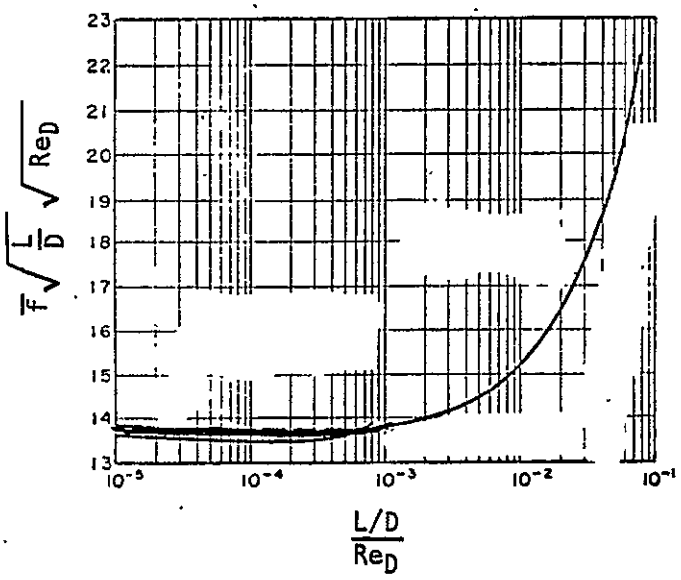

Figure 4-13. Effective Entrance Friction Factor (After Rivas and Shapiro, Ref. 4-5)

The theories discussed to this point have dealt solely with the calculation of C_D for relatively short orifices that do not produce fully developed flow. Some account must be made of the C_D for very long orifices and the transition from short to long orifices.

Regardless of the inlet conditions or the manner in which the boundary layer develops at the beginning of an orifice, the discharge coefficient of that orifice should approach, in an asymptotic fashion, the values of C_D predicted using standard friction factors (pipe flow) as the length of the orifice is increased. Therefore, a simple friction factor model should correlate well with C_D results obtained with long orifices. On the other hand, the boundary layer development theories presented in the previous section should correlate the data for very short orifices.

The approach that was selected to obtain a unified description of the discharge characteristics of orifices of all lengths (L/D) is summarized in the following discussion. The technique, basically, is to compute orifice coefficient curves for the two extreme cases: entrance flow (boundary layer plus a potential core)

and fully developed flow. These curves are then both plotted with respect to $\sqrt{(L/D)/Re}$. The solution for the orifice coefficients in the transition between the two extremes can be estimated by drawing a smooth "transition" curve between the two. (Note: For fully developed flow, i.e., simple friction factor model, the curve generated by holding L/D constant and varying Reynolds number is not the same curve that is obtained by holding Reynolds number constant and varying L/D. That is to say, the parameter $\sqrt{(L/D)/Re}$ is not "universal" for fully developed flow.)

The results of a sample calculation employing this technique are presented in Fig. 4-14. Three types of curves are depicted: (1) the universal curve, (2) fully developed flow curves with constant L/D and variable Reynolds number, and (3) fully developed flow curves with constant Reynolds number and variable L/D. The latter two types of curves have been smoothed into the "universal curve" in the transition regions. The difference between constant L/D and constant Reynolds number curves (fully developed flow) is quite striking.

It may be noted that the universal curve (boundary layer plus core) serves as an upper limit envelope for the C_D values. That is, no predicted value of C_D can be greater than that estimated by the universal curve at a given value of $\sqrt{(L/D)/Re}$.

The curves presented in Fig. 4-14 should be interpreted in the following manner. If one is interested in the variation of C_D with L/D at constant Reynolds number, one would enter the graph at the far left on the universal curve and follow this curve to the right until the curve for Reynolds number of interest is encountered. At this point, the curve for this Reynolds number should be followed.

On the other hand, if one is interested in the variation of C_D with Reynolds number at constant L/D, one would enter the graph at the far left on the curve for the L/D of interest and follow this to the right until the universal curve is encountered. At this point, the universal curve should be followed.

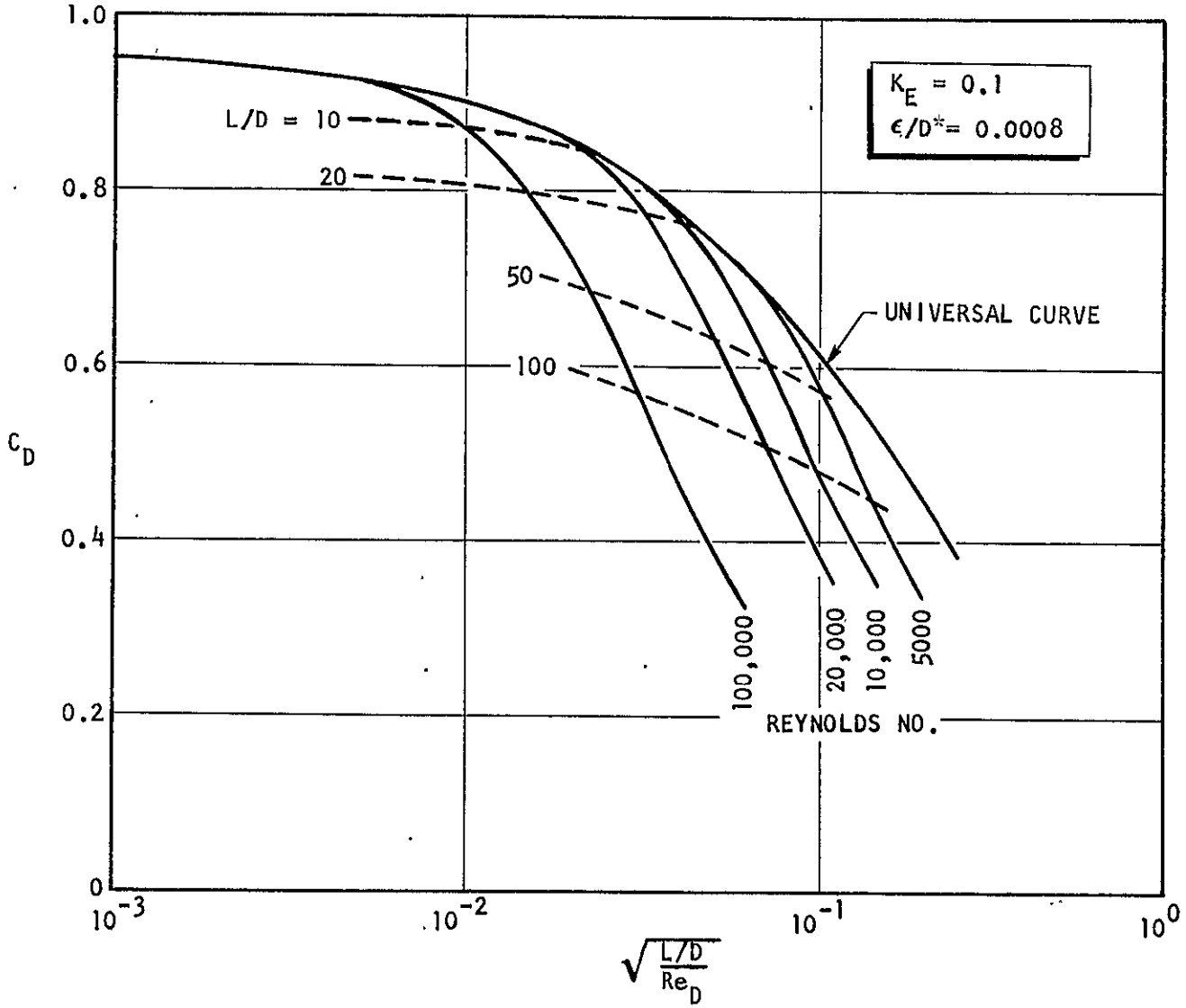

ϵ/D^* - SURFACE ROUGHNESS TO ORIFICE DIAMETER

Figure 4-14. Orifice Coefficient for Round Entrance Orifices

All of the curves in Fig. 4-14 were calculated with Eq. 4-25, the differences being attributable to the interpretation of $\bar{f}$ and the variation of $\bar{f}$ with the several parameters. For the universal curve, values of $\bar{f}$ are obtained from Fig. 4-13 while for the other curves, values of $\bar{f}$ are obtained from standard "friction fact charts."

The best procedure for predicting C_D is to first determine the Reynolds number at which a given orifice is to be operated, then compute Shapiro's universal curve as well as a curve based on simple friction for various L/D's. If the L/D of the orifice places its value of $\sqrt{(L/D)/Re}$ to the right of the intersection of the two curves, then use the simple friction factor value, if the point is to the left, use Shapiro's universal curve value.

4.3.2.2 Extension of the Orifice Model to Orifices With Sharp Entrances--Attached Flow. A qualitative sketch of the flowfield of an orifice with a sharp entrance is shown in Fig. 4-15.

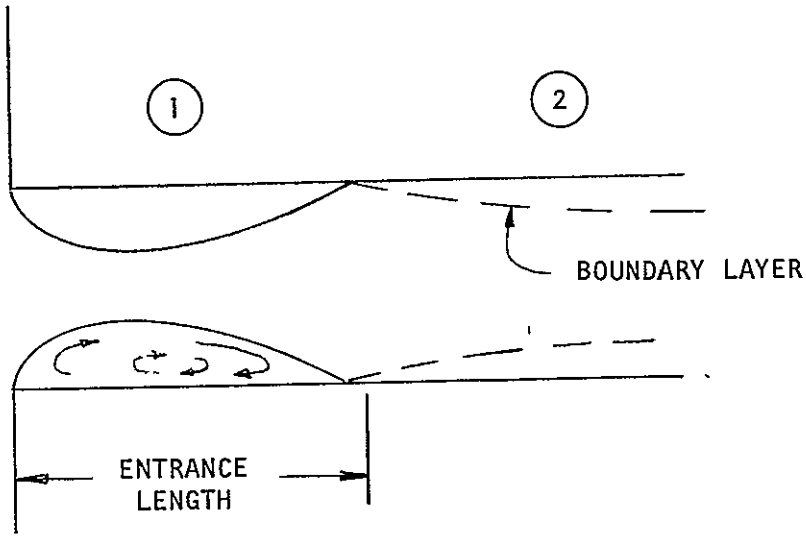

Figure 4-15. Flowfield for an Orifice With a Sharp Entrance

A simple extension of the model developed for rounded entrances was employed to correlate the data for sharp-edged orifices. As shown in Fig. 4-15, the flow-field is broken into two regions: (1) an entrance region in which the flow suffers a standard entrance loss (separated region), and (2) a full-flowing region at the start of which the boundary layer begins to grow. The L/D in the frictional calculations (i.e., region 2) must be reduced by the entrance length (L/D_e).

If it is assumed that a standard entrance loss coefficient of $K_E = 0.5$ is appropriate, the predicted values of orifice coefficient would be given by Eq. 4-27. (The value of K_E is actually a function of Reynolds number for $R_e < \sim 40{,}000$.)

$$C_D = \sqrt{\frac{1}{1.5 + f\,(L/D - L_e/D)}} \qquad (4\text{-}27)$$

This equation is identical to Eq. 4-26 with $K_E = 0.5$. In the equation used to generate the curves in Fig. 4-14, $K_E = 0.1$. The same families of curves given in Fig. 4-14 are given in Fig. 4-16, only with $K_E = 0.5$ and $L/D = L/D - L_e/D$. Recall that for the solid curves, Reynolds number is fixed while L/D is the variable.

This direct extension of Eq. 4-26 to sharp entrance cases is not strictly valid. The development that led to the expressions for the equivalent friction factor were based upon assumption of laminar flow. The boundary layer that develops in region 2 (see Fig. 4-15) for sharp-entranced orifices is undoubtedly turbulent. However, the values computed from Eq. 4-27 will be found to be in quite good agreement with the data.

4.3.3 Cross Velocity Model

The variational trends of orifice coefficient with cross velocity merit further discussion. Experimental results of cross velocity testing were presented in Section 4.2.2.

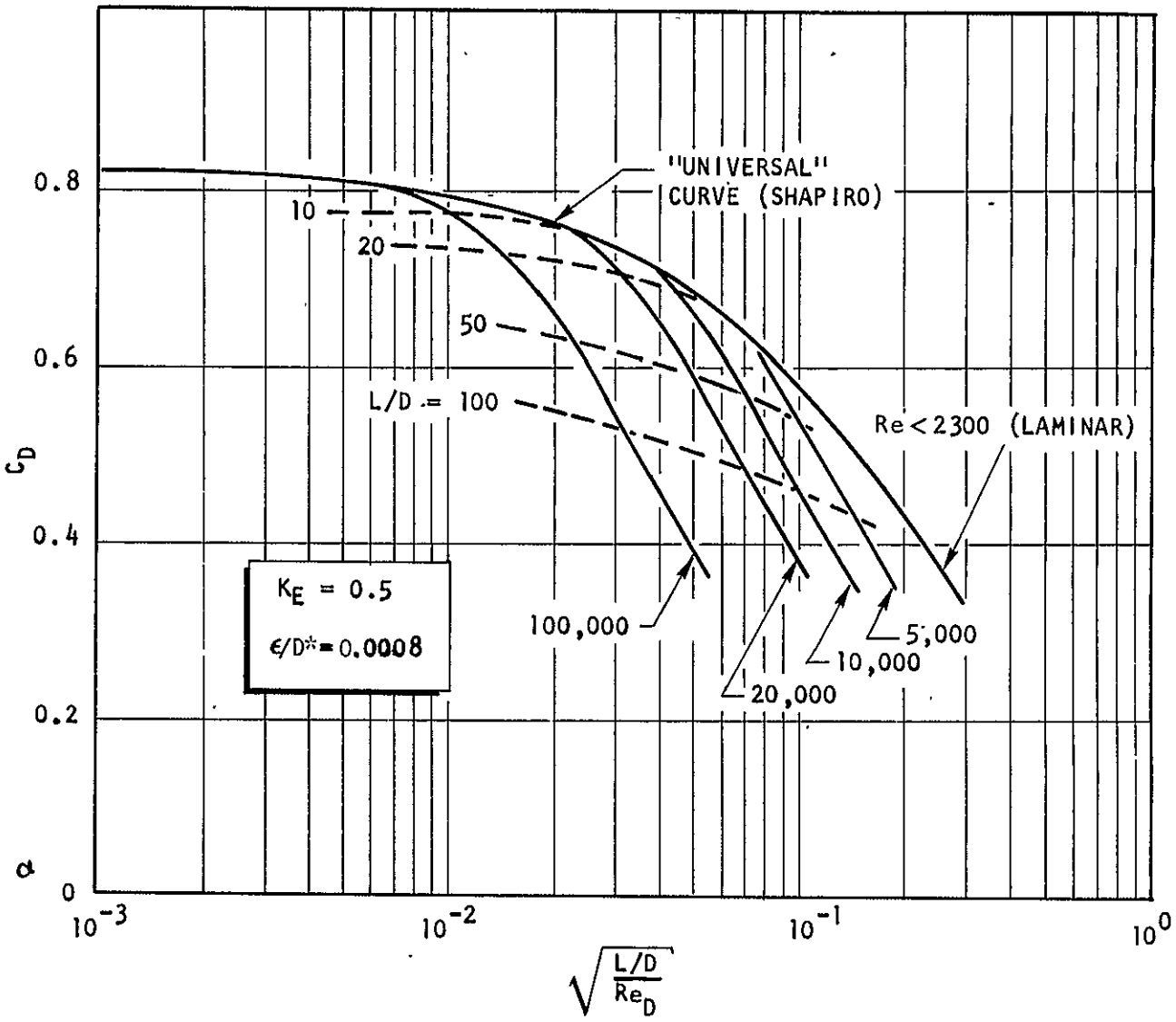

*ϵ/D - SURFACE ROUGHNESS TO ORIFICE DIAMETER

Figure 4-16. Orifice Coefficient for Sharp Entrance Orifices

The most interesting effect of imposition of cross velocity was the reduction of C_D with cross velocity for sharp entrance orifices and the increase of C_D with cross velocity for rounded-entrance orifices (see Fig. 4-6 and 4-7).

Qualitative sketches of the flowfield at the entrances to orifices with sharp and round configurations are shown in Fig. 4-17. Situations with and without cross velocity are depicted. These sketches are not meant to imply potential flow, only qualitative representation of the streamlines in a plane containing both the cross velocity vector and the centerline of the orifice.

With no cross velocity, both the sharp- and round-entrance orifices produce symmetrical flowfields. The flow into the sharp orifice separates at the entrance and reattaches downstream. From hydrodynamic considerations, it can be shown that the separation must occur such that the velocity vector at the corner is tangent to the wall. For orifices that are normal to this wall, the separation velocity vector is also normal to the centerline of the orifice. This radially directed momentum causes the formation of a vena contracta. The subsequent diffusion losses suffered by the flow in reattaching to the wall is the reason sharp entranced orifices yield C_D's that are lower than those for orifices with round entrances. With no cross velocity, all of the fluid available in the reservoir upstream passes through the orifice.

When a cross flow is imposed on the flowfield, some fluid must be bypassed and some must pass through the orifice. This requires that there be a "separation" stream surface generated within the flowfield (see Fig. 4-17). For the sharp entrance, the separation surface meets the wall downstream of the orifice and forms a separation line on the floor of the manifold channel. The flow direction around the perimeter of the orifice must still be everywhere tangent to the wall at the corner. The jet that is formed within the orifice is diverted from the centerline and the flowfield upstream of the orifice is highly distorted.

For the rounded entrance, no separation is necessary, as no "sharp corners" are present about which infinite velocities would be required. As a consequence, the

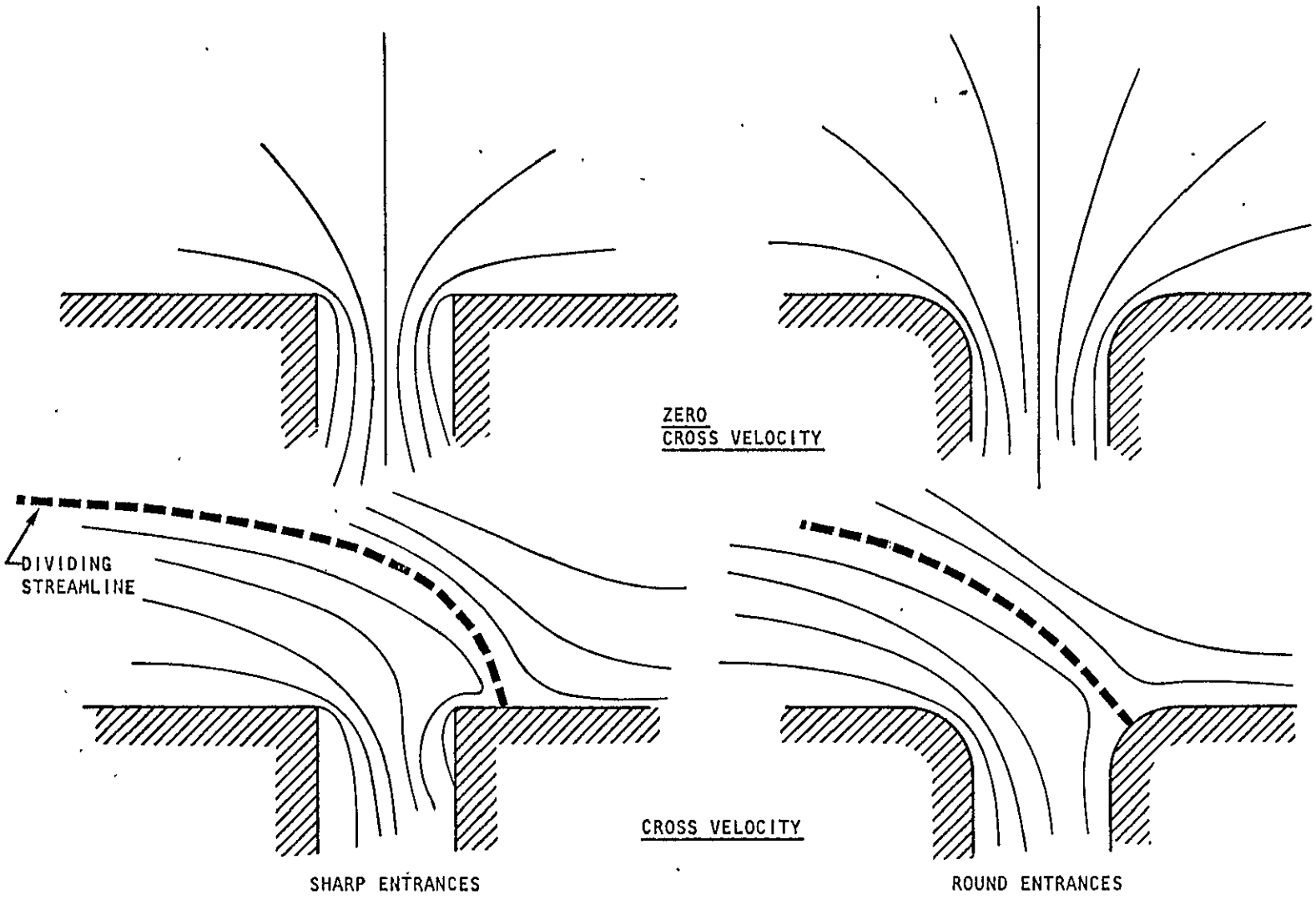

Figure 4-17. Effect of Cross Velocity on the Entrance Flowfield for Sharp and Round Inlets

separation surface could meet the channel wall inside the entrance to the orifice producing a stagnation pressure rise just upstream of the orifice. Thus, the round entrance could see an upstream pressure higher than the static pressure in the cross channel.

A "crude" model can be postulated for the effect of cross velocity on orifice coefficient employing the above qualitative reasoning. Suppose that the "true" value of C_D is really unchanged by the cross velocity, and only the apparent C_D varies with cross velocity because the actual ΔP across the orifice is unknown. The simplest description of the actual pressure drop would entail the assumption that the upstream pressure is equal to the static pressure in the manifold plus the velocity head for the round orifice (i.e., stagnation pressure) and minus the velocity head for the sharp orifice.

This can be expressed in equation form as follows:

$$\frac{C_{DA}}{C_D} = \sqrt{\frac{\Delta P_s \pm 1/2\rho V_c^2}{\Delta P_s}} \tag{4-28}$$

or

$$\frac{C_{DA}}{C_D} = \sqrt{1 \pm \frac{1/2\rho V_c^2}{\Delta P_s}} \tag{4-29}$$

where

C_{DA} = apparent C_D computed directed from test data

C_D = actual C_D at zero cross velocity (a constant)

ΔP_s = measured ΔP computed by subtracting downstream static pressure from upstream static pressure

$1/2\rho V_c^2$ = velocity head in the cross channel upstream of the orifice

The plus sign would be used with rounded entrances and the minus sign with sharp entrances.

Curves generated by Eq. 4-29 are presented in Fig. 4-18, wherein $C_D/C_{D_{V_{c=0}}}$ is shown as a function of the ratio of manifold velocity head to the static pressure drop across the orifice. These curves are extremely interesting because they provide direct design guidelines for the influence of cross velocity. As long as the manifold velocity head is small, compared to the pressure drop across the orifice, the effect of cross velocity will be small.

4.3.4 Correlation of the Data

4.3.4.1 Orifice Coefficient Model. The orifice coefficient data obtained with five of the shapes tested are plotted in Fig. 4-19 as functions of orifice L/D_H. The solid curves on each plot are the predicted functional relationships between C_D and L/D_H with K_E values of 0.5 and 0.7. (Hydraulic flip problems encountered with orifices having $L/D_H < 6$ render their characteristics highly unpredictable.)

In general, the data are fairly well represented by the theory. For the noncircular shapes, a value of 0.7 for K_E appears to correlate the results better than 0.5.

A comparison of the orifice coefficients for all of the orifice shapes tested is presented in Fig. 4-20. This comparison was obtained from the theoretical model. It can be seen that the effect of shape upon C_D is quite small, a fact that was verified by the data.

4.3.4.2 Cross Velocity Model. To correlate the results with this model, all cross velocity data, (C_D) at $L/D = 6$, was normalized by dividing each C_D value by the C_D found at a cross velocity of 10 ft/sec. The parameter $C_D/C_{D_{10}}$ was computed for both round and sharp data. These parameters are plotted versus cross velocity in Fig. 4-21. Since $C_D/C_{D_{10}} \neq 1$ at $V_c = 0$, an appropriate multiplier was applied to Eq. 4-29 to best fit the data. The value of $(C_D/C_{D_{10}})_{V_{c=0}}$ was then multiplied by $\sqrt{1 \pm 1/2\rho V_c^2/\Delta P_s}$ to produce the solid curve on each graph. For such a crude analysis, the curves correlate the data quite well. (For all the points in Fig. 4-21, ΔP_s was approximately equal to 20 psid.) Thus, Eq. 4-29 may be used to estimate the "apparent" discharge coefficient as

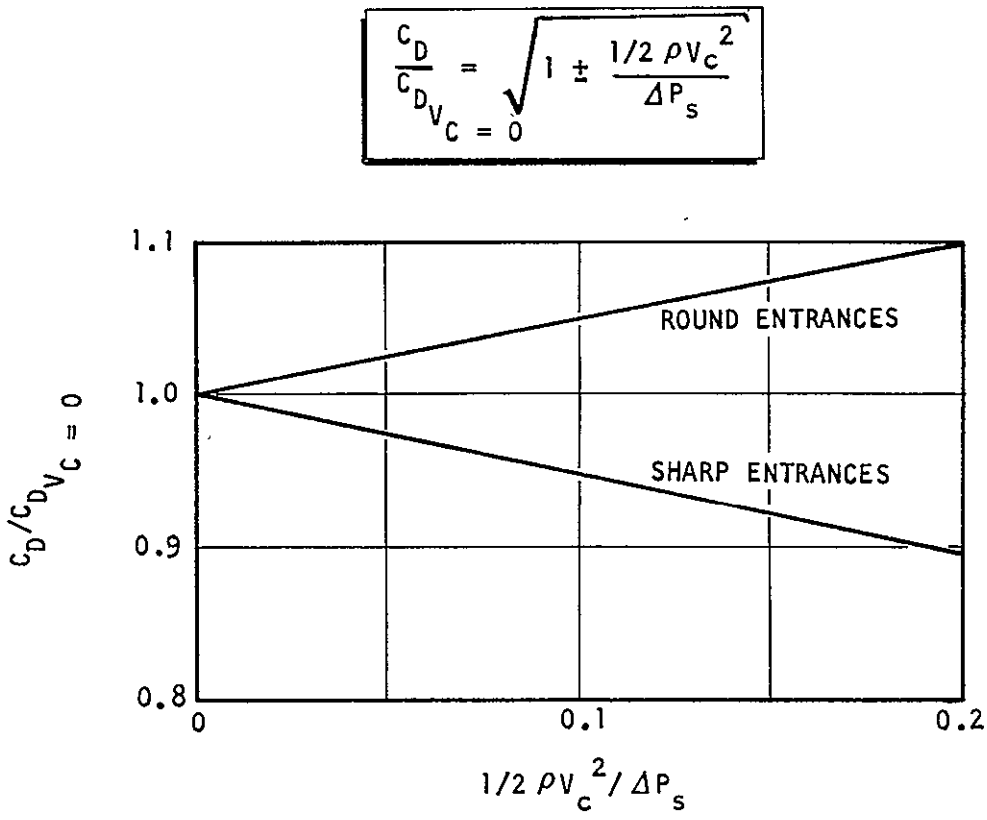

Figure 4-18. Effect of Cross Velocity on Orifice Coefficient (Normalized) for Orifices Normal to Manifold Only (Attached Flow)

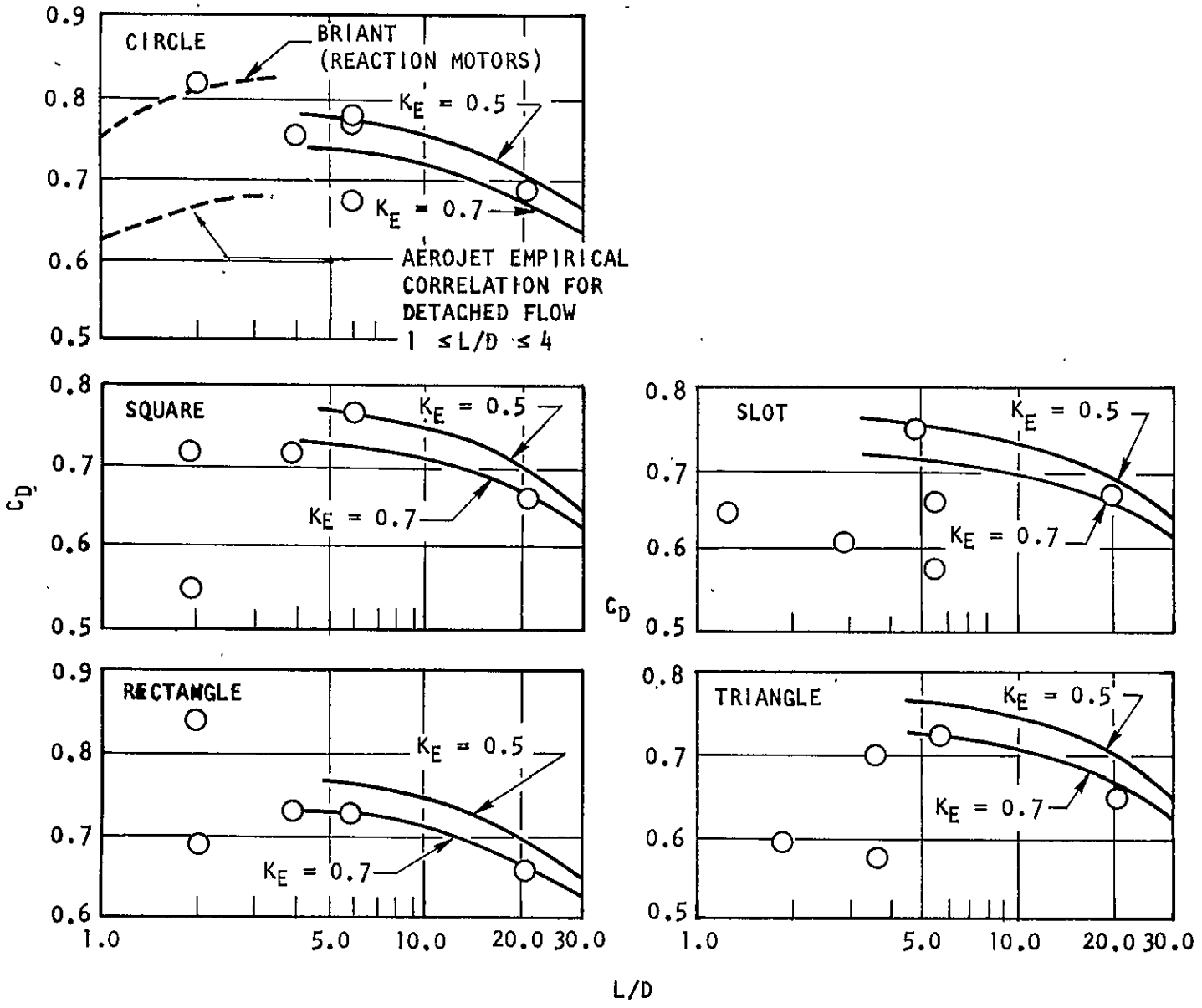

Figure 4-19. Variation of C_D With L/D for Various Orifice Shapes

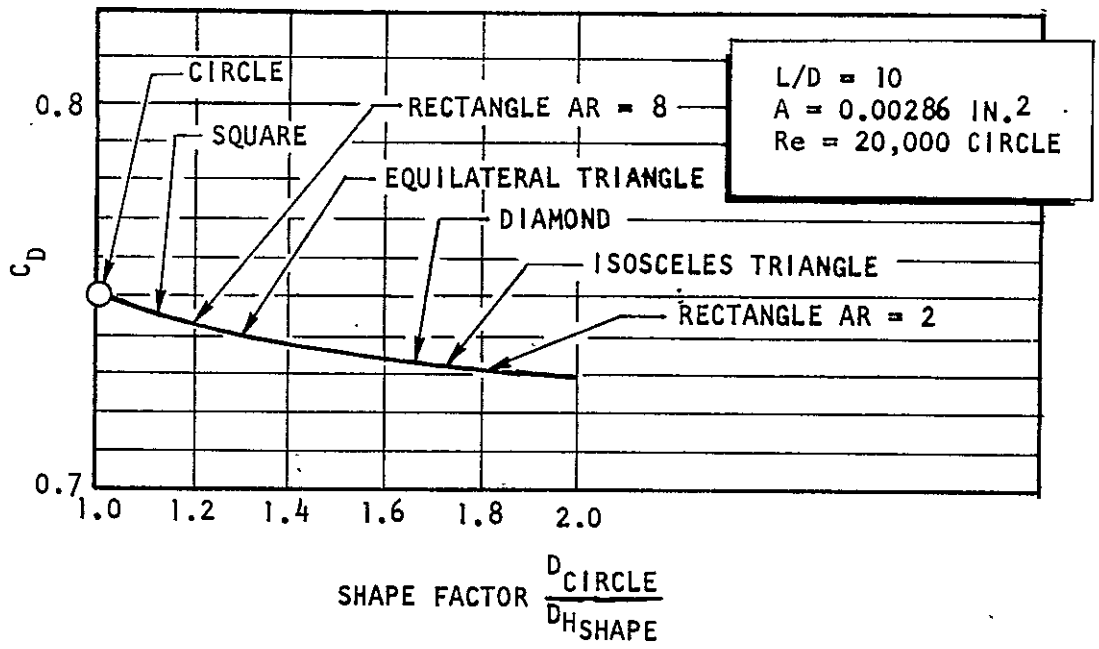

Figure 4-20. Comparison of C_D for Various Shapes

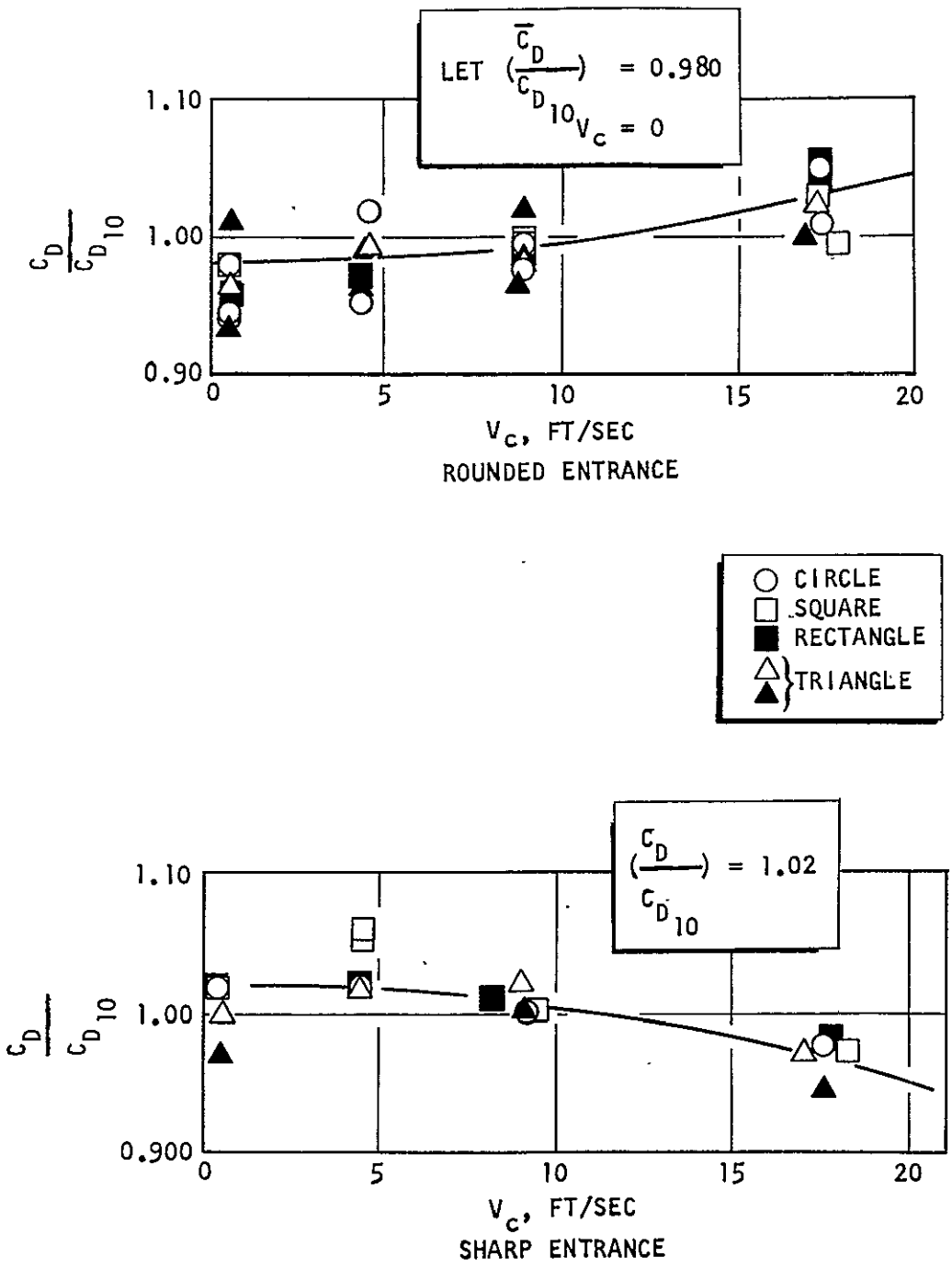

Figure 4-21. Correlation of Cross-Velocity Data

a function of both cross velocity and level of ΔP for sharp and well-rounded entrances. However, it must be emphasized that there are additional effects for orifices that are not perpendicular to the manifold channel as well as entrance conditions that are neither well rounded nor sharp. Equation 4-29 is far from being all encompassing; it does, however, show roughly how the sensitivity to cross velocity would vary with ΔP level. At very high ΔP's, the effects of cross velocity on C_D would be minimal.

5.0 SINGLE-ELEMENT LIQUID/LIQUID STUDIES

5.1 BACKGROUND

The quality of a jet issuing from an orifice affects the mixing and atomization characteristics resulting from impinging jets and is dependent, for example, on such factors as:

1. Orifice entrance conditions
2. Upstream pressure
3. Back pressure
4. Manifold-to-orifice-diameter ratio
5. Reynolds number
6. Manifold cross velocity
7. Orifice length-to-diameter ratio
8. Total injected momentum

To assess the general importance of these variables, element and/or orifice experiments were conducted over various ranges of all of the above-listed variables to determine their influence on mixing and atomization.

For unlike-impinging jets, rounded-inlet orifice geometry is less affected by the remaining parameters (items 2 through 8 above) than sharp-edge designs. From a mixing and dropsize standpoint, long L/D orifices are required to achieve fully developed flow and represent the most ideal element geometry. However, it is unrealistic to expect that state-of-the-art injector design practice can accommodate the orifice requirements necessary to achieve fully developed flow. In fact, most impinging jet injectors have orifice length-to-diameter ratios on the order of 5 to 7 with sharp-edge inlets. Consequently, some degradation in achievable mixing uniformity and spray dropsize can result over that ideally possible. The basis of the overall study was to determine if noncircular-shaped orifices, through greater design flexibility, could offer minimum degradation in the spray qualities

at design conditions that closely approximate those inherent in typical flight injectors. The standard chosen for comparison was an L/D of 10 with sharp-edge inlets. Circular orifice and noncircular orifice elements incorporating sharp inlets and an L/D of 10 are compared over identical ranges in flow conditions. To ensure maximum acceptability of the results, circular and noncircular elements having L/D's of 10 with rounded inlets were also studied. All of the results obtained during the study are not discussed in this Summary Report. For a comparison of the effect of the variables omitted, the reader is referred to the Phase I final report.

Generally, injector design criteria are specified for maximizing c* performance. The injector, however, in addition to providing high combustion performance, should also provide a compatible mixture ratio distribution near the chamber wall (so that neither chemical erosion nor high heat transfer rates will result) and an overall mass flux distribution dictated by combustion stability requirements. This study has concentrated at the single-element level to determine mixing and atomization characteristics as functions of element geometry and orifice hydraulics because these phenomena control combustion efficiency. No emphasis has been placed on the other requirements necessary for a complete injector design.

The mixing experiments were conducted using nonreactive propellant simulants, water, and trichloroethylene. These fluids have almost the exact densities as NTO/50-50 so that the orifice operating ΔP and flowrates should be similar to those of the actual propellants. The mixing uniformity is determined by catching the efflux spray from the element in a rectangular matrix of 841 tubes arranged in a 7- by 7-inch grid. Based on extensive experimental data, the collection distance has been specified at 2-1/2 inches from the injector face. Since the simulants are immiscible, the two liquids in each tube are separated and easily measured. The data are subsequently reduced and contour maps of the flowfield as well as mixing uniformity, percent mass collected, etc., are determined.

Spray dropsizes are determined using the molten wax technique where wax is heated above its melting point, flowed through one of the injector orifices where impingement occurs with a heated water jet issuing from the other orifice. The sprays

are then caught on a long, flat surface where they are washed into a catch basin and collected. Later, the sample is dried and sieved to determine the dropsize mass distribution.

The basic assumption in these approaches is that mixing and atomization are primarily controlled by the dynamics of impingement and the element geometry. This is, of course, valid for unlike impinging jets only when the chemical reactions occur downstream from the liquid-sheet breakup region. For hypergolic propellants this presents a major problem since reactive stream separation can occur. In addition, in most cases the combustion gas velocities can be sufficiently large that secondary breakup will occur. This latter phenomenon is being studied by several investigators; however, a detailed model is not available. Since for a given combustor, sprays from all element types will experience breakup, then comparisons under nonbreakup conditions should be qualitatively correct. For calculation of the vaporization efficiency, however, the actual dropsize characteristics as well as the size must be known. Since the physical properties of the simulant (wax) differ from those of the propellants, a correction must be supplied to obtain actual propellant dropsize.

5.2 PHYSICAL MODELS AND DIMENSIONAL ANALYSIS

Physical models describing the importance of specified parameters on atomization and mixing are presented in this section. Where appropriate, dimensional analysis is used to specify the nondimensional groups controlling these processes. While this approach is extremely powerful, it does not directly provide the form of the equation describing the physical process. However, if all pertinent parameters are specified, dimensional analysis does completely define the similarity variables (i.e., Re, We, M, etc.). Experiment is then required to show the analytical relationship between the various similarity variables. Dimensional analysis combined with experiment, therefore, sufficiently defines the problem so that design criteria can be specified. Although the specific form of the equation cannot be directly obtained by this approach, the selection of dimensionless parameters combined with the experimental studies, can lead to a better understanding of the

physics of the problem. The importance of this will become more evident in the following sections. In some cases, dimensional analysis is not warranted. In these instances, physical argument is used to support the selection of the pertinent parameters. Lastly, for some rather simplified cases, the equations defining the processes have been solved, and mathematical solutions are used as a basis for definition of pertinent parameters. Supporting studies are then used to extend them to more complex, but more realistic conditions.

5.2.1 Self-Atomizing Fan

Physical models for both mixing and atomization are considered. For the atomization model, since both impinging jets and self-atomizing fans produce sheets initially, the discussion of atomization is somewhat general in nature. The initial functional relationships developed are then used as a starting point in the subsequent sections for unlike impinging elements.

5.2.1.1 Mixing. A self-atomizing fan orifice utilizes the orifice inlet geometry to force the jet to dynamically form a sheet. The sheet then progressively changes from a broadening flat sheet to ligaments and finally droplets. The droplets thus formed then follow trajectories that are governed primarily by the initial direction (near the injector face) and the collisions between droplets from adjacent spray fans. Mixing between the oxidizer and fuel is initiated at the point of intersection of the fans. This is illustrated for edge impingement of fans in Fig. 5-1.

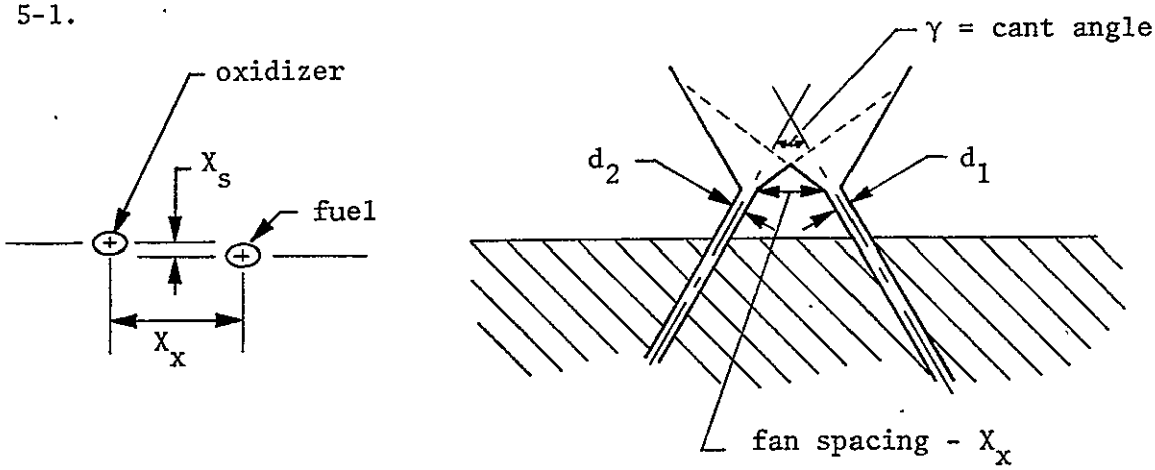

Figure 5-1. Sketch of Spray Mixing Between the Sprays From Two Adjacent Self-Atomizing Fans

"Page missing from available version"

In Ref. 5-1 the equations describing the overall processes have been formulated and a particular solution accomplished. Basically, the formulation assumes that the various processes are related such that:

$$(\bar{D}/d) = \left(\frac{d_L}{d}\right) \times \left(\frac{\bar{D}}{d_L}\right) \tag{5-2}$$

where

$\bar{D}$ = dropsize

d = jet size or characteristic dimension

d_L = ligament diameter

or that the final dropsize $(\bar{D}/d)$ is dependent on the entire process, i.e., the ligament size and its related characteristic dimension initial jet size, times the final dropsize divided by its characteristic dimension, the ligament size.

Dombrowski and John's equation in terms of dimensionless quantities is:

$$\frac{d_L}{d} = 0.96\left(\frac{\rho_L}{\rho_g}\,\frac{K_o^2}{d^4}\,\frac{1}{We^2}\right)^{1/6}\left\{1 + 2.6\left[(\rho_g/\rho_L)^4\,\frac{We^5}{Re^3}\,\frac{K_o}{d^2}\right]^{1/3}\right\}^{1/5} \tag{5-3}$$

$$\frac{\bar{D}}{d_L} = 1.18\left[1 + 3\,(d/d_L)^{1/2}\,\frac{We^{1/2}}{Re}\right]^{1/6} \tag{5-4}$$

where

ρ = density

We = Weber number $(\rho_L V^2 d/\sigma_L)$

Re = Reynolds number $(\rho_L Vd/\mu)$

g = gas

K_o = constant defined by Eq. 5-3

The solution assumes that the sheet thickness at any point is dependent on:

$$hr = K_o \tag{5-5}$$

where

h = sheet thickness

r = radius from the initial point of the sheet

This equation has been shown to be too simple since the sheet thickness also varies across its width for fixed radius (Ref. 5-2). However, the solution shows that:

$$\frac{hr}{d^2} = K \text{ and } K = f(\xi) \tag{5-6}$$

where

ξ = spray angle

Therefore, for a fixed spray angle (ξ), the sheet thickness for any nozzle will be similar and only related to r and d^2.

From Eq. 5-3 and 5-4, dropsize is a function of the following dimensionless grou

$$\bar{D}/d = f(\rho_L/\rho_g, We, Re, K_o/d^2) \tag{5-7}$$

It is important to recall that Eq. 5-2 was formulated on the basis that the flow is laminar and the velocity profile uniform. This is not the usual case encountered in rocket engine injectors. Zajac has extensively studied the influence of velocity profile and turbulence intensity on atomization (Ref. 5-3). Of importance to this study is that for laminar flow an additional parameter (P_c/P_j) that accounts for the velocity profile development was found to affect atomization. This term, P_c/P_j, is the jet centerline dynamic pressure divided by the

mean dynamic pressure. In addition, in comparing Zajac's equations for laminar and turbulent flow, they show that no additional parameter is included; however, the dependency of the various parameters does change. From the above discussion, the parameters included in Eq. 5-6 can be extended to include:

$$\bar{D}/d = f(\rho_L/\rho_g, \text{Re}, \text{We}, P_c/P_j, K_o/d^2) \tag{5-8}$$

for laminar or turbulent flow of only one fluid. This general functional relationship should be valid for the self-atomizing fan.

In summary, the parameters affecting mixing and atomization are given in Table 5-1. It should be noted that these are valid for the general case and for specific studies, some of the variables may not be varied. This, of course, would reduce the number of independent terms. Also note that the parameters given for mixing are not all dimensionless quantities. This is the result of the rather simple heuristic approach used to define the mixing process. If this element type were to be studied more extensively, then a more sophisticated approach would have been taken.

TABLE 5-1. SUMMARY OF PERTINENT PARAMETERS AFFECTING MIXING AND ATOMIZATION FOR SELF-ATOMIZING FANS

Mixing						Atomization					
1	2	3	4	5	6	1	2	3	4	5	6
E_m	X_s	X_x	γ	$\frac{\dot{W}_o V_o}{\dot{W}_f V_f}$	$\frac{\dot{W}_o V_o + \dot{W}_f V_f}{\dot{W}_f V_f}$	$\bar{D}/d$	ρ_L/ρ_g	Re	We	P_c/P_j	K_o/d^2

5.2.2 Unlike Doublets

Physical models are first considered for circular orifice and then noncircular orifice unlike-doublet elements. In both cases, the orifices are assumed to have rounded inlets and sufficient length to dampen entrance effects. The influence of other variables on the jet characteristics such as sharp-edge orifice inlets (cavitation), L/D, and manifold cross velocity are discussed in another section of this report.

5.2.2.1 Mixing. In the most general case, for circular orifices, mixing would intuitively be expected to be affected by the variables listed in Fig. 5-3.

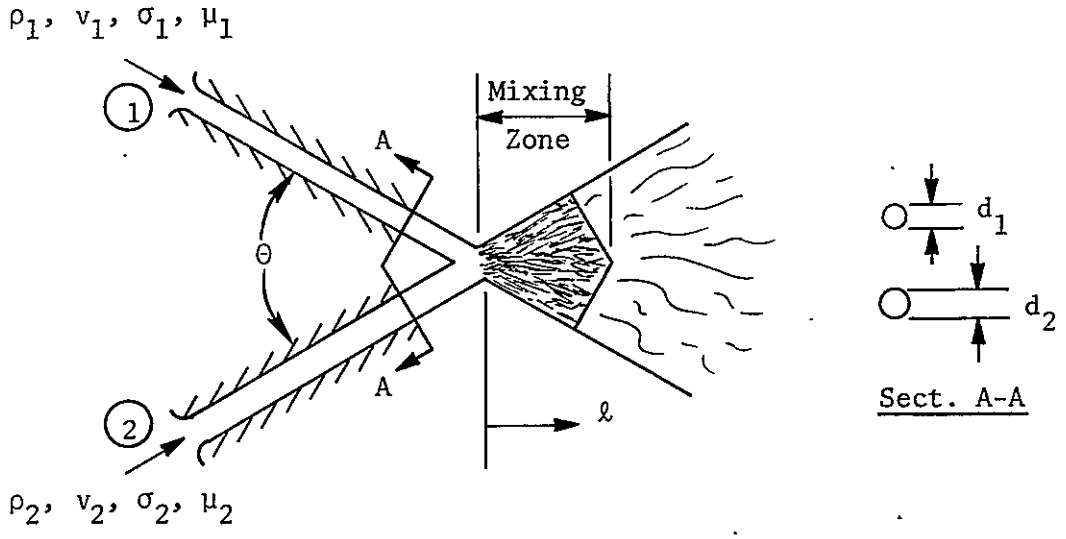

Figure 5-3. Typical Element Arrangement and Variables

If the problem is described by the entire set of variables shown above, then the mass and mixture ratio uniformity should be a function of:

$$E_m = f(\rho_1, \rho_2, V_1, V_2, d_1, d_2, \sigma_1, \sigma_2, \mu_1, \mu_2, \theta, \ell) \qquad (5\text{-}9)$$

Application of the Buckingham Pi theorem shows that a total of 10 independent terms are required to described the physical process specified in Eq. 5-9. However, if we limit ourselves to θ = 60 degrees and assume viscosity and surface tension are second-order functions (affecting mixing), then the number of independent terms is reduced to 5. In addition, experiment has shown that downstream of the mixing zone (see Fig. 5-3) the sprays are directed and, therefore, additional mixing does not take place. Limiting the consideration to ℓ >> the mixing zone length, further reduces the number of variables and, consequently, the number of independent terms to 4. These are:

$$E_m = f(\rho_1/\rho_2, V_1/V_2, d_1/d_2) \qquad (5\text{-}10)$$

The above specified dimensionless terms are somewhat arbitrary and other combinations could have been selected. The terms specified represent "fundamental" groups and more complicated groups must first be justified on the basis that experiment has shown them to have physical significance.

Rupe evaluated the effect of density, velocity, and diameter on the mixing uniformity and found the resultant mixing characteristics strongly dependent upon these variables. In particular, Rupe has shown that a given unlike impinging doublet injector (circular orifice) produces optimum mixing uniformity when:

$$\phi = (\rho_1/\rho_2)(V_1/V_2)^2 (d_1/d_2) = 1.0 \qquad (5\text{-}11)$$

Initially, Rupe's criteria were used in an attempt to understand the variables affecting noncircular orifice elements. However, reformulation for noncircular designs resulted in several possible forms of the criteria, depending upon the specification or grouping of the variables. This comes about since for circular geometry, Eq. 5-11 in terms of dynamic pressure or jet momentum ratio, is a dependent equation, while for noncircular orifice geometries, the equations are independent. Consequently, if the circular orifice mixing criteria were to be extended to other orifice geometries wherein the equations become independent, then the physical significance of ϕ must be known to select the proper form. During this study, experiments were conducted that clearly show that the physical significance of Rupe's criteria is that it is the centerline momentum ratio (Fig. 5-4). This is discussed in Appendix A, and is defined as:

$$M_{C_L} = \frac{\dot{W}_1 V_1}{\dot{W}_2 V_2} = \frac{\rho_1 V_1^2 A_1}{\rho_2 V_2^2 A_2} = \frac{\rho_1 V_1^2 d_1 (dx)}{\rho_2 V_2^2 d_2 (dx)} = \frac{\rho_1 V_1^2 d_1}{\rho_2 V_2^2 d_2} \text{ ; circular orifice} \qquad (5\text{-}12)$$

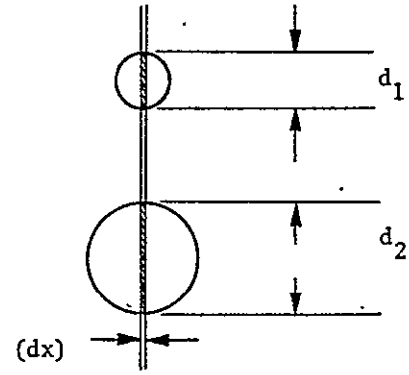

Figure 5-4. Geometric Definition of Centerline Momentum

It should be noted that Rupe's equation states that regardless of diameter ratio, the optimum mixing will always occur when ϕ is equal to 1. This statement is surprising in that intuitively it would be expected that the mass that does not directly impinge would tend to wrap around or pass by the other, thereby introducing a mixture ratio nonuniformity. Since the quantity of mass which does not impinge is related to d_1/d_2, it certainly could affect the required momentum ratio that results in maximum mixing uniformity.

Noncircular elements can be approached in an identical manner as circular orifice elements. Consider first the rectangular geometry shown in Fig. 5-5.

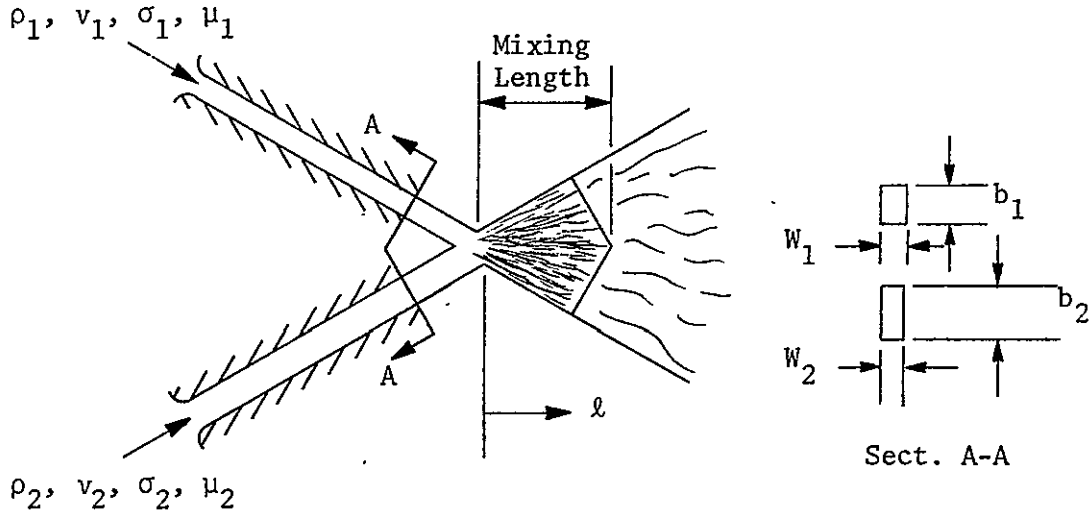

Figure 5-5. Typical Rectangular Orifice Element

In this example, the orifices have unequal widths so that the general case is considered. Application of the Buckingham Pi Theorem now results in six groups (assuming μ, σ second order and $\ell >>$ mixing length). These terms are:

(1)	(2)	(3)	(4)	(5)	(6)	
E_m	ρ_1/ρ_2	V_1/V_2	b_1/b_2	b_1/w_1	b_2/w_2	(5-13)

Other orifice shapes have also been considered, for example, two impinging triangular jets. Typical orifice cross-section geometries are shown in Fig. 5-6.

(a) Triangular (b) Mixed

Figure 5-6. Other Orifice Geometries Considered

For the shapes in Fig. 5-6, dimensionless groups identical to those obtained for the rectangular element are applicable. For noncircular orifices the centerline momentum ratio is:

$$MC_L = \frac{\dot{W}_1 V_1}{\dot{W}_2 V_2} = \frac{\rho_1 V_1^2 A_1}{\rho_2 V_2^2 A_2} = \frac{\rho_1 V_1^2 b_1 \, dx}{\rho_2 V_2^2 b_2 \, dx} = \frac{\rho_1 V_1^2 b_1}{\rho_2 V_2^2 b_2}; \text{ rectangular} \qquad (5\text{-}14)$$

One possible set of dimensionless groups describing mixing for each of the unlike doublet elements is provided in Table 5-2.

5.2.2.2 Atomization. Unlike impinging doublet elements utilizing immiscible fluids represent a major departure from the rather simple model of Dombrowski and Johns described in Section 5.2.1.2. For the unlike doublet, two fluids are involved, each having their own physical properties as well as hydraulic flow conditions. In an attempt to describe this particular problem, Zajac (Appendix E, Ref. 5-3) reformulated Eq. 5-2 for two adjacent sheets of differing fluids. The result for each sheet is:

$$\overline{D}_{1,2} = 1.88 \, D_{L_{1,2}} \left[1 + \frac{3\mu_{1,2}}{(\rho_{L_{1,2}} \, \overline{\sigma} \, D_{L_{1,2}})^{1/2}} \right]^{1/6} \qquad (5\text{-}15)$$

TABLE 5-2. SUMMARY OF π GROUPS FOR VARIOUS UNLIKE-DOUBLET GEOMETRIES (MIXING)

Configuration ↓ Group No. →	1	2	4	5	6	7
Circular 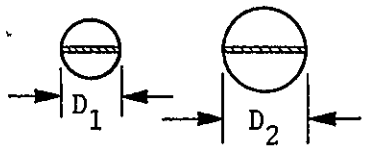	E_m	ρ_1/ρ_2	d_1/d_2	$\rho_1 V_1^2 D_1/\rho_2 V_2^2 D_2$		
Rectangular 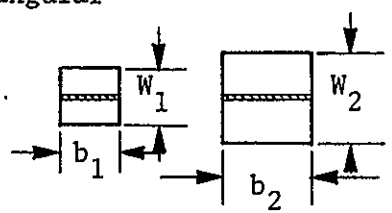	E_m	ρ_1/ρ_2	b_1/b_2	$\rho_1 V_1^2 b_1/\rho_2 V_2^2 b_2$	b_1/w_1	b_2/w_2
Triangular 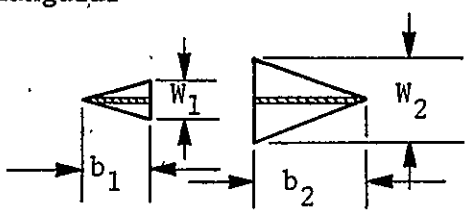	E_m	ρ_1/ρ_2	b_1/b_2	$\rho_1 V_1^2 b_1/\rho_2 V_2^2 b_2$	b_1/w_1	b_2/w_2
Mixed 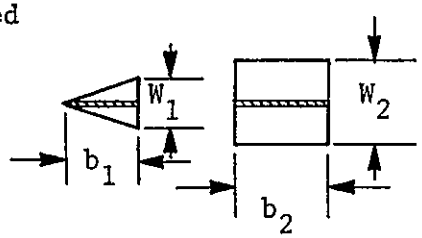	E_m	ρ_1/ρ_2	b_1/b_2	$\rho_1 V_1^2 b_1/\rho_2 V_2^2 b_2$	b_1/w_1	b_2/w_2

and

$$D_{L_1} = 1.81\left[\frac{2\,K_1^{\,2}\,\bar{\sigma}^2}{V_1^{\,4}\,\rho_g\,\rho_{L_1}\,(1 + P_D\,\rho_{L_1}/\rho_{L_2})}\right]^{1/6}\left[1 + 2.6\mu_1\left(\frac{K_1\,\rho_g^{\,4}\,V^8}{72\,V_1\,\bar{\rho}_{L_1}^{\,2}\,\bar{\sigma}^5}\right)^{1/3}\right]^{1/5} \tag{5-16}$$

$$D_{L_2} = 1.81\left[\frac{2\,K_2^{\,2}\,P_D\,\bar{\sigma}^2\,h_2/h_1}{V_2^{\,4}\,\rho_g\,\bar{\rho}_{L_1}\,(\rho_{L_1}/\rho_{L_2} + P_D)}\right]^{1/6}\left[1 + 2.6\mu_2\left(\frac{K_2\,\rho_g^{\,4}\,V^8}{72\,V_2\,\bar{\rho}_{L_2}^{\,2}\,\bar{\sigma}^5}\right)^{1/3}\right]^{1/5} \tag{5-17}$$

where

$\bar{D}$ = dropsize

D_L = ligament diameter

$\bar{\sigma}$ = average surface tension (see Ref. 5-3)

$\bar{\rho}$ = average density (see Ref. 5-3)

μ = viscosity

V = velocity

P_D = dynamic pressure ratio $\left[\rho_1\,V_1^{\,2}/\rho_2\,V_2^{\,2}\right]$

h = sheet thickness

1,2 = fluid 1 or 2

L,g = liquid, gas

These equations can be put into dimensionless groups as was done for the single-sheet model (Eq. 5-1). The resulting parameters are:

$$\bar{D}_1/d_1 = f(\rho_{L_1}/\rho_g,\ Re_1,\ We_1,\ \rho_{L_1}/\rho_{L_2},\ P_D,\ K_o/d_1^{\,2}) \tag{5-18}$$

$$\bar{D}_2/d_2 = f(\rho_{L_2}/\rho_g,\ Re_2,\ We_2,\ \rho_{L_1}/\rho_{L_2},\ P_D,\ d_1/d_2{}^*,\ K_o/d_2^{\,2}) \tag{5-19}$$

*$h_2/h_1 \propto d_2/d_1$

where

$$Re_{1,2} = \rho_{L_{1,2}} V_{1,2}\, d_{1,2}/\mu_{1,2} \text{ and } We_{1,2} = \rho_{L_{1,2}} V_{1,2}^2\, d_{1,2}/\sigma_{1,2} \qquad (5\text{-}20)$$

Note that the equations are functionally dependent on the conditions prevailing in each sheet.

If the above functional relationships are compared to that of the single sheet (Eq. 5-7), it becomes obvious that the complexity of the problem has been markedly increased.

The above relationship in addition to the above restrictions applies only to laminar flow and uniform velocity profile. For unlike doublets, Zajac has also investigated the effect of nonuniform velocity profile and found similar results as described earlier, i.e., a term $(P_c/P_j)_1$, or $(P_c/P_j)_2$, depending on the sheet being considered, accounts for this effect. Little data are available in the turbulent flow regime; however, it is expected that the trends found for single-sheet, like-impinging doublets would also apply. (It was shown that only the dependence of the parameters changed; no new variable was introduced.) Consequently, for turbulent flow and nonuniform velocity profile, Eq. 5-18 and 5-19 become:

$$\overline{D}_1/d_1 = f\left[\rho_{L_1}/\rho_g,\ Re_1, We_1, \rho_{L_1}/\rho_{L_2},\ P_D,\ K_o/d_1^2,\ (P_c/P_j)_1\right] \qquad (5\text{-}21)$$

$$\overline{D}_2/d_2 = f\left[\rho_{L_2}/\rho_g,\ Re_2,\ We_2,\ \rho_{L_1}/\rho_{L_2},\ P_D,\ d_1/d_2,\ K_o/d_2^2,\ (P_c/P_j)_2\right] \qquad (5\text{-}22)$$

These functional relationships are supported by the results obtained in Ref. 5-3.

Since noncircular unlike-impinging elements also produce sheets, then the mechanisms controlling atomization should be similar. In addition, simply from heuristic argument dropsize for noncircular orifices should include two additional geometric variables due to the additional degrees of freedom. The orifice length ratio (b_1/b_2) should be substituted for the orifice diameter ratio (d_1/d_2) and the additional geometric parameters are b_1/w_1 and b_2/w_2.

A complete set of variables for both circular and noncircular orifice unlike-doublet elements is given in Table 5-3.

TABLE 5-3. SUMMARY OF PARAMETERS AFFECTING ATOMIZATION FOR UNLIKE-DOUBLET INJECTORS

Configuration	Orifice	1	2	3	4	5	6	7	8	9	10
Circle 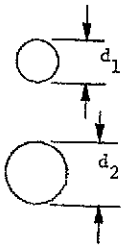	1	$\overline{D}_1/d_1$	$\overline{\rho}_{L_1}/\rho_g$	ρ_{L_1}/ρ_{L_2}	$Re_1 = \frac{\overline{\rho}_{L_1} V_1 d_1}{\mu_1}$	$We_1 = \frac{\overline{\rho}_{L_1} V_1^2 d_1}{\overline{\sigma}}$	$P_D = \frac{\rho_1 V_1^2}{\rho_2 V_2^2}$	K_o/d_1^2	d_1/d_2		
	2	$\overline{D}_2/d_2$	$\overline{\rho}_{L_2}/\rho_g$	ρ_{L_1}/ρ_{L_2}	$Re_2 = \frac{\overline{\rho}_{L_2} V_2 d_2}{\mu_2}$	$We_2 = \frac{\overline{\rho}_{L_2} V_2^2 d_2}{\overline{\sigma}}$	P_D	K_o/d_2^2			
Rectangular 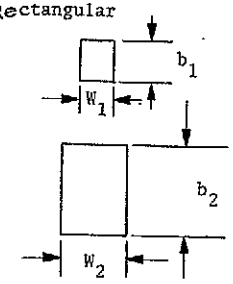	1	$\overline{D}_1/b_1$	$\overline{\rho}_{L_1}/\rho_g$	ρ_{L_1}/ρ_{L_2}	$Re_1 = \frac{\overline{\rho}_{L_1} V_1 b_1}{\mu_1}$	$We_1 = \frac{\overline{\rho}_{L_1} V_1^2 b_1}{\overline{\sigma}}$	P_D	K_o/b_1^2	b_1/b_2	b_1/w_1	b_2/w_2
	2	$\overline{D}_2/b_2$	ρ_{L_2}/ρ_g	ρ_{L_1}/ρ_{L_2}	$Re_2 = \frac{\overline{\rho}_{L_2} V_2 b_2}{\mu_2}$	$We_2 = \frac{\overline{\rho}_{L_2} V_2^2 b_2}{\overline{\sigma}}$	P_D	K_o/b_2^2			
Triangular 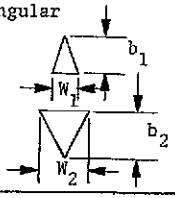	1	$\overline{D}_1/b_1$	ρ_{L_1}/ρ_g	ρ_{L_1}/ρ_{L_2}	Re_1	We_1	P_D	K_o/b_1^2	b_1/b_2	b_1/w_1	b_2/w_2
	2	$\overline{D}_2/b_2$	ρ_{L_2}/ρ_g	ρ_{L_1}/ρ_{L_2}	Re_2	We_2	P_D	K_o/b_2^2			

FOLDOUT FRAME

FOLDOUT FRAME

5.2.3 Unlike Triplets

5.2.3.1 Mixing. An unlike impinging triplet element has two outer jets directed to impinge on a central showerhead jet. A typical triplet element configuration (circular orifices) is shown in Fig. 5-7.

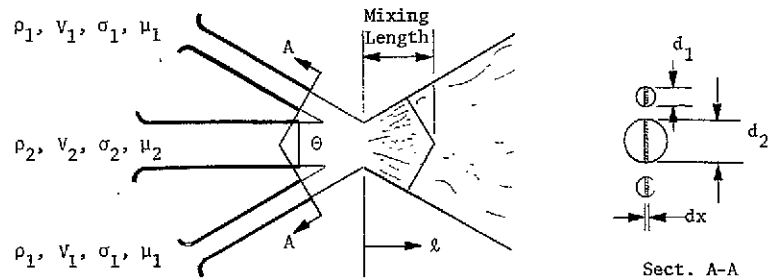

Figure 5-7. Typical Triplet Element Arrangement

It is obvious from the figure that no new parameter is introduced for the triplet configuration that was not specified for the circular unlike-doublet element. The centerline momentum ratio for this element is defined as:

$$\phi = \frac{\rho_1 V_1^2 2 d_1}{\rho_2 V_2^2 d_2} \tag{5-23}$$

It is interesting to compare this result with the empirical equation of Elverum and Morey (Ref. 5-4) describing mixing for a triplet element. Their equation is:

$$K = \frac{\dot{W}_1^2}{\dot{W}_2^2} \frac{\rho_2}{\rho_1} \left(\frac{A_2}{2A_1}\right)^{1.75} \tag{5-24}$$

In the terms of Eq. 5-23, the above equation can be converted to:

$$K = \left[\frac{\rho_1 V_1^2 2d_1}{\rho_2 V_2^2 d_2}\right] \left[\frac{d_2}{d_1}\right]^{0.5} \left[d\right]^{-0.75} \qquad (5\text{-}25)$$

where K = 0.66 for optimum mixing. The form of this equation is very similar to that of Eq. 5-23 except for the exponent on the second term and the constant. Letting K equal 0.66 (the optimum mixing value defined by the authors) and solving the equation in terms of ϕ results in:

$$\phi = 1.11 \, (d_1/d_2)^{1/2} \text{, for optimum mixing} \qquad (5\text{-}26)$$

This result is extremely informative in that it clearly shows that mixing should be a function of diameter ratio as well as ϕ. This suggests that for unequal orifice sizes the outer mass that does not directly impinge on the inner flow mass alters the value of ϕ where the overall spray uniformity is maximized.

A complete set of dimensionless quantities for mixing of triplet elements is given in Table 5-4.

TABLE 5-4. GROUPS FOR CIRCULAR ORIFICE UNLIKE TRIPLETS (MIXING)

Configuration	1	2	4	5
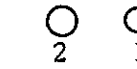	E_m	ρ_1/ρ_2	d_1/d_2	$\rho_1 V_1^2 2d_1/\rho_2 V_2^2 d_2$

5.2.3.2 Atomization. From consideration of symmetry, the two sheet models discussed above should apply to the triplet, which is composed of three sheets (but only two fluids). The resulting dependency of the various parameters on atomization can, however, be quite different. One additional parameter that might be important for the triplet is whether the central jet is greater or smaller than the outer jets. For the present study, only conditions wherein the central jet is larger than the outer jet were considered. See Table 5-3 for a complete list of pertinent variables affecting atomization.

5.3 ELEMENT DESIGN

Two major categories of element types were utilized: (1) spray nozzles and (2) unlike impinging elements. The spray nozzle-type injectors were off-the-shelf items purchased from Spray Systems, Incorporated. Three basic types were used--two designs provided swirling hollow-cone injection patterns (accomplished hydraulically or mechanically), while the third type produced a flat spray fan. Several types of impining unlike-doublet elements using differing orifice geometry were also used: (1) circular orifice element, (2) rectangular orifice element, (3) triangular orifice element, and (4) a rectangular and a triangular orifice element. All of the elements used in the study are described in this section. A more comprehensive description of the elements is contained in the appropriate final report for that phase of effort.

The determination of the appropriate set of element configurations (hardware dimensions and geometric variables) is dependent on the physical models defined in the preceding section. It is obvious from consideration of the large number of variables that affect atomization and mixing that some simplifications had to be made to reduce the scope of the effort consistent with program requirements.

5.3.1 Self-Atomizing Nozzle

Both hollow-cone nozzle and flat spray fan types were considered. For the cone nozzles, two designs provided a swirling hollow-cone injection pattern. One of the swirl designs (hydraulic) consisted of a swirl chamber into which the liquid entered through a tangential port and was then injected from the swirl chamber through a central orifice. The liquid swirls within the swirl chamber around an air core. This results in the fluid being injected into the engine combustion chamber in the form of a hollow conical sheet that is easily disintegrated into droplets. The other swirl type (mechanical) contains a centerbody with machined helical passages that impart a swirling flow pattern before fluid injection through the central orifice. The third design (the spray fan nozzles) contains circular orifices drilled from the back side of the injector face that intersect slots machined into the faces. The intersections form elliptical-shaped holes.

Since the entrance region is cricular, the fluid as it approaches the elliptical slot must contract along the major axis, resulting in the injected liquid producing a narrow fan-shaped sheet.

To minimize the number of variables, the fuel-to-oxidizer fan spacing (X_s) was held constant (X_s = 0 inch). This specification is certainly warranted from a design standpoint since previous studies (Ref. 5-5 and 5-6) have shown that the highest level of mixing occurs when the fans are aligned. This reduces the geometric variables to X_x and γ.

A complete summary of pertinent parameters for all of the nozzles is listed in Table 5-5a and for the element configuration in Table 5-5b. Note that for the selected configurations the fan cant angle (γ) is varied from 0 to 75 degrees. Also, the element interspacing (X_x) is varied from 0.5 to 1.0 inch.

To obtain comprehensive atomization data, single nozzles of differing equivalent diameters were also selected. Note in Table 5-5a that the range in size is from 0.062 to 0.124 inch for the swirl nozzles and from 0.018 to 0.072 inch for the fan nozzles.

5.3.2 Unlike-Doublets Circular Orifices

A limited number of circular unlike-doublet elements were evaluated as a baseline for comparison with the noncircular elements. Two designs were evaluted, one having rounded inlets and the other having sharp-edge entrances. The specific designs are presented in Table 5-6. For these elements the orifice L/D's are about 10 and the impingement angle is 60 degrees.

5.3.3 Unlike-Doublets Noncircular Orifices

Three basic unlike-doublet-type noncircular elements were studied (1) rectangle-on-rectangle, (2) triangle-on-triangle, and (3) rectangle-on-triangle.* The

*These designs are included in Appendix A; no further references will be made to them in this section.

TABLE 5-5. SUMMARY OF SELF-ATOMIZING INJECTOR NOZZLES AND ELEMENT CONFIGURATIONS

(a) Nozzles

Nozzle Type	Manufacturer* Part No.	Equivalent Orifice Diameter, inch**	Spray Angle, degrees
Vee-Jet-VV (Spray Fan)	800050	0.018	80
	8001	0.026	
	8002	0.036	
	8006	0.062	
	8008	0.072	
Hydraulic Swirl	1/8 B-1	0.062	
	1/8 B-2	0.078	
	1/8 B-3	0.094	
	1/8 B-05	0.047	
Mechanical Swirl	1/4 M-26	0.086	

(b) Elements

Element Type	Manufacturer Part No.		Equivalent Orifice Diameter, inch		Spacing Between Elements, inch	Fan Cant Angle, degrees	Fan Inclination Angle, degrees
	Oxidizer	Fuel	Oxidizer	Fuel			
Vee-Jet-VV	8006	8006	0.062	0.062	0.5	0 to 75	0
	8006	8006	0.062	0.062	1.0		
	8008	8006	0.072	0.062	0.5		
Hydraulic Swirl	1/8 B-3	1/8 B-2	0.094	0.078	0.5	10 to 70	0

*Spraying Systems, Inc.

**The equivalent orifice diameter represents an equivalent circular orifice passing the same flow as the actual elliptical orifice assuming separated flow.

TABLE 5-6. SUMMARY OF CIRCULAR ORIFICE UNLIKE-DOUBLET ELEMENTS

Element	Entrances	L/D	d_o, inch	d_f, inch
1	Sharp	10	0.072	0.062
2	Rounded	10	0.0706	0.0628

Legend: o = oxidizer
f = fuel

Rounded Inlet

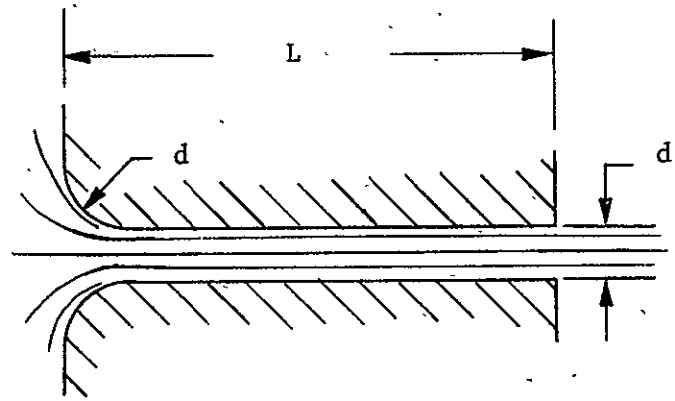

Sharp-Edge Inlet

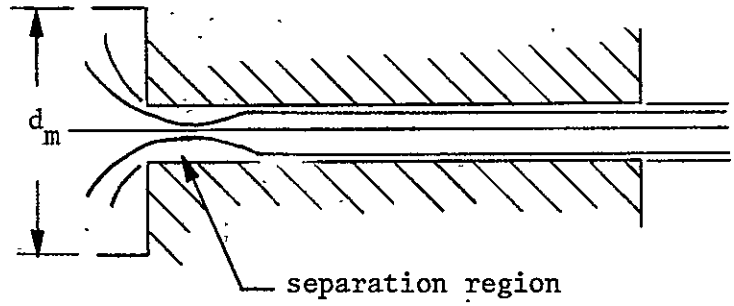

selection of the variables to be investigated was somewhat more difficult for these element configurations than for the previous cases considered. This is primarily the result of increased geometric terms. Investigating all of the above listed parameters for each noncircular element configuration would have been an extensive task so that the number of variables was reduced. For this initial study of noncircular orifices, W_1 and W_2 were set equal ($W_1 = W_2$). This results in eliminating either b_1/W_1 or b_2/W_2 since they are dependent when combined with b_1/b_2. Additionally, the study was conducted using only two fluids, so that ρ_1/ρ_2 was constant.

A complete list of all noncircular orifice unlike-doublet elements is presented in Tables 5-7 and 5-8. Table 5-7 lists the rectangular elements having rounded entrances, while for the rectangular and triangular orifice elements listed in Table 5-8 the entrances are sharp. All elements have orifice L/D's of ≈ 10 and an impingement angle of 60 degrees. The rounded entrance designs were added to the program after some question arose about the validity of data being obtained with separated jets (but not flipped). Also, note that for the sharp-edge entrance elements, only one element was designed for an area ratio of 0.926. This element combined with data obtained earlier, during a Rocketdyne-sponsored program, are presented in the mixing section of this report for completeness. Justification of all of the above described designs is discussed below.

5.3.4 Unlike-Triplet Circular Orifices

During the last several years the triplet element has gained wider use and, consequently, it was desirable to determine more definitive design criteria than that provided by Ref. 5-4. Elements were selected in a practical size range, 0.030 to 0.0575 inch. A complete listing of all configurations chosen for evaluation is presented in Table 5-9.

TABLE 5-7. UNLIKE-DOUBLET ELEMENT GEOMETRY MATRIX, ROUNDED INLETS

$\frac{b_f}{b_o} = \frac{A_f}{A_o}$	Oxidizer Aspect Ratio, $AR_o = b_o/w_o$ ($W_f = W_o = W$)			
	0.278	1.000	3.600	6.00
1.000		1.000	3.600	6.000
		0.0490	0.0258	0.0200
		0.0490	0.0930	0.1200
		0.0490	0.0930	0.1200
0.625	AR_f = 0.174	0.625	2.250	3.750
	W = 0.1175	0.0620	0.0327	0.0253
	b_o = 0.0327	0.0620	0.1177	0.1518
	b_f = 0.0204	0.0388	0.0736	0.0949
0.391		0.391	1.410	2.350
		0.0783	0.0413	0.0320
		0.0783	0.1487	0.1920
		0.0306	0.0581	0.0751

Legend: A = area
AR = aspect ratio (b/w)
o,f = oxidizer and fuel

TABLE 5-8. UNLIKE-DOUBLET ELEMENT GEOMETRY MATRIX, SHARP-EDGE INLETS

(a) Rectangular-Rectangular Orifices

$\frac{b_f}{b_o} = \frac{A_f}{A_o}$	Oxidizer Aspect Ratio, $AR_o = b_o/w_o$			
	1.52	2.72	5.42	8.10
0.737	AR_F = 1.0	2.0	4.0	
	W = 0.0532	0.0376	0.0266	
	b_o = 0.0722	0.1022	0.1444	
	b_f = 0.0532	0.0751	0.1064	
0.926*				7.5
				0.0200
				0.1620
				0.1500

(b) Triangular-Triangular Orifices

$\frac{b_f}{b_o} = \frac{A_f}{A_o}$	Oxidizer Aspect Ratio, $AR_o = b_o/w_o$		
	1.07	1.12	2.66
0.736	AR_F = 0.0845	0.836	1.92
	W = 0.081	0.1064	0.0532
	b_o = 0.0948	0.0722	0.1414
	b_f = 0.0685	0.1064	0.1024

Legend: A = orifice area
AR = aspect ratio (b/w)
o,f = oxidizer and fuel

*This element was designed to complement a set of elements studied under a company-sponsored independent research study (S.A. 60218).

TABLE 5-9. SUMMARY OF CIRCULAR ORIFICE UNLIKE-TRIPLET ELEMENTS (ROUND INLETS)

Element*	d_o, inch	d_f, inch	d_f/d_o
1	0.030	0.030	1.00
2	0.020	0.020	1.00
3	0.043	0.030	0.70
4	0.0575	0.030	0.52

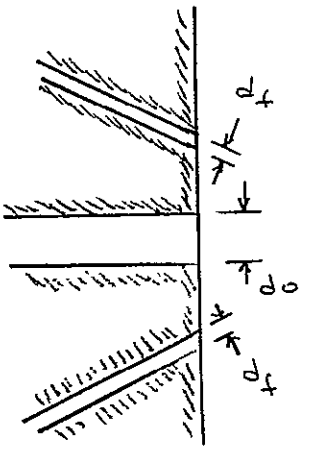

Typical Triplet Elements

*All elements have L/D ≈10 and the impingement angle of the outer jets is 60 degrees.

5.4 MIXING STUDIES

The objective of the mixing experiments was to generate sufficient data so that element design criteria could be established, as well as define optimum mixing levels for all element types. Due to the large number of element types investigated, complete injector design criteria for all elements could not be determined. Initial tests were conducted to establish which element configuration had the greatest potential for achievement of uniform mixing. More extensive study of that element configuration was then accomplished. As is established from the data, the rectangular orifice element resulted in the highest level of E_m and was, therefore, more thoroughly studied. The experimental results and design criteria for all elements studied are presented below. It should be noted that variables such as manifold cross velocity and orifice L/D were also investigated. These results are not presented in this summary; however, the data are contained in the appropriate phase final report. For the results presented herein, several general restrictions can be placed on the data. These are:

- ρ_f/ρ_o = const, μ_f/μ_o = const, σ_f/σ_o = const
- $W_f = W_o$; noncircular shapes

5.4.1 Experimental Results

A summary of the experimental results for most of the element types investigated is presented in a separate report (Ref. 5-7). The results contained in this section have been limited to the data required to establish the "best" element geometry for maximizing mixing using specific orifice geometry (i.e., L/D, entrance, etc.). The data are presented in terms of the mixing uniformity (E_m) which is defined as the sum of the mass-weighted deviations in mixture ratio from the injected mixture ratio. As such it represents an average measure of the uniformity of the spray distribution. It should be pointed out that the overall mixing uniformity of an entire injector is strongly influenced by interelement mixing so that the magnitude of the mixing measured from single elements should not be

expected to quantitatively match that of multielement injector designs. However, an element that produces the most uniform elemental mixing requires less dependence on interelement mixing to achieve the desired overall uniformity.

Lastly, for the tabulated results (Ref. 5-8), two mixture ratios are included: (1) mixture ratio based on cold-flow propellant simulants $(MR)_{CF}$ and (2) mixture ratio based on hot-fire propellants $(MR)_{NTO/50\text{-}50}$. This is done because the density of the simulants does not exactly match those of NTO/50-50 and in predicting the c* mixing efficiency (discussion in a latter section) the collected simulant mixture ratio of the sample must be converted to an equivalent propellant MR. The simulant mixture ratio relates to the dynamics of the impingement or mixing process as well as to the spray uniformity (E_m), so that for the purposes of this section the pertinent variable is $(MR)_{CF}$.

5.4.1.1 Self-Atomizing Nozzles. The mixing levels attained with the hollow-cone nozzle were extremely low ($E_m \approx 45$ percent) and rather insensitive to geometric parameters. These results are presented in detail in the Phase I final report. No further reference will be made to these results.

For the self-atomizing fan element the variables influencing mixing have been limited to:

$$E_m = f(\gamma, X_x, \dot{W}_o V_o/\dot{W}_f V_f, \dot{W}_o V_o + \dot{W}_f V_f) \qquad (5\text{-}27)$$

Momentum ratio was varied by changing mixture ratio and total momentum was varied by changing total flowrate. The cant angle (γ) was varied from 0 to 75 degrees and the fan spacing (X_x) was set at two values (0.5 and 1.0 inch). The total momentum was varied from 0.003 to 0.07 lbf and the momentum ratio was varied from 0.5 to 2.0.

The results showing the effect of γ and X_x on E_m for an o/f orifice diameter ratio of 1 are presented in Fig. 5-8. Note that for spacings (0.5 and 1.0 inch), the mixing tends to maximize between 45- and 60-degree cant angle. This value of

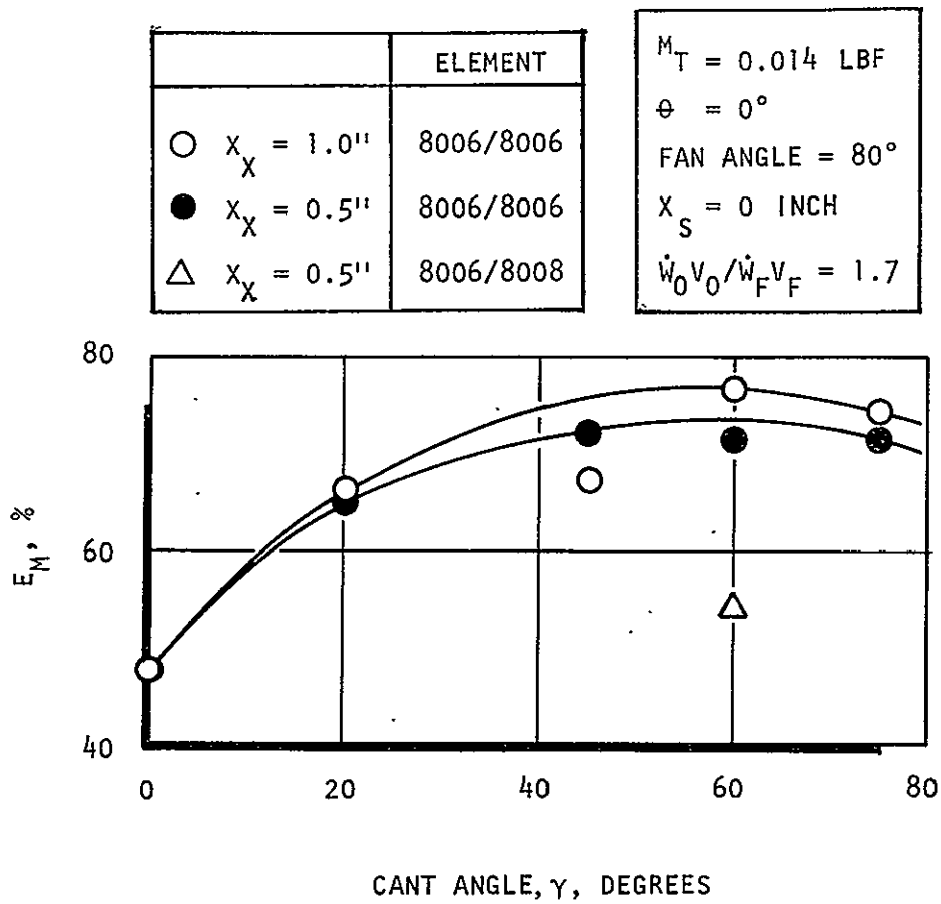

Figure 5-8. Mixing Uniformity as a Function of Inter-Fan Cant Angle for the Spray Fan Elements

cant angle where maximum mixing uniformity is attained is close to that found for like-doublet element pairs (Ref. 5-5). For spacings of 1.0 inch, the mixing levels attained are slightly higher than those attained for 0.5-inch spacings. This result suggests that impingement too close to the initial fan-formation zone inhibits the intermixing process. This could be the result of the fans not having sufficient opportunity to form into ligaments and/or droplets before coming together. Greater interspray mixing should occur if droplets are interacting and colliding rather than the two sheet edges.

In addition to the above results, the mixing uniformity (E_m) obtained for o/f orifice diameters of 0.072/0.062 taken at γ of 60 degrees is also presented. Note that the value of E_m is considerably lower (i.e., 18 percent) than that found for equal orifice sizes. The measured mass distribution data show that the outer portion of the thicker sheet passed through the mixing region without coming into contact with the mass from the thinner sheet (concentrated in the central portion of the spray).

In Fig. 5-9 and 5-10, the influence of both momentum ratio and total momentum on E_m are presented for the unequal orifice size configuration. For fixed orifice geometry and only one set of fluid simulants, momentum ratio is defined as:

$$\text{momentum ratio} = K_1 (MR)^2 \tag{5-28}$$

where $K_1 = \rho_f A_f / \rho_o A_o = 0.51$

so that momentum ratio is uniquely related to mixture ratio. For these experiments the total momentum was essentially constant. The data presented in Fig. 5-9 show that mixing uniformity maximizes at a momentum ratio of about 1.0. The uniqueness of this value, however, must await more data where differing orifice geometry was used.

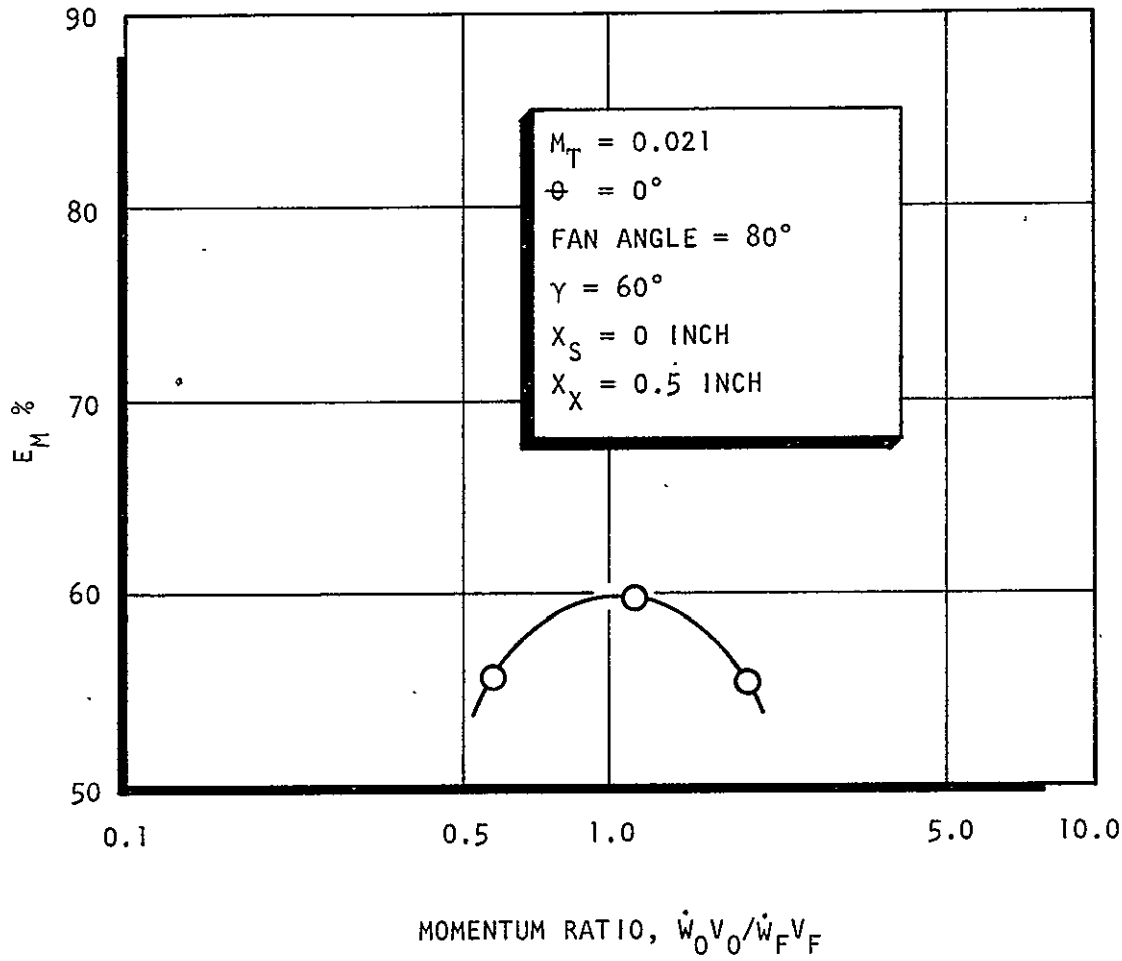

Figure 5-9. Mixing Uniformity as a Function of Momentum Ratio for Spray Fan Elements

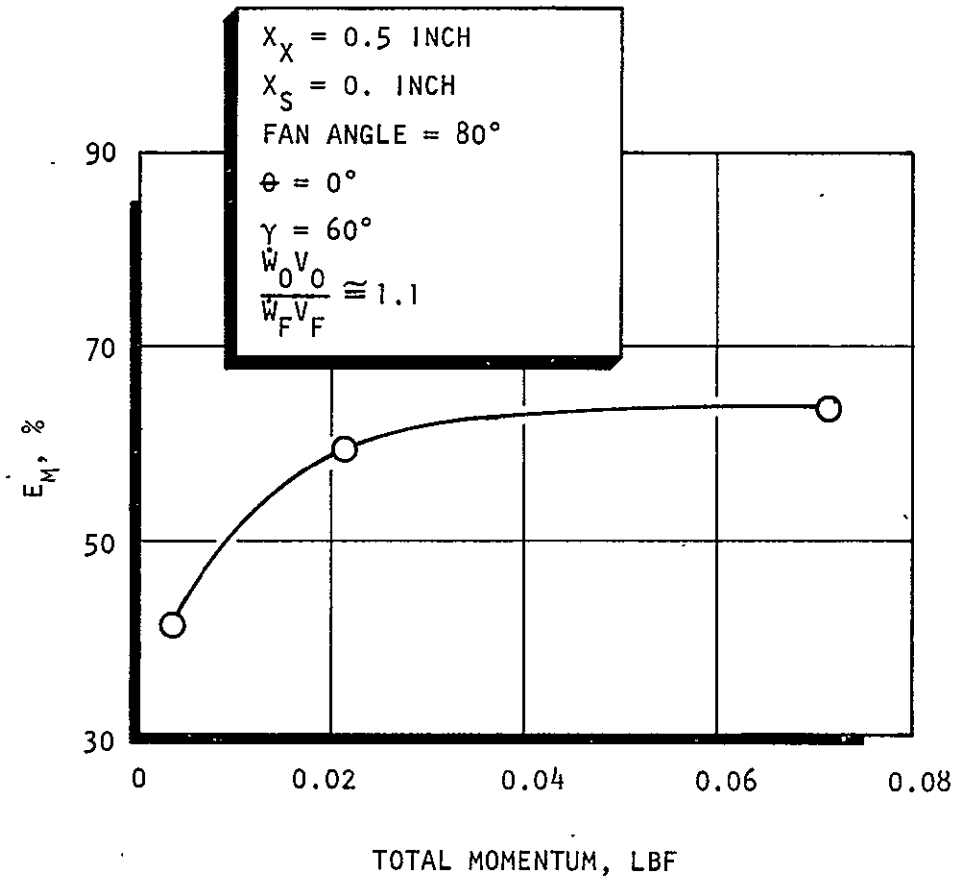

Figure 5-10. Mixing Uniformity as a Function of Total Momentum for Spray Fan Elements

For fixed-orifice conditions and constant mixture ratio, the total momentum is:

$$\text{total momentum} = K_2 W_T^2 \tag{5-29}$$

where

$$K_2 = \frac{1}{\rho_o A_o \left(1 + \frac{1}{MR}\right)^2} = \frac{1}{\rho_f A_f (1 + MR)^2}$$

Consequently, for fixed miture ratio and orifice geometry the total momentum is uniquely related to total flowrate. The effect of total momentum on E_m is illustrated in Fig. 5-10. The sensitivity of mixing to total momentum was rather surprising; however, the results suggest that increasing the total momentum above about 0.04 lbf (for constant relative o/f momentum ratio) does little to further improve mixing.

5.4.1.2 Circular-Orifice Elements. The results for elements comprised of circular elements are presented in this section.

5.4.1.2.1 Circular Unlike-Doublet Element. The circular orifice unlike-doublet element was chosen as the baseline for comparison with noncircular orifice unlike-doublet types. Consequently, only one design was chosen for evaluation--a sharp-edge inlet orifice with an L/D of 10. This element configuration, under the single-orifice study, was shown to provide full flowing orifices. After publication of the Phase I final report, question arose as to the validity of the data obtained with orifices having inlet separation where fluid cavititation could have occurred. To ensure that the conclusions given in the Phase I report were valid, additional experiments were run using an element having rounded-entrance inlets where cavitation could not occur.

For only one element configuration and using one set of fluids from Table 5-2, the mixing should only be a function of:

$$E_m = f(\phi) \tag{5-30}$$

The basis for the development of the dimensionless groups was that the jets were turbulent and insensitive to inlet conditions. For a specific geometry this was indeed the case; however, when the geometry was changed, then it would be expected that the mixing levels might also change. For the two element designs investigated in this study, the following parameters were changed:

- Entrance condition
- Manifold-to-orifice-diameter ratio

The mixing data obtained using the rounded-inlet element over a range of ϕ are presented in Fig. 5-11. These results show a rather flat region in E_m around the ϕ of 1.0 operating conditions. In addition, the scatter of the data is larger than can be explained by experimental measurement limitations. No explanation for these results was evident at the time these data were obtained. Subsequently, however, Zajac under a JPL-sponsored study (Ref. 5-3) showed that for well-contoured inlets the transition from laminar to turbulent flow was extended beyond the range of Reynolds number typically given of 2300 to about 10,000. Since the design flowrate for the subject injector element was in this transition zone it was suspected that this phenomenon could account for the data scatter. During a related program (Ref. 5-9), an injector element having almost the exact orifice dimensions was being studied. As part of that study, mixing experiments were conducted over a wide range in flowrate. In addition, turbulence intensity measurements of the effluent jets were also obtained. For completeness of the discussion, the results of this study are presented in Fig. 5-12. Note that the jets are experiencing transition from laminar flow to turbulent flow in the range of the measurements where E_m varies considerably. Once both jets are reasonably fully turbulent, the value of E_m also is more stable. The Reynolds number for the data presented in Fig. 5-11 ranged from about 12,000 to 25,000. It appears from these results that the measured data scatter and the resulting unusual mixing characteristics were due to the jets undergoing transition flow. The results illustrated in Fig. 5-12 show that the maximum mixing level attained is about 83-percent E_m, depending on the actual flow Reynolds number. The level in mixing uniformity is dependent on the value of ϕ for which the data were taken. In subsequent discussions it is shown that this level can be increased if the value of ϕ is changed.

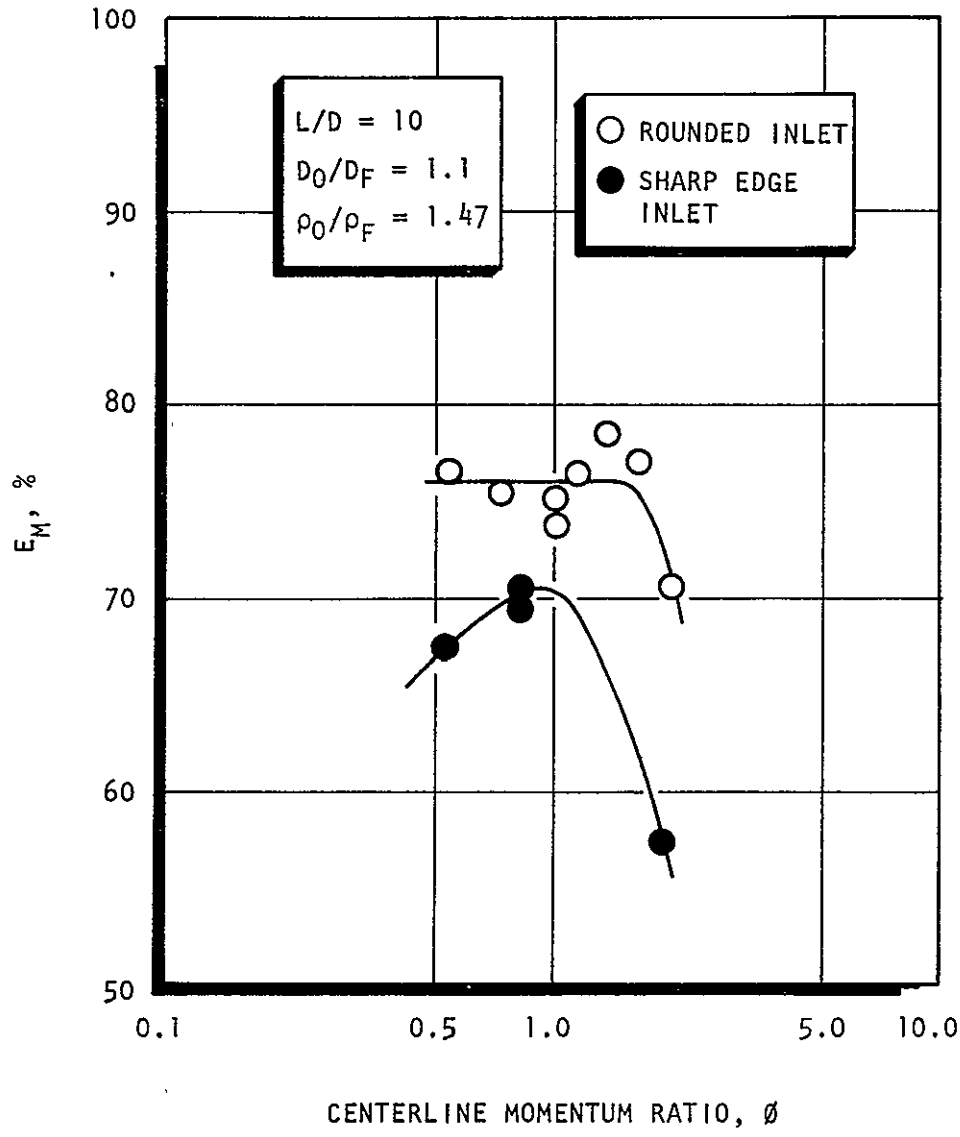

Figure 5-11. Mixing Uniformity as a Function of Centerline Momentum Ratio for Circular Unlike Doublets With Sharp and Rounded Entrances

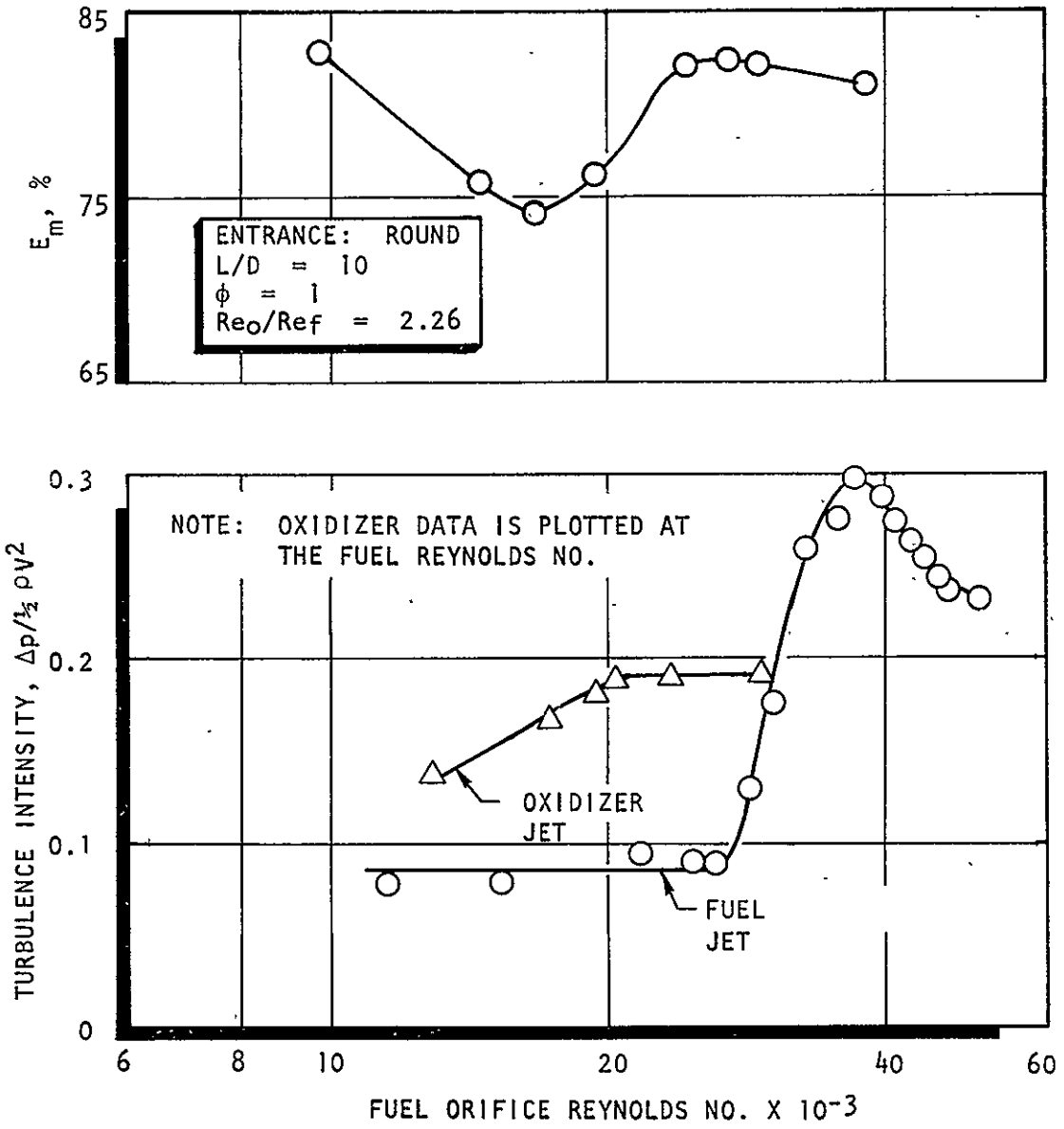

Figure 5-12. Mixing Uniformity and Jet Turbulence Intensity for a Circular Unlike Doublet (Rounded Inlets) as a Function of Fuel Orifice Reynolds No. (Re_o/Re_f = 2.26)

The sharp inlet (L/D of 10) results are also presented in Fig. 5-11. These show that E_m maximizes at a value of ϕ equal to 1.0 and that the maximum value of E_m is about 71 percent. It was surprising to find for unequal orifice sizes that the mixing uniformity maximized at a value of ϕ equal to 1. This could be a universal value for unlike-doublet elements; however, only four data points were obtained at three values of ϕ so that the maximum has not been experimentally determined. (The maximum has arbitrarily been drawn through the ϕ of one point.)

The maximum value of E_m is a function of the injected flowrate (or momentum), as illustrated in Fig. 5-13. Note that these characteristics are presented in terms of the fuel orifice Reynolds number for easy comparison with the rounded-inlet results (Fig. 5-12). The characteristics are considerably different from those observed for the circular element. However, unusual trends were not expected, since, for the sharp-edge inlet, turbulent flow should occur over the entire flowrate range. Note that increasing the flowrate resulted in a steady decrease in mixing uniformity.

Lastly, using the same injector element, but reducing the manifold entry diameter by one-half, one test was conducted to determine the sensitivity of the jets to upstream manifold geometry. This resulted in a loss in E_m of about 3 percent when the entry diameter was reduced.

5.4.1.2.2 Circular Unlike-Triplet (Round Inlet Elements). The triplet element was investigated during Phase IV. This element was incorporated into the program primarily to determine if the potential for increased mixing uniformity could be realized. Based on the designs presented in Table 5-9 and the parameters varied during the experimental program, mixing should be a function of:

$$E_m = f(\phi, d_f/d_o, \dot{W}_T) \tag{5-31}$$

The mixing results from the two elements having a diameter ratio equal to 1.0, but differing orifice sizes are presented in Fig. 5-14a. The data are presented in terms of E_m versus ϕ (centerline momentum ratio). Note that about a 1-percent

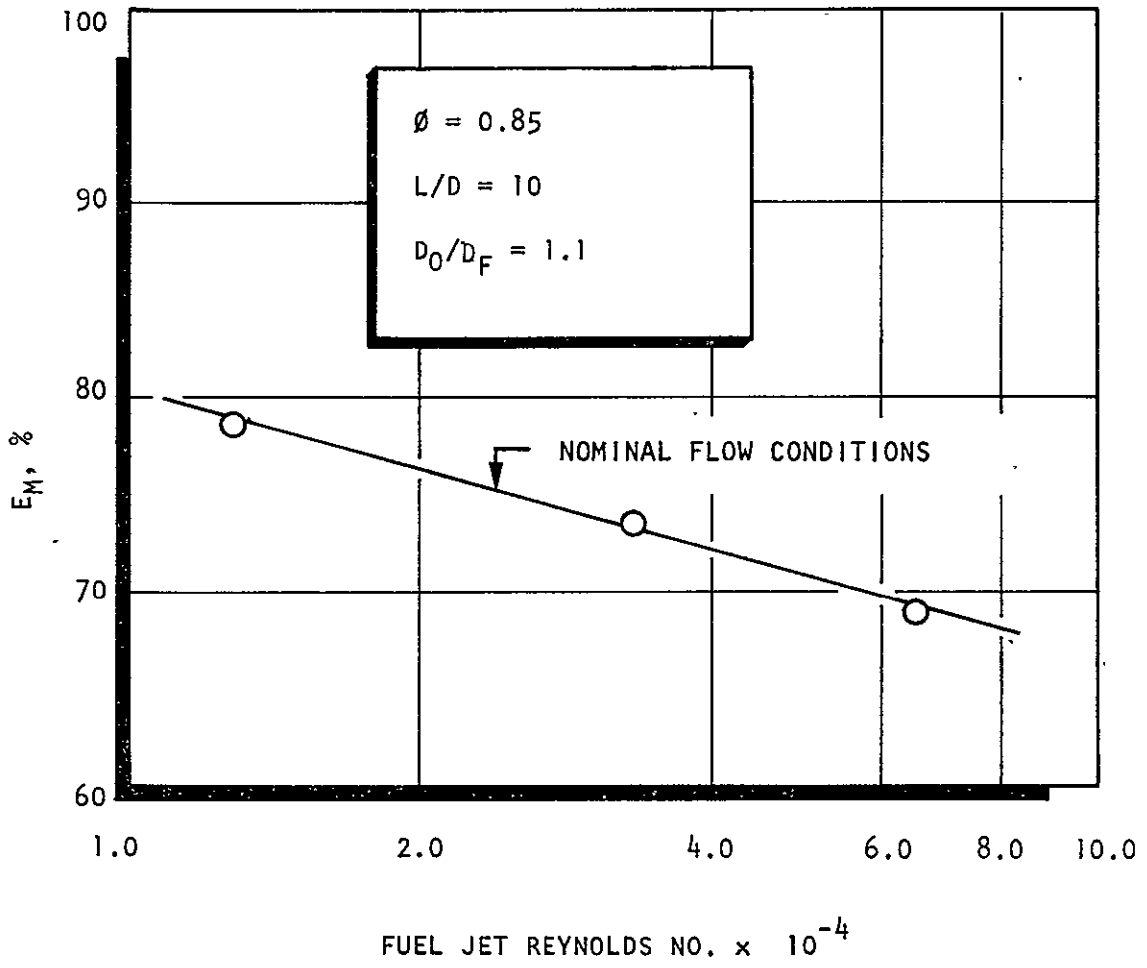

Figure 5-13. Mixing Uniformity as a Function of Fuel Jet Reynolds Number for a Circular Unlike Doublet (Sharp Entrance)

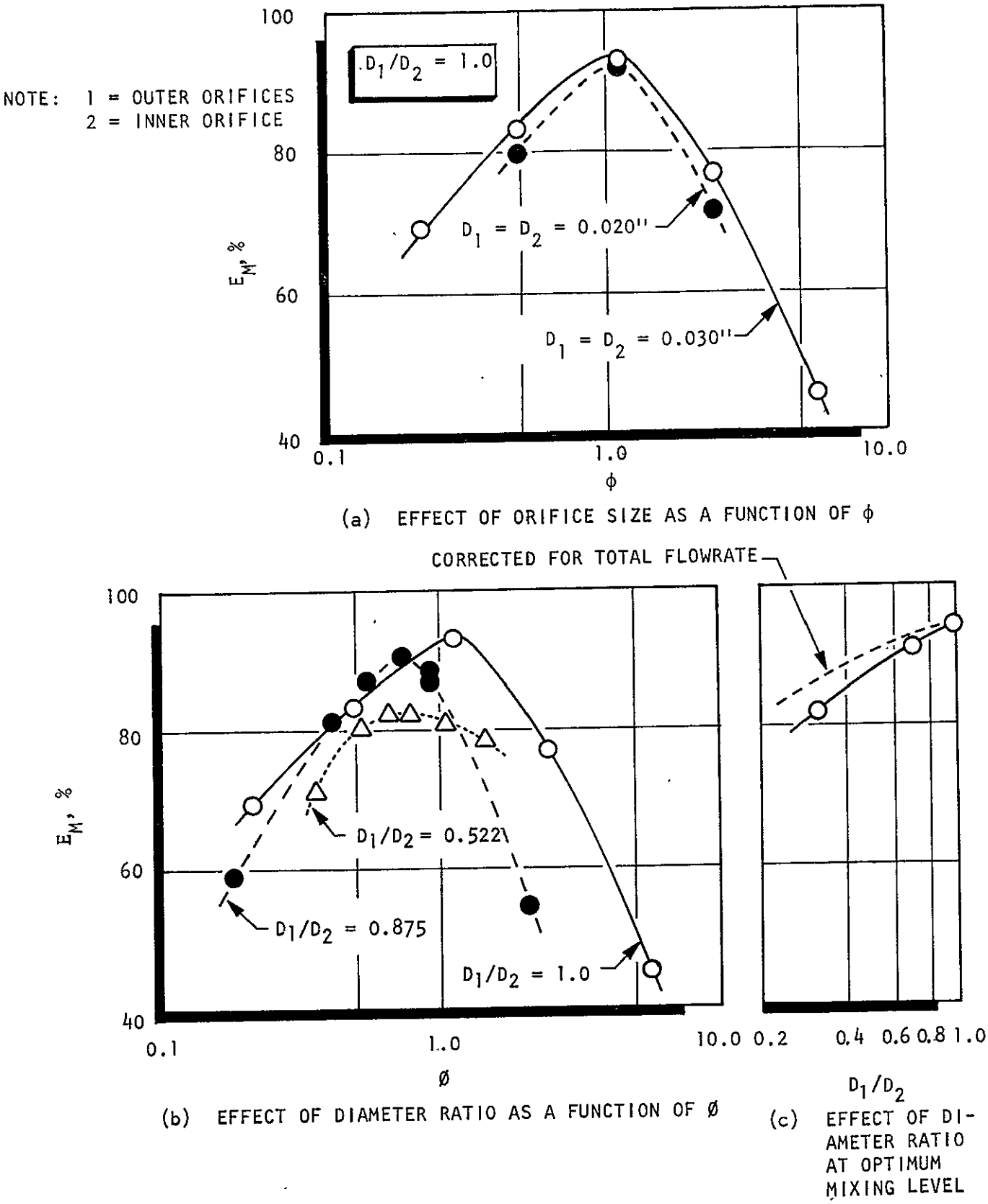

Figure 5-14. Effect of Oxidizer Diameter and Diameter Ratio Upon Unlike Triplet Mixing, Presented as a Function of Ø

difference in mixing uniformity occurred, with the larger element producing the higher values of E_m. In addition, for both elements, the mixing uniformity maximized at a value of ϕ equal to 1.0. This was expected since the diameter ratio is 1.0 for both elements. The overall mixing levels obtained with these elements (L/D = 10, round inlets) are high--the maximum level being 93 percent.

The effect of diameter ratio on the mixing uniformity is presented in Fig. 5-14b and 5-14c. These results show that the optimum value of E_m occurred at a value of ϕ other than 1 when the diameter ratios (d_f/d_o) were less than 1.0. Study of the mass contour plots suggests that the inner jet, being larger than the outer jets, is wrapping around the outer jets producing oxidizer-rich zones on the periphery of the spray. Therefore, it is reasonable to expect that the momentum ratio producing optimum overall spray mixing would be different from 1.0 to compensate for the mass that does not undergo direct impingement.

Unequal diameter ratios, in addition to causing a shift in the momentum ratio producing optimum mixing uniformity, also result in a lowered maximum value in E_m. The values of ϕ producing $(E_m)_{max}$ are cross plotted in Fig. 5-14c to illustrate the effect of diameter ratio on element mixing. The maximum value of E_m was obtained at a diameter ratio of 1, which is different from that found for unlike-doublet elements. (Unlike-doublet elements produce relatively low values in E_m for a diameter ratio of 1.) The dashed line shown in this plot is an attempt to correct the data for total flowrate effects on mixing. The total flowrate was varied and trends in E_m similar to those found for the unlike doublet occurred. The results are plotted in Fig. 5-15. Note that E_m decreases with increased flowrate. The ΔE_m, shown by the dashed line in Fig. 5-14, was obtained from these results, assuming a constant flowrate of 0.078 lbm/sec.

5.4.1.3 Noncircular-Orifice Elements. For the noncircular-orifice elements, specific "optimum" design criteria were sought as well as a valid comparison of the results with circular-orifice geometry. Consequently, a large number of rectangular elements were studied. Referring to the dimensionless groups listed in

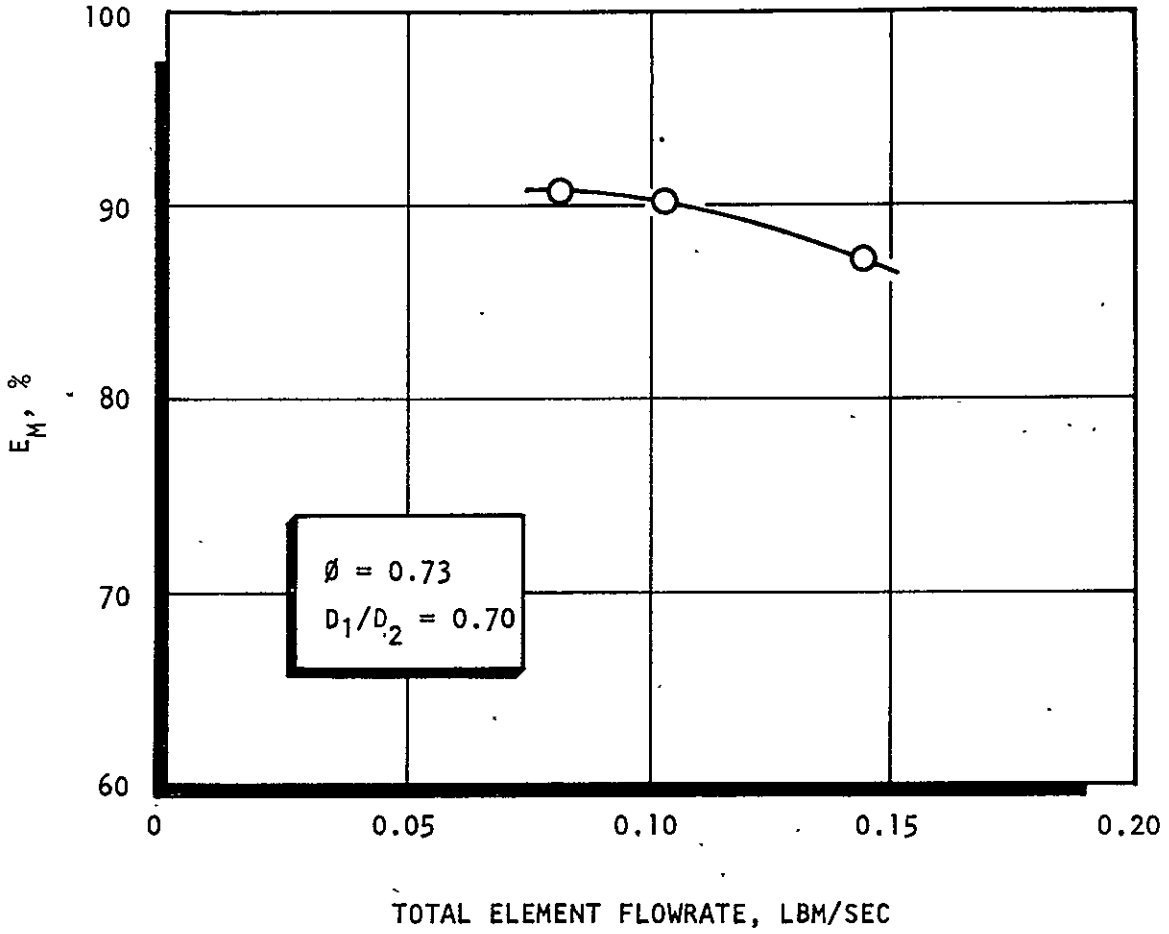

Figure 5-15. Effect of Total Flowrate Level Upon Unlike Triplet Mixing

Table 5-2 for the noncircular orifice, some simplifications can immediately be made based on the use of only one set of fluid simulants (i.e., ρ_1/ρ_2 = const). In addition, for each of the rectangular and triangular orifice configurations, the oxidizer and fuel orifice widths were identical and, consequently, one of the geometric groups must be eliminated. Based on the configurations listed in Table 5-2 (rectangular and triangular elements), the parameters affecting mixing are:

$$E_m = f(b_1/b_2, \phi, b_1/W_1) \tag{5-32}$$

5.4.1.3.1 Rectangular Elements (Rounded Entrances). A complete summary of the test conditions and measurements is presented in Ref. 5-8. The results of these tests are presented in Fig. 5-16 through 5-18. It is obvious from these plots that the mixing uniformity varies as a function of b_f/b_o, AR_o, and ϕ. For these particular designs, the highest level of mixing was not always attained at a value of ϕ equal to 1.0. It is believed that the slight shifts in the value of ϕ where the maximum values of E_m occur, is due to slight variations in geometry (e.g., $W_1/W_2 \neq 1$) or irregularities along the orifice length. It should be noted, however, that the optimum is never far from a value of ϕ equal to 1.0. The maximum value of E_m was about 88 percent. This value was obtained at one aspect ratio for each series of elements having constant b_f/b_o. The impact of this result on injector design criteria is discussed in a latter section of this report.

5.4.1.3.2 Rectangular Elements (Sharp-Edge Inlets). Three elements were designed with b_f/b_o of 0.737 and the fourth element had a b_f/b_o of 0.926. The experimental mixing results for all of the injector elements are presented in Fig. 5-19 and 5-20. For completeness, two additional element configurations evaluated under a Company-sponsored program (Ref. 5-10) are also included in Fig. 5-20. Again, the mixing uniformity tends to maximize at a value of ϕ equal to 1.0 The maximum mixing uniformity (E_m) attained with these configurations was about 85 percent. This range is somewhat less than that obtained with the rounded-inlet designs (88 percent). Here again the results suggest that flow development affects the quality of mixing produced by impinging jets.

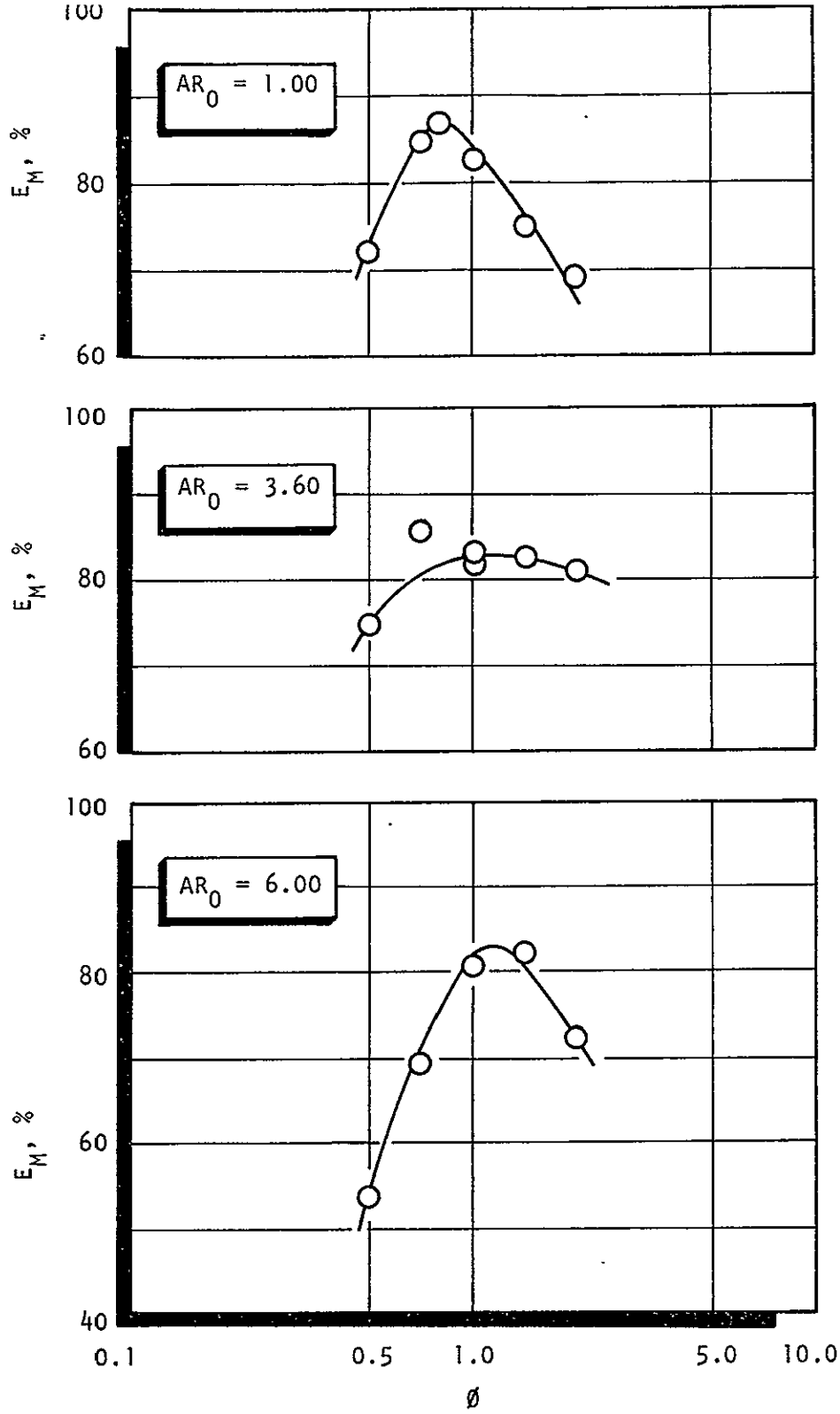

Figure 5-16. Rectangular Unlike-Doublet Mixing, E_m, as a Function of Ø and AR_o for b_f/b_o = 0.391 (Rounded Entrances)

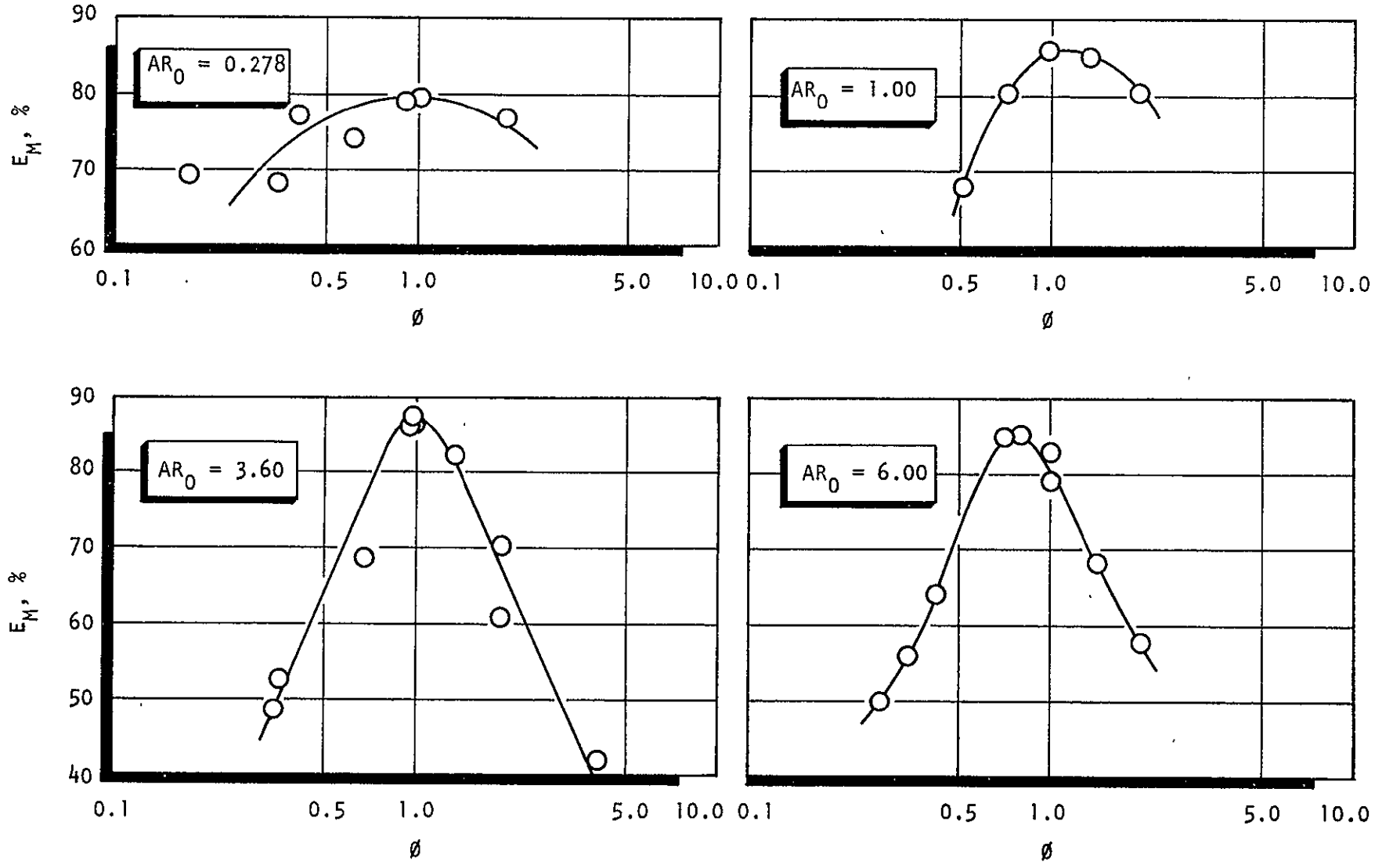

Figure 5-17. Rectangular Unlike-Doublet Mixing, E_m, as a Function of ø and AR_o for b_f/b_o = 0.625 (Rounded Entrances)

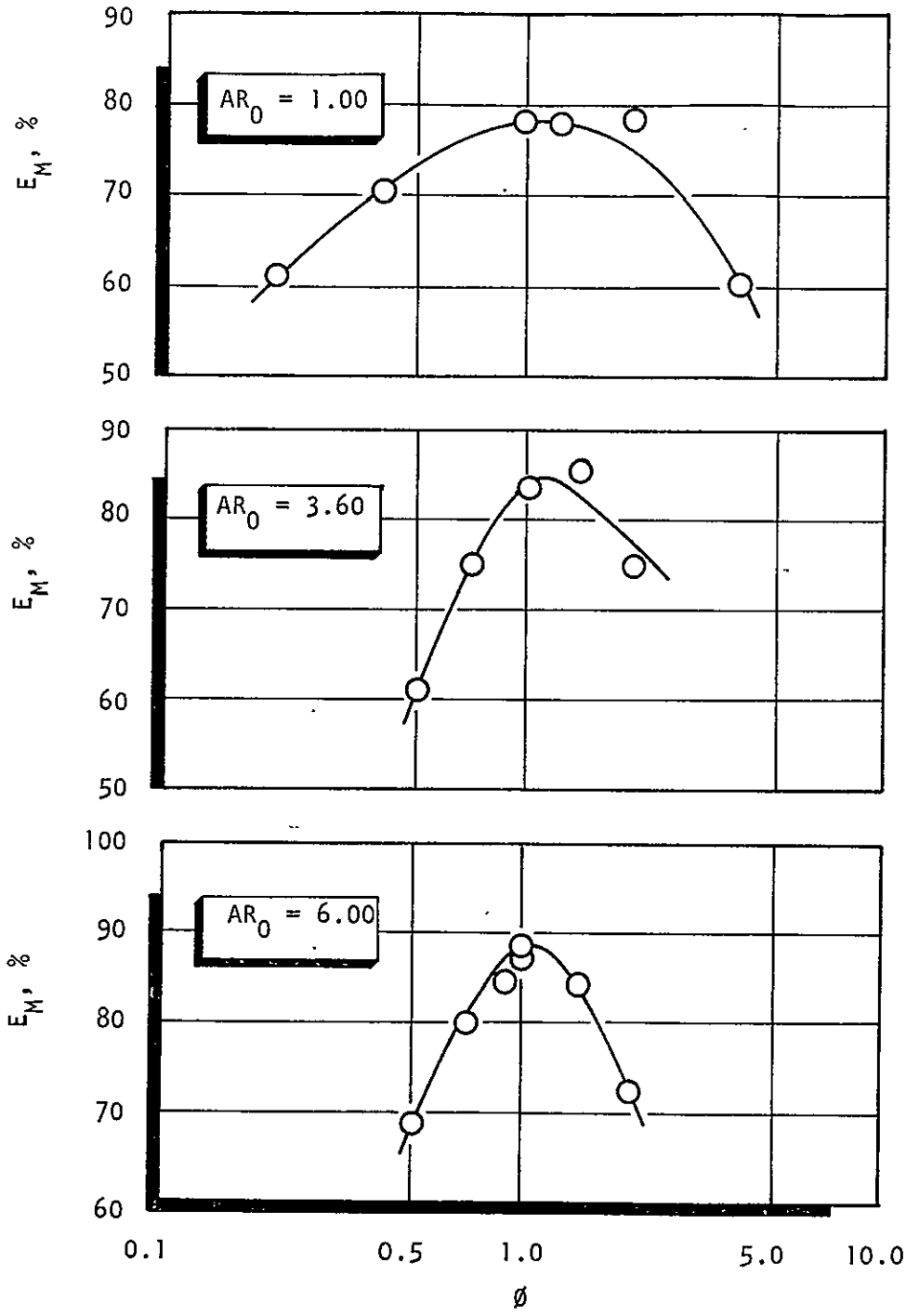

Figure 5-18. Rectangular Unlike-Doublet Mixing, E_m, as a Function of Ø and AR_o for b_f/b_o = 1.00 (Rounded Entrances)

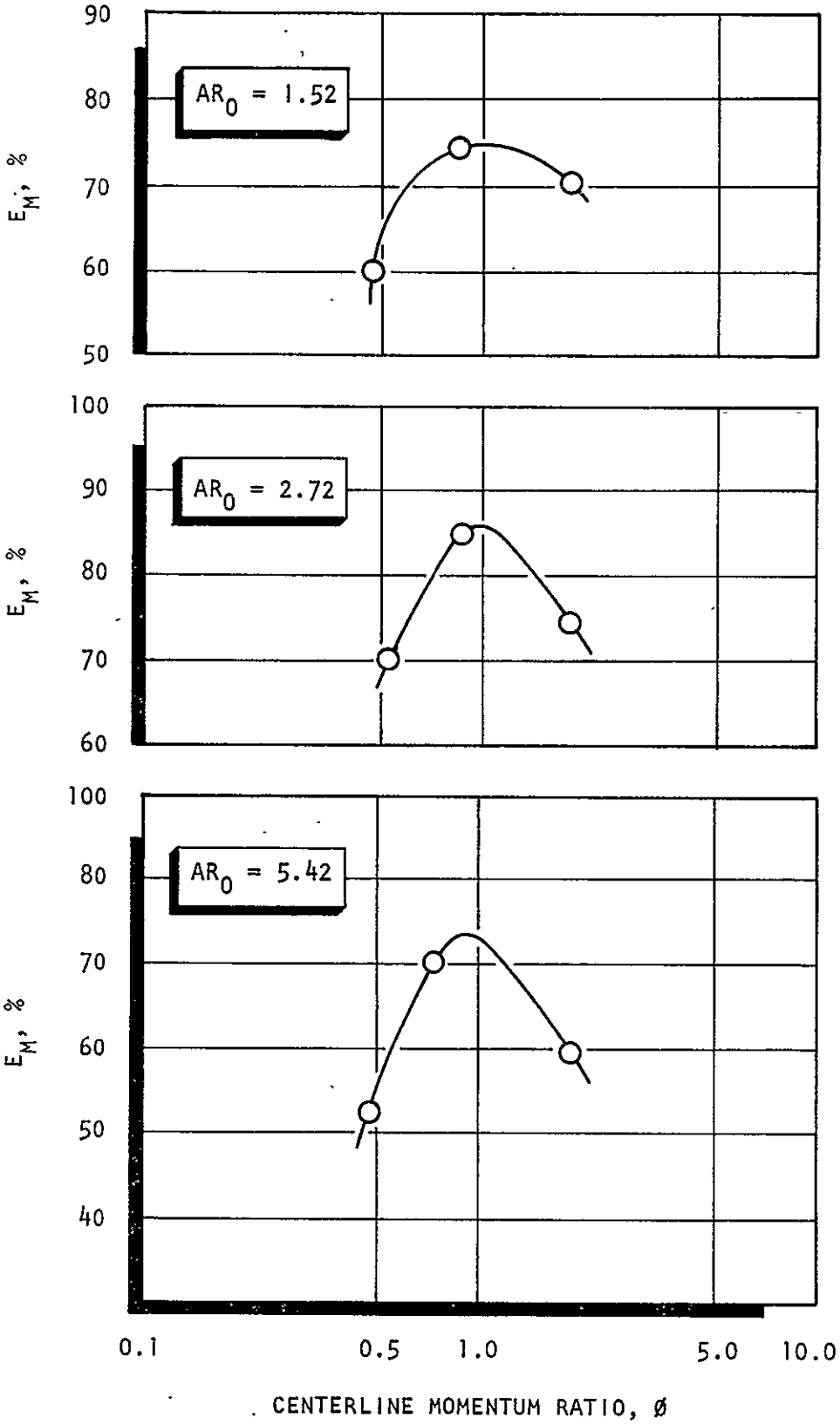

Figure 5-19. Mixing Uniformity for Rectangular Unlike Doublets as a Function of Ø and AR_o for b_f/b_o = 0.737 (Sharp Entrances)

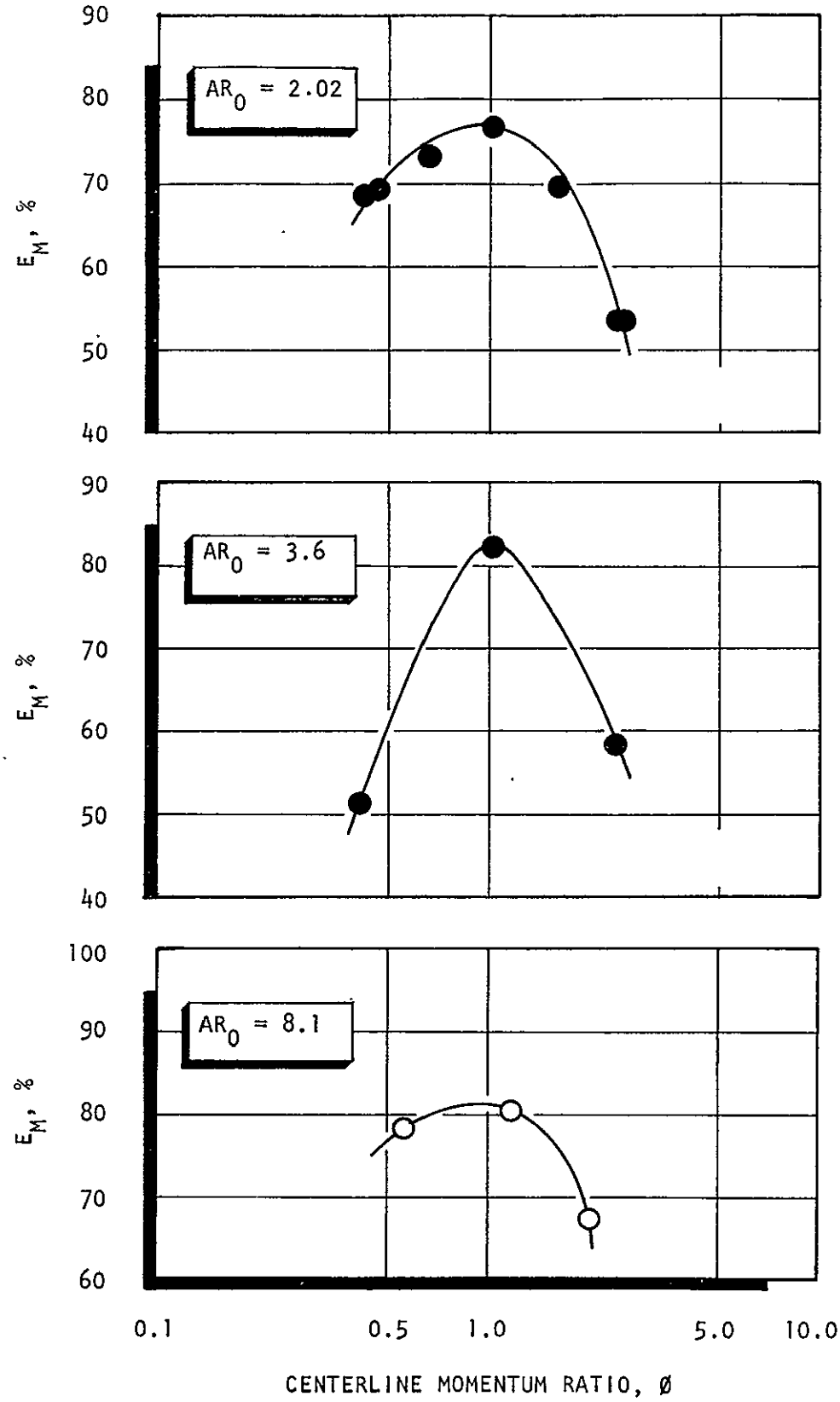

Figure 5-20. Mixing Uniformity for Rectangular Unlike Doublets as a Function of Ø and AR_o for b_f/b_o = 0.926 (Sharp Entrances)

5.4.1.3.3 Triangular Elements (Sharp-Edge Inlets). The mixing experimental results for the three triangular orifice elements evaluated are presented in Fig. 5-21. These results are similar to those obtained with both circular and rectangular orifice elements. Interestingly, the maximum level in E_m obtained with this element is the same as that obtained with the sharp-edge inlet rectangular orifice.

5.4.2 Element Design Criteria

The design criteria established for obtaining maximum mixing uniformity (E_m) of each element type are presented in this section. In addition to the results presented in preceding sections, other data are also presented to support and/or extend the results of this study. The discussions for unlike-doublet elements are presented (for each element type), first for round inlet designs and then for sharp-edge inlet designs. Finally, other parameters are then discussed that can further affect the mixing characteristics. It should be noted that for the non-circular designs, only the rectangular unlike-doublet injectors were varied sufficiently such that generalized design criteria could be obtained. For the other configurations only limited design criteria can be defined.

5.4.2.1 Self-Atomizing Nozzles. Since very little was done in terms of optimization of these elements, comprehensive design criteria cannot be given. For the self-atomizing fan nozzle the results obtained over the range of parameters investigated suggest that the highest level of mixing will occur when:

1. Nozzles for fuel and oxidizer are identical
2. Cant angle = 60 degrees
3. Fans aligned ($X_s = 0$)
4. Fans spaced about 1.0 inch apart (X_x = 1.0 inch)
5. The momentum ratio (oxidizer/fuel) equal to 1.0
6. The total injected momentum greater than about 0.04 lbf

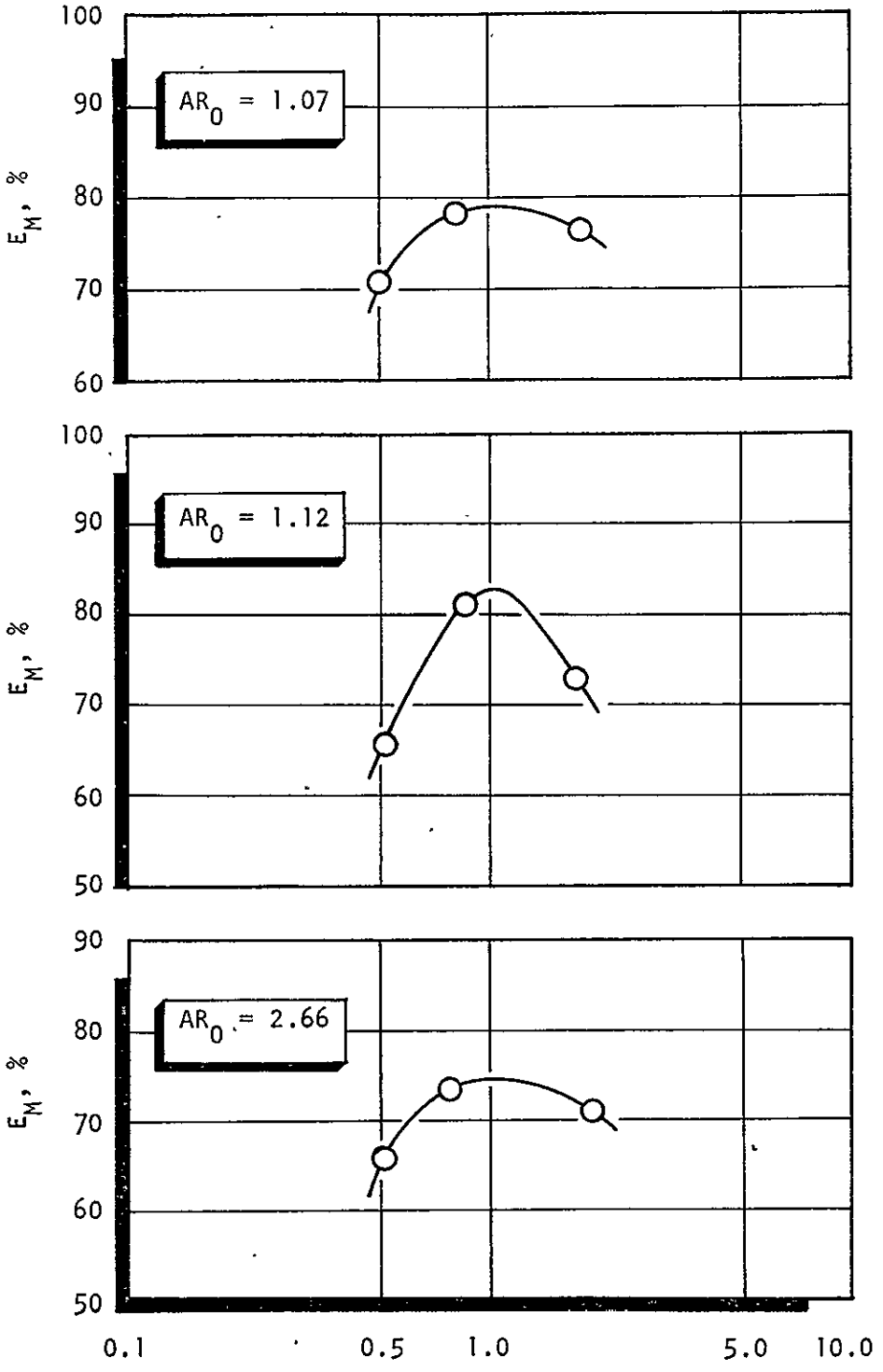

Figure 5-21. Mixing Uniformity for Triangular Unlike Doublets as a Function of Ø and AR_o for b_f/b_o = 0.736 (Sharp Entrance)

The maximum level of E_m attained with the self-atomizing fan was 77 percent. However, higher efficiencies could probably have been attained if the injected momentum were greater.

5.4.2.2 Unlike Doublets.

5.4.2.2.1 Circular Orifices. Although unlike-doublet injector design criteria have been available for years (Ref. 5-11 and 5-12), the design recommendations specified by Rupe were rather stringent considering current design practice. The injector design guidelines were:

1. Rounded entrances
2. Sufficient L/D (~100) to obtain fully developed turbulent flow
3. ϕ equal to 1.0

As stated earlier, it is surprising that the requirements defined by item 3 above is not a function of diameter ratio. In fact, most investigators now believe that $(\phi)_{opt}$ is indeed a function of diameter ratio. As a result, the data of Rupe and others were reviewed to determine if a relationship could be defined. The data definitely indicate that the optimum ϕ is a function of d_f/d_o although the data are rather limited. Analytical fit of the available data suggests that the relationship might be:

$$(\phi)_{opt} = 1.0\ (d_f/d_o)^{1/3} \tag{5-33}$$

over the range:

$$0.5 < d_f/d_o \leq 1.0 \tag{5-34}$$

The practical significance of diameter ratio effects on $(\phi)_{opt}$ is limited since (practical) diameter ratios are generally between 0.80 and 0.90. Thus, use of Eq. 5-33 rather than the one proposed by Rupe will not markedly alter the results. Before this equation is generally accepted, additional experiments should be conducted to verify the relationship.

Under conditions 1 and 2 above, the jet characteristics and the spray distribution are both controllable and predictable and conditions defined by Eq. 5-33 guarantee maximum E_m.

In terms of engine design parameters, ϕ is:

$$(\phi) = \left(\frac{1}{MR}\right)^2 \frac{\rho_o}{\rho_f} \left(\frac{d_o}{d_f}\right)^3 \tag{5-35}$$

and for the optimum value of (ϕ) using Eq. 5-33b

$$(d_f/d_o) = \left[\left(\frac{1}{MR}\right)^2 \rho_o/\rho_f\right]^{0.3} \tag{5-36b}$$

For a given propellant combination the mixture ratio and densities are fixed so that the diameter ratio of the orifices are also fixed.

For NTO/50-50 propellants:

$$d_f/d_o = 0.87 \text{ when } \phi = (\phi)_{opt} \tag{5-37}$$

This value of diameter ratio will result in the optimum element design regardless of the orifice L/D or inlet conditions; however, these variables will control the level of mixing uniformity that can be achieved. For example, in Fig. 5-22 for fixed diameter ratio of 0.82, the mixing uniformity characteristics are shown (data obtained from Ref. 5-11). These results were obtained with an orifice L/D of 22, round inlets and a threaded length of orifice to induce turbulence. Note that for this design the maximum level in E_m is 85 percent. Two other configurations are also presented in Fig. 5-22: (1) L/D of 10, round inlets; and (2) L/D of 10, sharp-edge inlets. These results show the effect of these design parameters on the mixing uniformity. Interestingly, for the L/D of 10 round inlet element, the maximum level in E_m attained was equal to that of the long L/D design. This occurred probably because the high orifice Reynolds numbers resulted in reasonably fully developed turbulent flow. Lastly, for most injector designs, it is not

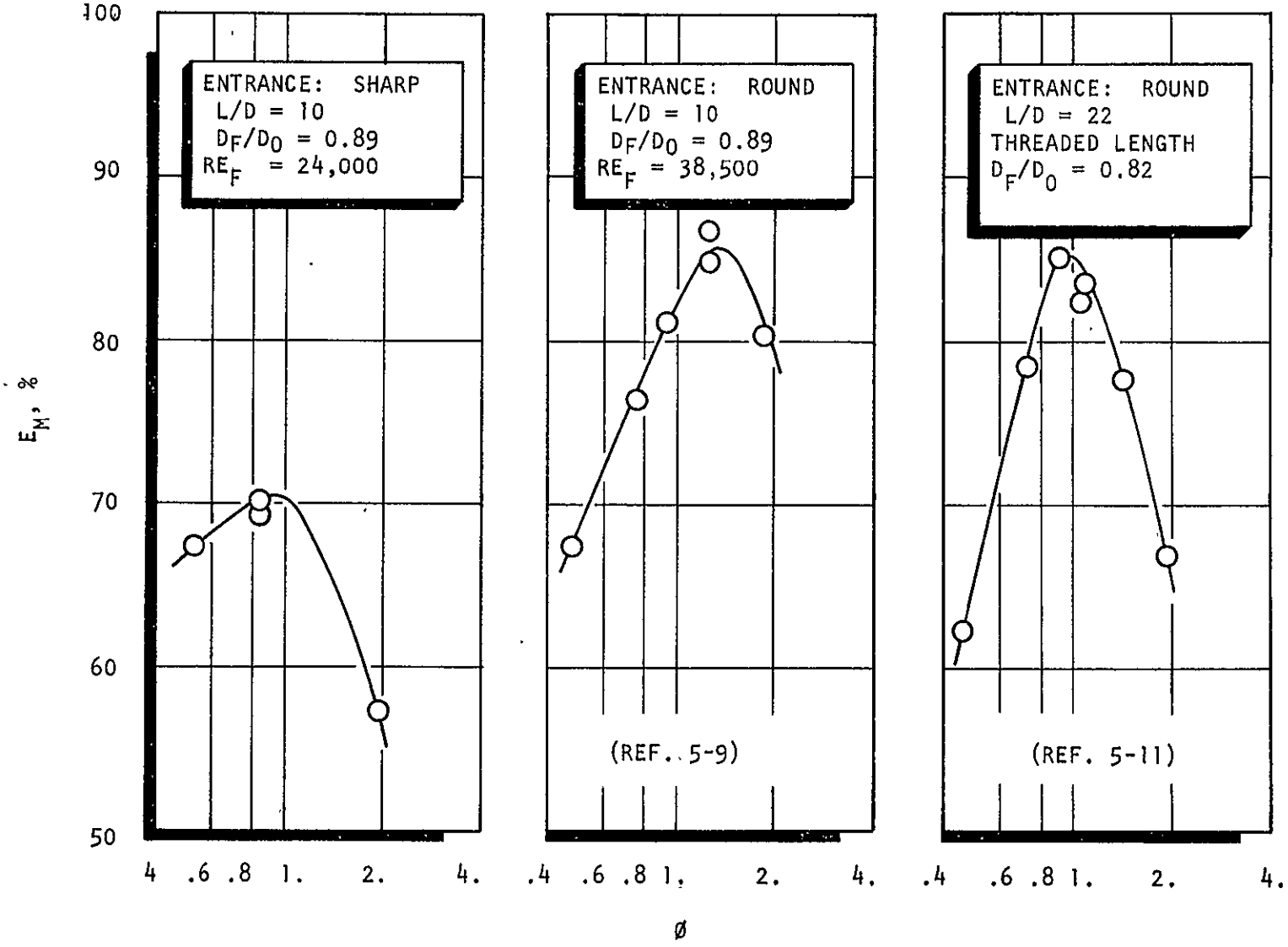

Figure 5-22. Comparison of the Mixing Uniformity of Circular Unlike Doublets With Sharp, Rounded, and Rounded and Threaded Entrances

possible to round the orifice inlets since the back sides are not accessible; for these cases, the entrances are sharp edged. The mixing attainable with sharp-edge inlet orifices having L/D's of 10 are also presented in Fig. 5-22. The results for the sharp-edge inlet design were obtained with full flowing jets.

Measurement of orifice coefficients and visual inspection conclusively showed that the flow did not flip, although at the orifice exit the jets were somewhat "bushy." Comparison of the maximum level of mixing attainable with this design shows that it is considerably below that obtained with rounded entrances--70- versus 85-percent E_m. This represents a considerable drop in mixing uniformity over that attainable with rounded-inlet orifices.

As mentioned earlier, the optimum element design criteria specifies a particular orifice diameter ratio. Rupe has shown that the maximum value of E_m attainable at $(\phi)_{opt}$ depends on diameter ratio. Therefore, the selection of propellant combination and/or operating conditions has a significant effect on the level of elemental mixing that can be achieved using a circular orifice unlike doublet. A plot of Rupe's results, for long L/D orifices (22) and a threaded orifice section, showing these characteristics, are presented in Fig. 5-23. Note that the smaller the diameter ratio (d_f/d_o) the greater the maximum value of mixing uniformity. For fully developed turbulent flow the elemental mixing can be predicted from Fig. 5-23 once the d_f/d_o is determined.

It was shown in the Results section that a valid assessment of the level in E_m that can be achieved with either sharp-edge or round inlets is dependent on the total flowrate (or momentum). It is also important for round inlet designs to ensure that the jets are turbulent. Measurement of turbulence intensity within the jets has shown that transition to turbulent flow occurred between a Reynolds number of 10,000 and 30,000.

5.4.2.2.2 Noncircular Orifices. The noncircular orifice injector design criteria, for round and sharp-edge inlets, developed in this program are limited to:

$$E_m = f(b_f/b_o, \phi, AR_o) \qquad (5\text{-}38)$$

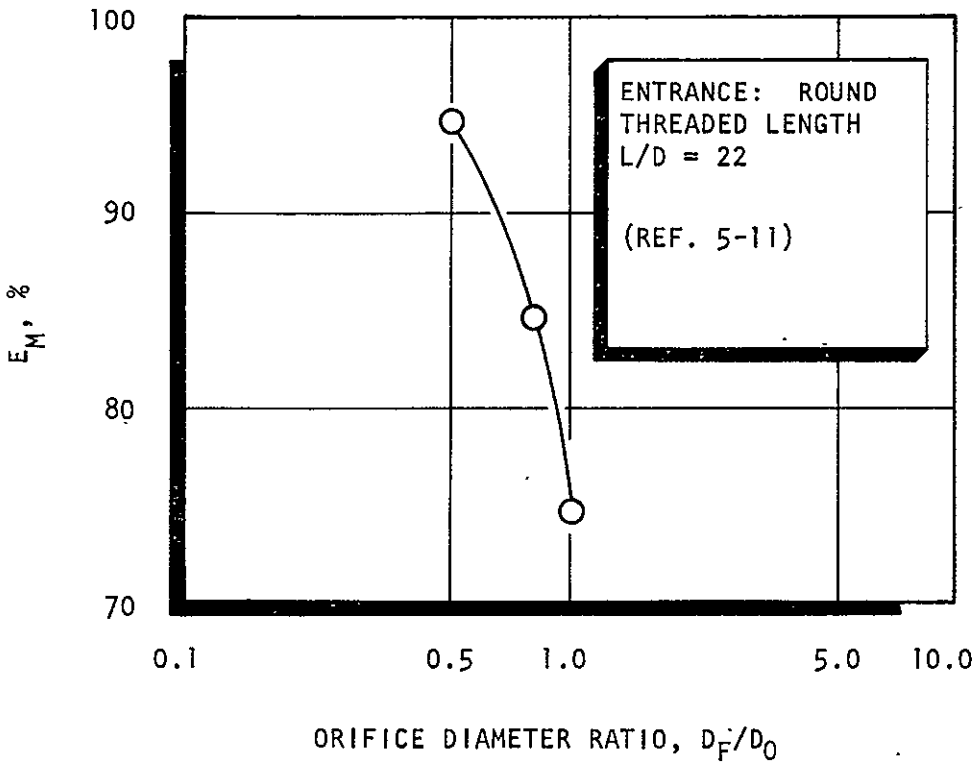

Figure 5-23. Mixing Uniformity for Circular Unlike Doublets as a Function of Diameter Ratio (Rounded and Threaded Entrance)

One of the major considerations of the design engineer is the required length of orifice and inlet configuration. In Fig. 5-24, the data shown in the plot on the right were generated by the authors of Ref. 5-31, and are for round orifice inlets and an L/D of ≈ 29. This design should (1) represent near fully developed turbulent flow, and (2) since the inlets were rounded, separation at the orifice inlet definitely did not occur. It is unfortunate that only three data points were obtained and that none were taken at a ϕ of 1. Note however, that the mixing curve through the data has been drawn such that it maximizes near the maximum value obtained rather than at ϕ of 1. (This is conservative since a higher value would result if the curve were maximized at ϕ of 1.) This was done since the orifice widths for this design were not exactly equal so that the actual value ϕ where $(E_m)_{max}$ occurs is unknown. The maximum level of E_m shown is ≈ 88 percent. In the central plot on Fig. 5-24, mixing results are presented for a rounded-inlet design having an L/D of 10. These results show that the mixing maximized at ϕ of 1 ($W_1 = W_2$) and the maximum level in E_m is 87 percent. These results suggest that within experimental error, no loss in E_m occurred as the L/D was reduced. (It should be pointed out that these two sets of data were taken at different facilities. However, duplicate tests at other conditions have been performed at both test facilities with reasonable check.)

The data obtained using a sharp-edge inlet element with an L/D of 10 are also presented in Fig. 5-24. The results show that for this orifice configuration the maximum level in E_m is 86 percent, which is only 1 percent lower in E_m than that obtained for the rounded inlet L/D of 10 design. These results suggest that for these orifices the flow develops rapidly and is relatively insensitive to inlet condition or L/D (between 29 and 10). In addition, although the sharp-edge orifices might experience separation, this phenomenon does not appear to have affected the mixing characteristics.

For the triangular orifices, only designs having L/D's of 10 and sharp-orifice inlets were evaluated. The mixing uniformity results presented earlier in Fig. 5-21 show that for this design E_m also maximized at ϕ equal 1 ($W_1 = W_2$) and the maximum level was 83 percent. This level, like that for the rectangular elements, does not necessarily represent the maximum level attainable with sharp-edge inlet orifices.

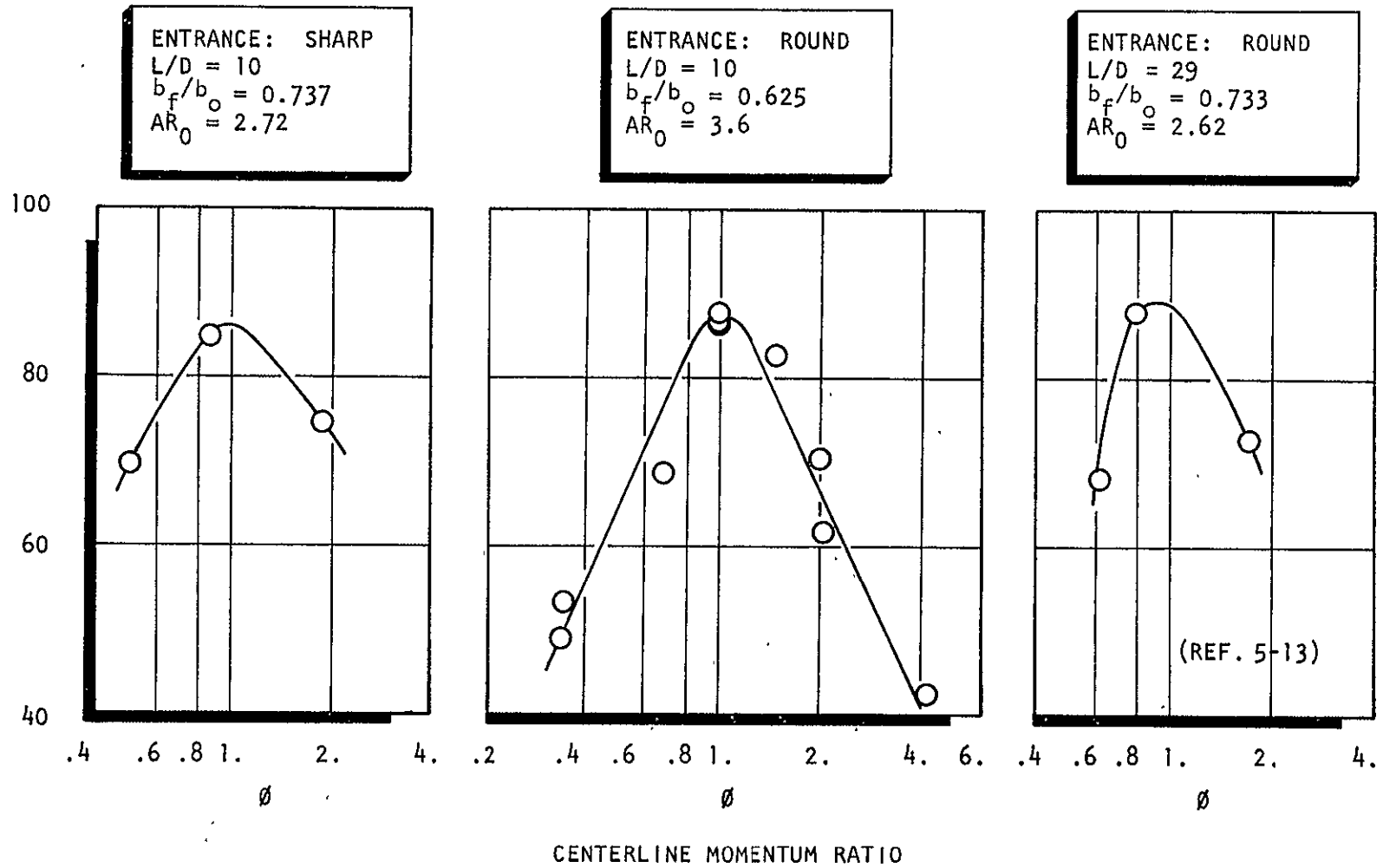

Figure 5-24. Mixing Uniformity for Rectangular Unlike Doublets as a Function of Centerline Momentum Ratio

Since all elements result in their respective optimum levels in E_m at about $\phi = 1$ then for the noncircular shapes where $W_1 = W_2$:

$$(\phi)_{opt} = 1.0 = \left(\frac{1}{MR}\right)^2 \left(\frac{\rho_o}{\rho_f}\right) \cdot \frac{b_o}{b_f} \quad (5\text{-}39)$$

and for NTO/50-50 $b_f/b_o = 0.622$. Equation 5-39 shows that as was the case for the circular orifice element design criteria, noncircular orifices are also restricted to a specified value of b_f/b_o once the propellants and mixture ratio are selected. However, for noncircular shapes, an infinite number of designs can be specified, all having the same b_f/b_o ratio but differing aspect ratio (AR). For injector design it is important to select the aspect ratio for a given b_f/b_o, which will result in the highest level in E_m.

The initial step in determining the optimum element geometry for each element set is to define the values of $(E_m)_{max}$ at ϕ of 1. These results for the rectangular element configurations (rounded and sharp-edge inlet) are presented in Fig. 5-25. The results are presented in terms of $(E_m)_{max}$. (E_m at $\phi = 1.0$) as a function of the oxidizer aspect ratio for constant values of b_f/b_o. No data points are plotte since the values plotted do not actually represent data but a point along a curve fit of the data. Comparing the sharp-edge inlets with the round-inlet results shows that mixing is more dependent on the geometry for sharp inlets than for rounded inlets. The round-inlet rectangular orifice results suggest that the optimum design aspect ratios (AR_o) for b_f/b_o of 0.391 and 1.0 lie outside the range studied. However, the optimum configuration appears to be close to the end of the range evaluated. The range was selected based on practical EDM machining capabilities, and there was, of course, no *a priori* guarantee that the optimum configuration would be included.

A curve fit of the data was accomplished to determine if a maximum value in $(E_m)_{max}$ could be predicted, and the results are presented in Fig. 5-26. The correlating factor is $AR_o/(b_f/b_o)^3$. Note that for the rounded-inlet designs, the data suggest that the maximum attainable E_m is 88 percent. In addition, the result

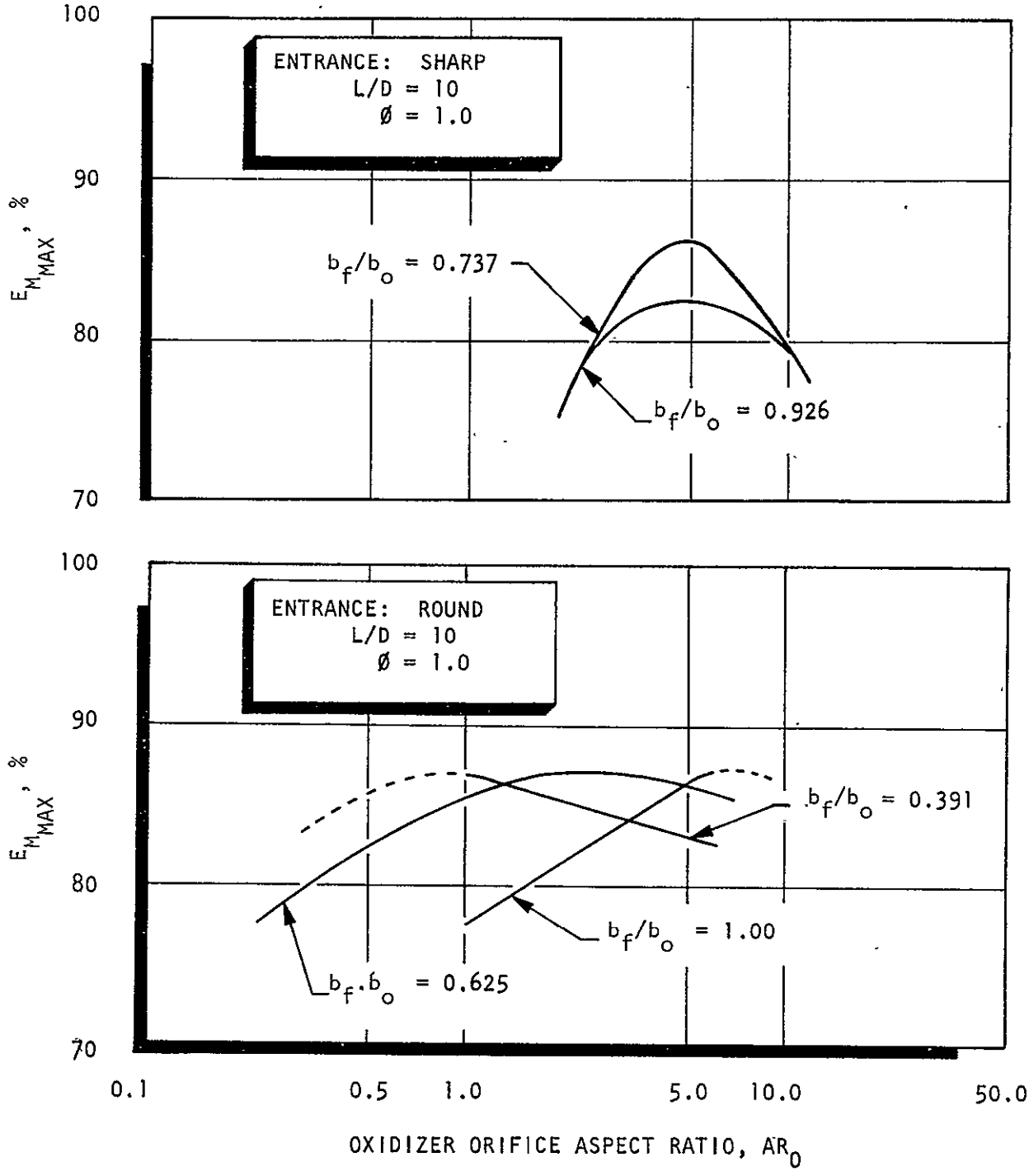

Figure 5-25. Mixing Uniformity for Rectangular Unlike Doublets as a Function of Oxidizer Orifice Aspect Ratio (Ø = 1.0)

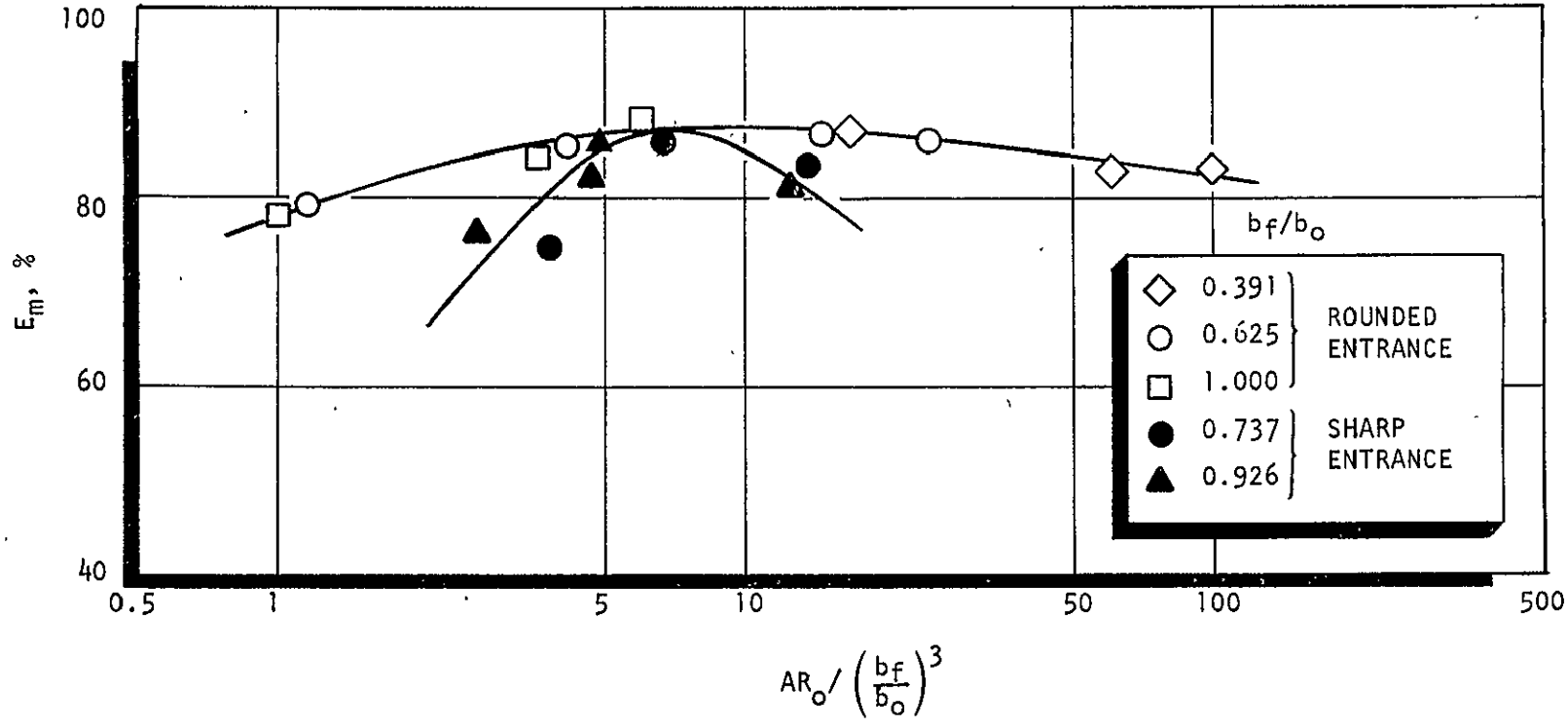

Figure 5-26. Mixing Uniformity for Rectangular Unlike Doublets as a Function of $AR_o/(b_f/b_o)^3$ (Sharp and Rounded Entrance Data Shown)

show that wide latitude in the selection of an aspect ratio for a given b_f/b_o ratio can be given without suffering a significant loss in mixing uniformity. The results for the sharp-edge rectangular elements are also presented in Fig. 5-25 and 5-26. For this configuration (i.e., sharp edge) optimum design configurations were, in every case, within the range evaluated. In Fig. 5-26, the data were fit to the same correlation as that for the rounded-inlet elements. The curve drawn through the data suggest that the maximum value in E_m is also about 88 percent. Based on the results presented in Fig. 5-26, the design criteria for the rectangular elements is:

$$\left[AR_o/(b_f/b_o)^3\right]_{opt} = 8 \qquad (5\text{-}40)$$

so that in conjunction with Eq. 5-39, the optimum AR_o providing the maximum value of $(E_m)_{max}$ (i.e., 88 percent) can be calculated.

For the triangular elements the maximum level in $(E_m)_{max}$ should also be a function of b_f/b_o ratio. From the results shown in Fig. 5-27, the maximum level in $(E_m)_{max}$ for a b_f/b_o of 0.737 is 83 percent. This level is 3 percent lower than that achievable with the round-inlet rectangular orifice element. Since only one set of triangular elements was evaluated, design criteria can only be presented for this specific case. From Fig. 5-27, the optimum element design is:

Triangular orifice:

$$b_f/b_o = 0.736$$

$$(AR)_{opt} = 1.3$$

5.4.2.3 Unlike Triplet. The triplet element results presented previously show that mixing is a function of:

$$E_m = f(\phi,\ d_f/d_o,\ W_T) \qquad (5\text{-}41)$$

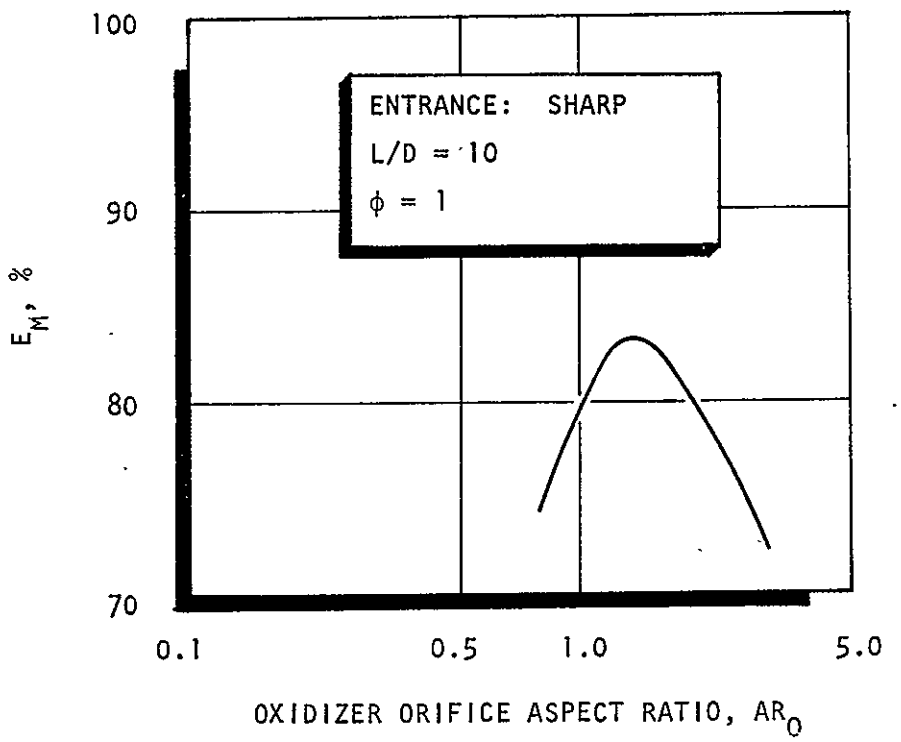

Figure 5-27. Mixing Uniformity as a Function of Oxidizer Orifice Aspect Ratio for a Triangular Unlike Doublet for b_f/b_o = 0.736 (Sharp Entrance)

The results show that the highest level of mixing is obtained when the diameter ratio is unity. However, the centerline momentum ratio is related to the optimum E_m in the following manner:

$$(\phi)_{opt} = C(d_f/d_o)^n \tag{5-42}$$

From the data presented in Fig. 5-14, optimum values of ϕ were determined. For the diameter ratio of 0.52 the curve is very flat in the region of the optimum so that a range was considered for this case. These values were fit to the above equations and the resulting equation is:

$$(\phi)_{opt} = 1.0\ (d_f/d_o)^{0.7} \tag{5-43}$$

In Fig. 5-28, Eq. 5-43 is compared to that proposed by Elverum and Morey. Over the ranges evaluated the curves give reasonably close predictions. The authors of Ref. 5-4 propose two separate fits of their data but conclude that they are only valid at a value of d_f/d_o of 1.2. Note that Eq. 5-43 also fits this point, suggesting that the proposed equation predicts the optimum ϕ reasonably well. In terms of rocket engine parameters, Eq. 5-43 can be reformulated as:

$$\frac{d_f}{d_o} = \left[\left(\frac{1}{MR}\right)^2 \frac{\rho_o}{\rho_f}\ 1/2\right]^{0.27} \tag{5-44}$$

and for NTO/50-50 propellants:

$$d_f/d_o = 0.76 \tag{5-45}$$

This diameter ratio is sufficiently close to optimum so that only a 4-percent loss in E_m results over the maximum attainable (see Fig. 5-4) value.

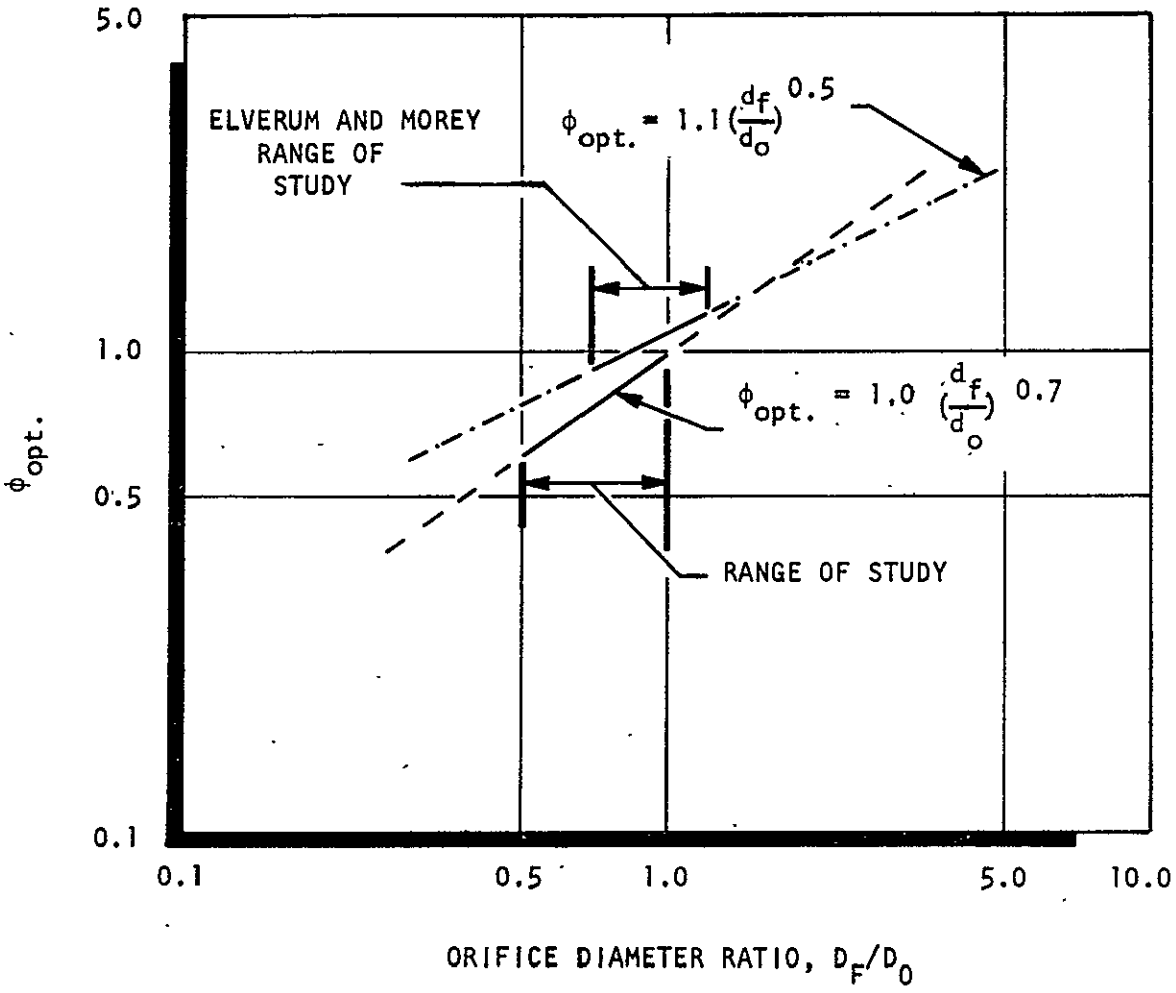

Figure 5-28. Optimum Centerline Momentum Ratio for Circular Unlike Triplets as a Function of Fuel to Oxidizer Orifice Diameter Ratio

5.4.3 Comparison of Mixing Characteristics for Circular and Noncircular Unlike-Doublet Elements

5.4.3.1 Rounded Inlets. Several comparisons are made between the circular and noncircular unlike doublets in Fig. 5-29. In the upper plot, the long L/D rounded-entrance data are shown. These results can be compared with the L/D of 10 rounded-entrance results shown on the middle plot on the left. These latter results at a specific d_f/d_o show that reducing the L/D to 10 did not affect the level of mixing attained. Of importance (although not illustrated), is that the noncircular orifice elements (rounded entrance) provide the same high level of $(E_m)_{max}$ regardless of b_f/b_o ratio while the circular orifices are a strong function of d_f/d_o. As a consequence, the rectangular orifice, through its greater geometric flexibility (see Fig. 5-26 and Eq. 5-40) can always be designed for the maximum E_m possible. The maximum E_m of the (rounded-entrance) rectangular orifice elements exceeds that of the circular orifice doublets for $d_f/d_o \geq 0.76$. If the propellant combination is NTO/50-50 then the optimum d_f/d_o is 0.87 (see Eq. 5-37) and the circular and noncircular element will provide nearly the same value of E_m, so that for these propellants the selection would be based on considerations other than mixing. An exception would be the cases where the design Reynolds number for the circular element is less than about 25,000. For Reynolds numbers less than this value, the circular element will probably be in transition and, consequently, the overall mixing E_m could drop to as low as 74 percent. As an example, for a 0.03-inch orifice with a ΔP of 50 psi, the fuel Reynolds number will be 18,000* so that this restriction is within the range encountered in real engine applications. In such a case, mixing of the noncircular doublet would be superior. Also, it is possible that noncircular orifices might provide even higher values of E_m if the width (W) ratio were other than 1.0. This is suggested from the circular data, which show increasing E_m with differences in orifice diameters.

5.4.3.2 Sharp-Edge Inlets. The sharp-edge inlet circular and noncircular results are presented in the lower plot in Fig. 5-29. At these conditions, the circular orifice element results in considerably lower values of $(E_m)_{max}$ than either the triangular or rectangular orifice unlike doublet elements. The specific mixing levels are shown in the following listing.

*The fuel is 50-50.

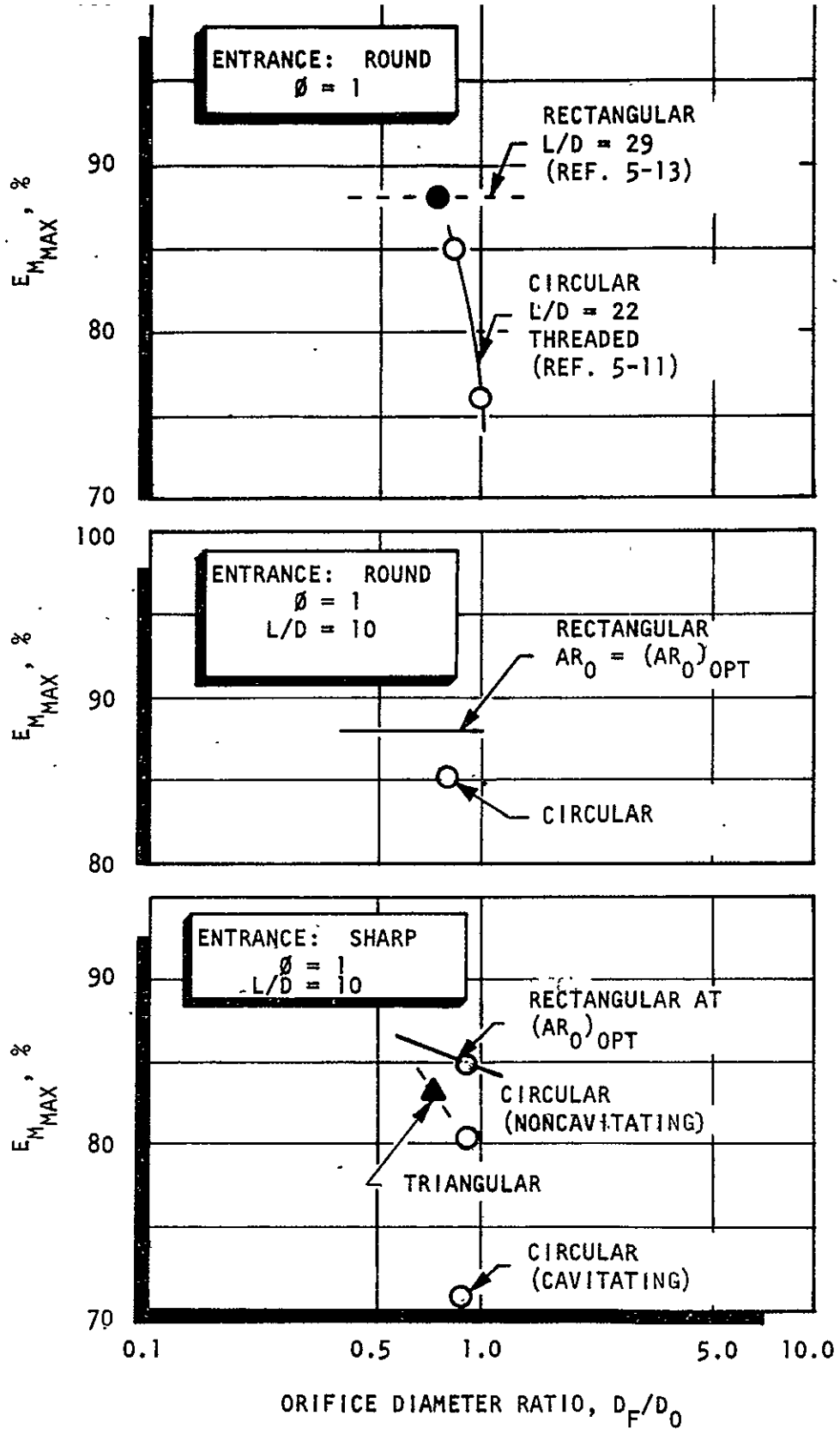

Figure 5-29. Mixing Uniformity Comparisons

Element	d_f/d_o	b_f/b_o	$(E_m)_{max}$, %
Circular Orifice Element	0.84	--	70.5** to 80.0***
Rectangular Orifice Element	--	0.74	86***
Triangular Orifice Element	--	0.74	83***

*L/D = 10

**Cavitated

***Noncavitated

It is obvious from these results that if it is required to design the orifices with sharp-edge inlets and cavitation can be avoided, then the noncircular elements will provide 3 to 6 percent greater elemental mixing uniformity (E_m). On the basis that the mixing characteristics for the circular element with sharp-edge orifices are similar under hot-fire conditions, circular elements would not be recommended.

It has been stated in Ref. 5-13 that the lower value in mixing uniformity (with sharp-entrance orifices) is caused by cavitation of the fluid in the flow separation region. This contention was arrived at through the use of a cavitation model (Ref. 5-14) which the author of Ref. 5-14 clearly stated is only good for Reynolds numbers greater than 50,000. For these experiments, the nominal Reynolds number for the fuel is 13,000. Furthermore, the authors of Ref. 5-13 fail to state that the correlation presented by Hall (Ref. 5-14) did not match for L/D's greater than 6. Indeed, at an L/D of 10, Hall's predictions were high by a factor of about 2.0.

Because of the rather wide circulation of that report and the apparent acceptance of the results, Rocketdyne, under company funds conducted a study to measure the pressure within the separation cavity as a function of upstream pressure to define the conditions required to produce cavitation. These results to be published (Ref. 5-9) conclusively demonstrate that the lower value of $(E_m)_{max}$ of 70.6 percent is caused by orifice cavitating. The results of that study also conclusively show that for noncavitated jets the $(E_m)_{max}$ is only 80 percent.

5.5 ATOMIZATION STUDIES

Selected element types were investigated to determine comparative atomization characteristics. The elements selected were:

1. Self-atomizing nozzles (spray fans)
2. Sharp-inlet circular orifice unlike doublet
3. "Near-optimum" rectangular and triangular orifice unlike doublets (sharp entrance)
4. Round-inlet circular orifice unlike triplet

Each element was evaluated over a range in flowrate (injection velocity) keeping the relative flowrates (mixture ratio) constant. Additional parameters were varied for specific configurations. For the unlike-doublet elements, hot wax was used in one orifice and heated water in the other. In this way, the dropsize for each orifice could be determined in separate tests simply by interchanging fluids.

The measured dropsize distributions are presented in terms of the mass median dropsize ($\overline{D}$). This droplet diameter is the size in a given sample for which half of the sample weight is made up of droplets of larger diameter and the other half of the mass is made up of droplets of smaller diameter. The mass median diameter was chosen rather than some other arbitrary statistical dropsize diameter because the distribution data were determined by sieving, which gives $\overline{D}$ directly.

A summary of the results is presented below.

5.5.1 Experimental Results

A complete tabular summary of all of the atomization tests can be found in Ref. 5-8. Only the results in terms of selected parameters are presented herein.

5.5.1.1 Self-Atomizing Fans. For the self-atomizing fan elements, single orifices were evaluated. The equivalent diameter range studied was from 0.018 to 0.072 inch. During the experiments the flowrate was varied and the resulting atomization characteristics determined. In addition, to minimize the number of variables studied, a single fluid was used for the determination of dropsize. Consequently, ρ_L/ρ_g, μ, and σ remained constant. Since neither surface tension nor viscosity varies, Reynolds number is directly related to Weber number ($Re = K\sqrt{We}$); therefore, one of these terms must be excluded from the correlation. In addition, since all nozzles were 80-degree fan designs, K_o/d^2 is also constant. Finally, for the self-atomizing fans, the velocity profile in the sheet is reasonably uniform since the flow has virtually zero distance to develop so that P_c/P_j should be close to 1.0. From the above discussion, the number of independent parameters affecting atomization is, therefore, reduced to the rather simple function:

$$\overline{D}/d = f(We) \tag{5-46}$$

All of the results are presented on a single plot in Fig. 5-30. The data fit the line drawn in the figure by ±10 percent, except for two points, which are within experimental repeatability. The equation describing these results is:

$$\overline{D}/d = 4.8\left(\frac{1}{We}\right)^{1/3} \tag{5-47}$$

It is of interest to compare this result with that of Hasson and Mizrah (Ref. 5-15)

$$\overline{D} = C'\,(\sigma_L\, K/C_D{}^2\, \Delta P)^{1/3}\,(\rho_L\, \mu_L)^{1/6} \tag{5-48}$$

$$K = A/\sin(\theta/2) \tag{5-49}$$

Converting this equation to Weber number and letting ρ_L, μ_L, and θ equal constants results in:

$$\frac{\overline{D}}{d} = K'\left(\frac{1}{We}\right)^{1/3} \tag{5-50}$$

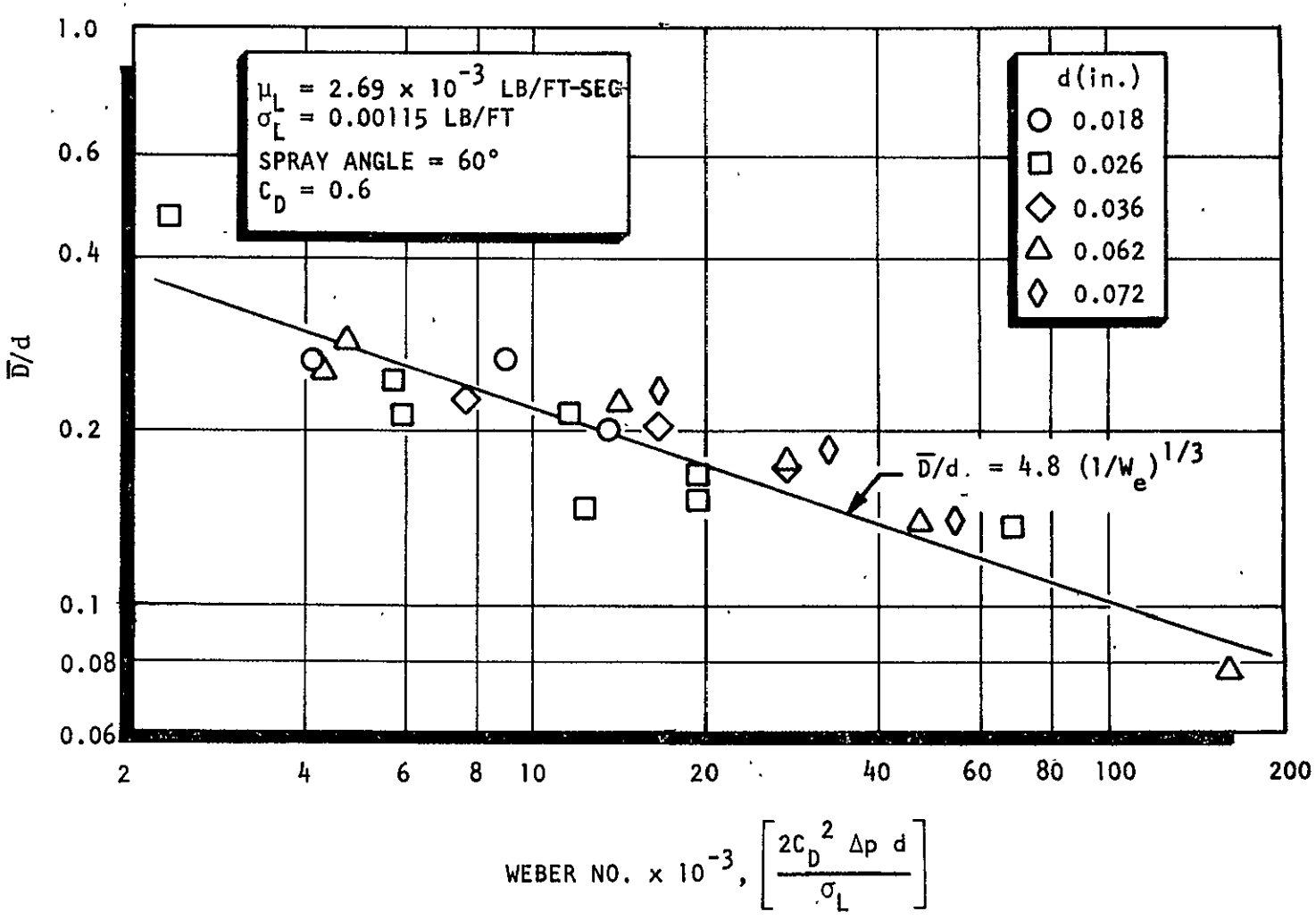

Figure 5-30. Relative Droplet Diameter as a Function of Weber Number for Self-Atomizing Spray Fans

The agreement of the equations is important in that it extends the applicability of the results to other fluids, since the Ref. 5-15 equation also includes the effect of ρ_L and μ_L.

5.5.1.2 Circular Orifice Elements. For the circular orifice elements, experiments were conducted using both unlike-doublet and triplet elements. For the unlike-doublet elements the entrances were sharp and the L/D was 10. During the program, it was not apparent that the heated wax having a vapor pressure that is almost atmospheric resulted in the jets encountering hydraulic flip. As a consequence, the jets are probably laminar and the jet diameter about $\sqrt{0.611}\,d$. Therefore, these unlike-doublet results would not be representative of an element operating under unflipped conditions. The unlike doublet results are therefore not presented herein; however, subsequent study on a NASA contract (NAS7-726) has resulted in equations that extended the work of Dickerson et al. (Ref. 5-5) for turbulent unlike-doublet elements so that the equation can be utilized to predict the dropsize for the circular unlike-doublet injector.

The dropsize equation for the fuel orifice (smaller size orifice) of the unlike doublet, for turbulent flow is:

$$\overline{D}_f = 1.05 \times 10^5 \, V_f^{-1.07} \, d_f^{0.293} \, P_D^{0.165} \, (d_o/d_f)^{0.023} \qquad (5\text{-}51)$$

where

$$P_D = \frac{\rho_f V_f^2}{\rho_o V_o^2} \qquad (5\text{-}52)$$

Note that this equation does not include the effect of P_c/P_j, since measurements of this type were not taken. It is unfortunate that the element that is used more than any other has been studied the least. Facilities are available and techniques developed to ensure that hydraulic flip will not occur so that experiments could be conducted to determine the dropsize characteristics of the unlike element (turbulent flow).

A more extensive study was conducted with the triplet elements wherein orifice diameter, L/D and total flowrate were varied. For this study, dropsize should be a function of:

$$\text{Inner jet:} \quad \frac{\overline{D}_f}{d_f} = f\left[We_f,\ P_D,\ (P_c/P_j)_1\right] \tag{5-53}$$

$$\text{Outer jet:} \quad \frac{\overline{D}_o}{d_o} = f\left[We_o,\ P_D,\ d_f/d_o,\ (P_c/P_j)_2\right] \tag{5-54}$$

The centerline pressure ratio (P_c/P_j) is a function of L/D and Reynolds number and since the Reynolds number for these tests is related to Weber number, then Eq. 5-53 and 5-54 can be converted to:

$$\text{Inner jet:} \quad \frac{\overline{D}_f}{d_f} = f(We_f,\ L/D,\ P_D) \tag{5-55}$$

$$\text{Outer jet:} \quad \frac{\overline{D}_o}{d_o} = f(We_o,\ L/D,\ d_o/d_f,\ P_D) \tag{5-56}$$

and, finally, the dynamic pressure for these tests was held constant so that this variable can also be eliminated.

Data were taken over a wide range in orifice Reynolds number, keeping the centerline momentum ratio equal to 1, since that is where mixing was thought to maximize. In addition, the inlets were rounded to ensure that the orifices would not experience hydraulic flip. This resulted in most of the data being taken in the laminar region ($Re \leq 10{,}000$). A few data points were taken in the turbulent (or transition) zone; however, these data were insufficient to develop a correlation. Finally, some data were obtained on the Ref. 5-3 study with an L/D of 50 and equal orifice diameters. These data are included herein for completeness.

The data are presented in terms of We, L/D, and $\overline{D}/d$ in Fig. 5-31. Note that it was possible to collapse the L/D effect by simply multiplying Weber number by L/D. These results are presented for the laminar flow ($Re \leq 10{,}000$) only. For these

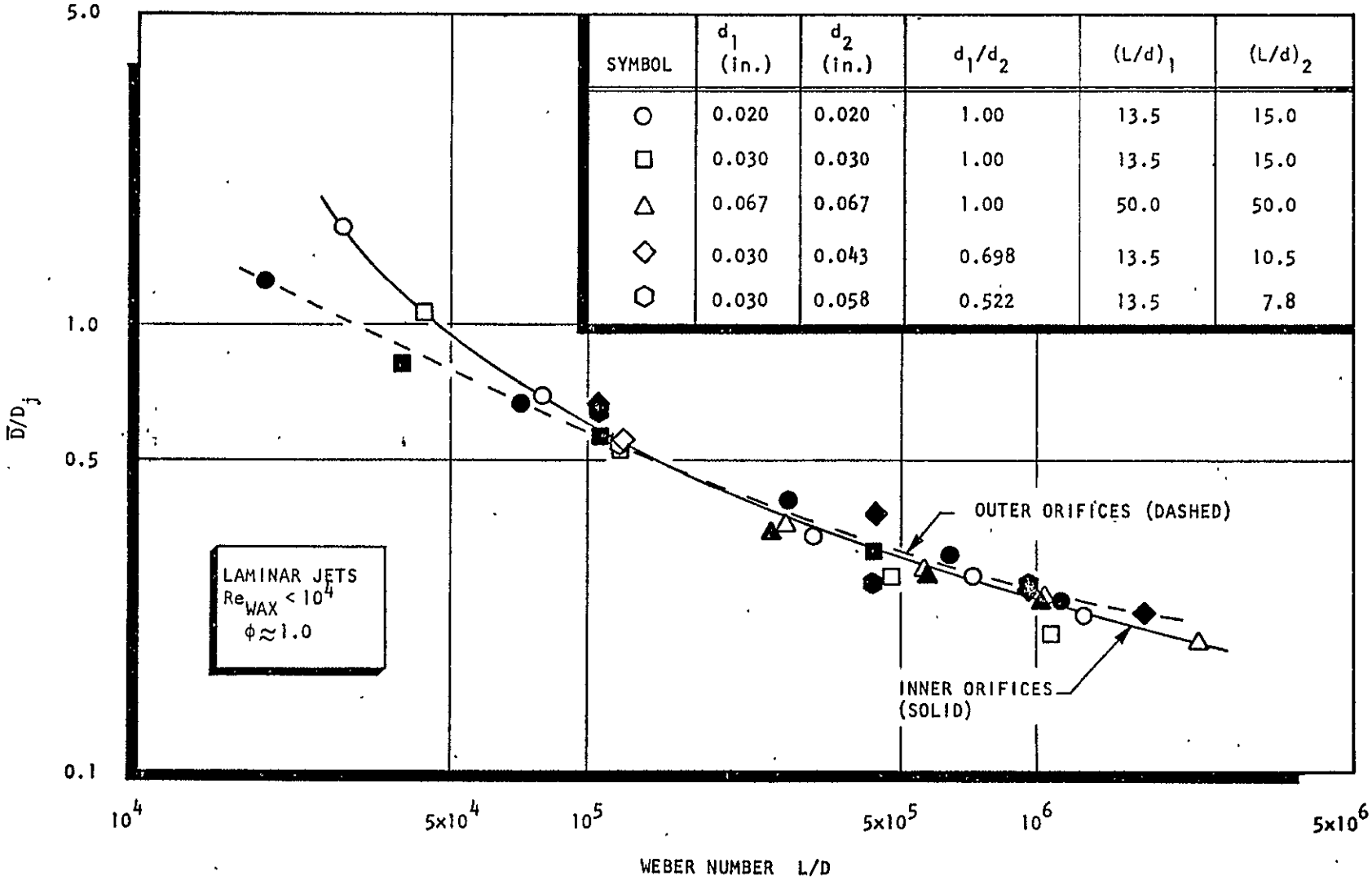

Figure 5-31. Correlation of Relative Droplet Diameter With Weber No. and Orifice L/D for Unlike Triplets (Both Central and Outer Orifice Results Shown)

results the inner and outer jets yield quite similar lines when plotted in this manner. A straight line could not be drawn through the entire set of data showing that over that range in Weber number, no single power function will describe the data. For values of (We L/D) greater than about 10^5, $\overline{D}/d$ is proportional to Weber number to the one-third power. This power relationship is identical to that found for the self-atomizing fan element.

5.5.1.3 Noncircular Orifice Elements. Based on the arguments given above, single set of fluid simulants, equal widths as well as a constant impingement angle of 60 degrees, the number of variables affecting atomization can immediately be reduced to:

$$\overline{D}_1/b_1 = f(We_1, P_D, b_1/W_1) \tag{5-57}$$

$$\overline{D}_2/b_2 = f(We_2, P_D, b_1/b_2, b_1/W_1) \tag{5-58}$$

However, as discussed in the Results section, atomization tests for these were limited to the specific "optimum" design and others were not evaluated. Consequently, the variables listed in Eq. 5-33 and 5-34 are further reduced to:

$$\overline{D}_1/b_1 = f(We_1, P_D) \tag{5-59}$$

$$\overline{D}_2/b_2 = f(We_2, P_D) \tag{5-60}$$

It is important to note, however, that these simplifications impose a large number of restrictions on the atomization results, i.e.:

$$b_1/b_2 = \text{const};\ b_1/W_1 = \text{const},\ \rho_{L_1}/\rho_{L_2} = 1.30$$

$$Re = K_1 \sqrt{We},\ \phi = 60 \text{ degrees},\ \mu_{L_1}/\mu_{L_2} = 6.06$$

$$\text{and } \sigma_1/\sigma_2 = 3.56$$

Therefore, caution should be exercised in extrapolation of these results to other fluids or operating conditions.

Only two noncircular elements were evaluated: (1) rectangular orifice, $(b_f/b_o)/AR_o$ = 0.737/2.72; and (2) triangular orifice, $(b_f/b_o)/AR_o$ = 0.736/1.12. The data were taken over a range in flowrate keeping the mixture ratio constant. This resulted in the data being obtained at constant dynamic pressure ratio. The results are presented in Fig. 5-32 in terms of $\overline{D}$ and injection velocity since the orifice size was not varied sufficiently for a determination of the pertinent geometric parameter (i.e., b, w, or hydraulic diameter). In addition, injection velocity was used instead of Weber number since only V_j was varied. The results show trends similar to those found for the circular orifice elements.

5.5.2 Element Design Criteria

Design criteria for atomization are generally dictated by overall system ΔP requirements and the necessity of achievement of a specified level of spray vaporization. Given these requirements, combustion models are generally used to determine, as a function of combustor geometry, the initial median dropsize necessary to achieve the vaporization efficiency. Then for several candidate element types, using the maximum allowable ΔP, the element geometry (i.e., orifice size, impingement angle, etc.) is specified for zero combustion gas velocity. This results in extremely conservative estimates since gas velocity tends to result in secondary breakup, reducing initial dropsizes. The results are then scrutinized to determine the practicability of the resulting specifications (fabrication, number of elements, size, etc.). Element type(s) are then selected. Element design criteria for atomization then become an analytical description of atomization for specific elements, which includes all variables affecting dropsize.

5.5.2.1 Self-Atomizing Fans. As determined in the previous section, for wax droplets the equation describing atomization is:

$$\overline{D}/d = 4.8\left(\frac{1}{We}\right)^{1/3} \qquad (5\text{-}61)$$

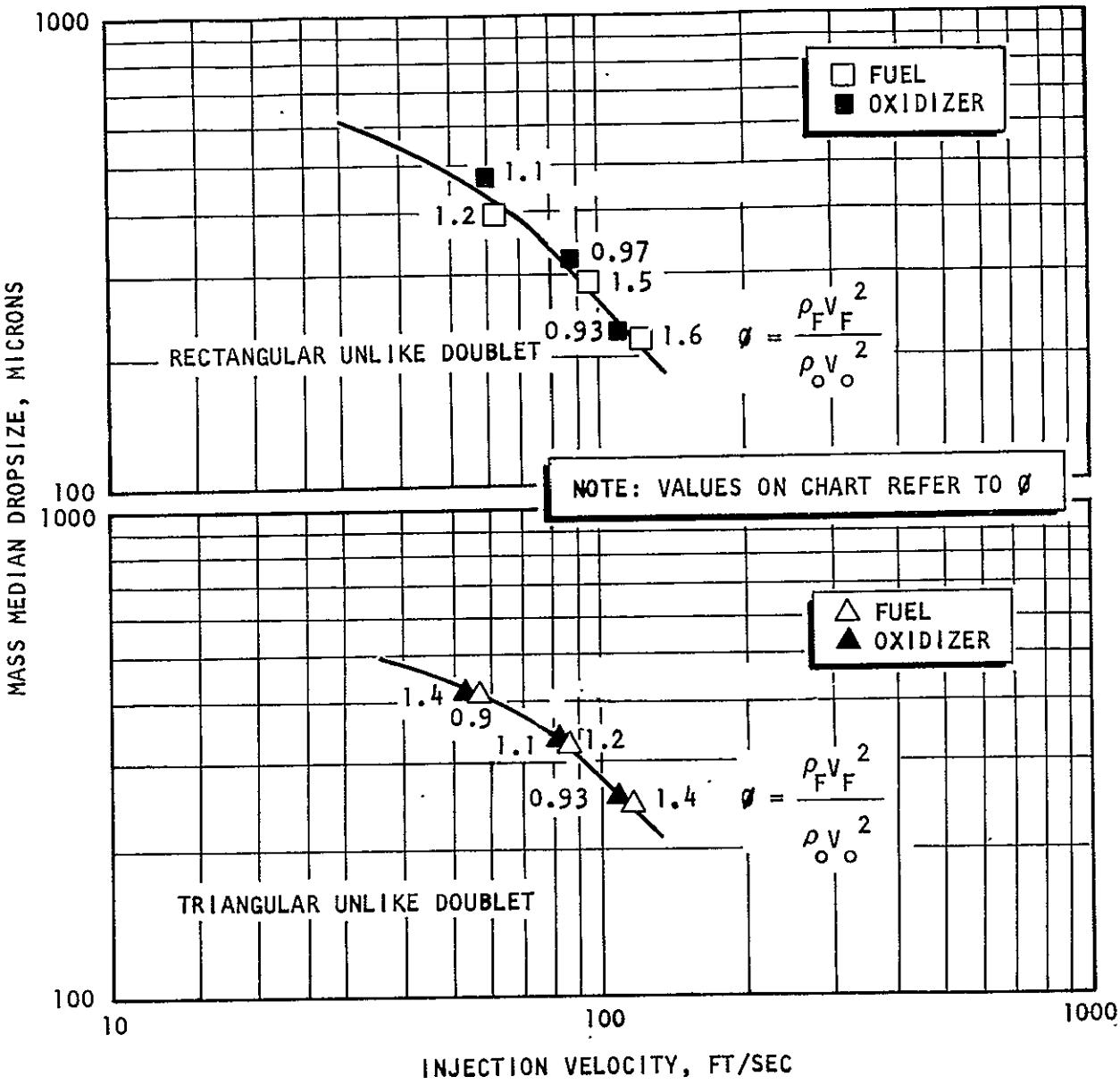

Figure 5-32. Effect of Injection Velocity on Mass Median Dropsize for Rectangular and Triangular Orifices (Simulant: wax/H_2O)

Use of Eq. 5-61 will provide the wax dropsize for zero velocity environmental gas. Since the results agree with those of Ref. 5-15, a proposed correction for physical properties is:

$$(\bar{D}/d)_{wax} \Big/ (\bar{D}/d)_{propellant} = \left[\frac{(\rho_L \mu_L)_{wax}}{(\rho_L \mu_L)_{propellant}} \right]^{1/6} \quad (5\text{-}62)$$

This correction should be adequate for the self-atomizing fan; however, caution should be used in extending it to other element types.

5.5.2.2 Unlike-Doublet Elements. Since detailed experiments were not conducted to develop empirical equations describing atomization characteristics for this element type, no design criteria can be specified. The data obtained are for a point design.

5.5.2.3 Unlike-Triplet Elements. For the unlike-triplet elements, a more extensive investigation was conducted; however, the results presented in Fig. 5-31 clearly show that the dropsize characteristics are nonlinear in log-log space. Consequently the best approach to determine dropsize for laminar jets is to directly use the results shown in Fig. 5-31.

5.5.3 Comparison of Atomization Characteristics for Circular and Noncircular Elements

The comparison of dropsize is done on the basis of cold-flow measured wax dropsizes. Because atomization for all of the unlike-doublet elements is dependent upon ϕ, a comparison of these elements is made at the value of ϕ, which is optimum for mixing. All elements under comparison have the same orifice area, although the shapes are different.

For all of the element types, except the triplet element, comparison of the wax dropsize characteristics for the fuel orifice is shown in Fig. 5-33 at equivalent thrust-per-element sizes. The results are shown in terms of the mass median dropsize as a function of injection velocity. The circular orifice unlike-doublet

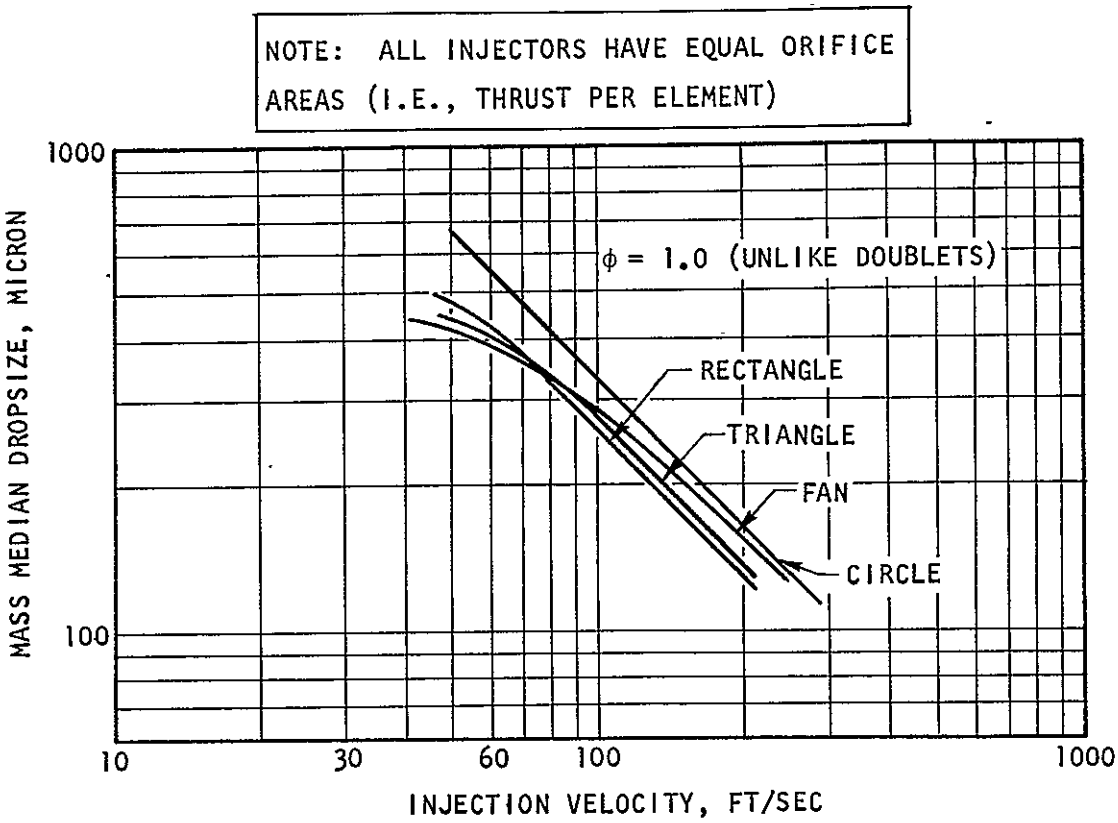

Figure 5-33. Comparison of Wax Dropsize Characteristics for Noncircular and Circular Orifice Designs

line was determined using Eq. 5-51. These results are for turbulent flowing orifices. Note that the circular unlike doublet produces dropsizes slightly larger than the noncircular designs. The smaller dropsizes produced by the noncircular designs are thought to occur due to total liquid contact across the entire width of the jets producing maximum momentum interchange.

The triplet element results were not included in Fig. 5-33 since they were primarily taken in the laminar flow regime. Most injectors operate in the turbulent flow regime so that the most valid comparison is for turbulent flow. However, since only laminar triplet data are available, a comparison between the circular orifice unlike doublet, triplet, and like doublet (laminar flow) was made. The results are presented in Fig. 5-34. Note that for laminar flow the triplet produced the largest dropsizes, while the like and unlike doublets produced the smallest. The L/D for these injectors is 50.

5.6 HOT-FIRE STUDIES

5.6.1 Experimental Results

Hot-firing experiments were conducted to gain information concerning the operational characteristics of single elements using the various orifice types under actual engine conditions.

Based on the results of cold-flow experimental studies, four injector elements were selected for the hot-fire evaluations. The element types chosen were:

1. Unlike-doublet circular orifices, sharp inlet, d_f/d_o = 0.89, L/D = 10
2. Unlike-doublet rectangular orifices, $(b_f/b_o)/AR_o$ = 0.736/2.72
3. Unlike-doublet triangular orifices, $(b_f/b_o)/AR_o$ = 0.736/1.12
4. Unlike-doublet, self-atomizing fan nozzle, 8006/8008 (see Table 5-5b)

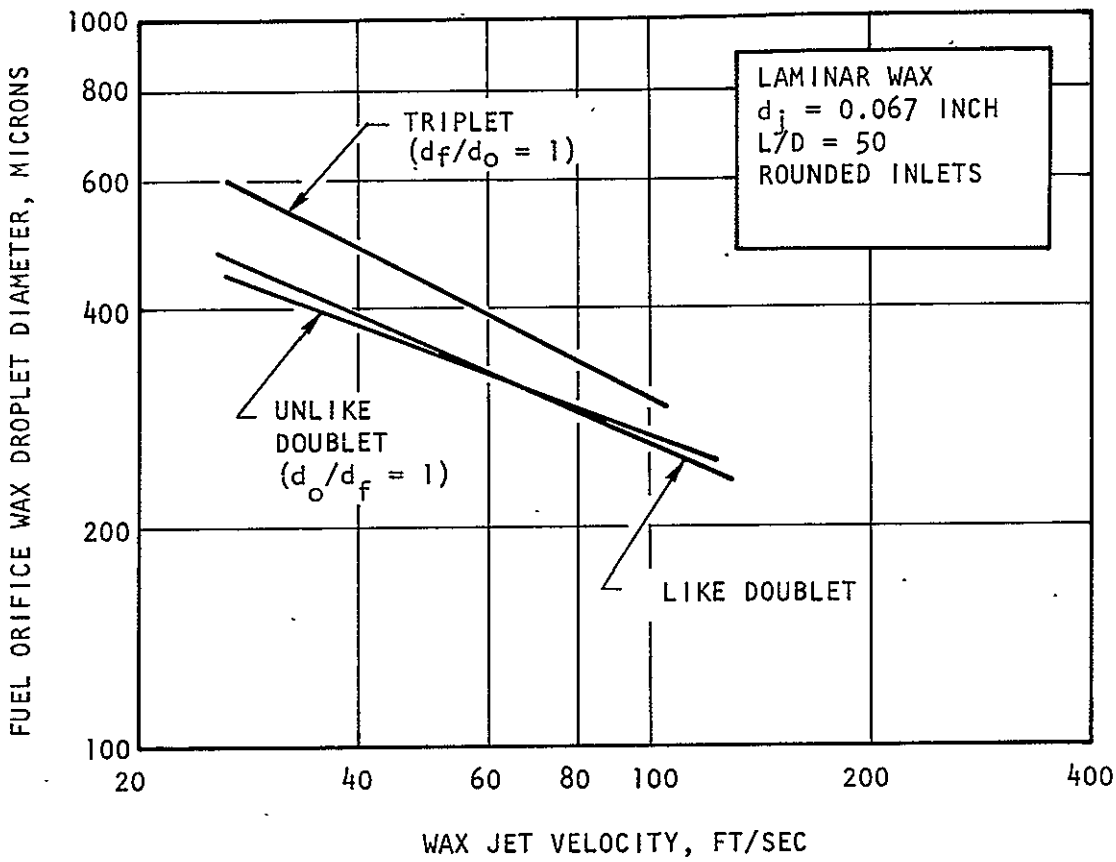

Figure 5-34. Comparison of Wax Droplet Diameters for a Triplet, an Unlike Doublet, and a Like Doublet for Laminar Flow (R_e < 10,000), Ref. 5-3

All of the foregoing configurations had orifice sizes identical to those previously cold-flow evaluated. The injectors were fired in a combustion chamber with contraction ratio, $\varepsilon_c = 4.0$.

5.6.1.1 Self-Atomizing Fan Element. Hot-firing test results for the self-atomizing fan are presented in Fig. 5-35, 5-36, and 5-37. Shown in these figures are the influence upon characteristic velocity efficiency of mixture ratio, characteristic chamber length, and chamber pressure.

Figure 5-35 shows the variation of η_{c^*} with mixture ratio for chamber (characteristic) lengths of 30 and 60 inches. For the tests shown, chamber pressure was approximately 100 psia. (Adjustments have been made by minor interpolation to 100 psia as noted.) Characteristic velocity efficiency (at L* = 30 inches) falls some 16 percentage points as mixture ratio is varied from 1.0 to 2.0. The same trend is suggested by the data for L* = 60 inches.

The improvement in η_{c^*} with L* suggested in Fig. 5-35 is amplified in Fig. 5-36. Here, η_{c^*} is shown as a function of L* for chamber pressure of 100 psia and mixtuer ratio close to 1.5. It may be noted that η_{c^*} increases from about 66 percent to slightly over 80 percent with an increase of L* from 15 to 60 inches. Extrapolation of these data to larger values of L* suggests that the maximum efficiency obtainable for the single element at $P_c = 100$, MR = 1.6 lies between 83 and 85 percent.

The variation of η_{c^*} with chamber pressure is depicted in Fig. 5-37 for L* = 30 inches and mixture ratio about 1.6. A striking improvement of efficiency with increased chamber pressure is noted. This increase is attributed mainly to improved mixing and atomization, resulting from higher injection velocities at elevated pressures rather than the absolute level of pressure. In this engine, the chamber throat area remained fixed as well as the injector orifice areas. Thus, increased pressure required increased flowrates and, subsequently, higher injection velocities

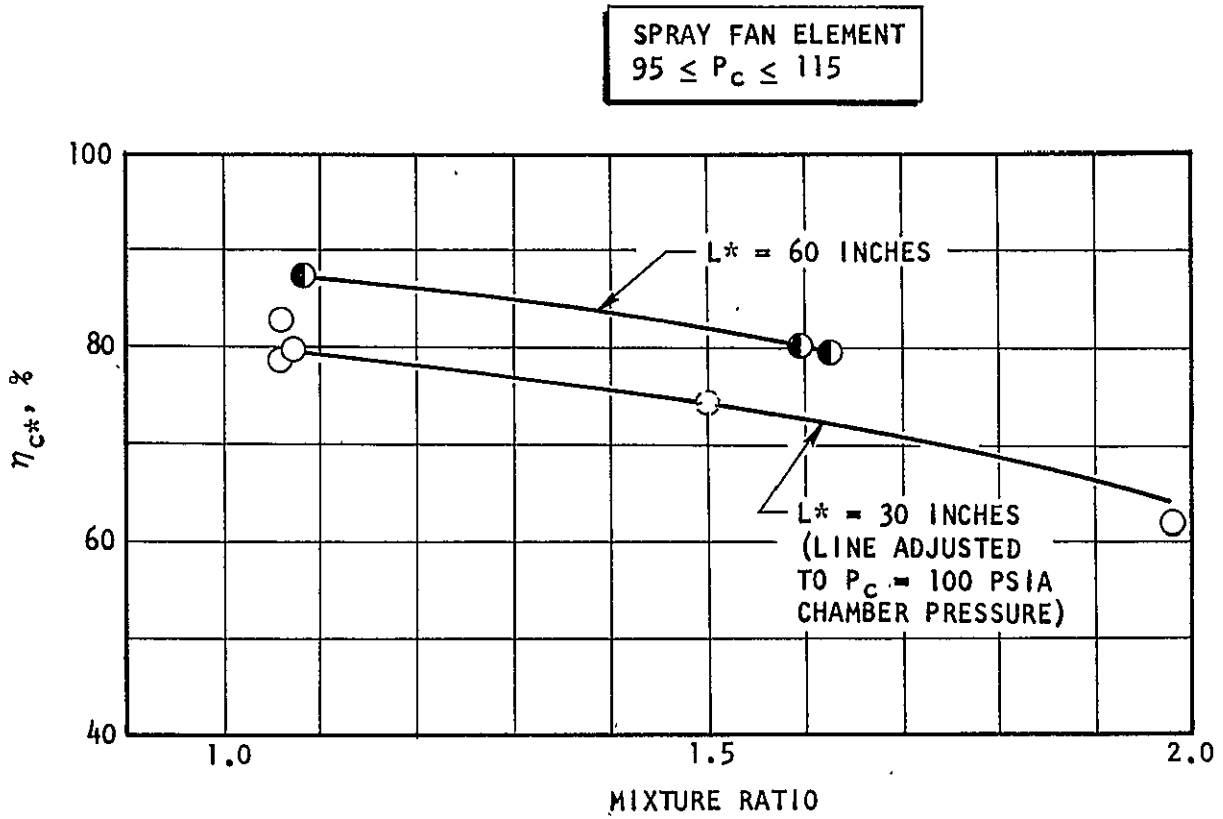

Figure 5-35. Variation of c* Efficiency With Mixture Ratio for the Spray Fan Element

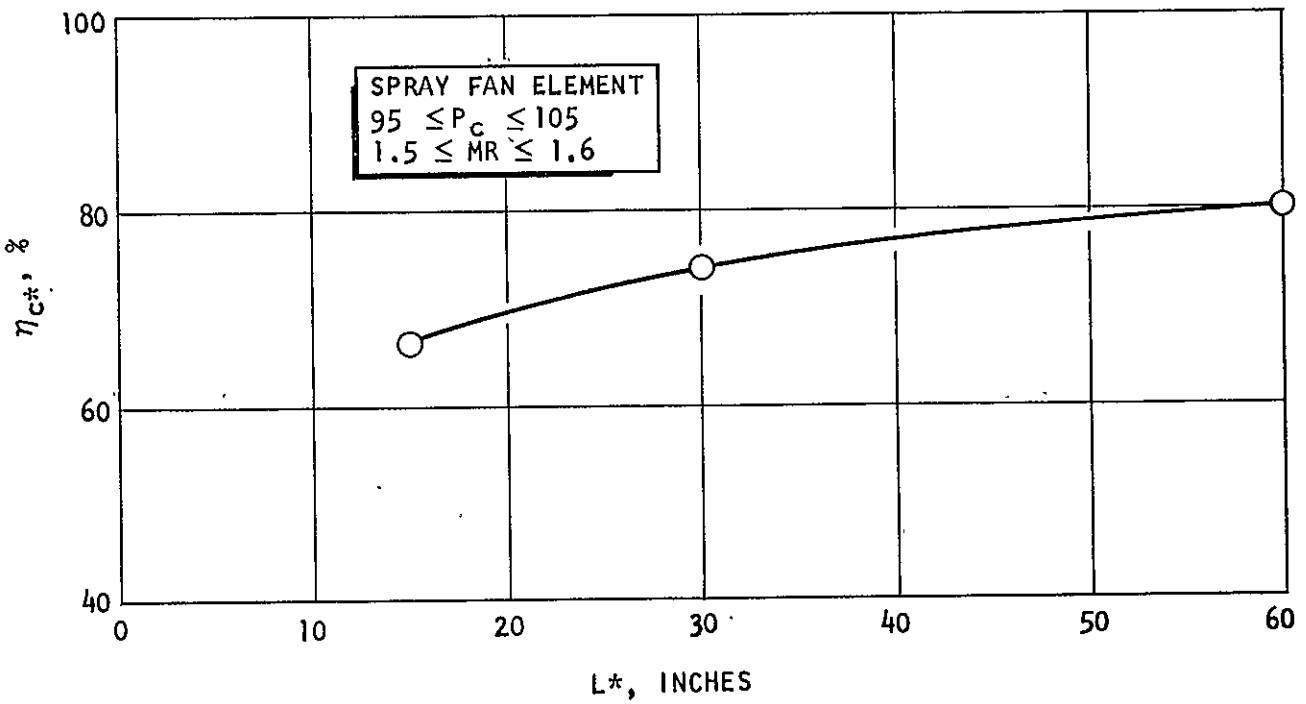

Figure 5-36. Variation of c* Efficiency With L* for the Spray Fan Element

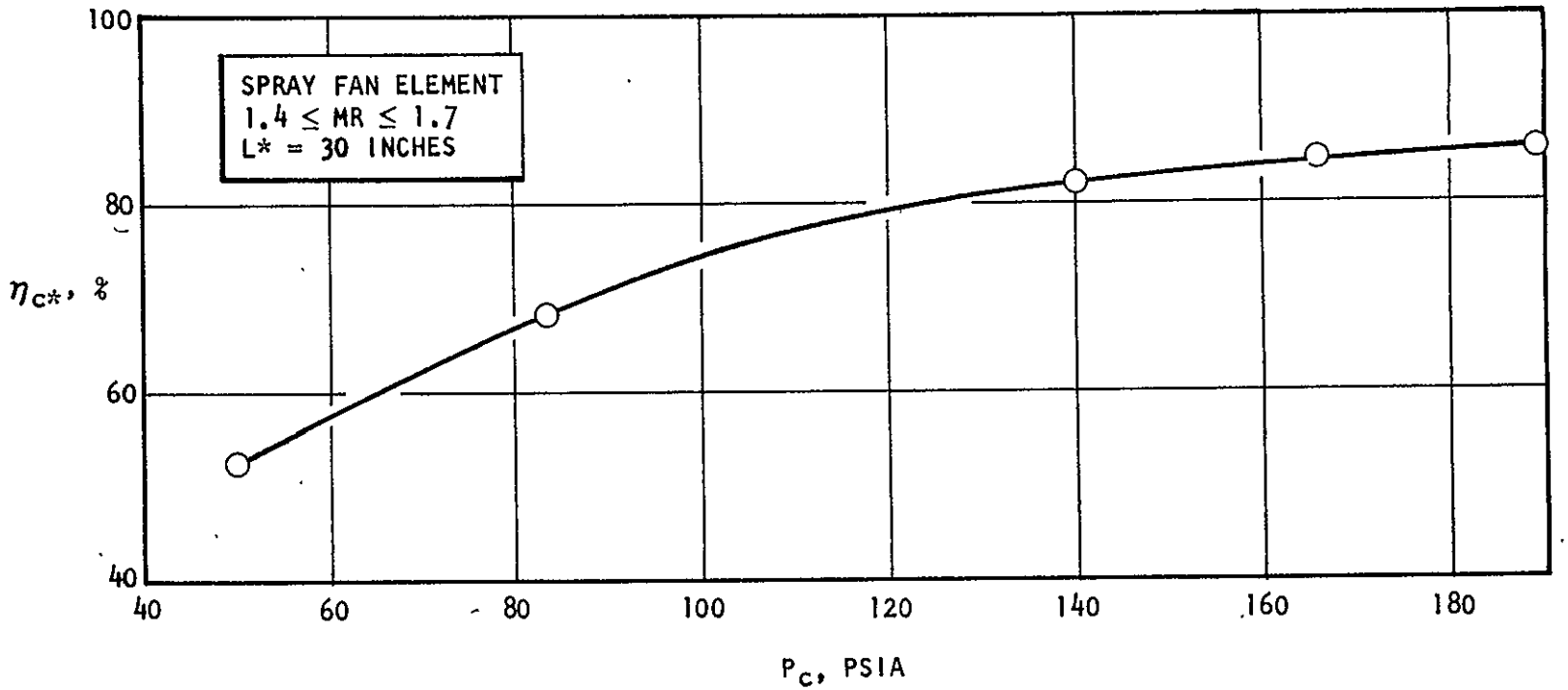

Figure 5-37. Variation of c* Efficiency With Chamber Pressure for the Spray Fan Element

5.6.1.2 Unlike-Doublet Elements. Characteristic velocity efficiency as a function of mixture ratio, L*, and P_c, respectively, for the three types of impinging jet unlike doublets is shown in Fig. 5-38, 5-39, and 5-40. These injectors were similar in design except for orifice shape. Orifice shapes tested were the circle, triangle, and rectangle. (Note that the circle-on-circle injector was tested with both sharp and rounded entrances to the orifices.)

It is evident from the data shown in Fig. 5-36 and 5-38 that the impinging jet unlike doublets have produced performance results that are quite different from those of the fan-type element. Rather than maximizing at "optimum" mixture ratio as suggested by cold flow, efficiency is actually lowest at this mixture ratio. Further, as noted in Fig. 5-38, performance for the impinging-type elements decreases with increasing chamber pressure, in contrast to the fan elements.

Variations of c* efficiency with characteristic chamber length are shown in Fig. 5-40 for P_c = 100 psia and MR = 1.5. As expected, efficiency increases significantly with increased L* from 15 to 60 inches. The efficiency for the rectangular orifice element increases some 16 percentage points while that of the triangular orifice element increased 22 percentage points.

5.6.2 Discussion of Hot-Fire Results

The selection of the elements to be evaluated under hot-fire conditions was determined on the basis of the cold-flow results. The cold-flow experiments provided design criteria for optimizing mixing and predicting wax dropsizes under stagnant conditions. On the basis of direct comparison of these results, the elements with the greatest potential for achieving high performance were chosen. The major hypothesis for this approach is that chemical reaction does not alter the mixing and atomization characteristics from those obtained under the nonreactive (cold-flow) conditions. The hot-fire results presented above clearly show that the unlike-doublet elements (both circular and noncircular) behaved contrary to all predictions while the self-atomizing fan performed as expected.

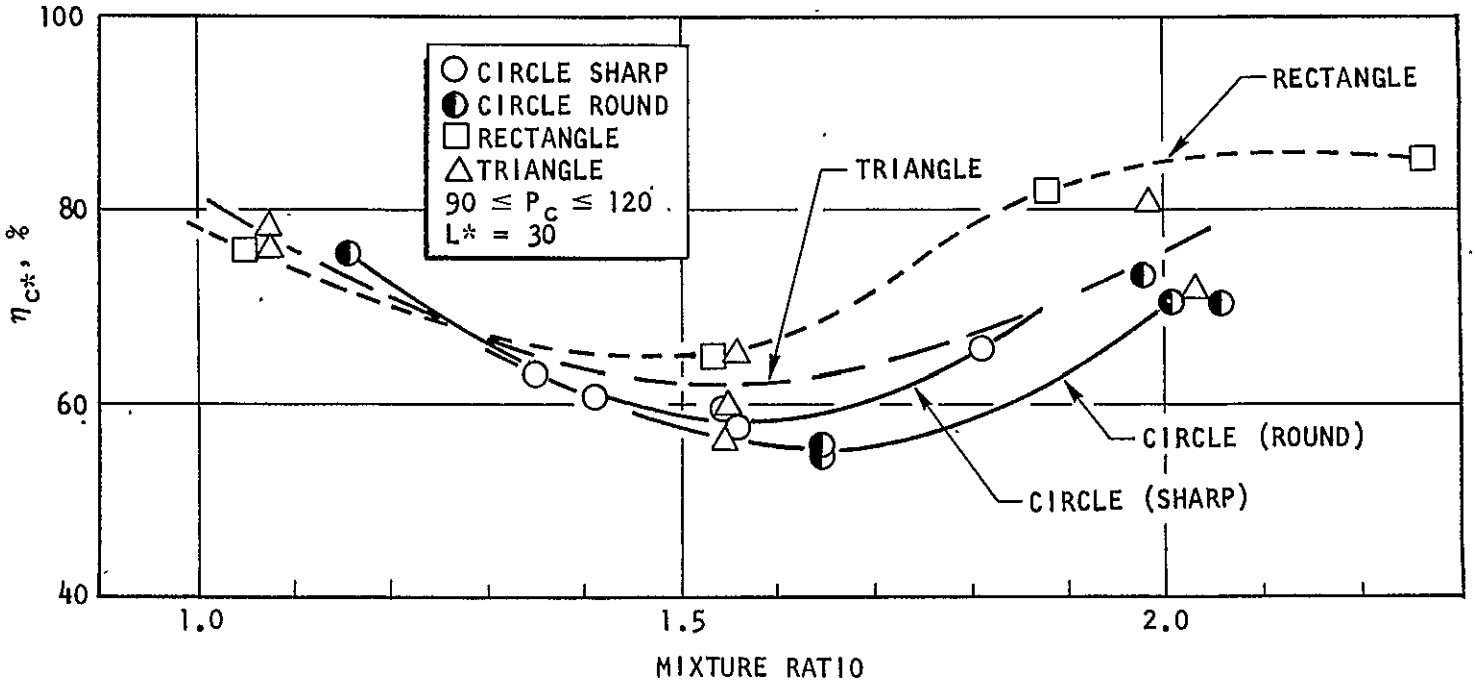

Figure 5-38. Variation of c* Efficiency With Mixture Ratio for Circular and Noncircular Unlike Doublets

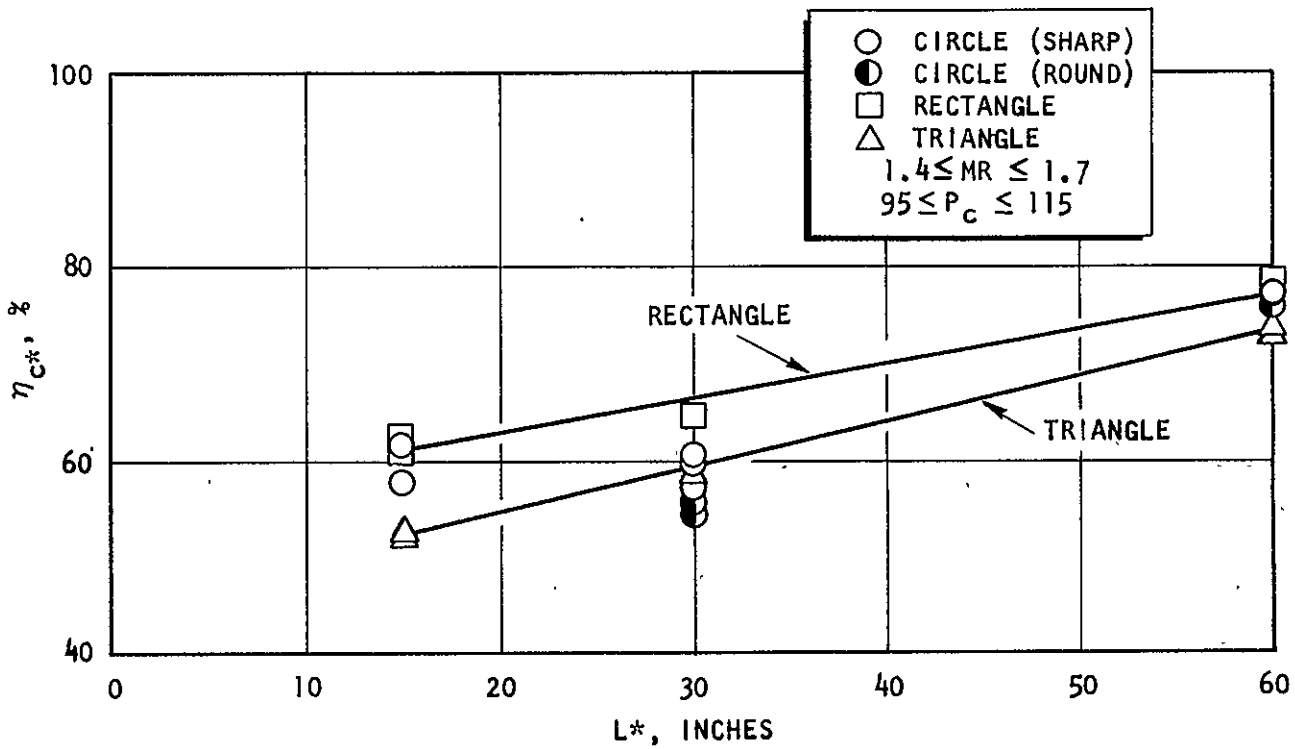

Figure 5-39. Variation of c* Efficiency With Characteristic Chamber Length for Circular and Noncircular Unlike Doublets

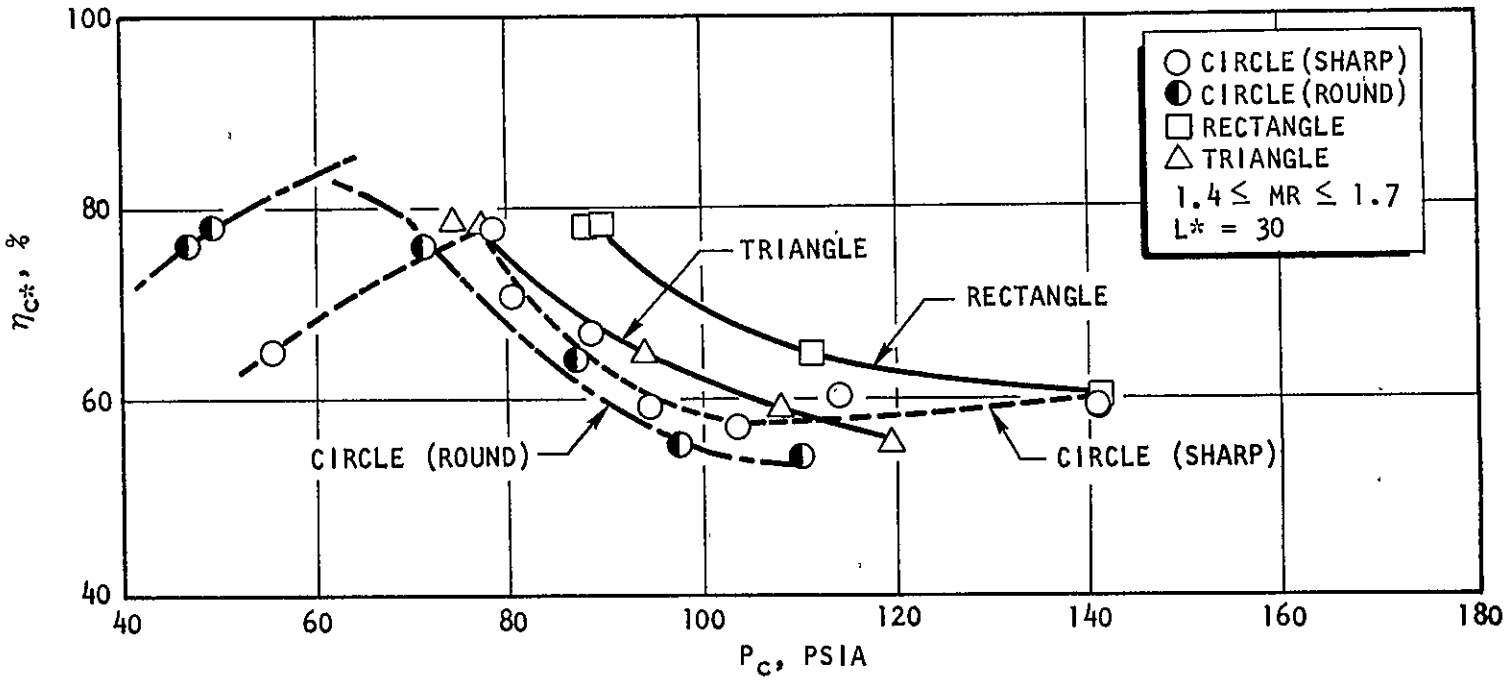

Figure 5-40. Variation of c* Efficiency With Chamber Pressure for Circular and Noncircular Unlike Doublets

5.6.2.1 Self-Atomizing Fan Element. In Fig. 5-41, the cold-flow mixing limited performance predictions for a mixture ratio of 1.1 and 1.6 at a chamber pressure of 100 psia are compared to those obtained in hot-firing experiments. The results are presented in terms of c* efficiency and chamber characteristic length (L*). (Unless vaporization has been completed, the level of c* efficiency measured in hot-fire testing is not representative of the mixing losses alone. Therefore, the most straightforward method of comparing the predicted levels of mixing with hot-fire data is to compare cold-flow predictions with hot-fire results obtained at a chamber length long enough that complete vaporization has occurred. (That is, the maximum level of c* efficiency obtained with increasing chamber length is dependent upon the level of mixing attained by the injector.) As shown in Fig. 5-41 excellent agreement is found between the cold-flow predicted mixing limited c* efficiency and the extrapolated values of the hot-fire results. The ability to predict the mixing-limited c* efficiency has been previously demonstrated (e.g., Ref. 5-5 and 5-6). The above result combined with previous data illustrates the accuracy of the cold-flow mixing technique and analytical model in predicting the level of mixing efficiency attainable in rocket engines.

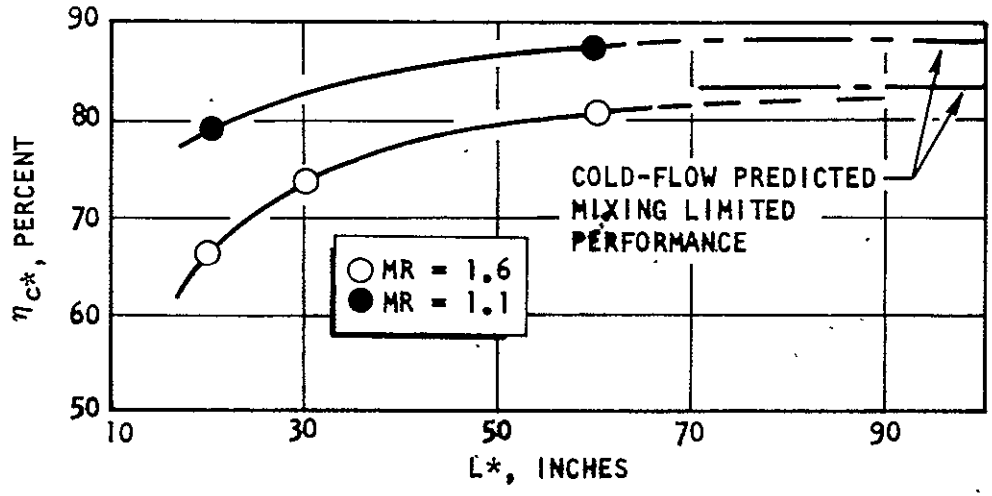

Figure 5-41. Comparison of Cold-Flow Predicted Mixing Limited c* Efficiency With Actual Hot-Fire Results; Self-Atomizing Fan

5.6.2.2 Unlike Doublets. Since the unlike-doublet elements directly impinge oxidizer on fuel jets, this configuration is susceptible to reactive stream separation (The self-atomizing fan on the other hand should mix as impacting droplets and/or ligaments and consequently should not experience reactive stream separation.) While no verified physical models exist for predicting reactive stream separation, considerable experimentation has been conducted. The results of these studies have demonstrated that two types of reactive stream separation can occur: steady state and cyclic or popping. The range of operating conditions and element geometry within these phenomena is certainly within the range covered in this study. Of importance to this study is that both the circular and the noncircular orifice elements experienced reactive stream separation. Since the mechanisms controlling blowapart are not well understood, it cannot be stated that noncircular orifice element designs do not exist that will result in blowapart-free operation.

The hot-fire results were analyzed to determine if the centerline momentum ratio (ϕ) or the dynamic pressure ratio (P_D) could be related to the loss in η_{c*} caused possibly by reactive stream separation. It was suggested by Clayton (Ref. 5-16) that popping was related to the hydraulic unsteadiness associated with impingement of equal dynamic pressure jets, and that at equal dynamic pressure ratios, the tendency to produce combustion disturbances is maximized. This conclusion was surprising since for the elements evaluated by Clayton, optimum mixing also occurred at equal dynamic pressure ratio. Since noncircular orifice elements do not necessarily optimize mixing when the P_D is unity, the results of this study were analyzed to determine the validity of that conclusion. Both the cold-flow and hot-fire results for the circular and rectangular element are compared in Fig. 5-42 in terms of ϕ and P_D. In the upper curves the cold-flow and hot-fire results are presented in terms of ϕ. Note that both element types provide optimum mixing at ϕ of 1. The hot-fire results show that for both elements the performance is a minimum at the point where optimum mixing occurred. suggesting that the more uniform the mixing the greater the tendency for reactive stream separation which resulted in a lowering of η_{c*}. In the lower curves, note that for the rectangular element, optimum mixing occurs at P_D of 1.4 while for the circle, the

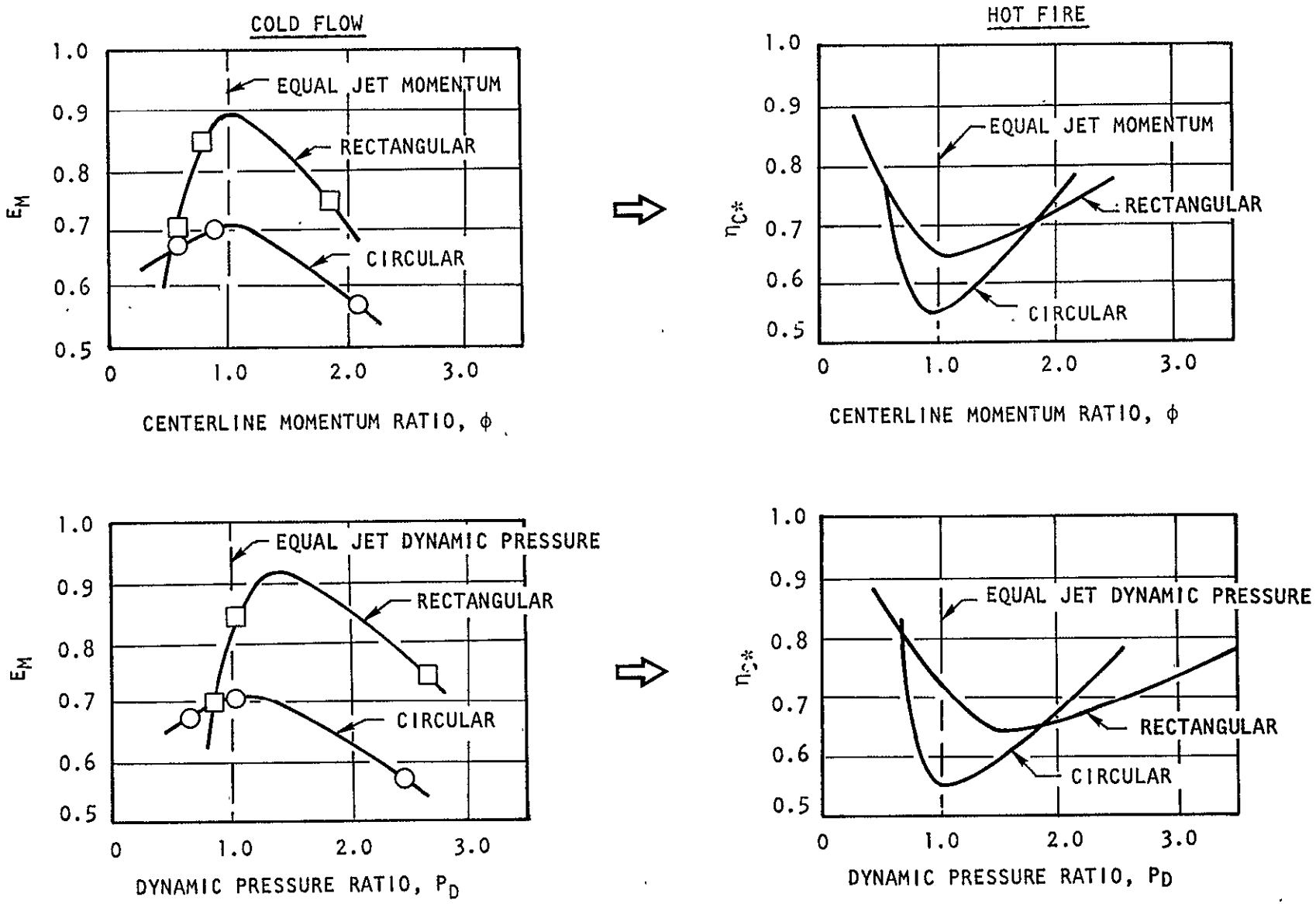

Figure 5-42. Comparison of Cold-Flow and Single-Element, Hot-Fire Results for Circular and Rectangular Unlike Doublets

optimum is at 1.0. The hot-fire results confirm that the lowered performance is related to mixing and not to dynamic pressure ratio since for the rectangular element the minimum performance occurred at P_D of 1.4 (at optimum E_m) rather than 1.0. On the basis of these results, it is unlikely that noncircular orifice unlike-doublet elements can afford added design flexibility that will result in the avoidance of reactive stream separation.

6.0 SINGLE-ELEMENT GAS/LIQUID STUDIES

The gas/liquid studies reported herein are composed primarily of cold-flow mixing, cold-flow atomization, and hot-fire experimental investigations of the effect of geometrical parameters upon the performance of rectangular concentric tube injector elements. (A small amount of cold-flow data was obtained for another element type, a showerhead triplet. Reporting of the results of that element is limited to a discussion at the end of the gas/liquid section to avoid confusion of the concentric tube presentation with another type of geometry.) To avoid unnecessary repetition of certain lengthy terms, a list of abbreviations to be employed throughout this section is presented in Table 6-1.

TABLE 6-1. LIST OF ABBREVIATIONS FOR GAS/LIQUID INJECTOR ELEMENT STUDIES

Term	Abbreviation
Gas/liquid	G/L
Rectangular Concentric Tube Element	RCTE
Circular Concentric Tube Element	CCTE
Showerhead Triplet Element	STE

6.1 TECHNICAL APPROACH

The technical approach adopted for the G/L study is outlined in block diagram from in Fig. 6-1.

The objective of the program was to determine experimentally the influence of element geometry upon injector performance employing the RCTE. To solve this problem, the concept of "performance" had to be broken down into fundamental components; one related to the quality of mixing provided by a given element and one related to the degree to which that element is capable of atomizing the liquid propellant. This was accomplished by assuming that thrust chamber c* efficiency

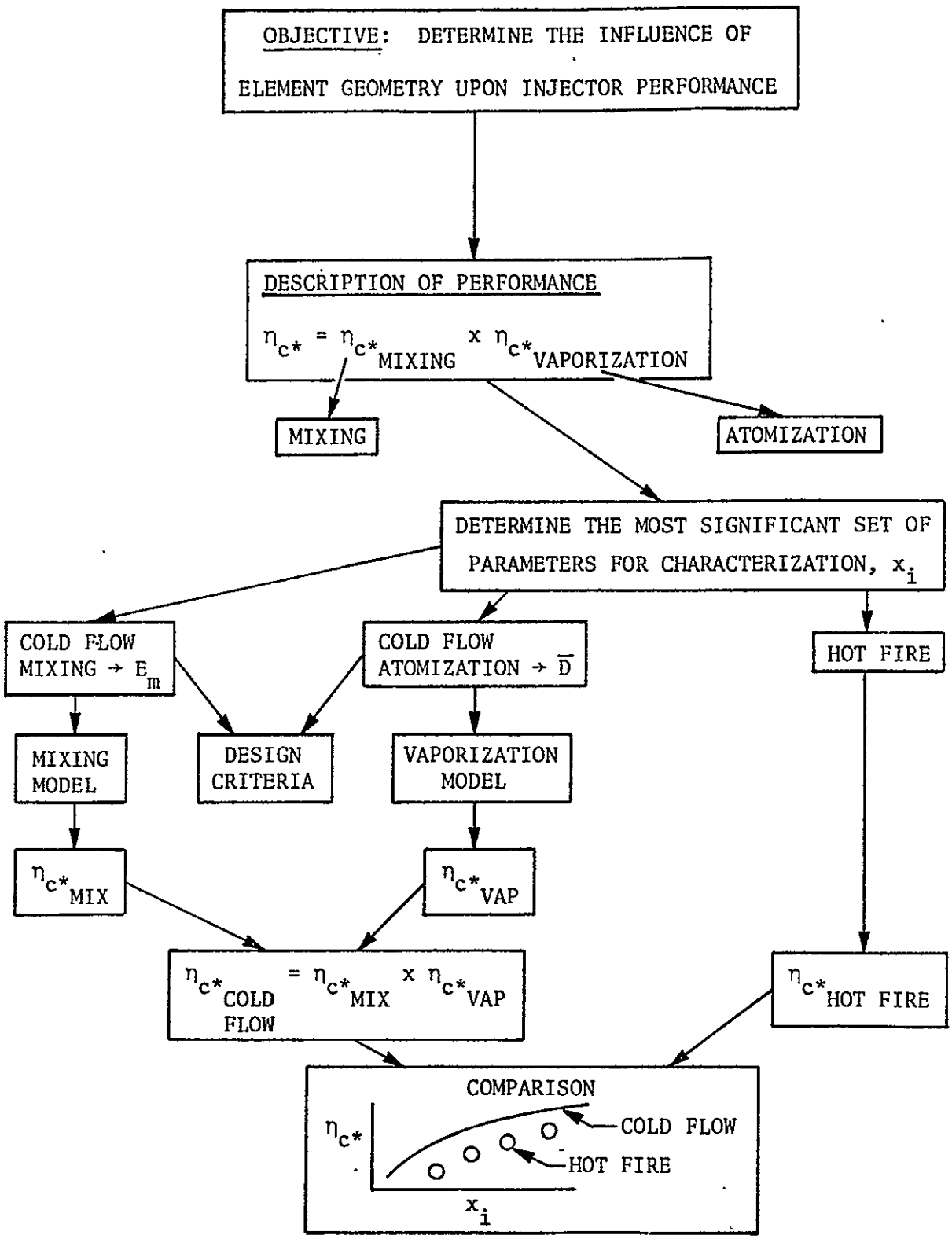

Figure 6-1. Technical Approach for the Characterization of Gas/ Liquid Rectangular Concentric Tube Injector Elements

is approximated, to the first order, by the product of a mixing limited and a vaporization limited c* efficiency (Fig. 6-1.). Under this assumption, the performance problem is greatly simplified and can be investigated along two essentially independent paths.

The next step in the approach was to single out those geometrical and operational parameters that (1) most influence the mixing and atomization processes, and (2) could be varied over significant ranges employing practical experimental techniques within the scope of the program. This was accomplished by the application of dimensional analysis.

With the selected parameters as guidelines, a set of model hardware and an experimental approach were formulated. The model hardware was designed to allow variation of the selected geometrical parameters. The experimental plan included independent cold-flow mixing, cold-flow atomization, and hot-fire experimentation.

Primary element comparisons and design criteria are obtained from the cold-flow results. The hot-fire experimentation was performed to ensure that the trends indicated by the cold-flow results were essentially correct.

To compare cold-flow and hot-fire performance trends, the cold-flow results were converted to equivalent mixing limited and vaporization limited c* efficiencies (see Appendix B). The product of these efficiencies was termed $\eta_{c^*_{C.F.}}$ and was compared to the hot-fire efficiency, $\eta_{c^*_{H.F}}$.

It was not the goal of this study to "predict" performance. However, the hot-fire trends must serve as a "yardstick" for the credibility of the cold-flow design criteria.

A CCTE was carried along throughout the program to serve as a basis of comparison for the RCTE results. It should be emphasized, in the beginning, that the comparisons between circular and rectangular G/L elements made in this report are not intended to imply that circular elements are either "worse" or "better" than noncircular overall ranges of injector design. These results should be viewed in

the light of changes in performance (at the conditions and over the ranges stipulated in this document) produced by variations of shape alone.

6.2 DEFINITION OF SIGNIFICANT PARAMETERS AND TEST PLAN FORMULATION

6.2.1 Dimensional Analysis

As could be envisioned, intuitively, the mixing and atomization processes associated with concentric tube injector elements are highly complex. To single out the individual parameters that should most influence these processes, the method of dimensional analysis was applied to the problem. This method, attributed to Buckingham, stipulates that if there are M physical parameters involving N dimensions, then there are M-N dimensionless groups that will completely characterize the physical problem.

The first task in the development of a dimensional analysis is to identify all of the parameters involved in the problem. Great care must be taken to ensure that all of the parameters are included. At this point, a discussion of the flowfield and the physics associated with concentric tube element mixing and atomization is appropriate

Injector face geometries for both a CCTE and a RCTE are shown in Fig. 6-2 and a cross section of a concentric tube element with physical processes identified is presented in Fig. 6-3. The standard concentric tube element (often called coaxial element) is composed of a single tube within a larger orifice. Liquid, usually oxidizer, is injected through this central tube while gas, usually fuel, is injected through the annulus between the central post and the orifice (Fig. 6-3). Atomization of the liquid and subsequent mixing of the gas and liquid is produced by shear between the gas and liquid. The bulk of the energy required for the mixing and atomization processes is provided in the gas component in the form of velocity head

In many cases, the performance of the elements may be improved by recessing the the central tube (Fig. 6-3) to allow more efficient momentum (or energy) exchange between the two fluids. There are situations, however, in which recess can be detrimental, either from a performance or a hardware compatibility standpoint.

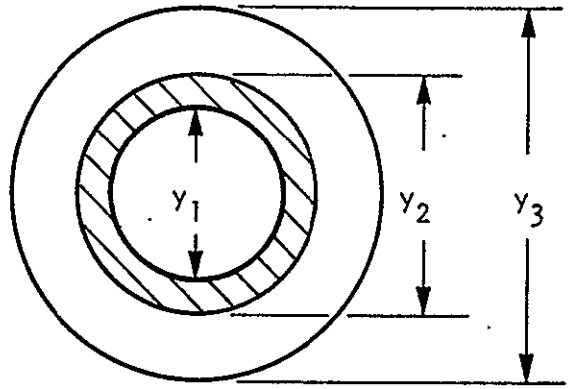

(a) CIRCULAR

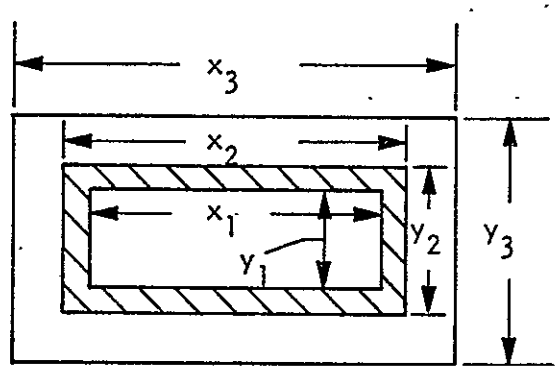

(b) RECTANGULAR

Figure 6-2. Typical Face Geometry for Circular and Rectangular Concentric Tube Elements

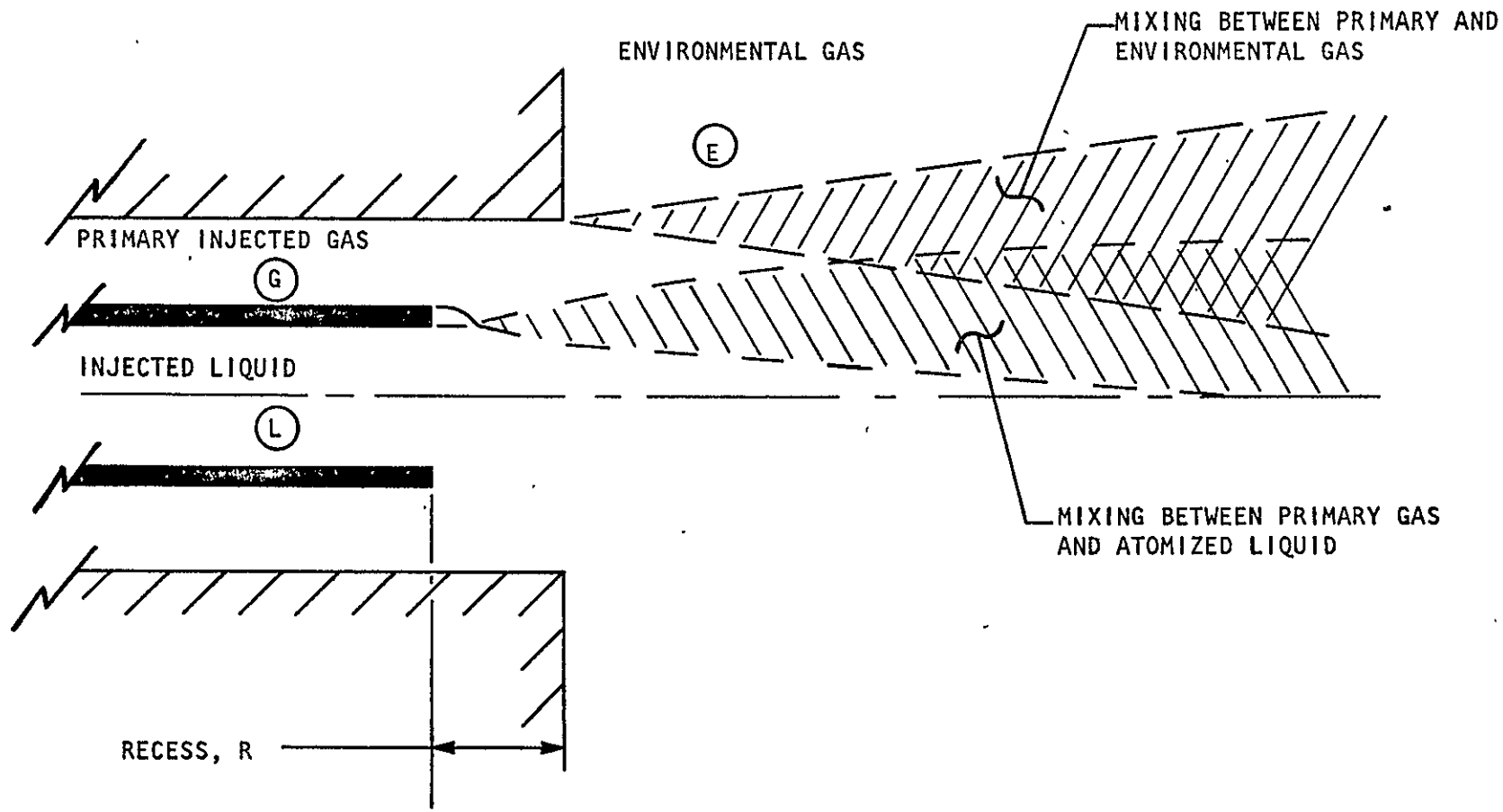

R-9271
154

Figure 6-3. Typical Concentric Tube Element Flowfield

These situations arrise at extremely low mixture ratios ($\dot{\omega}_L/\dot{\omega}_G \leq 1$). Recess causes the liquid to be drawn out through the gas to the outer edge creating a high mixture ratio at walls.

With the physical processes in mind, it is very important to note that there is a significant difference between a cold-flow model of these processes and the actual operation of an element with chemically reactive propellants. In the cold-flow situation there is no vaporization of the liquid component and there is no energy release due to combustion. Thus, cold-flow results should not be expected to "predict" levels of performance exactly. However, cold-flow trends in performance with the geometrical and operational variables should be representative of actual trends. These modeling restrictions are not as important in the cold-flow modeling of liquid/liquid injector processes due to the fact that the majority of the mixing and atomization of liquid/liquid propellants occurs before significant combustion interaction.

In addition to the primary mixing of the injected liquid and gas components, there is a competitive mixing of the environmental gas with the injected gas. This secondary mixing is detrimental to the performance of the element as it severly degrades the momentum of the primary gas jet. The importance of the secondary mixing is diminished, however, with increased central tube recess.

The variables that were selected as representative of the concentric tube element performance are listed in Table 6-2, along with their basic physical dimensions. Many variables have been eliminated from the analysis. For example, the compressibility of the liquid has been neglected, gravitational forces have been neglected, and all temperatures, specified heats, and thus heat transfer have been neglected. In all, there are 19 variables considered, having a total of three dimensions. According to the Buckingham π theorem (see Ref. 6-1), with M = 19 variables and N = 3 dimensions, there are 19-3 = 16 dimensionless groups that will completely characterize the problem.

The results of the dimensional analysis are presented in Table 6-3. These groups are the fundamental groups. More meaningful combinations can be obtained by

combining two or more groups and replacing one of the variables employed in the new group. For example, the mixing of the primary gas with the environment is a free turbulent mixing process and is little dependent upon the viscosity of the gases (Reynolds number). A better group may be $(\rho_G V_G - \rho_E V_E)/\rho_G V_G$ to replace V_E/V_G. However, no attempt has been made in this report to regroup the variables a priori. Reather, the quantities that appear in the groups, which could be varied were studied, and the results used to suggest which dimensionless groups would be most appropriate.

It is obvious upon inspection of the results shown in Table 6-3 that the task of investigating the concentric tube flow-field is formidable. Therefore, the next task in the formulation of the experimental approach was to significantly reduce the number of variables for further study.

TABLE 6-2. PHYSICAL VARIABLES AND THEIR DIMENSIONS

Variable	Liquid	Gas	Environment	Dimensions*
Geometry	X_1, X_2, X_3, y_1, y_2, y_3, R			L
Density	ρ_L	ρ_G	ρ_E	ML^{-3}
Velocity	V_L	V_G	V_E	LT^{-1}
Compressibility		K_G	K_E	$ML^{-1}\ T^{-2}$
Viscosity	μ_L	μ_G	μ_E	$ML^{-1}\ T^{-1}$
Surface Tension	σ_L			MT^{-2}

*M = mass
L = length
T = time

TABLE 6-3. DIMENSIONLESS GROUPS REQUIRED FOR THE DESCRIPTION OF GAS/LIQUID CONCENTRIC TUBE ELEMENT MIXING AND ATOMIZATION

Group No.	Group	Name and Type
1	x_1/y_1 (Aspect Ratio)	Geometry
2	x_2/y_2	
3	x_3/y_3	
4	y_2/y_1	
5	y_3/y_2	
6	R/y_1 (Relative Recess)	
7	ρ_g/ρ_L	Density Ratio
8	ρ_E/ρ_G	Density Ratio
9	V_G/V_L	Velocity Ratio
10	V_E/V_G	
11	$\rho_G V_G (y_3-y_2) /\mu_G$	Reynolds Number
12	$\rho_L V_L (y_1) /\mu_L$	Reynolds Number
13	$\rho_E (V_G-V_E) y_3/\mu_E$	
14	$V_G/ \sqrt{K_G/\rho_G}$	Mach Number
15	$V_E/ \sqrt{K_E/\rho_E}$	Mach Number
16	$\rho_G (V_G-V_L)^2 y_1/\sigma_L$	Weber Number

Since most of the basic results to be generated under this contract would come from cold flow, it was natural, first, to examine which of the parameters involved in the problem could be varied over a significant range and yet maintain the study within the scope of the contract.

Realistically, the only parameters that could be varied included the geometry, the gas density, the gas velocity, and the liquid velocity. These parameters were, therefore, selected as the primary experimental variables. Since all the dimensionless groups could not be varied, independently, it was decided that presentation of the results in terms of any of these groups would be inappropriate unless justification could be presented. Thus, only in the case of certain of the geometri groups, are results presented in dimensionless form. However, where possible, the results are employed to suggest which terms should be investigated in more detail.

In addition to these restrictions, it was also decided that the scope of the program did not allow an independent variation of all of the geometrical groups. The rationale employed to limit the experimental scope and the basis of the test plan are presented in the next section.

6.2.2 Test Plan Formulation

In formulating the test plan, the most important consideration was the original objective of the study: "determine the influence of shape upon the performance of concentric tube injector elements". Therefore, the first question that one should ask is, "Exactly what does a rectangular concentric tube element accomplish that a circular element cannot?".

Study of Table 6-3 will show that all of the groups can be varied equally well by either a CCTE or a RCTE except groups No. 1, 2, and 3. It is clear, upon reference to Fig. 6-2 that these groups are available only to RCTE's. Thus, these three groups embody the only possible advantages or disadvantages available with non-circular (rectangular) shape.

The experimental plan, therefore, was limited to a parametric variation of these geometrical groups at a nominal baseline set of operating conditions. Some variations about the nominal conditions were selected to show relative sensitivity of the various elements. However, the restriction to baseline conditions was necessary, again, to reduce scope.

Operating conditons selected as baseline are those of an 800-psia chamber pressure, liquid oxygen, gaseous hydrogen (LOX/GH_2) rocket engine with contraction ratio approximately 2.3:1 and nominal flow per element of 0.43 lb/sec. A listing of the baseline conditions is presented as Table 6-4.

TABLE 6-4. BASELINE OPERATIONAL PARAMETERS

Parameter	Symbol	Nominal Value
Chamber Pressure, psia	P_C	800
Propellant Properties		LOX/GH_2
Mixture Ratio	MR	6
Gas Density, lbm/ft^3	ρ_G	0.27
Liquid Density, lbm/ft^3	ρ_L	70
Chamber Contraction Ratio	ε_c	≈ 2.3
Flow Per Element, lbm/sec	$\dot{W}_T$	0.432
Fuel Injection Velocity (gas), ft/sec	V_G	≈ 1000
Oxidizer Injection Velocity, liquid, lbm/sec	V_L	≈ 50

The set of concetric tube elements selected for experimental evaluation is shown in Fig. 6-4 to relative scale (letters and numbers appearing under each element are element code numbers).

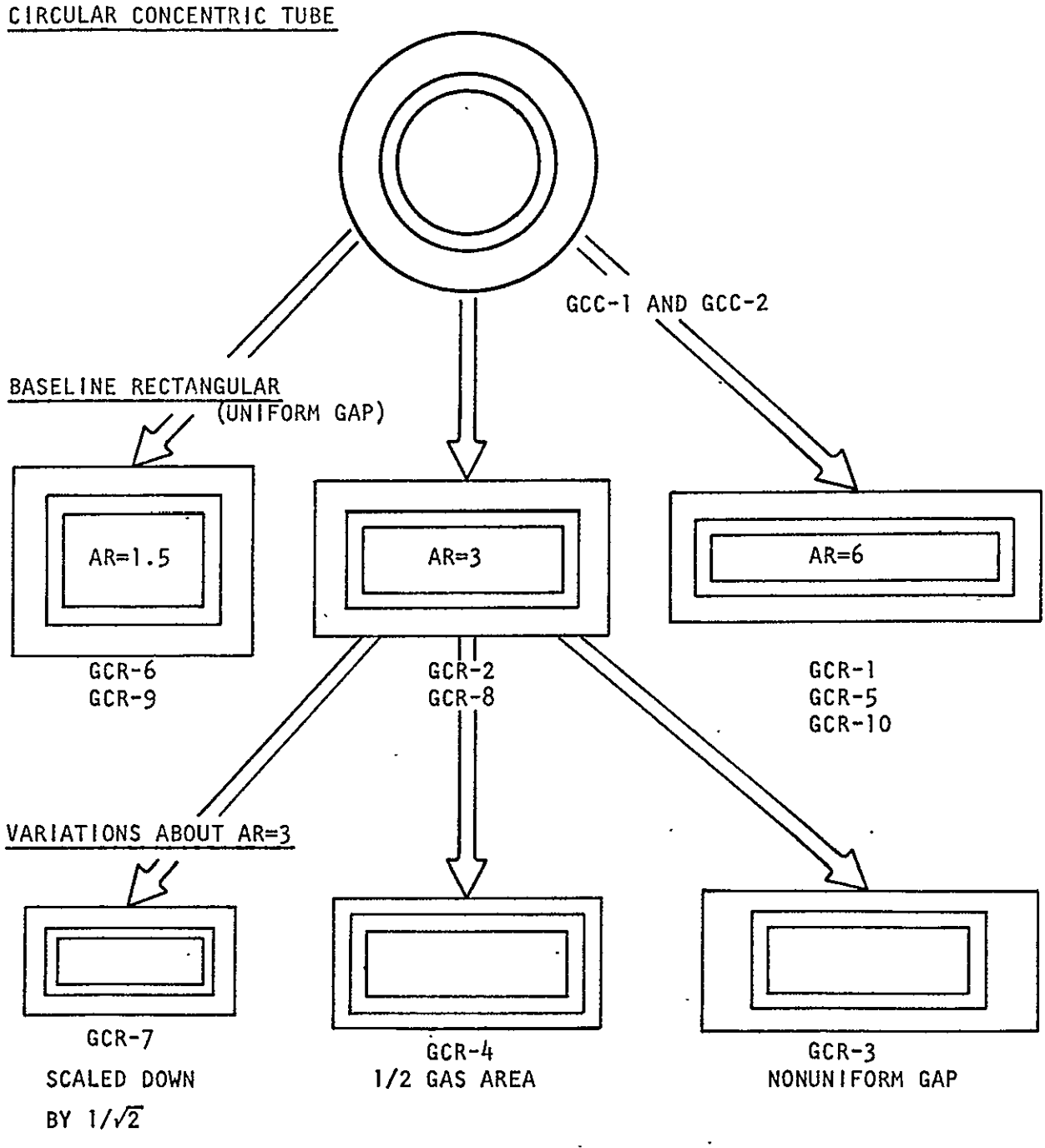

Figure 6-4. Rectangular Concentric Tube Element Comparisons

The element comparison was accomplished in two stages: (1) comparison between a CCTE and "baseline" RCTE's, and (2) a comparison of one baseline RCTE with three variations of geometrical parameters about this baseline (Fig. 6-4).

The primary geometrical variable selected for comparison is the liquid orifice dimension ratio, x_1/y_1 termed the element aspect ratio (AR) (see Fig. 6-2). Values of 1.5, 3.0 and 6.0 were chosen for this ratio. Certain ground rules were established for the primary baseline comparison; all baseline liquid areas were equal, all baseline gas annulus areas were equal, gas annulus gap was uniform, and all central tube wall thickness were equal. This was stipulated to ensure that all baseline elements would produce respectively equal gas velocities and liquid velocities at the baseline operating conditions. The equivalence of post tube wall thickness was a fabrication consideration.

Under these ground rules, all the geometrical dimensionless groups become directly related to the aspect ratio, x_1/y_1.

The central post aspect ratio of 3.0 was selected for further parametric study. These additional elements are labeled "variations about AR = 3" in Fig. 6-4. One of these elements, GCR-7, is a direct scale model of the baseline AR = 3 element, reduced by a factor of $1/\sqrt{2.}$ This reduces all of the areas by a factor of 1/2. The other two variations, GCR-4 and GCR-3, employ the exact center post of GCR-2 (basic AR = 3 element) and have respectively one-half the gas annulus area (uniform gap), and a nonuniform gas gap (same gas area as GCR-2), see Fig. 6-4.

These latter three variations were designed to test the effects of element size, velocity ratio, and nonuniform gas annulus distribution upon performance.

A complete list of all of the elements, their dimensions, and the objective of each is presented as Table 6-5. (Two additional elements, GST-1 and GST-2, appear in Table 6-5. These are the "showerhead triplet elements" and are discussed in a separate section at the end of major section 3.0.) The code number meaning is explained in Table 6-5. The hardware designed to implement the test plan is described in Ref. 6-3.

TABLE 6-5. GAS/LIQUID ELEMENT GEOMETRY

(See also Fig. 6-2 and 6-4)

Element* Code No.	x_1 (in.)	x_2 (in.)	x_3 (in.)	y_1 (in.)	y_2 (in.)	y_3 (in.)	Aspect Ratio x_1/y_1	Gas Area $(x_3/y_3 - x_2/y_2)$	Liquid Area x_1/y_1	Element Description
GCC-1	0.160	0.200	0.305	0.160	0.200	0.305	1.0	0.0416	0.0201	Circular concentric tube from Phase II
GCC-2	0.1604	0.2005	0.292	0.1604	0.2005	0.292	1.0	0.0354	0.0202	Circular concentric tube from Phase III
GCR-1	0.346	0.386	0.450	0.058	0.098	0.162	5.97	0.0351	0.0201	Rectangular concentric tube from Phase II, AR=6
GCR-2	0.245	0.286	0.3592	0.0825	0.1211	0.1936	2.97	0.0349	0.0202	Baseline RCTE, uniform gap, AR=3
GCR-3	0.245	0.286	0.4039	0.0825	0.1211	0.1721	2.97	0.0349	0.0202	Nonuniform gas gap, AR=3
GCR-4	0.245	0.286	0.3249	0.0825	0.1211	0.1615	2.97	0.0178	0.0202	1/2 baseline gas area, AR=3
GCR-5	0.350	0.3876	0.4518	0.0595	0.0981	0.1625	5.88	0.0354	0.0208	Baseline RCTE, uniform gap, AR=6
GCR-6	0.1735	0.2122	0.2922	0.1165	0.1611	0.2333	1.49	0.0340	0.0202	Baseline RCTE, uniform gap, AR=1.5
GCR-7	0.1750	0.2020	0.2535	0.058	0.0851	0.1379	3.02	0.0178	0.0101	$1/\sqrt{2}$ scale model of GCR-2
GCR-8	0.2450	0.286	0.3590	0.0825	0.1211	0.1950	2.97	0.0354	0.0202	Remake of GCR-2 with copper gas port for hot fire
GCR-9	0.1735	0.2122	0.2903	0.1165	0.1611	0.2350	1.49	0.0340	0.0202	Remake of GCR-6 with copper gas port for hot fire
GCR-10	0.350	0.3876	0.450	0.0595	0.0981	0.1620	5.88	0.0349	0.0208	Remake of GCR-5 with copper gas port for hot fire
	x_1 (in.)			y_1 (in.)	D_j (in.)					
GST-1	0.320	---	---	0.055	0.020	---	5.82	0.0352	0.0088	Showerhead triplet with 28 each 0.020 in. dia. orifices
GST-2	0.320	---	---	0.055	0.030	---	5.82	0.0352	0.0088	Showerhead triplet with 12 each 0.030 in. dia. orifices

*Code No. Definition

GCC ≡ Gas/Liquid Concentric Tube - Circular

GCR ≡ Gas/Liquid Concentric Tube - Rectangular

GST ≡ Gas/Liquid Showerhead Triplet

6.3 EXPERIMENTAL RESULTS

All gas/liquid experimental results are presented in this section. These include cold-flow mixing, cold-flow atomization, and hot-fire results. Cold-flow mixing results are presented in terms of the mixture ratio uniformity parameter, E_m (see Appendix B), cold-flow atomization results are presented in terms of the mass median droplet diameter, $\overline{D}$ and the hot-fire results are presented in terms of η_{c^*}. In the section devoted to correlation of the results, cold-flow results are transformed from E_m and $\overline{D}$ into $\eta_{c^* \text{ mix}}$ and $\eta_{c^* \text{vap}}$ by means of analytical combustion models (see Appendix B).

The format of the presentation will be the same for all three sections and is listed below. (The discussion of the hot-fire results does not include a "Generalization of the Results" section.)

1. Nominal Conditions (Baseline Comparisons)
2. Variations About AR = 3
3. Generalization of the Results

This format has been adopted to focus attention upon the primary objective of the study, the determination of the effect of element shape upon injector performance at a fixed set of nominal conditions. A broad discussion of methods of generalizing the results is incorporated in separate material at the end of each section and may either be studied or ignored and will not influence the general results of the program. These generalizations are highly interesting and important and warrant incorporation in the report, however; it is suggested that they be studied upon and a second reading of the report, if desired.

The nominal, or baseline conditions are listed in Table 6-4 and the element comparison scheme has been outlined in Fig. 6-4.

6.3.1 Mixing Studies

The objective of the mixing studies was to determine the effect of element geometry and to some extent, operational parameters upon the mixture ratio uniformity parameter, E_m (see Appendix B). Mass fluxes and mixture ratios at discrete points in the flowfield produced by a given element were measured by means of a two-phase sampling probe that was positioned 2 inches downstream of the injector element exhaust plane. None of the Phase II mixing results are included in this presentation as these data were obtained at a sampling distance of 5 inches. Since mixing efficiency is a function of length, the two sets of data cannot be compared on a one-to-one basis.

All of the Phase III mixing cold-flow data are presented in Ref. 6-2.

6.3.1.1 Nominal Conditions (Baseline Comparison). The mixing results for four baseline injector elements are presented in Fig. 6-5. Data, E_m, are plotted with respect to actual centerpost recess in Fig. 6-5a and with respect to relative recess, R/y_1, in Fig. 6-5b. The relative recess appears to offer the better representation of the results. A cross plot of Fig. 6-5b is presented as Fig. 6-6 wherein E_m is shown as a function of aspect ratio, x_1/y_1, for constant values of centerpost recess. (Note. Results presented at aspect ratio unity are those for a circular concentric tube element, not a rectangular element of aspect ratio unity.

The representations of Fig. 6-6 show that the quality of mixture ratio uniformity improves dramatically with increased aspect ratio at the nominal operating conditions. This result was so interesting that a more detailed analysis of the data was undertaken in an attempt to explain exactly how the change in shape, alone, could improve the mixing to such a degree. The results of this extended analysis are presented in Fig. 6-7 and 6-8.

In these two figures, mass fraction flux (mff), mass fraction per unit area, contours for the liquid and the gas component are shown for each of the four elements at zero recess. (The mass fraction flux is computed by dividing the local value of the mass flux of the i^{th} component, $\dot{W}_i/A$, (liquid or gas) by the total injected

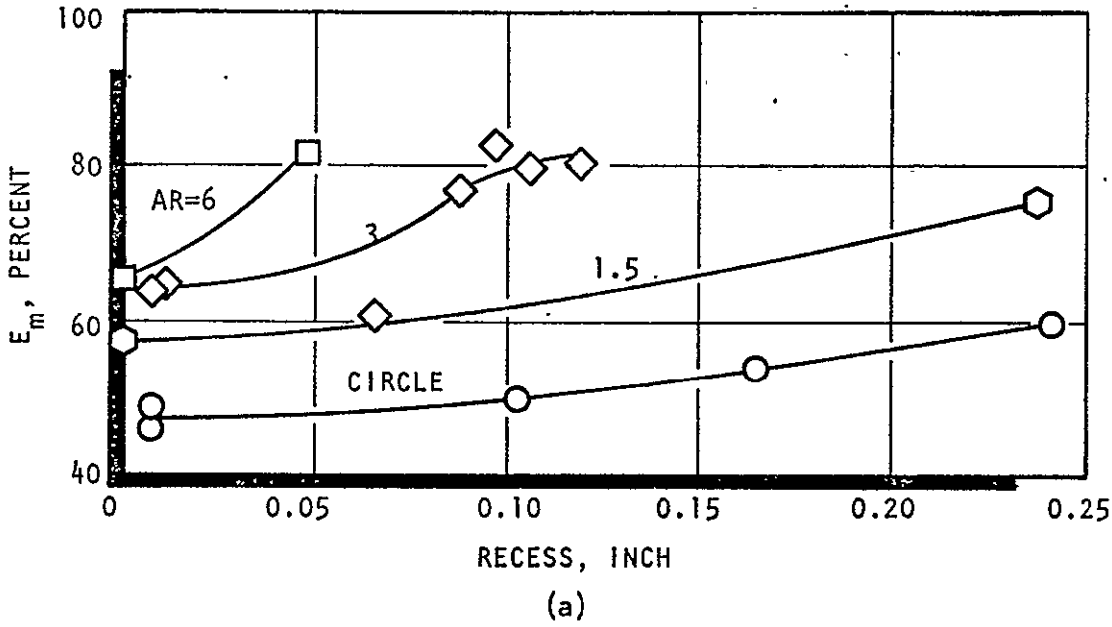

(a)

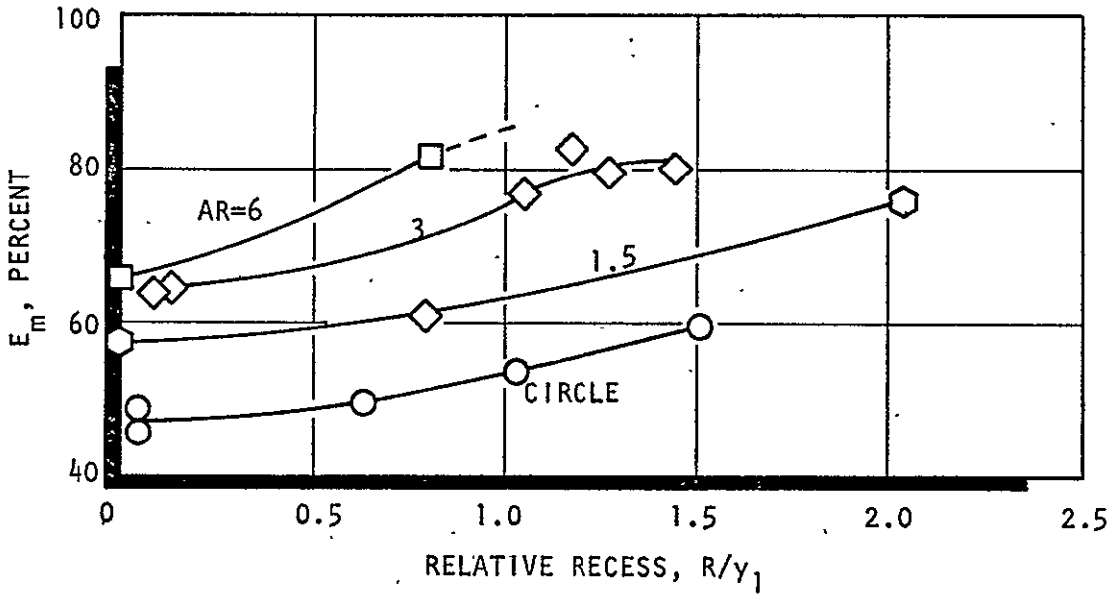

(b)

Figure 6-5. Mixture Ratio Uniformity Comparison of the Four Baseline Elements (at Nominal Conditions) as a Function of Center-Post Recess

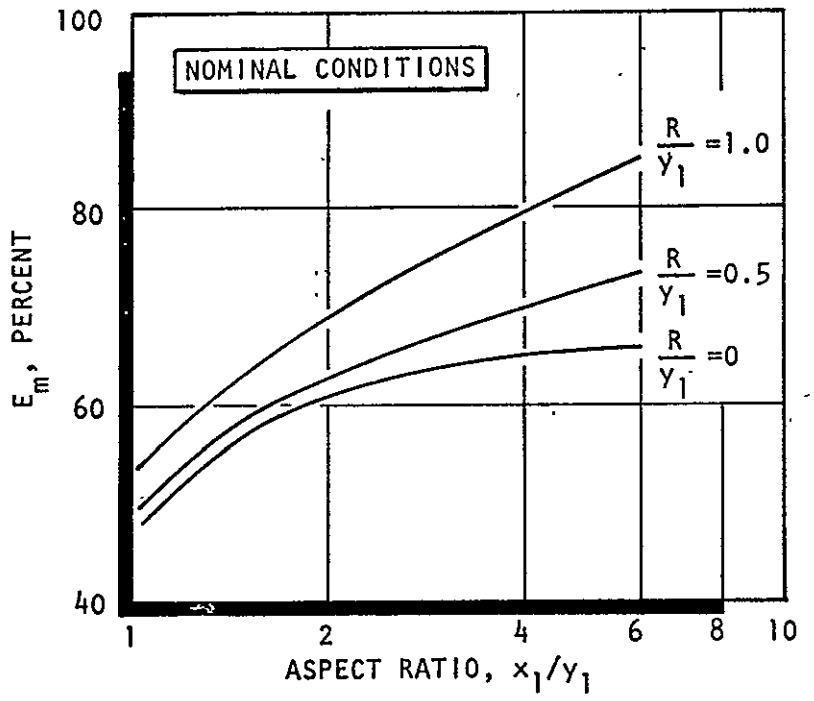

Figure 6-6. Mixture Ratio Uniformity Comparison as a Function of Aspect Ratio (nominal conditions)

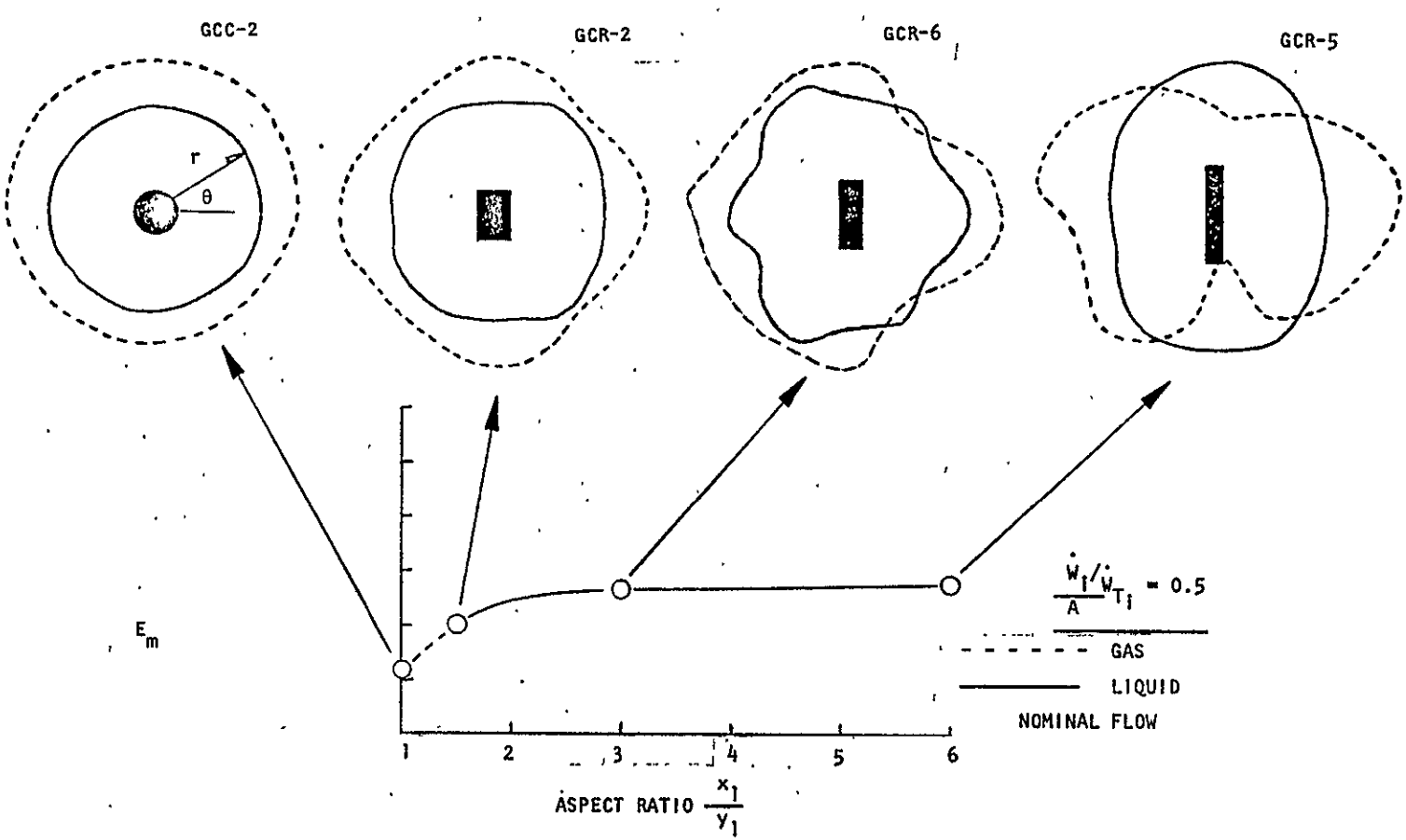

Figure 6-7. Effect of Liquid Port Aspect Ratio Upon Flowfield, R/y = 0 (constant mass fraction flux contours)

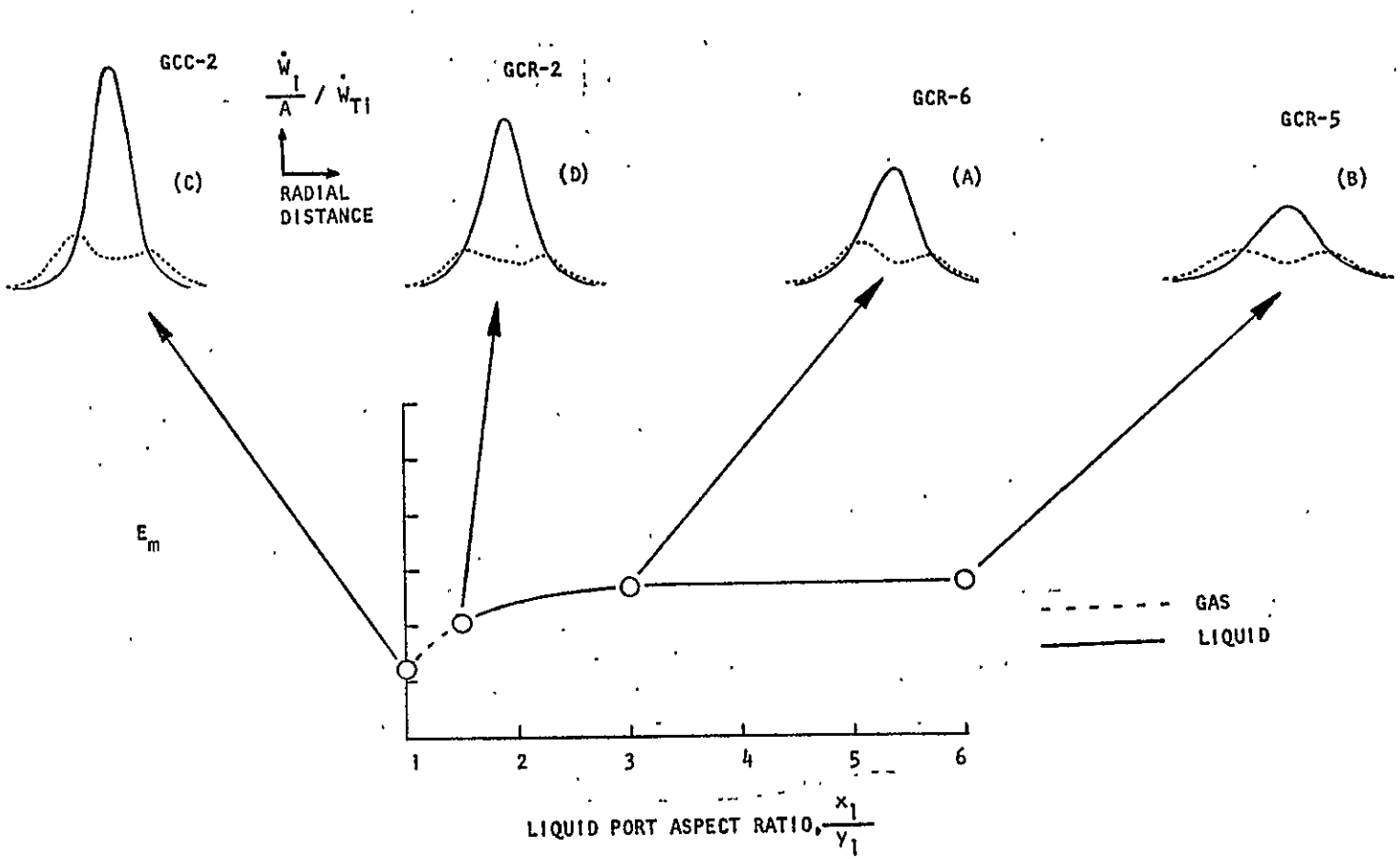

Figure 6-8. Effect of Liquid Port Aspect Ratio Upon Flowfield (mff variable)

mass flow for the i_{th} component, W_{Ti}. At a point in the flowfield where the local mixture ratio, $\dot{W}_{Li}/\dot{W}_{Gi}$, is equal to the injected mixture ratio, the values of the mass fraction flux for the liquid and gas components would be equal. Thus, for an element that could produce perfect mixing, E_m = 100 percent, the liquid and gas mass fraction flux contours would be, everywhere, superimposed, one upon the other.) In Fig. 6-7 constant mass fraction flux contours ($\frac{\dot{W}_i}{A}/W_{Ti}$ = 0.5) are presented for the liquid and gas components. (The value mff = 0.5 was selected arbitrarily and the comparison could have been made at other values. Only one contour value was selected to avoid confusion.) These contours are obtained by plotting the distance from the centerline of the element, in polar coordinates, at which the given value of mff is found in the sampling plane, which is normal to the element centerline. Here again, if the elements had produced perfect mixing, the two contours would lie directly upon one another. For the circular element, the value of 0.5 for the mff is achieved much closer to the element centerline than that of the gas component. There are no points in the flowfield that are "on mixture ratio" for this value of mff. Physically this means that the liquid is "coring" or remaining in the center of the flowfield and has not been spread out in the radial direction by the gas.

This is a classic problem for circular concentric tube elements operating at high mixture ratios (>4:1) and having relatively low gas-to-liquid velocity ratios.

The influence of element shape is quite evident in Fig. 6-7. The "warping" of the flowfield causes contours to approach each other or intermingle, and thus, the degree of mixing is increased without the necessity of increasing the gas velocity or decreasing the liquid velocity.

Exactly the same result can be noted in Fig. 6-8, wherein the value of mff for the liquid and gas component is plotted as a function of the radial distance from the element centerline along a fixed ray in the collection plane (i.e., mff =f(r), θ = constant). Here, the coring problem encountered by the circular element can be seen plainly. The increased aspect ratio systematically reduces the "coring."

There is another interesting potential advantage of RCTE's that can be deduced from Fig. 6-7. The mff contours for the highest aspect ratio element (GCR-5) suggest that the flowfield can be "tailored" to provide "fuel-rich"and "oxidizer-rich" zones that can be employed to ensure thrust chamber/injector compatibility in the outer zone of the chamber wall. Center post recess produces approximately the same change in the character of the contour plots as does increased aspect ratio. Recess has the ability to reduce "coring."

6.3.1.2 Variations About AR = 3. Continuing with the investigation of the effect of shape, as outlined in Fig. 6-4, the next task was to study the influence of element area ratio, element scale, and deviation from uniform gas annulus gap with aspect ratio, x_1/y_1, equal to 3.0

The effect of a reduction in the gas annulus area (with uniform gap) is presented in Fig. 6-9. This comparison could not be made at the nominal flowrates due to the fact that the gaseous nitrogen employed as a fuel simulant was already at a velocity of 950 ft/sec in the baseline element. A reduction in the gas area at the nominal conditions would have caused the nitrogen to choke. The comparison was made, therefore, at one-half the nominal total flowrate. The mixture ratio and gas density were held at nominal values (6.0 and 0.27 lbm/ft^3, respectively).

The value of E_m dropped off for the baseline AR = 3 element (GCR-2) as the total flow was reduced. At one-half the nominal flowrate, the liquid velocity was 21 ft/sec and the gas velocity was reduced from 935 to 468 ft/sec. At these flow conditions, the element with reduced gas area (GCR-4) was operating with the same liquid velocity but with a gas velocity of 935 ft/sec. It can be seen that this increase in gas-to-liquid velocity ratio produced a significant increase in E_m. This change in E_m is ascribed totally to the change in gas velocity, as the density and mixture ratio were held constant.

The effect of element size is shown in Fig. 6-10. Here again, the comparison was not made at the nominal flowrate. The scaled-down model, GCR-7 $\left[\frac{1}{\sqrt{2}}\right.$ reduction of GCR-2$\left.\right]$, had liquid and gas area exactly one-half those of the large

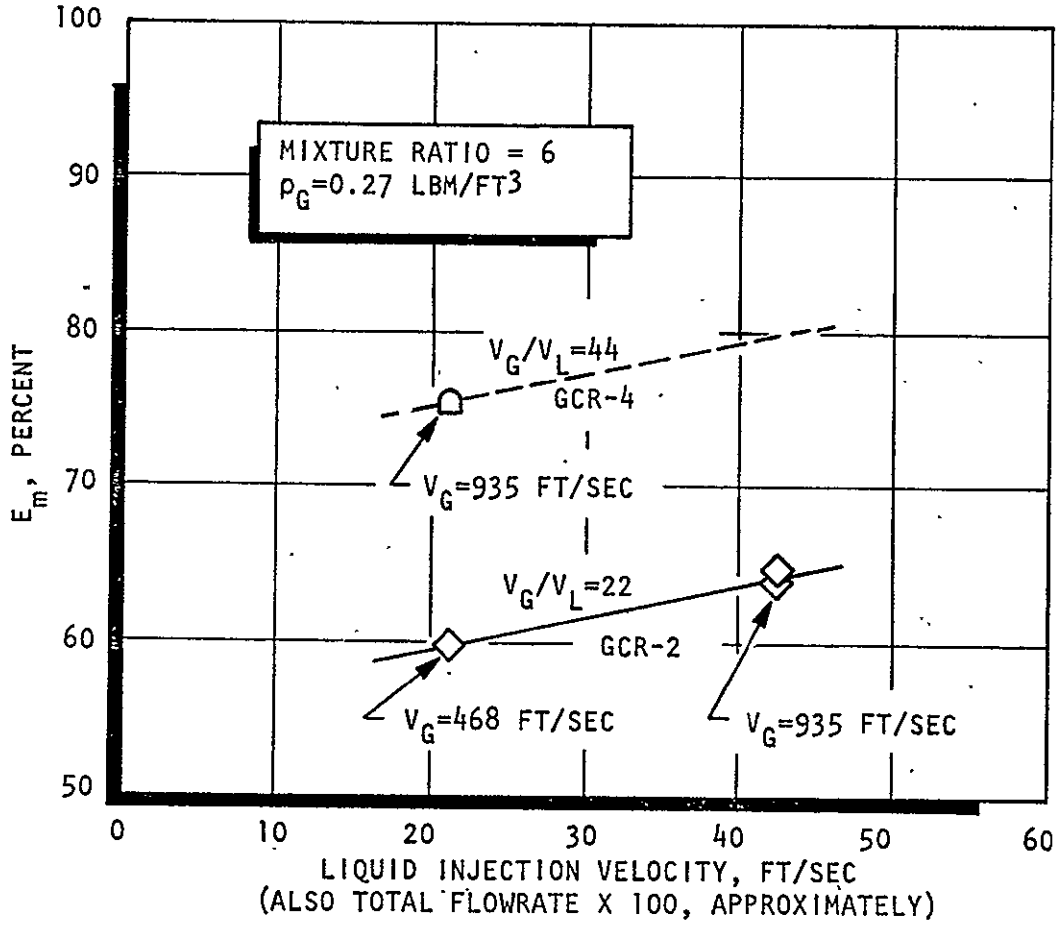

Figure 6-9. Effect of Variation of Gas to Velocity Ratio at Constant Mixture Ratio and Constant Gas Density (GCR-2 and GCR-4).

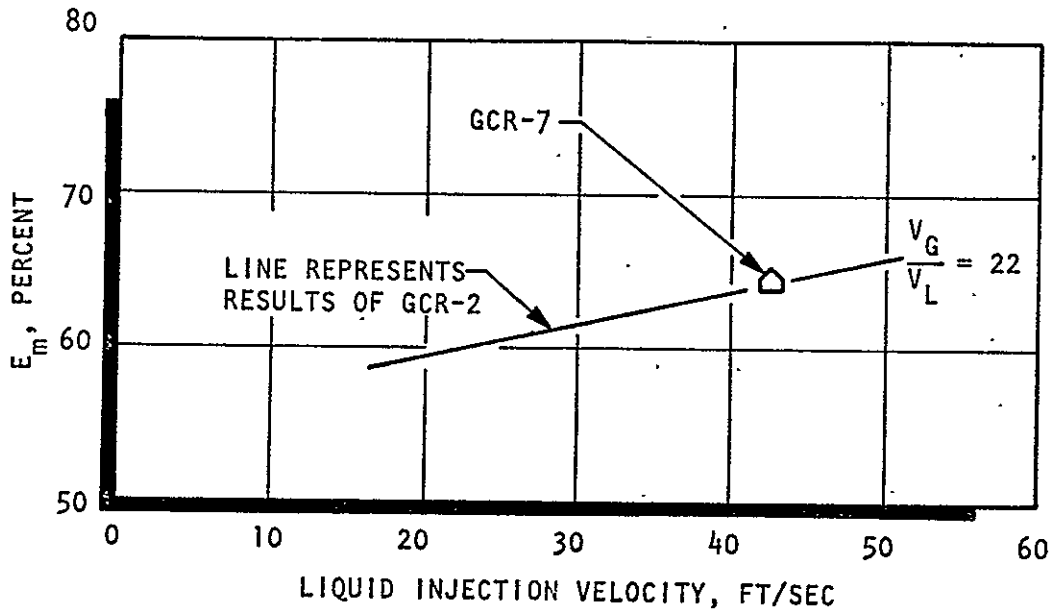

Figure 6-10. Effect of Element Size at Constant Density and Mixture Ratio (GCR-2 and GCR-7)

element. Comparison was made at nominal mixture ratio, density, and velocities, thus, the total flow in GCR-7 was exactly one-half that in GCR-2. This meant that the mass fluxes $(\dot{W}_i/A_i)$ for both elements were identical. The curve of E_m for GCR-2 is shown as a function of liquid velocity. This curve is reproduced from Fig. 6-9. The data point for GCR-7 is plotted on the same scale. It can be seen that the value of E_m is unaffected by size as long as the mass flows per unit area are preserved along with densities, velocities, and mixture ratio. This is a highly important result and suggests, at least at this scale, that thrust per element has no effect upon mixing of an individual element. This is not to say, however, that improved interelement mixing cannot be improved with lower thrust per element and thus the mixing of the injector improved overall (i.e., more elements).

The effect of variation of the gas port aspect ratio (change of x_3/y_3 with gas annulus area and centerpost configuration held constant) is shown in Fig. 6-11. This change produced a nonuniform gas gap. Here, values of E_m for GCR-2 and GCR-3 are plotted as functions of centerpost recess. This result, alone, is relatively uninteresting in that it merely says that the level of mixing dropped when the gas port aspect ratio was changed from 1.86 to 2.347. The more interesting aspects of this experiment are presented in Fig. 6-12. Here again, mff contours are employed Gas and liquid contours for mff = 0.5 are presented for GCR-2 and GCR-3 at their respective points of centerpost recess at which maximum mixing level was encountered. These points are marked by arrows in Fig. 6-11.

The contours for element GCR-2 (Fig. 6-12) suggest that there is "too much" gas concentration in the y direction and that a redistribution of some of the gas to the x direction should tend to cause the contour lines to more closely coincide. As a matter of fact, the design of GCR-3 was based upon analysis of these contours and its objective was exactly that stated. What happened is obvious. The redistribution of the gas component from y to x was greatly "overdone."

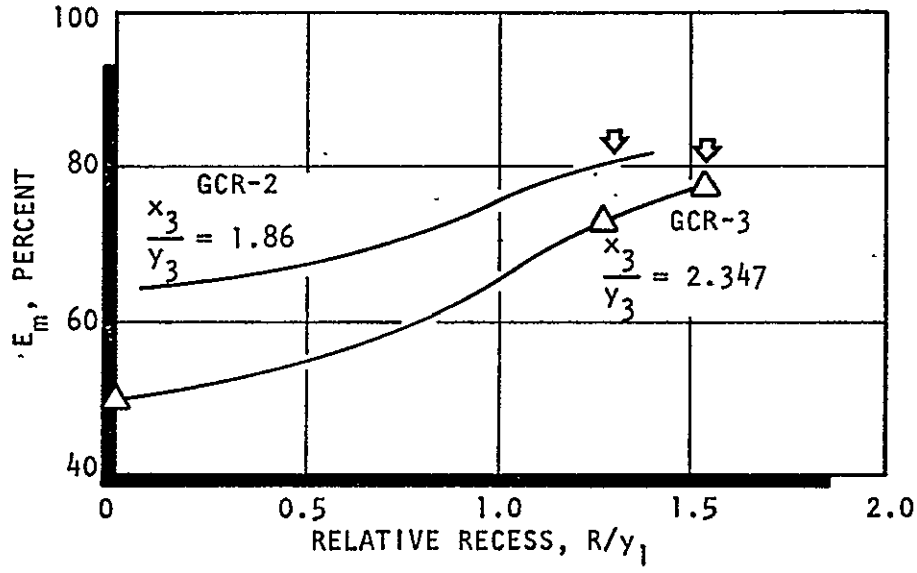

Figure 6-11. Effect of Variation of Gas Port Aspect Ratio Upon Mixing at Nominal Conditions (GCR-2 and GCR-3)

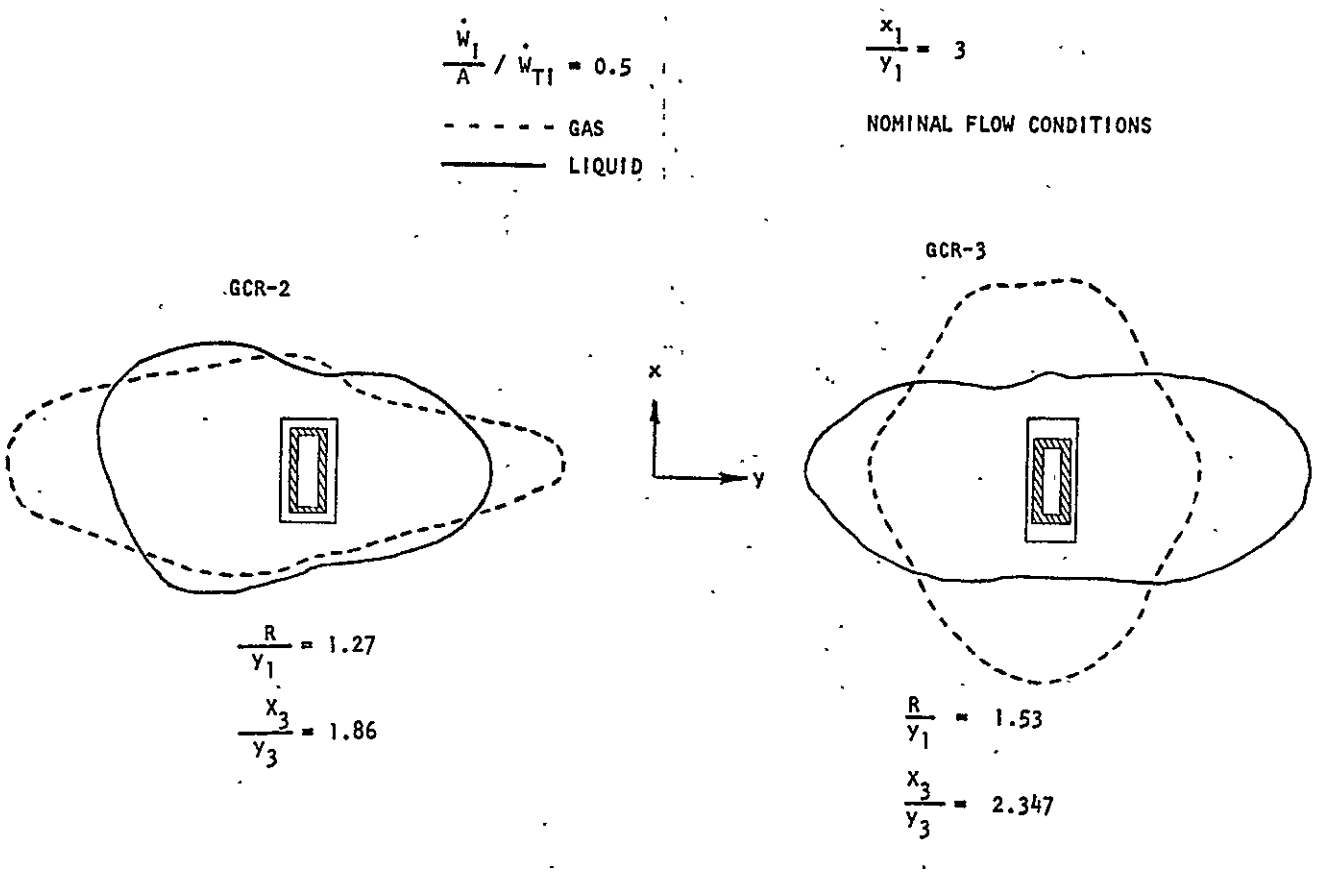

Figure 6-12. Effect of Gas Port Aspect Ratio on Flowfield Development

As a result, the mixing uniformity dropped; however, the character of the flowfield was changed. This result suggests that an optimum value of x_3/y_3 must exist between the values that were tested. The inferences of these data are presented in Fig. 6-13, which is highly speculative, but interesting. If the trends suggested in Fig. 6-13 are correct, then RCTE's offer yet another degree of freedom to the injector designer to aid in improving mixing with element geometry.

6.3.1.3 Generalization of the Results. Mixing uniformity cold-flow tests conducted with RCTE's proved to be relatively time consuming and, therefore, costly. This was due to the fact that the flow-fields were highly nonaxisymmetric and a great number of sampling points had to be incorporated to obtain accurate results. On the other hand, cold-flow tests with the circular concentric-tube element (GCC-2) proved to be quite economical due to the axisymmetric nature of the flowfield. Therefore, it was decided that an appreciation of the influence of the flow parameters upon the mixing characteristics of G/L CTE's could best be obtained with the CCTE. An extensive set of data was obtained with element GCC-2 covering a broad range of gas velocity (350 to 935 ft/sec), gas density (0.135 to 1.5 lbm/ft^3), and liquid velocity (2 to 100 ft/sec). The results of this parametric study are presented in Fig. 6-14 through 6-17. It must be pointed out that even this extensive parametric variation does not show the independent effects of velocity ratio and mixture ratio. This is due to the fact that the entire set of results was obtained with one element; thus, the area ratio, A_G/A_L, was not a variable. As a result, the mixture ratio was a dependent variable as shown in Eq. 6-1.

$$MR = K\left(\frac{V_L}{\rho_G V_G}\right) \tag{6-1}$$

where K is a constant

It has been shown (see Fig. 6-9) that a variation of velocity ratio (by variation of area ratio) produces a change in mixing with constant density and constant mixture ratio. This type of comparison is not allowed by the restrictions of Eq. 6-1.

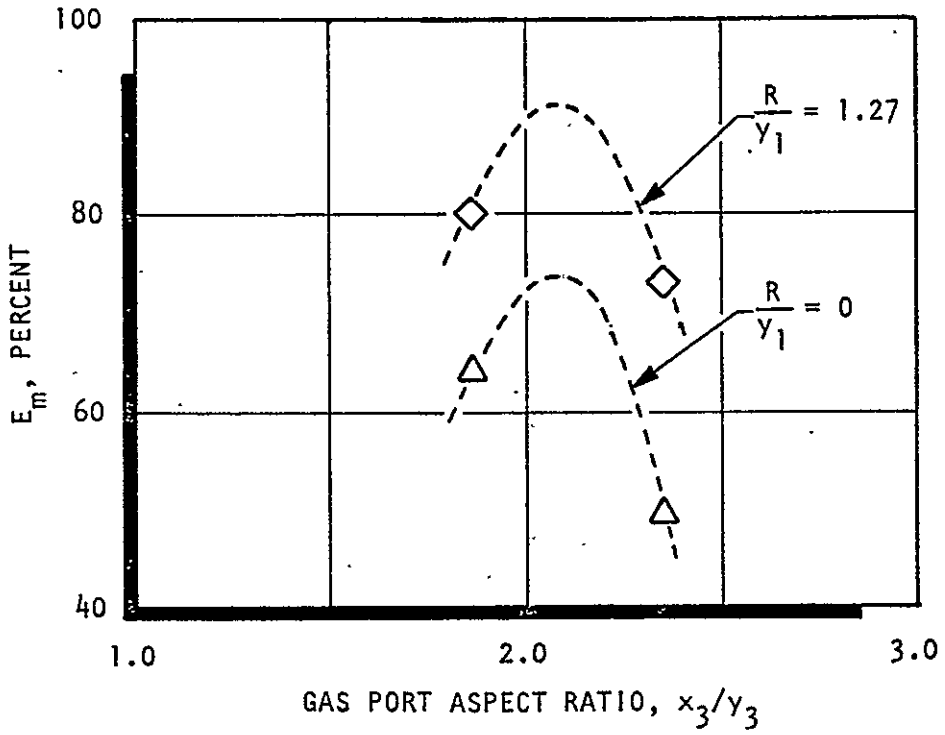

Figure 6-13. Mixture Ratio Uniformity Trends Inferred From Analysis of the Effects of Gas Port Aspect Ratio, x_3/y_3

Figures 6-14 through 6-16 show the variation of E_m with liquid velocity along lines of constant density with gas velocity a constant in each figure. One of the many possible cross plots is presented in Fig. 6-17, wherein the variation of E_m with liquid velocity is shown along lines of constant gas velocity with gas density everywhere constant. Lines of constant mixture ratio have been included in Fig. 6-16 and 6-17 to illustrate the fact that this quantity is dependent upon the other variables, and also to show that even though the parametric roles of V_G, ρ_G and V_L are quite clear, the interpretation of performance variations with constant mixture ratio throttling (V_G = const) are not straightforward.

Figures 6-14 through 6-17 show clearly that the liquid velocity is the parameter which most influences the mixing performance of a concentric tube element. In addition, the lines of constant mixture ratio in Fig. 6-16 and 6-17 show that for this particular element, no combination of variables can produce high levels of mixing as long as the mixture ratio is maintained at high values. However, based upon the results shown in Fig. 6-9 for a RCTE, it can be expected that a change in area ratio which increases the velocity ratio V_G/V_L at high mixture ratio will produce a higher mixing level. Great care must be taken not to associate directly the effects of changes in velocity ratio shown by these data with a change in velocity ratio at constant mixture ratio. These additional data are required to complete the story.

These data, however, provide certain broad design criteria. In general, one can conclude that "good mixing," with zero post recess may be achieved with high gas velocity, high gas density, and low liquid velocity. The most important of these being low liquid velocity.

6.3.2 Atomization Studies

Results of the atomization studies are presented with the same format that was employed for the mixing results. The data are presented in Ref. 6-2.

Atomization results are interpreted in terms of the mass median droplet diameter, $\overline{D}$, obtained from a given sample of "frozen" wax droplets. The value of $\overline{D}$

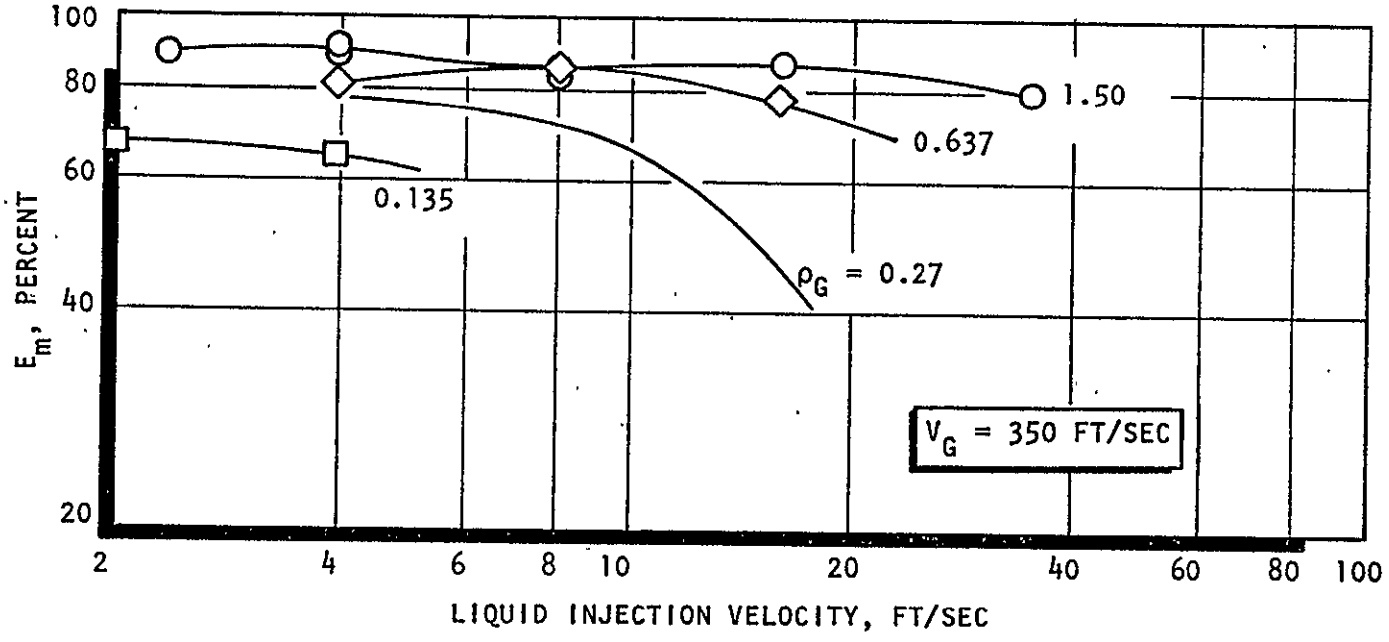

Figure 6-14. E_m as a Function of V_L Along Lines of Constant ρ_G. Circular Concentric Tube Element. (Limited data points shown for reference curves are "best fit" of actual data)

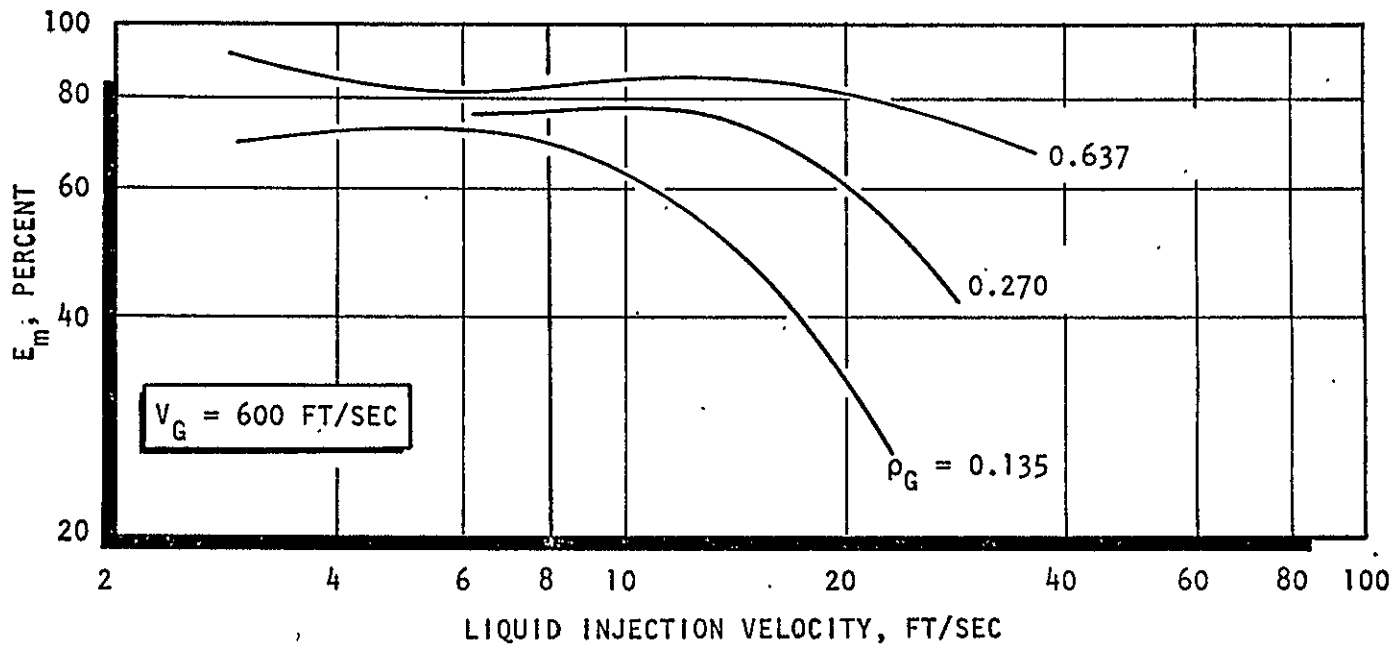

Figure 6-15. E_m as a Function of V_L Along Lines of Constant ρ_G. Circular Concentric Tube Element (data points not shown)

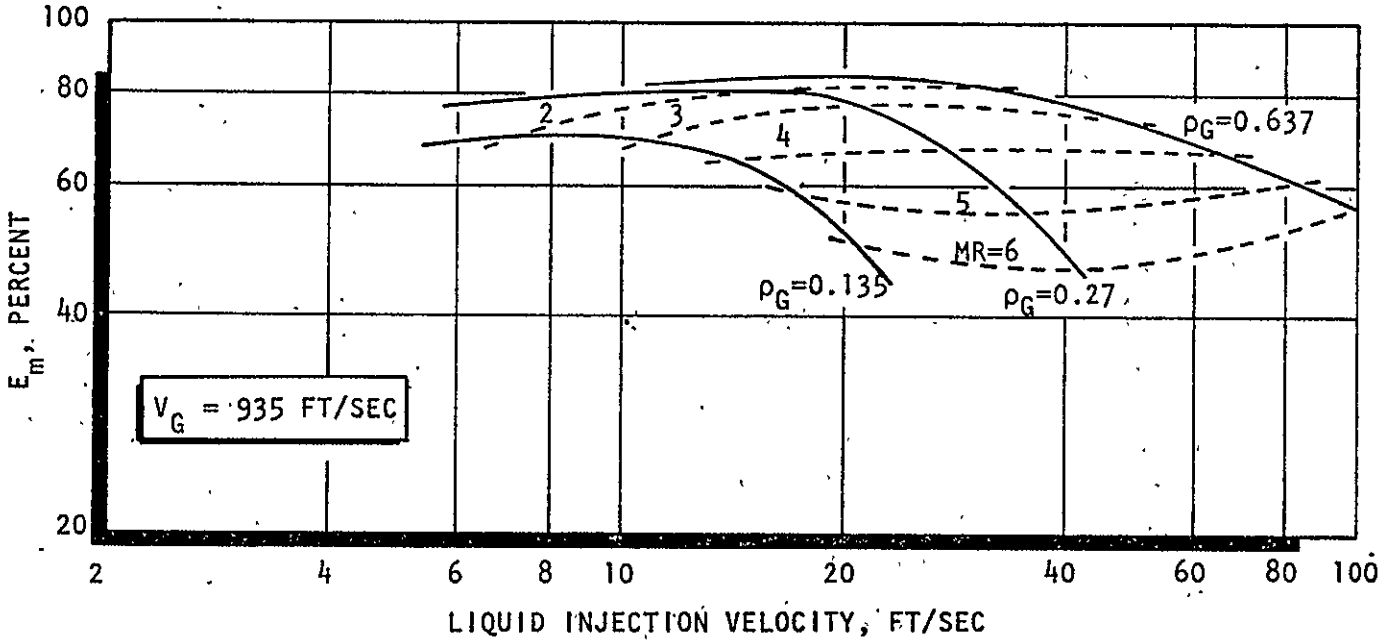

Figure 6-16. E_m as a Function of V_L Along Lines of Constant ρ_G and Mixture Ratio. Circular Concentric Tube Element (data points not shown)

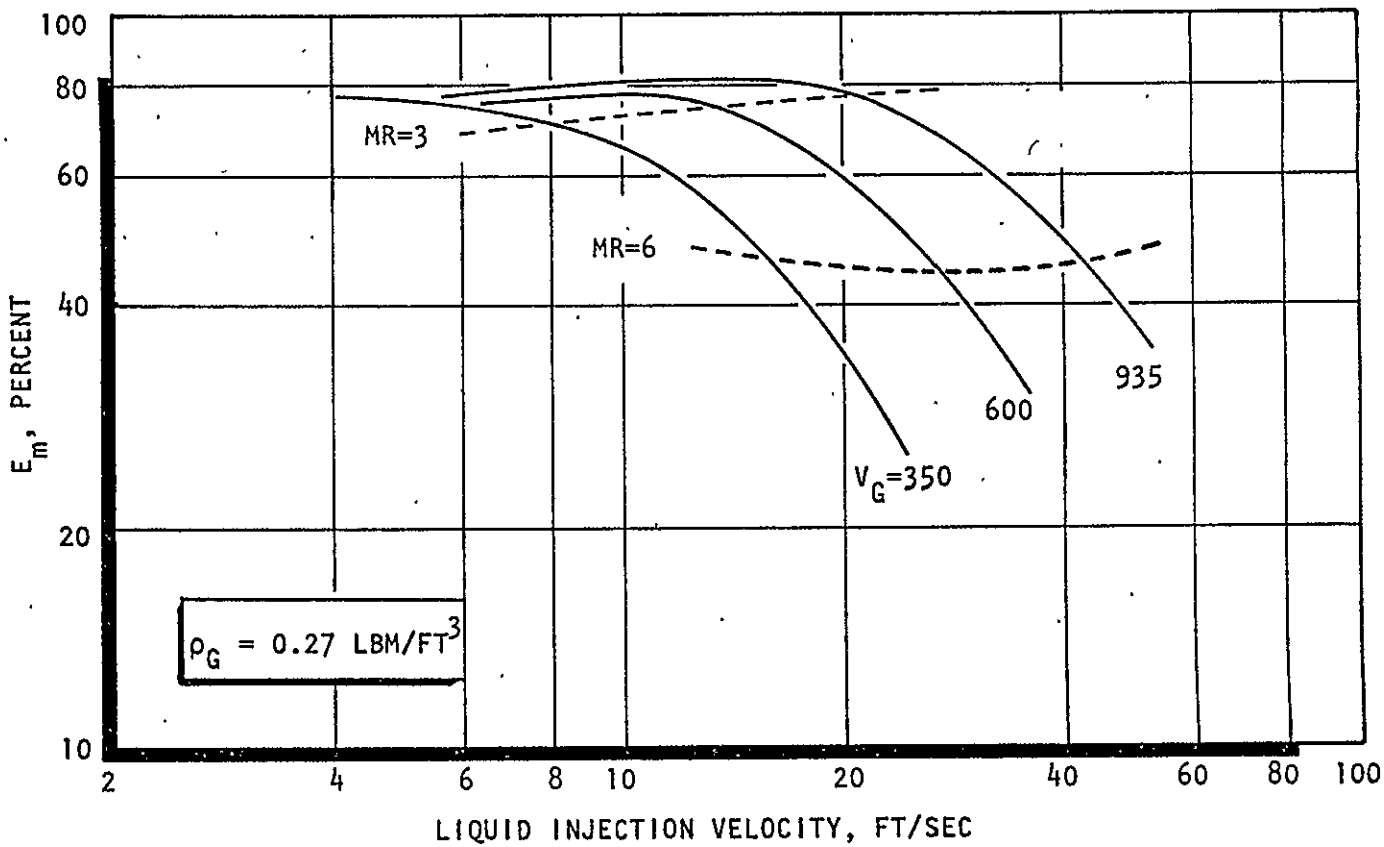

Figure 6-17. E_m as a Function of V_L Along Lines of Constant V_G and Mixture Ratio. Circular Concentric Tube Element (data points not shown)

is merely a shorthand method of evaluating the atomization characteristics of an injector element. Unfortunately, $\overline{D}$ by itself does not completely describe the nature of a given droplet sample. The droplet size distribution function is required in addition to $\overline{D}$ to perform a complete vaporization limited performance calculation (see Appendix B). A typical droplet diameter distribution is shown in Fig. 6-18, wherein the cumulative wieght fraction of the wax droplet sample is shown as a function of the normalized droplet diameter, $D/\overline{D}$. By definition, these distribution functions pass through the value of 0.5 for cumulative weight fraction when $D/\overline{D} = 1$. The data shown in Fig. 6-18 represent the results of three different atomization experiments conducted with two different RCTE's. One distribution function fits the data for these three tests quite well. This distribution function was employed for all performance analysis throughout the remainder of the study.

Both Phases II and III atomization data are presented in this section.

6.3.2.1. Nominal Conditions-Baseline Comparison. The nominal conditions-baseline comparison is shown in Fig. 6-19. Here the droplet mass median diameters normalized with respect to the characteristic size of the element are plotted as a function of the relative recess, R/y_1, of the liquid centerpost. Two basic conclusions can be drawn from these results: (1) droplet diameter is reduced with increased centerpost recess, and (2) relative droplet diameter increases with increased aspect ratio. The effect of recess is well known and has been documented many times in the past. The effect of aspect ratio, however, is quite surprising and warrants further discussion.

A crossplot of these data is presented in Fig. 6-20 wherein the relative dropsize is shown as a function of aspect ratio along lines of constant relative recess. Two important items concerning Fig. 6-20 must be kept in mind when evaluating the data: (1) relative dropsize is shown (not dropsize) and the value of y_1 is continually decreasing with increased aspect ratio; and (2) although these curves are drawn to the aspect ratio unity, the data at unity were obtained with a circular element, not a RCTE with aspect ratio unity, and should not be expected to fall on the curves.

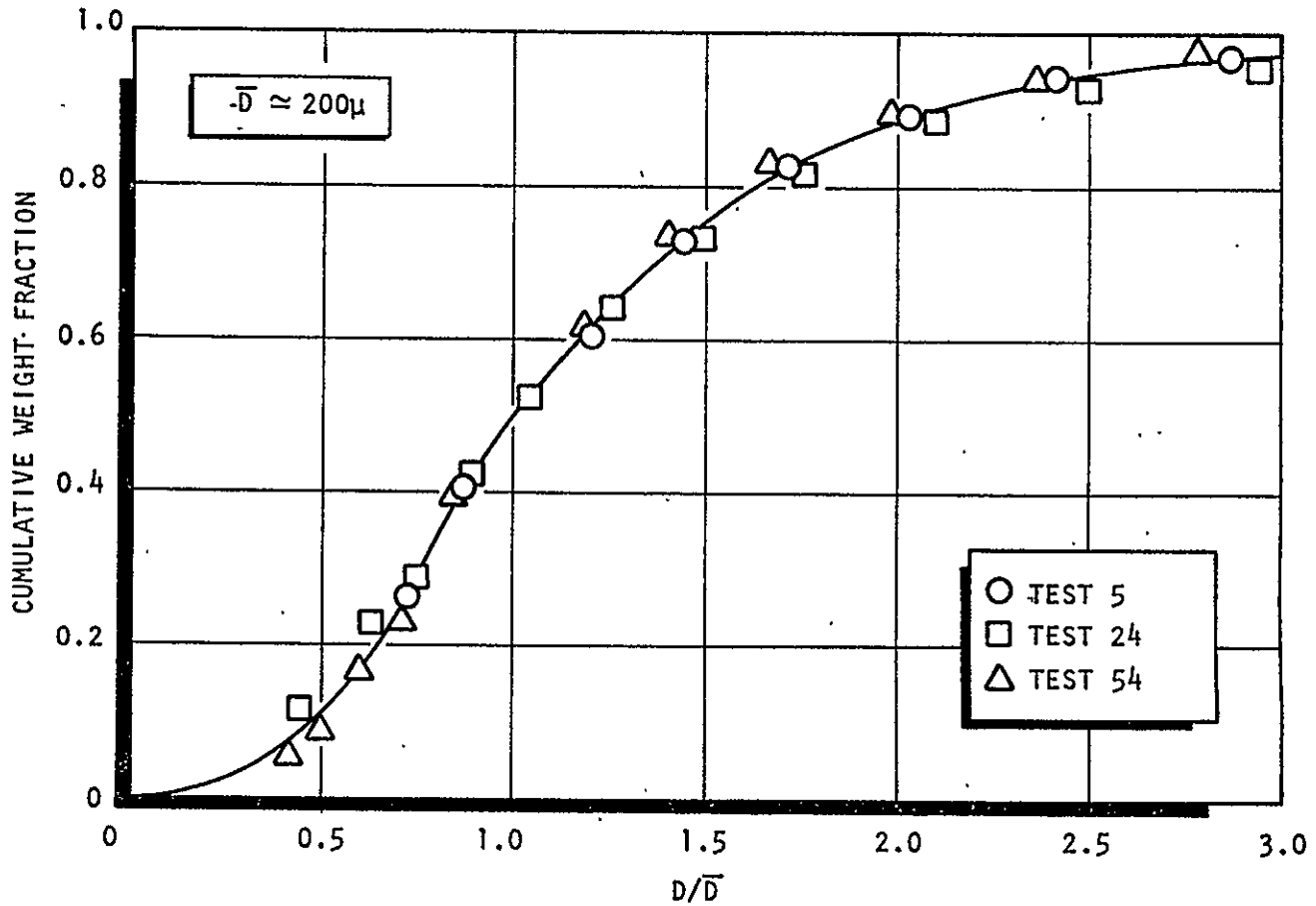

Figure 6-18. Typical Dropsize Distribution Function. Gas/Liquid Rectangular Concentric Tube Element (GCR-2), and Circular Concentric

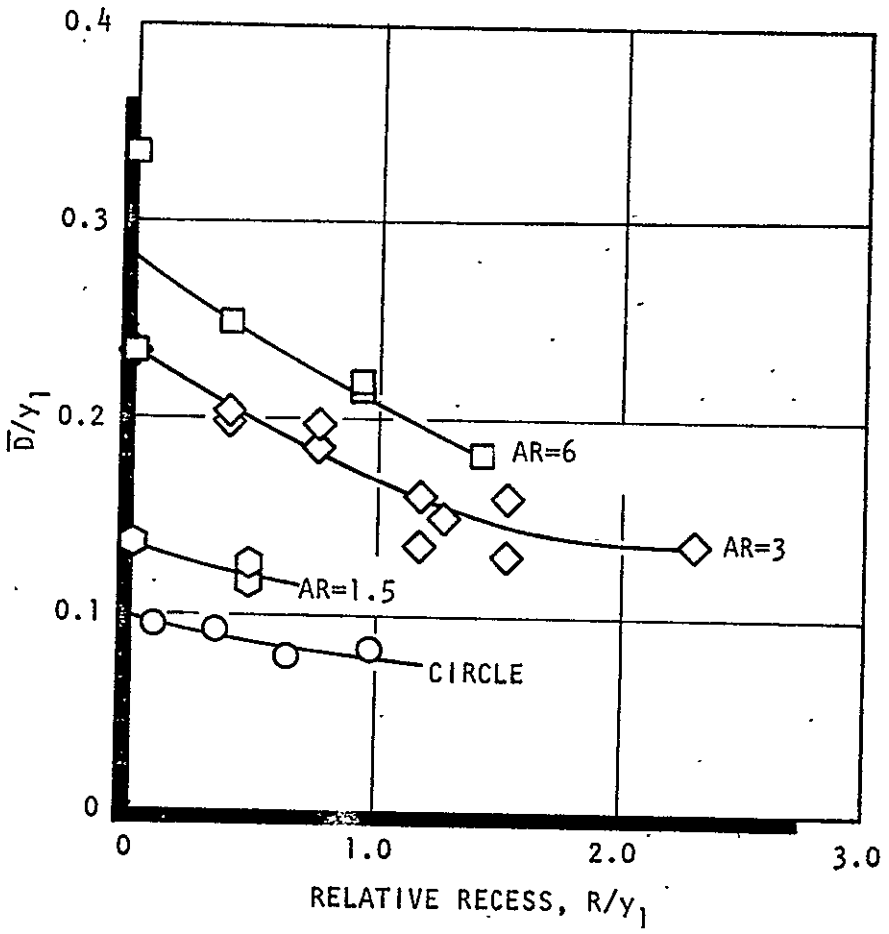

Figure 6-19. Normalized Droplet Diameter as a Function of Center-Post Relative Recess for the Four Baseline Elements at Nominal Conditions

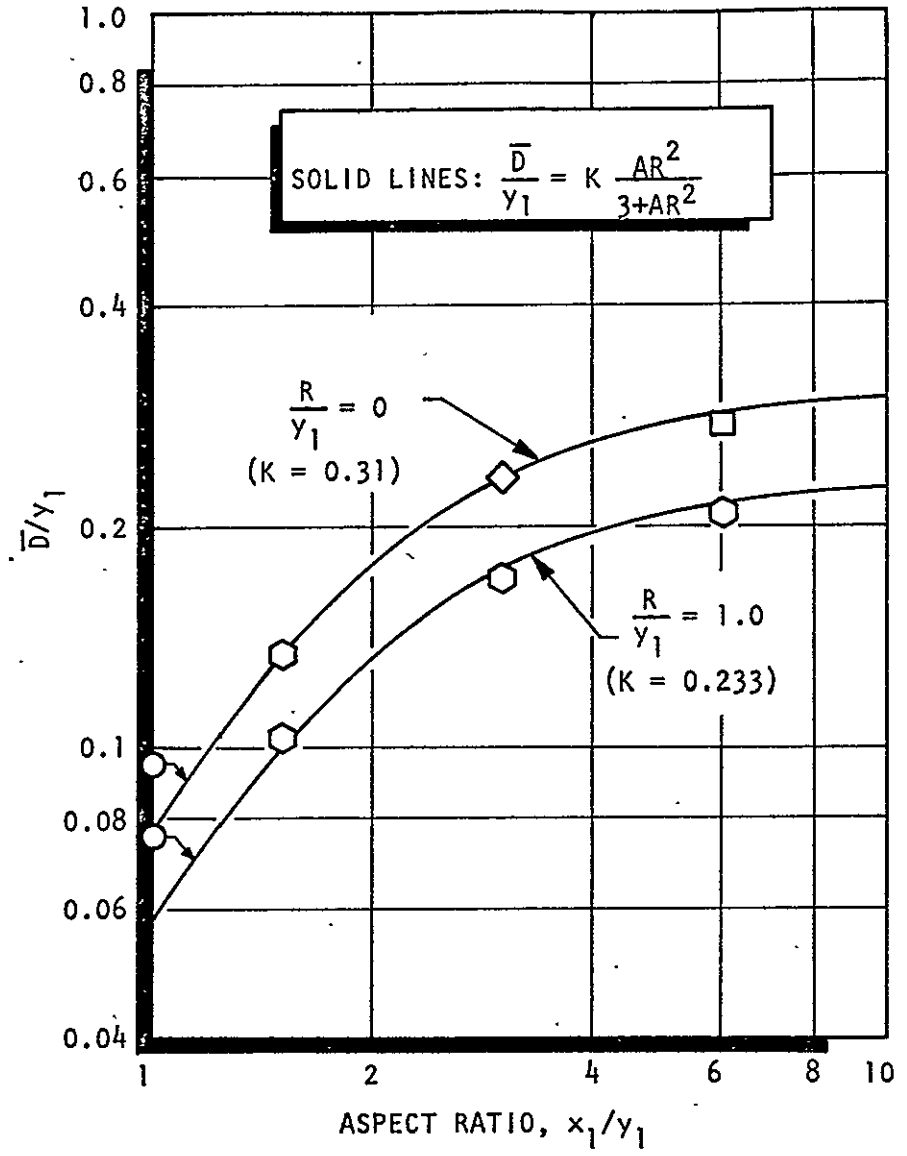

Figure 6-20. Normalized Droplet Diameter as a Function of Aspect Ratio for Constant Values of Relative Recess (baseline elements at nominal conditions)

It was found that a relatively simple algebraic function could be employed to correlate the RCTE dropsize results. This function is presented as Eq. 6-2.

$$\frac{\overline{D}}{y_1} = K \left[\frac{AR^2}{3 + AR^2} \right] \tag{6-2}$$

where K = f(recess). The curves that are drawn through the data in Fig. 6-20 were generated with Eq. 6-2. The implication that these curves fall below the CCTE data at aspect ratio unity is purely speculation and has not been shown. It is interesting to note that Eq. 6-2 states that, geometrically, dropsize is a function of the term:

$$\overline{D} = f \left\{ y \left[\frac{AR^2}{3 + AR^2} \right] \right\} \tag{6-3}$$

It must be remembered that the liquid port area, $X_1 y_1$, was held constant as aspect ratio was varied.

It is interesting to speculate upon what a correlation of droplet diameter based upon the hydraulic diameter of the liquid orifice would yield as a functional relationship. If it had been assumed that the correlating parameter was $\overline{D}/D_H$ where D_H = hydraulic diameter, the following would have been the result:

$$\overline{D} = f \left\{ y_1 \left[\frac{AR}{1 + AR} \right] \right\} \tag{6-4}$$

The similarity between this function and Eq. 6-3 is striking. However, hydraulic diameter alone is not sufficient to describe the data. The difference between Eq. 6-3 and Eq. 6-4 also points out the danger of adopting complex combinations of variables as correlating parameters early in an experimental study.

The variation of actual dropsize with aspect ratio is shown as a function of aspect ratio in Fig. 6-21. The curve through these data was obtained from Eq. 6-3 by adding the additional restriction that the product $x_1 y_1$ is a constant and is

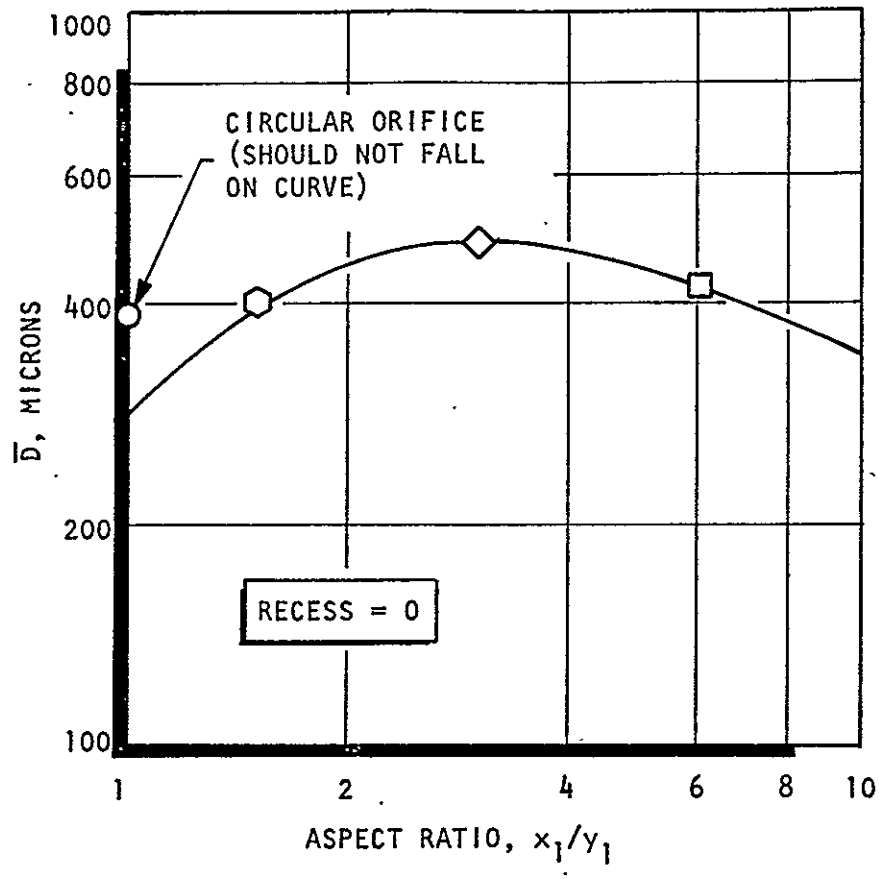

Figure 6-21. Variation of Wax Droplet Diameter With Aspect Ratio (baseline elements, nominal conditions)

equal to the liquid area, A_L. This restriction adds the additional relation:

$$y_1 = \sqrt{\frac{A_L}{AR}} \tag{6-5}$$

Combination of Eq. 6-2 and 6-4 yields:

$$\overline{D} = K\sqrt{\frac{A_L}{AR}} \left[\frac{AR^2}{3 + AR^2}\right] \tag{6-6}$$

where

$K = 0.310$

$\sqrt{A_L} = 513$ microns

$AR = X_1/y_1$

These results can be interpreted quite simply from the implications of Eq. 6-3. This relation states that the characteristic dimension for atomization is a complex quantity at low aspect ratios and approaches y_1 as $AR \to \infty$. Physically, this is reasonable. At low apsect ratios, although y_1 is reduced by an increase in aspect ratio, X_1 is increased. Evidently, the increase in the X dimension is more detrimental to atomization than the decrease in y_1 is beneficial for atomization. As the aspect ratio increases to larger and larger values, the characteristic thickness of the liquid jet quite naturally approaches the value of y_1.

6.3.2.2 Variations About AR = 3. Only two of the three variations about the aspect ratio three baseline element were investigated during the atomization study (element scale and nonuniform gas gap).

The effects of variation of element size and gas port aspect ratio are presented in Fig. 6-22. The effect of size is shown in Fig. 6-22a wherein the relative dropsize is presented as a function of actual recess for both GCR-2 (the larger element) and GCR-7 (the smaller element). What is shown in this figure is the reduction in dropsize produced by a $\sqrt{2}$ reduction in the characteristic size of the element.

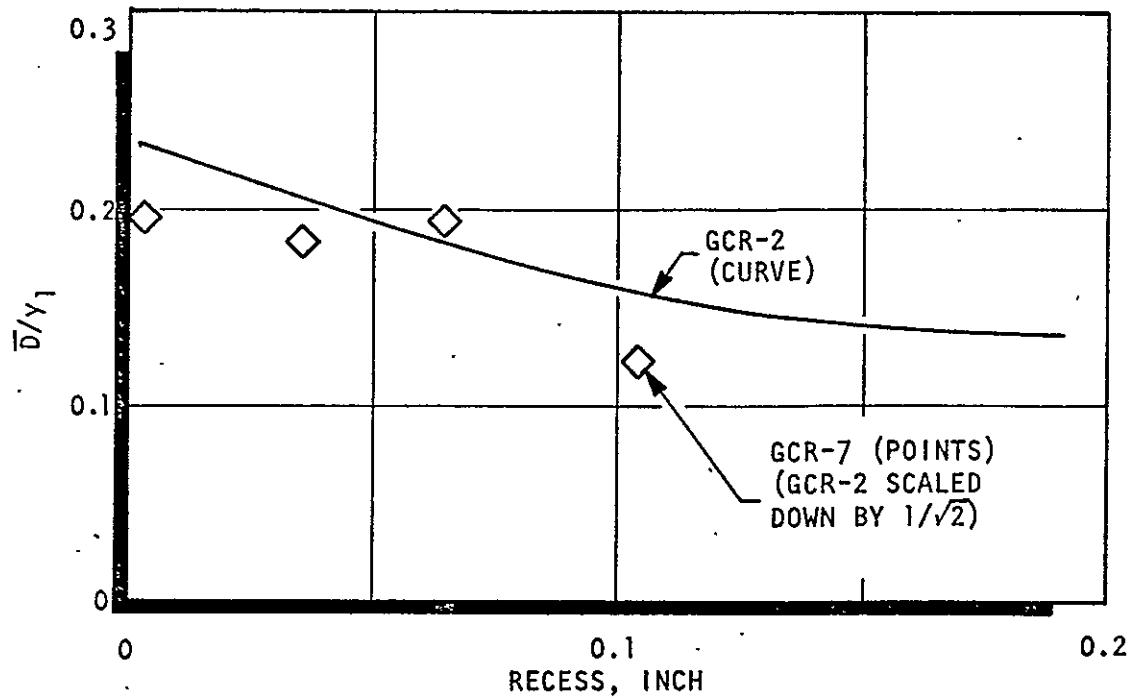

(a) EFFECT OF ELEMENT SIZE

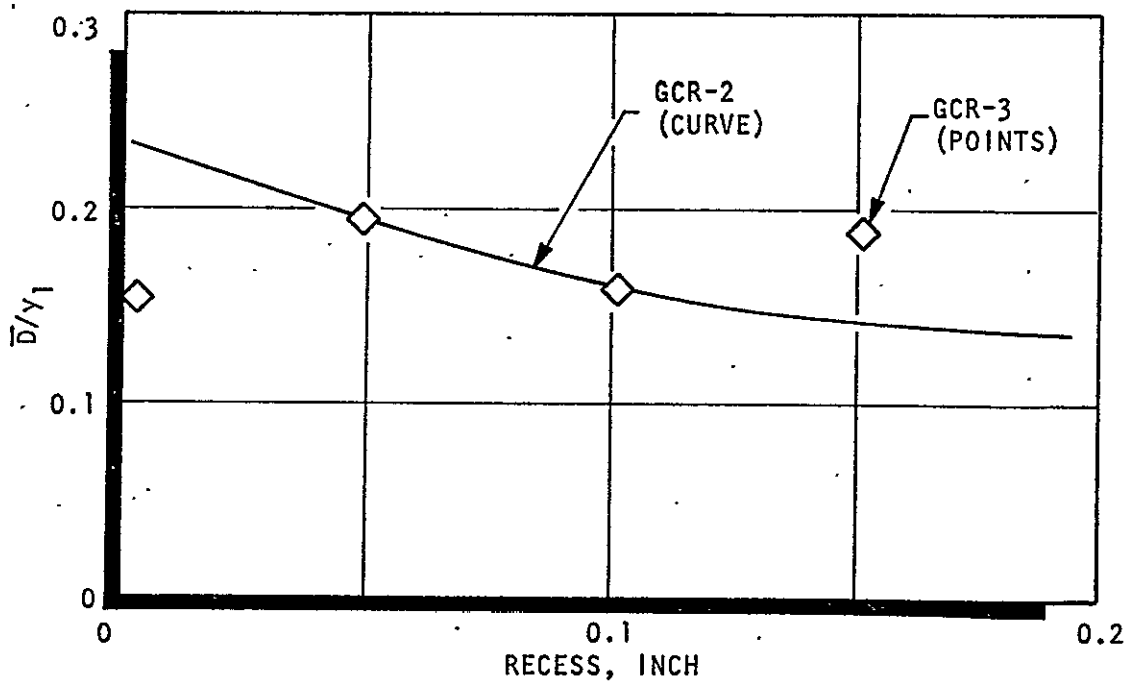

(b) EFFECT OF NONUNIFORM GAS GAP

Figure 6-22. Effect of Element Size Reduction and Nonuniform Gas Gap Upon Atomization (AR = 3, MR = 6, ρ_G = 0.27 lbm/ft^3, V_G = 950 ft/sec)

If the characteristic dimension, y_1, had been sufficient to describe the droplet variation the points for GCR-7 would have fallen directly on the curve for GCR-2. At zero recess the GCR-7 element actually provided a dropsize reduction of roughly $1.2\ \sqrt{2}$.

This result suggests that the effect of element size upon dropsize is stronger than the first power of a characteristic dimension. However, the limited amount of data plus the fairly large degree of uncertainty associated with dropsize data preclude any valid speculation as to the second order effects of element size.

The effect of the gas port aspect ratio is shown in Fig. 6-22b. At zero recess the element having a nonuniform gas gap (GCR-3) produced a $\overline{D}$ significantly smaller than the baseline element. However, the dropsizes for the two elements approach one another at moderate recess. There appears to be considerable scatter in these data such that a firm conclusion as to the gas gap effect cannot be drawn. The results seem quite rational except for the data point at the greatest recess for element GCR-3.

Atomization experiments with element GCR-4 (1/2 nominal gas area) were not conducted as discussed earlier. However, it can be postulated that an improvement in atomization would have been realized with this element at the nominal flowrate and mixture ratio. This improvement would be attributable to the doubling of the gas velocity at constant liquid velocity and gas density. The magnitude of the improvement, however, is unknown for these elements (see, however, Ref. 6-4 for other elements.)

6.3.2.3 Generalization of the Results. The bulk of the parametric atomization data was obtained with the baseline AR = 3 element (GCR-2). As a result, these data were employed in an attempt to generalize the results to operating conditons other than the nominal set. The influence of a parametric variation of gas velocity, gas density, and liquid velocity, at mixture ratio equal to 6.0, is depicted in Fig. 6-23. In this figure the relative dropsize, $\overline{D}/y_1$, is shown as a function of liquid injection velocity along lines of constant density and constant gas velocity. The parametric variations of V_L, V_G, and ρ_G are not independent and are subject to

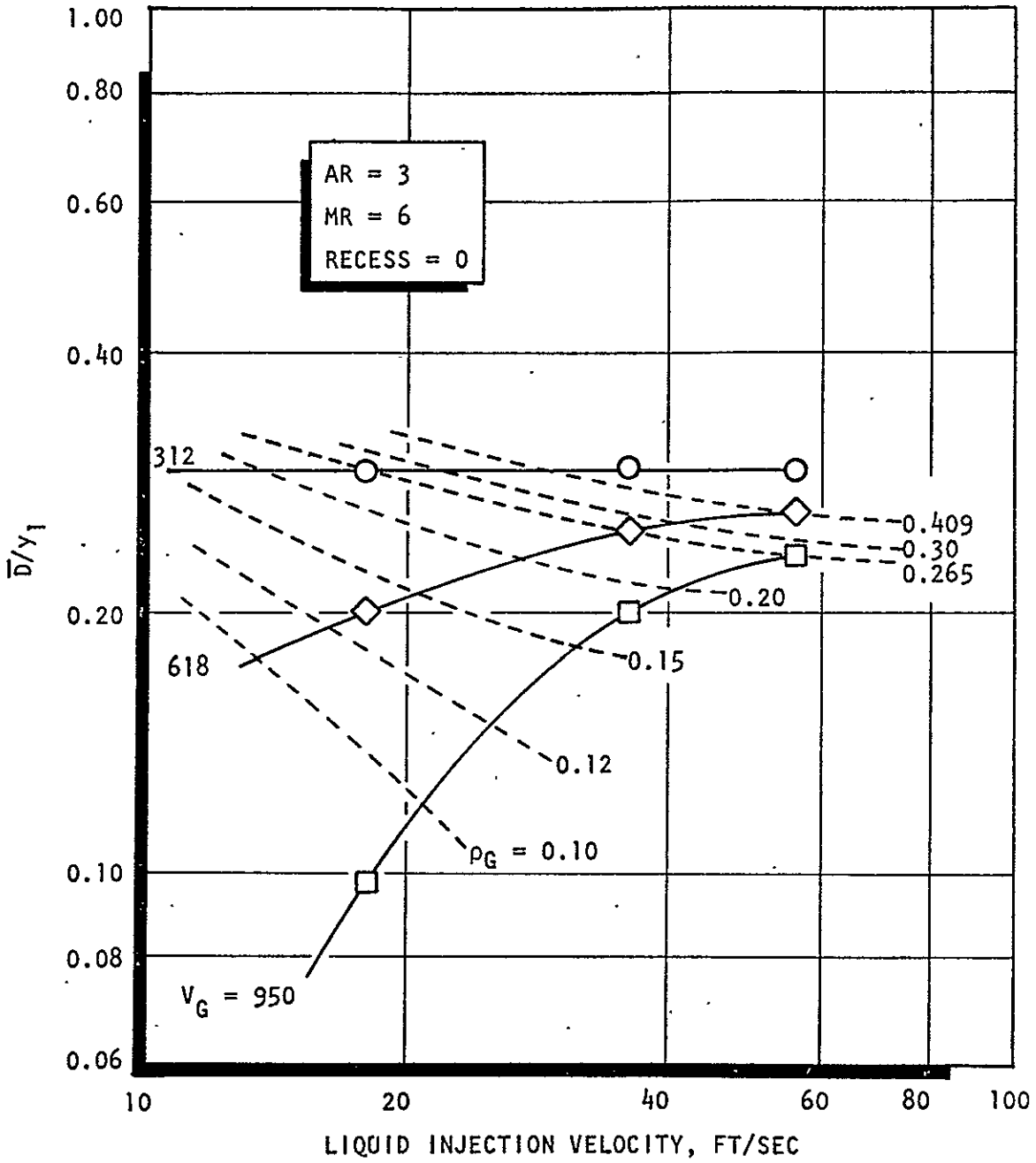

Figure 6-23. Effect of V_L, V_G, and ρ_G Upon Dropsize at Constant Mixture Ratio for the Baseline AR=3 RCTE (GCR-2)

the restrictions of Eq. 6-1 with mixture ratio a constant. It was found through further analysis of data at other mixture ratios that the effect of mixture ratio could be incorporated by casting the results shown in Fig. 6-23 into the form shown in Fig. 6-24. Here, $\overline{D}/y_1$ is plotted as a function of $\rho_G V_G^2$ along lines of constant liquid velocity.

The restrictions of Eq. 6-1 still apply here; however the mixture ratio is allowed to vary in addition to the other parameters. A physical interpretation of the data in this form is quite clear. With a fixed liquid velocity, the droplet size is significantly reduced by increasing $\rho_G V_G^2$. However, as the liquid velocity is increased, the value of $\rho_G V_G^2$ required to produce the same droplet diameters is increased. The fact that the product $\rho_G V_G^2$ improves the correlation of the data suggests strongly that the Weber number is a key parameter for the description of atomization process (see Table 6-3). This method of presentation is extended to the other baseline elements in Fig. 6-25 through 6-27.

In Fig. 6-25, the atomization results for both the Phase II (GCC-1) and the Phase III (GCC-2) CCTE's are presented. This figure is significant in that the direct correlation between low-density, "open-air" atomization and high-density atomization can be accomplished. These data incorporate large variations in gas density (0.055 to 0.27 lb/ft^3), liquid velocity (4 to 55 ft/sec), and gas velocity (300 to 1000 ft/sec).

A very interesting result can be found in Fig. 6-27 in which the dropsize data from the Phase II (GCR-1) and the Phase III (GCR-5) AR = 6 elements are presented. Here again, the Phase II and Phase III data correlate well except for a set of points which has been pointed out in the figure. It is believed that these points constitute limiting dropsizes. That is to say that a dropsize can be achieve, regardless of how low the liquid velocity is or how high the value of $\rho_G V_G^2$ is, such that a smaller droplet cannot be realized. The smallest dropsizes shown in Fig. 6-27 are on the order of 100 to 110 microns. It is reasonable to suppose that such a limit does exist. As the droplets become smaller and smaller, they are more easily accelerated by the gas stream (the acceleration is proportional to 1/D). If the droplets are accelerated rapidly to the gas velocity, the ΔV between the droplets and the gas goes rapidly to zero and further droplet breakup is halted. This

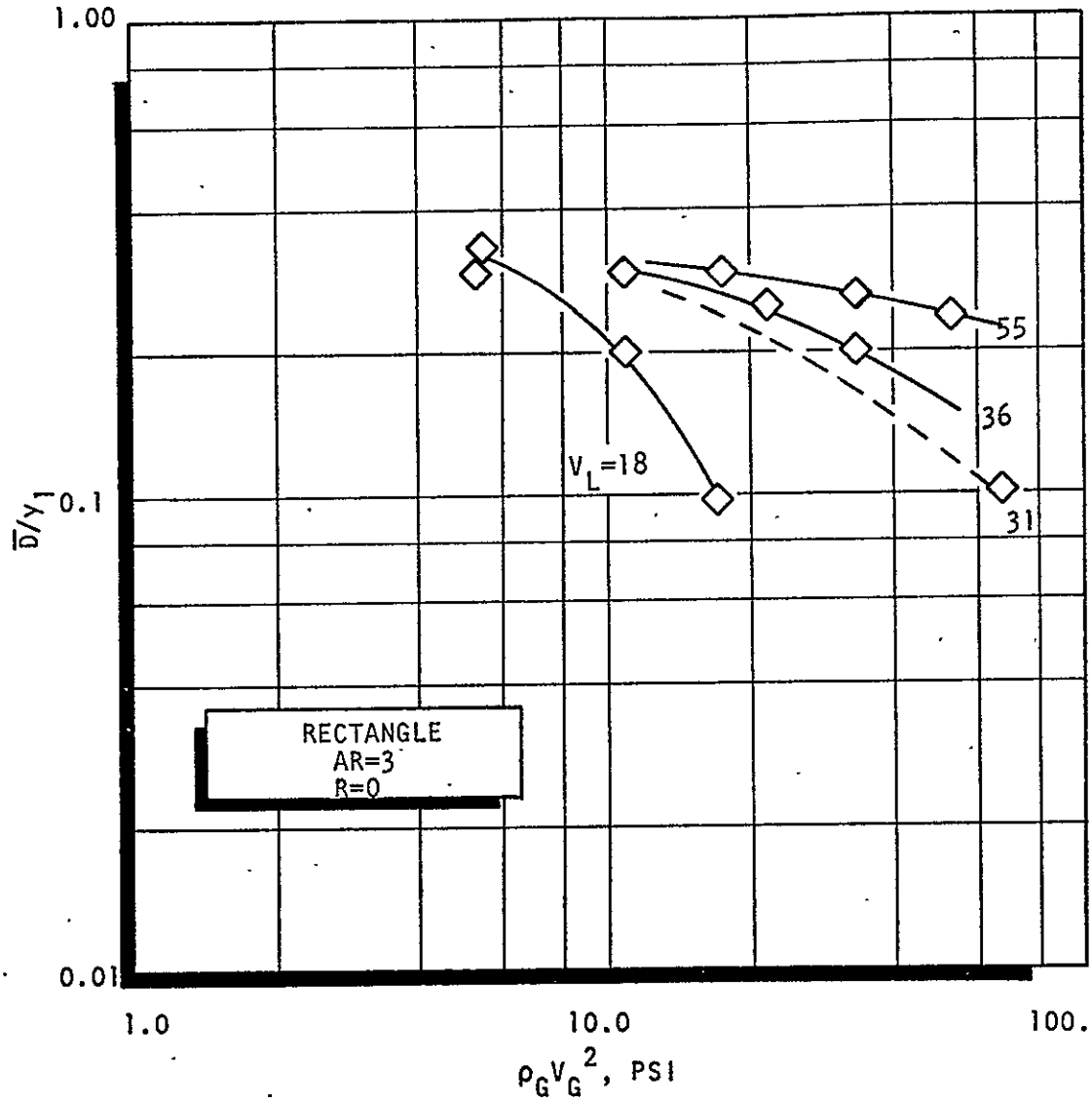

Figure 6-24. Variation of Dropsize With $\rho_G V_G^2$ and V_L. Baseline AR=3 Element (GCR-2)

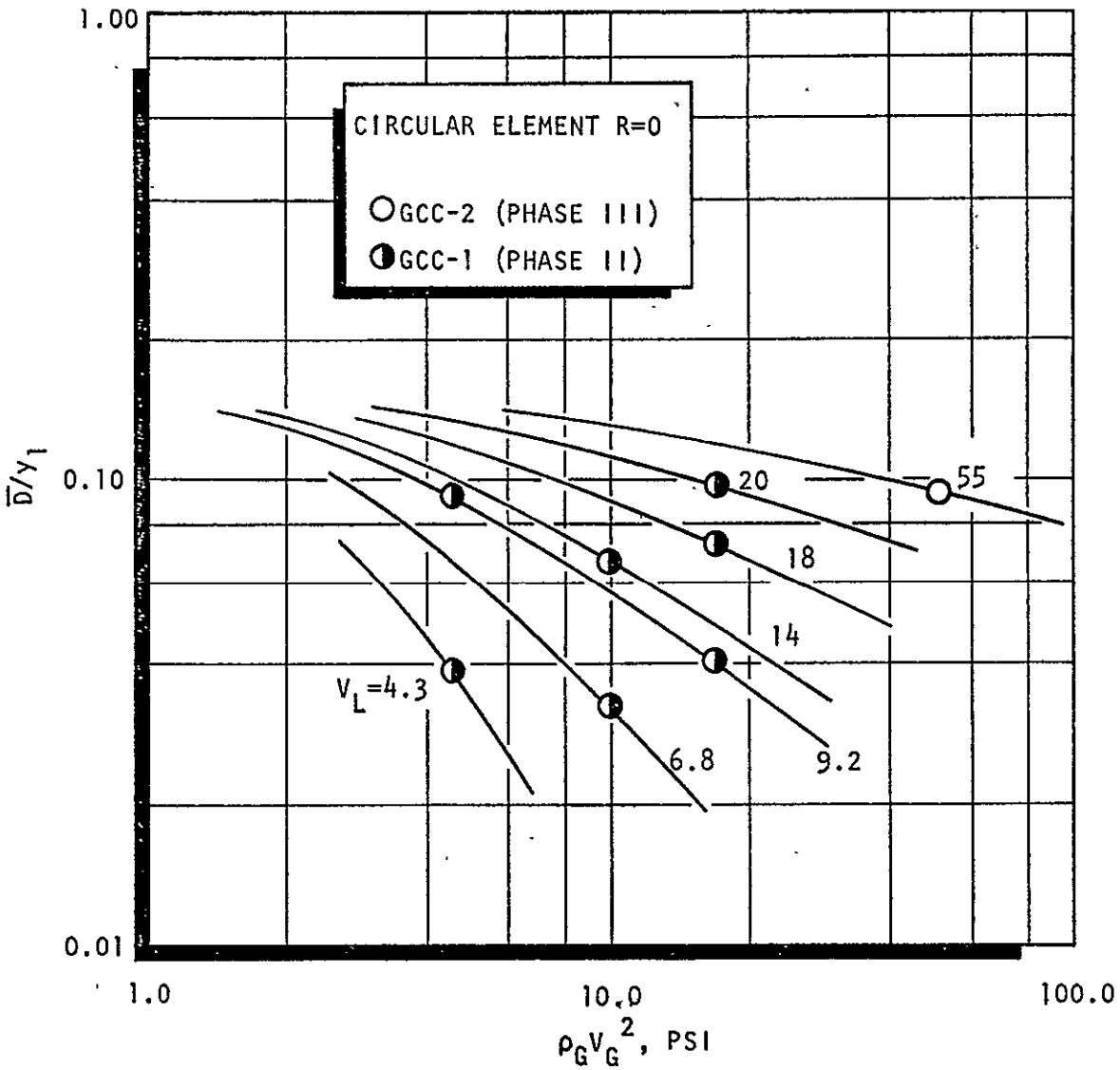

Figure 6-25. Variation of Dropsize With $\rho_G V_G^2$ and V_L. Baseline Circular Element. (Note: Solid lines are estimates based upon the limited data shown)

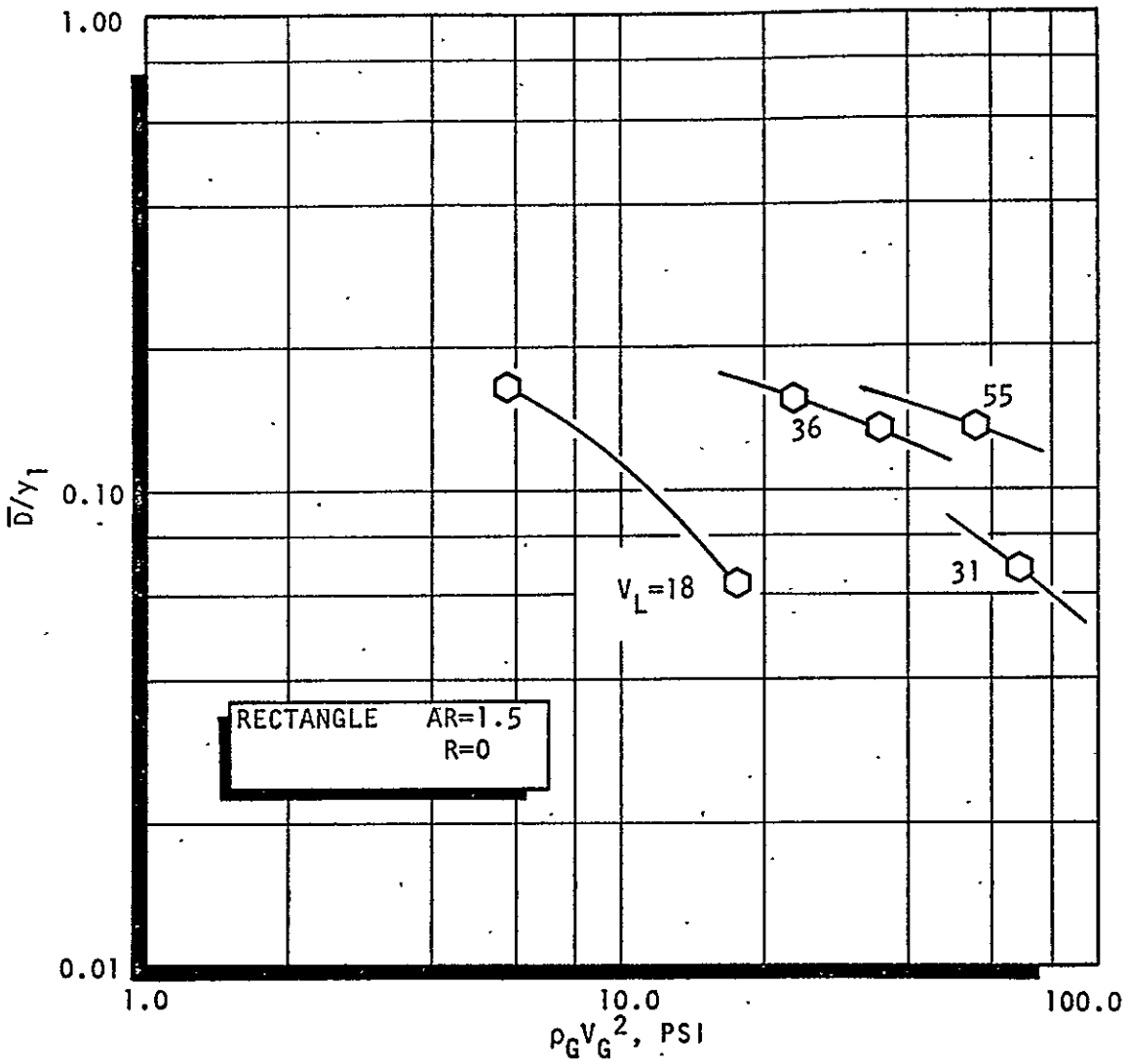

Figure 6-26. Variation of Dropsize With $\rho_G V_G^2$ and V_L. Baseline AR=1.5 Element (GCR-6)

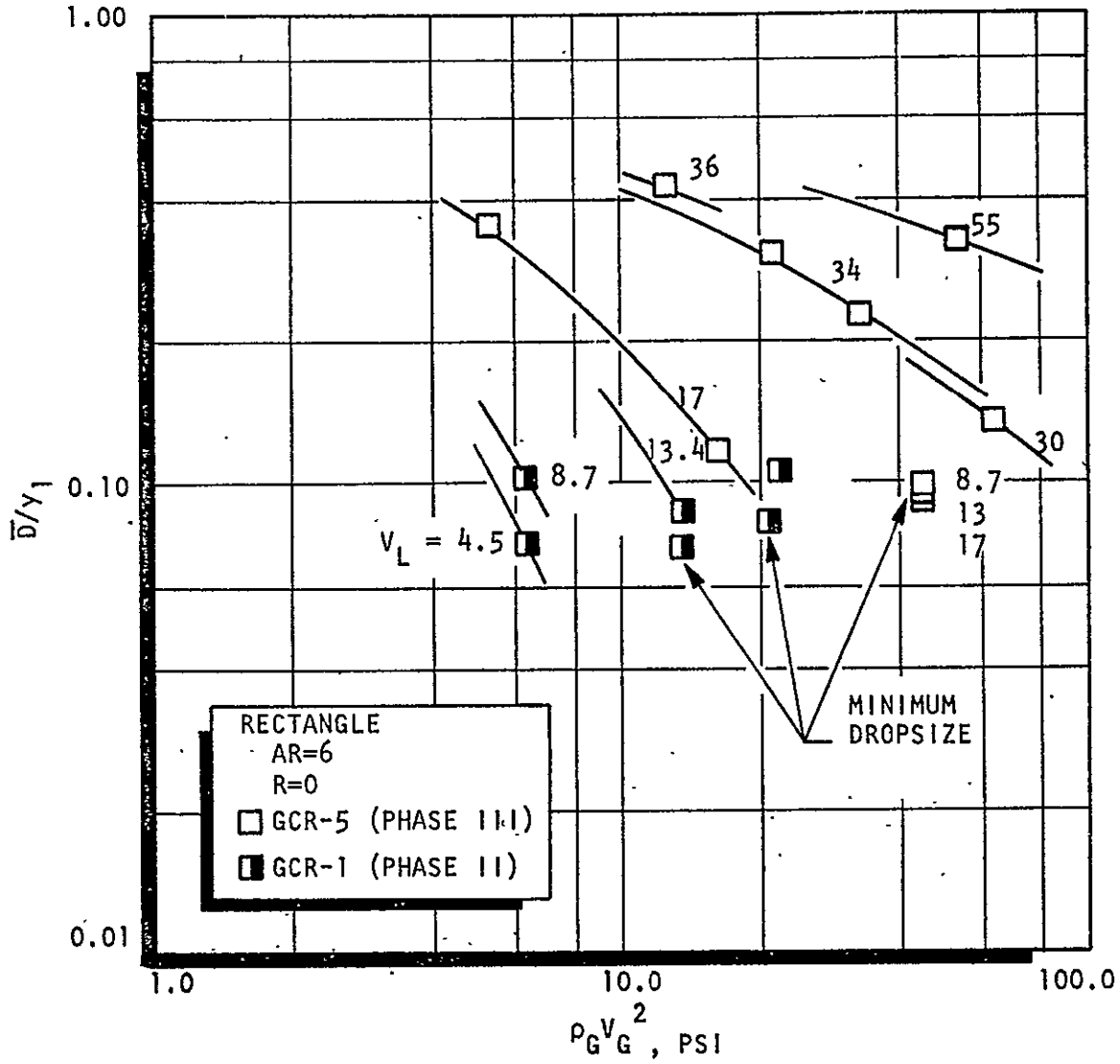

Figure 6-27. Variation of Dropsize With $\rho_G V_G^2$ and V_L Baseline AR=6 Element

would not be the case, however, if the droplet were held in place until breakup occurred. In that case, smaller droplets could be obtained from droplets less than 100μ with increased gas velocity.

Further dropsize comparisons for the baseline elements are presented in Fig. 6-28 through 6-30 as functions of $\rho_G V_G^2$ for three different liquid velocities.

Finally, the effect of liquid velocity variation upon dropsizes with centerpost recess is shown in Fig. 6-31. Once again, the limiting dropsize phenomenon appears in these data. Actually, the dropsize at the breakoff point is approximately 200μ.

This is a rather large dropsize and smaller droplets should have been achieved for for this element. The premature breakoff at this point has not been explained.

6.3.3 Multishowerhead Triplet Results

The basic multishowerhead triplet (MST) element mixing and atomization results are discussed briefly in this section (for data, see Ref. 6-2). The specification for the two MST elements tested (GST-1 and GST-2) may be found in Table 6-5.

A face pattern view of the two MST elements is shown in Fig. 6-32. In each case, two rectangular gas jets are impinged at an included angle of 60 degree upon a set of showerhead liquid orifices. The total gas and liquid areas are equal, respectively, for the two elements.

The objective of the test series was to determine the effect of the size and number of the liquid jets upon mixing and atomization. The basic results are presented in Fig. 6-33. It can be seen that the number of orifices had little effect on the mixing characteristics of the element. However, dropsize was greatly improved with the larger number of orifices (smaller jets) at low gas velocity. At higher gas velocity the jet size had no effect.

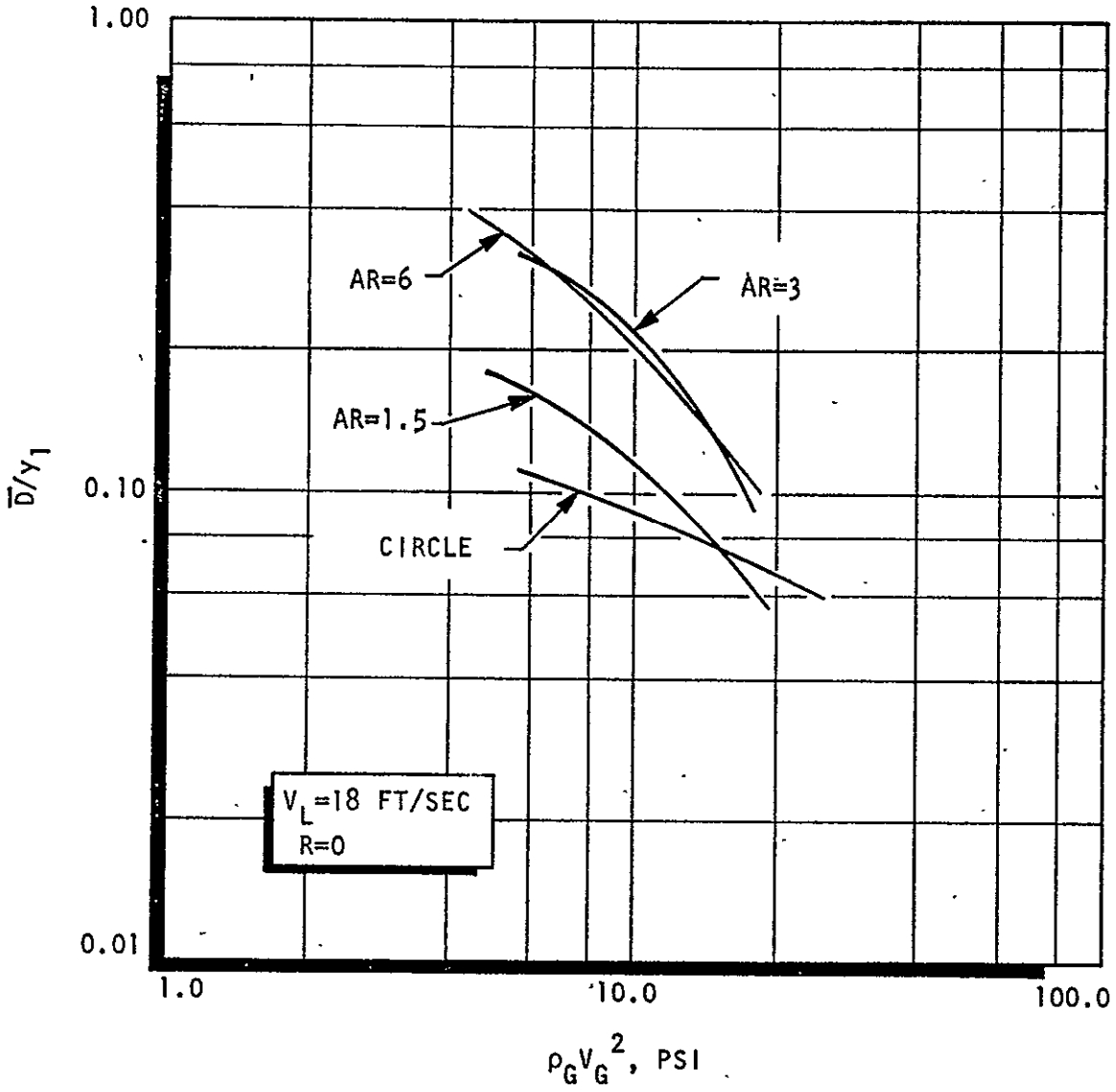

Figure 6-28. Baseline Element Dropsize Comparison

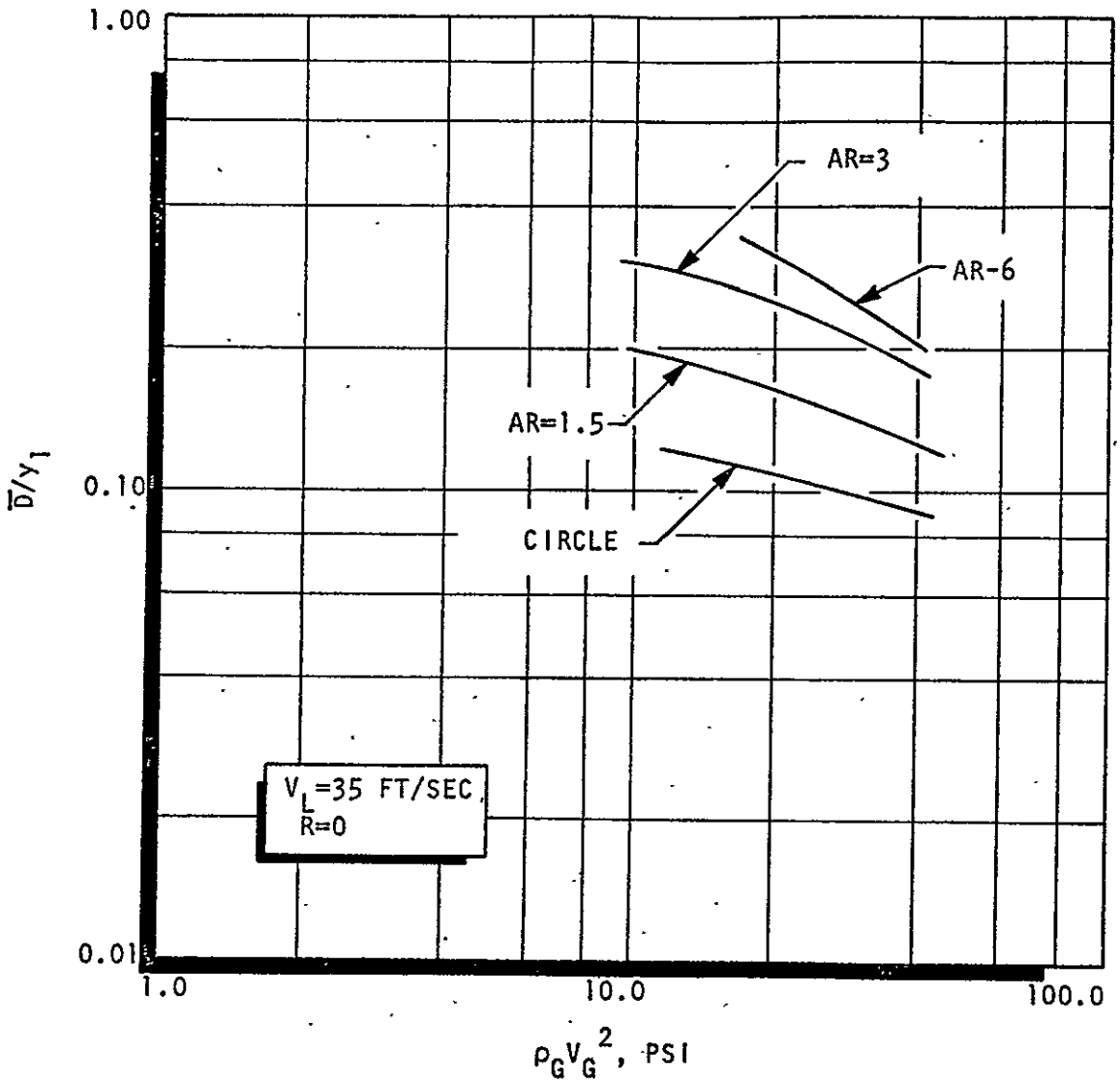

Figure 6-29. Baseline Element Atomization Comparison

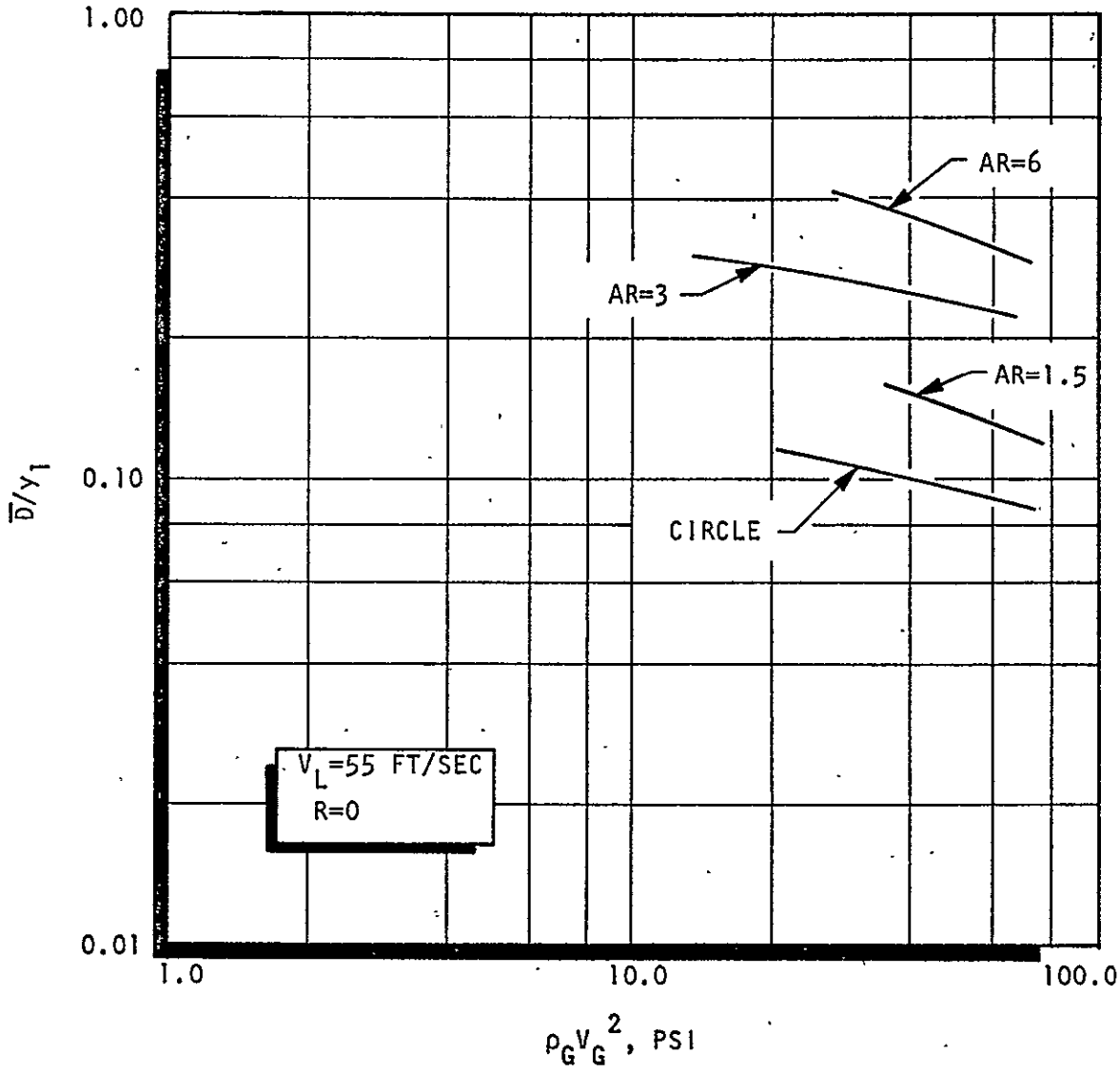

Figure 6-30. Baseline Element Atomization Comparison

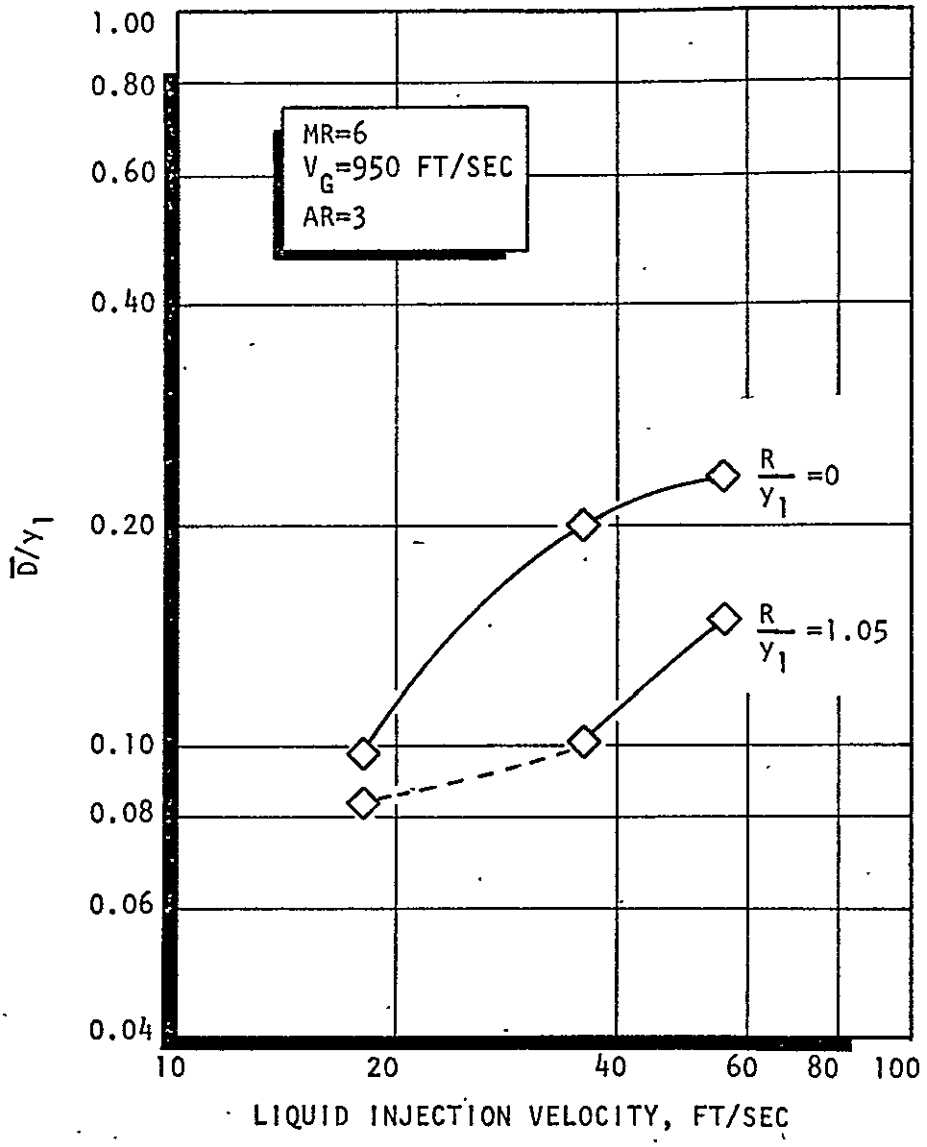

Figure 6.31. Dropsize Variation With V_L Showing the Effect of Center-Post Recess (GCR-2)

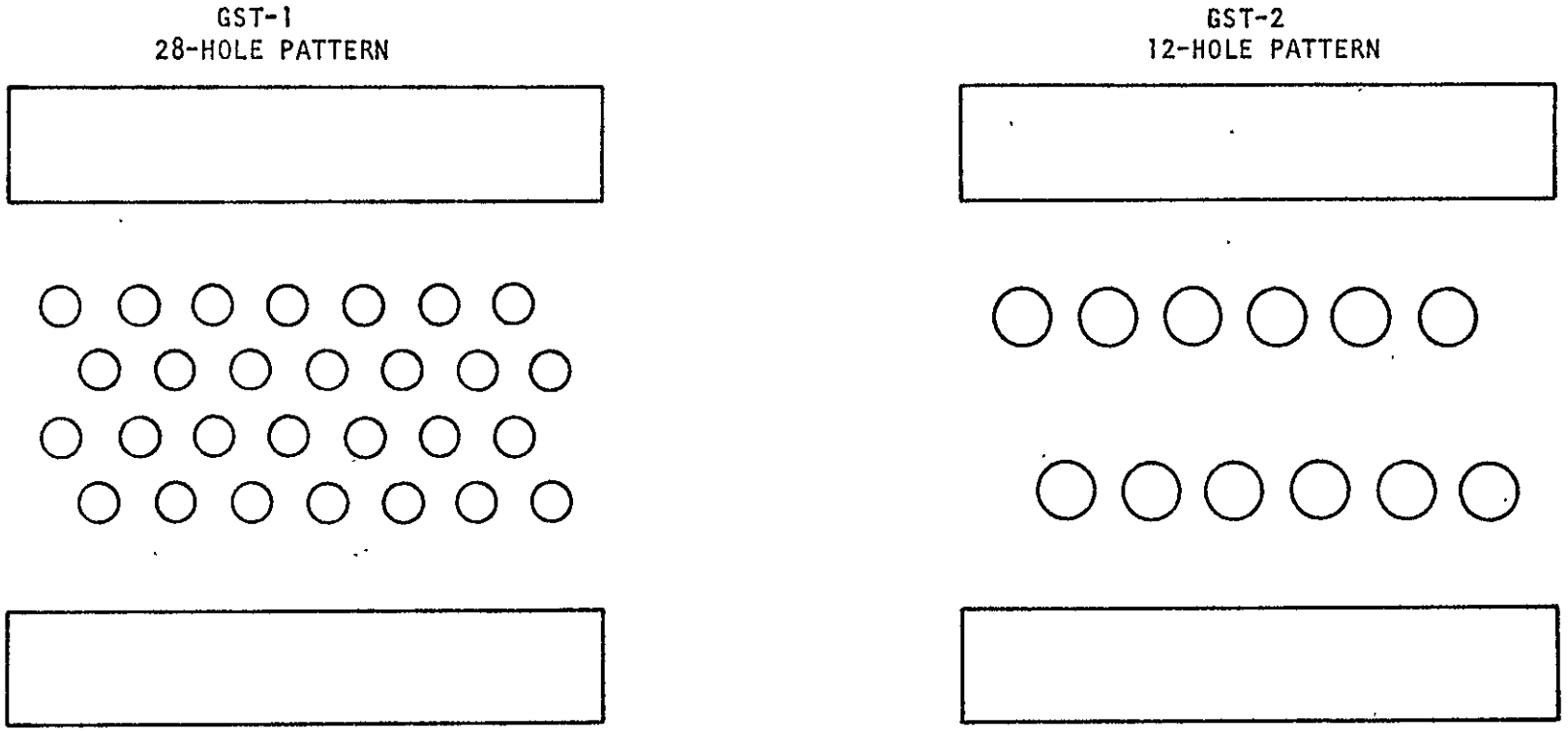

Figure 6-32. Multishowerhead Triplet-Element Face Pattern

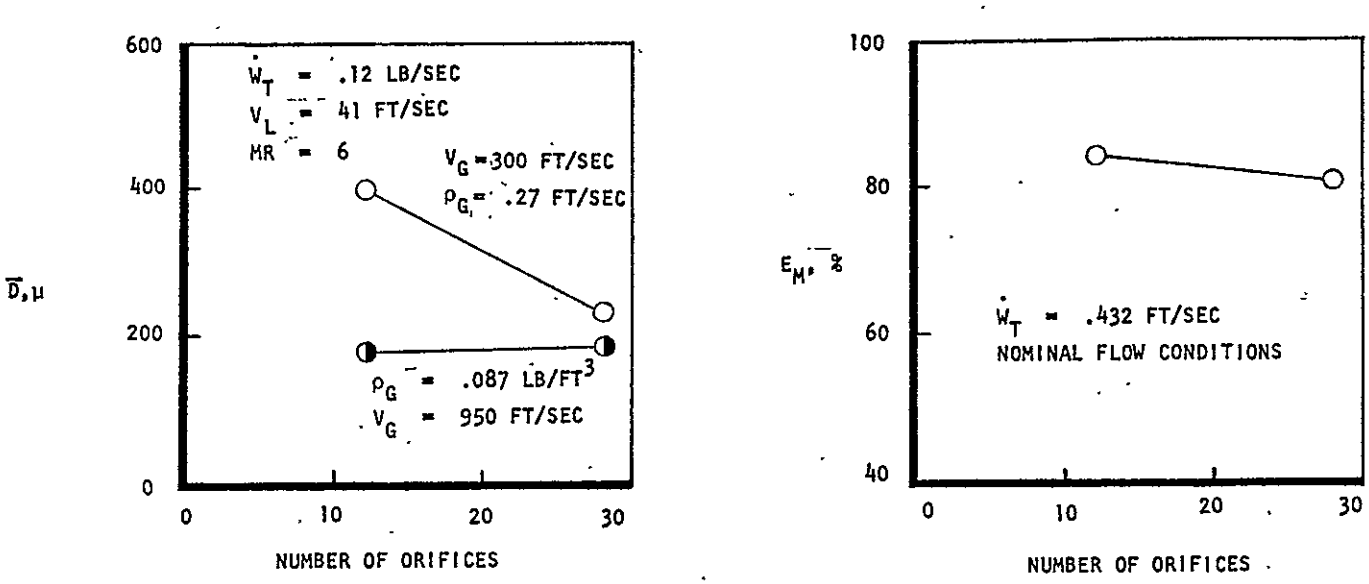

Figure 6-33. Atomization and Mixing Results for the Multishowerhead Triplet Elements (GST-1 and GST-2)

The truly interesting aspect of these data is that the mixing uniformity is relatively high and the droplet diameters are quite small. Further atomization characteristics of the 28-orifice element (GST-1) are presented in Fig. 6-34. Dropsize is shown as a function of liquid velocity along lines of constant gas velocity and gas density. The trend with constant gas density suggests that there is an optimum operating point for atomization. This is logical in view of the fact that this element is subject to agglomeration of the liquid jets of the gas velocity is not high enough. The diameter of each jet is already 500 microns. This is as small as some of the droplets produced by the concentric tube elements. Evidently, below the optimum operating point the benefit of reduced liquid velocity is overcome by the agglomeration produced by the "pushing together" of the liquid jets.

In all, these are very interesting elements and should be investigated in more detail. The brief mention of their results in this report is not from a lack of technical interest but rather from limitations dictated by the scope of the program.

These elements were not included in the hot-fire experiments under this study.

6.3.4 Hot-Fire Studies

Results of the gas/liquid hot-fire studies are presented in this section. The values of η_{c^*} have been corrected for static-to-throat stagnation pressure (a 4.2 percent increase) and for bulk heat loss to the chamber walls (roughly a 1 to 2 percent effect). A bulk heat loss correction was selected for this chamber due to its large L/D (6.7) and large surface area to cross-sectional area ratio. Tables of the experimental data may be found in Ref. 6-2.

The single-element thrust chamber was 4 inches in length from the injector-to-throat plane. The chamber diameter was 0.6 inch and the throat diameter was 0.395 inch giving a contraction ratio, $\varepsilon_c \cong 2.3{:}1$. Details of the chamber design may be found in Ref. 6-3.

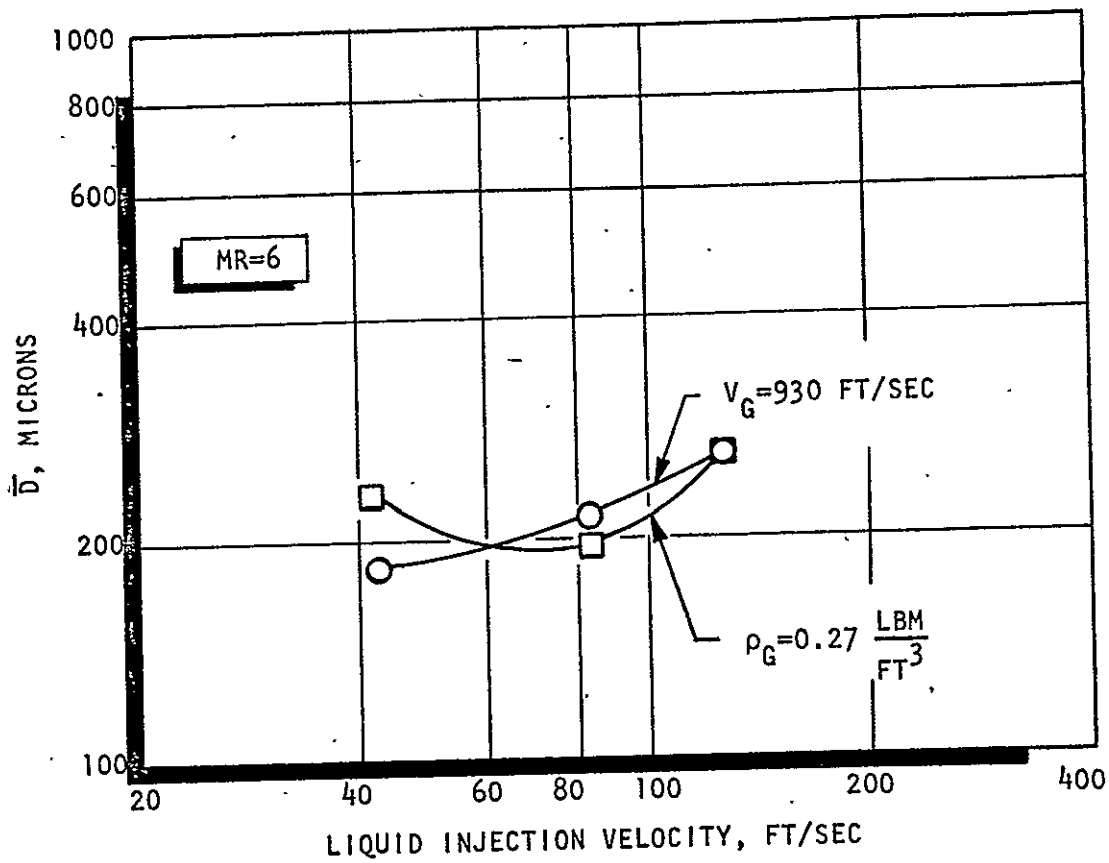

Figure 6-34. Variation of Dropsize for the MST-1 Element as a Function of Liquid Velocity Along Lines of Constant V_G and ρ_G

6.3.4.1 Nominal Conditions-Baseline Comparison. Hot-fire c* efficiency results for the four baseline elements are presented in Fig. 6-35. Values of η_{c^*} are shown as functions of the operating static pressure (not the computed throat stagnation pressure). The elements were throttled over a range of chamber pressure to ensure that a valid interpolation to the baseline 800 psia could be made. Data obtained at several values of center-post recess are presented for the baseline circular element and the baseline AR = 3 element.

In general, the performance dropped off slightly with increased chamber pressure (throttling up). For the two elements fired with center-post recess, the performance was improved substantially as recess was increased.

The variation of c* efficiency with aspect ratio, at zero recess and nominal conditions, is presented in Fig. 6-36. The performance first improved markedly with aspect ratio and then suddenly fell off again at the highest aspect ratio.

The effect of center-post recess upon η_{c^*} is shown in Fig. 6-37 for the circular and the AR = 3 baseline elements at nominal conditions. For both elements, the performance was significantly improved with recess. However, the difference in performance between the elements was maintained, approximately. The performance of the recessed (R/y_1 = 1.411) AR = 3 rectangular concentric tube element was notably high for a single-element injector (η_{c^*} = 95 percent).

6.3.4.2 Variations About AR = 3. Charactersitic velocity efficiency for the three variations about the aspect ratio 3.0 baseline element is presented in Fig. 6-38. A detailed comparison of the data with those obtained with the baseline AR = 3 element is presented in the next section in which the cold-flow and hot-fire results are correlated. One trend of note that is evident in these results is that the scaled-down model of the baseline AR = 3 element (GCR-7) appears to be more sensitive to throttling than its larger counterpart.

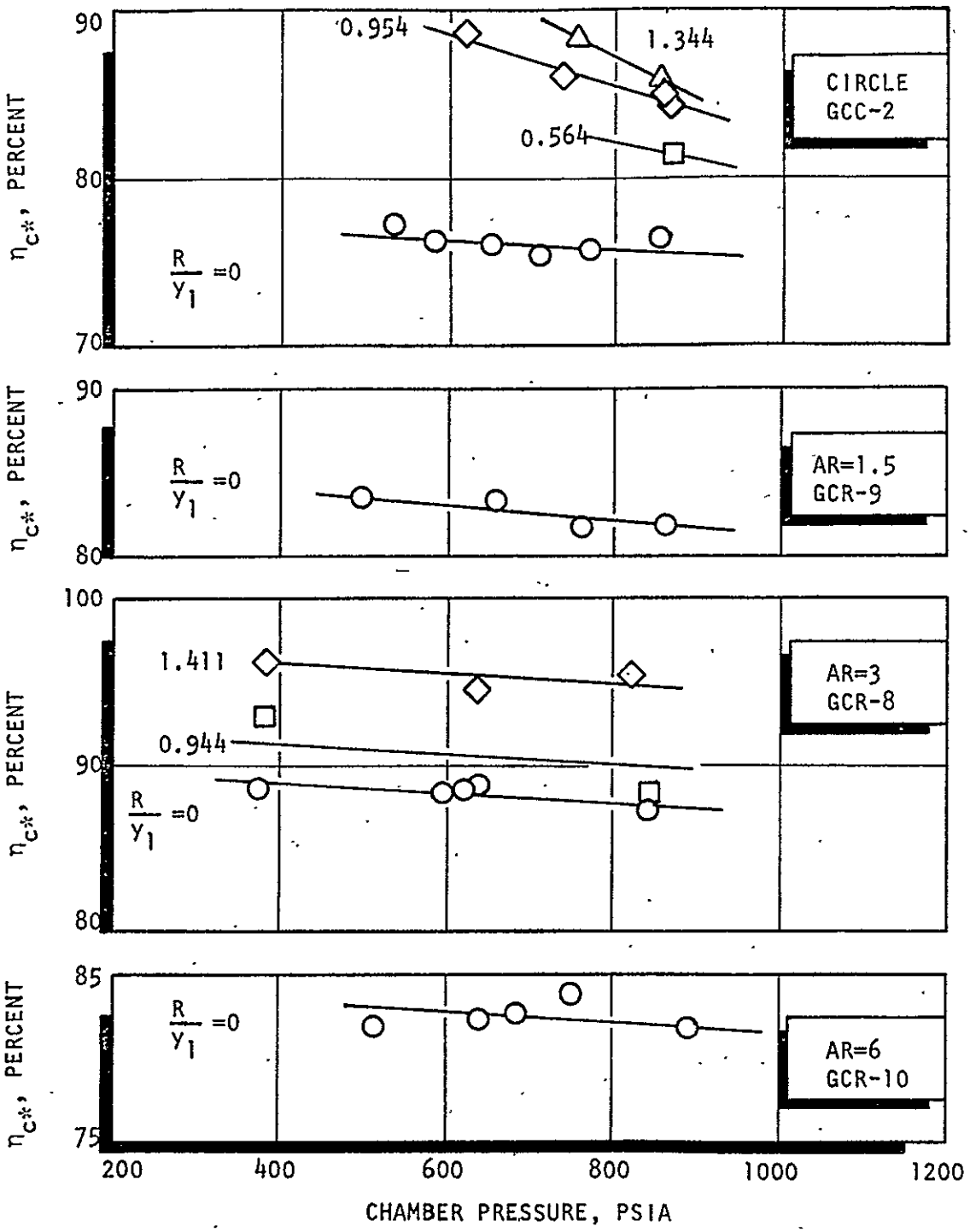

Figure 6-35. Characteristic Velocity Efficiency as a Function of Chamber Pressure (Baseline Elements)

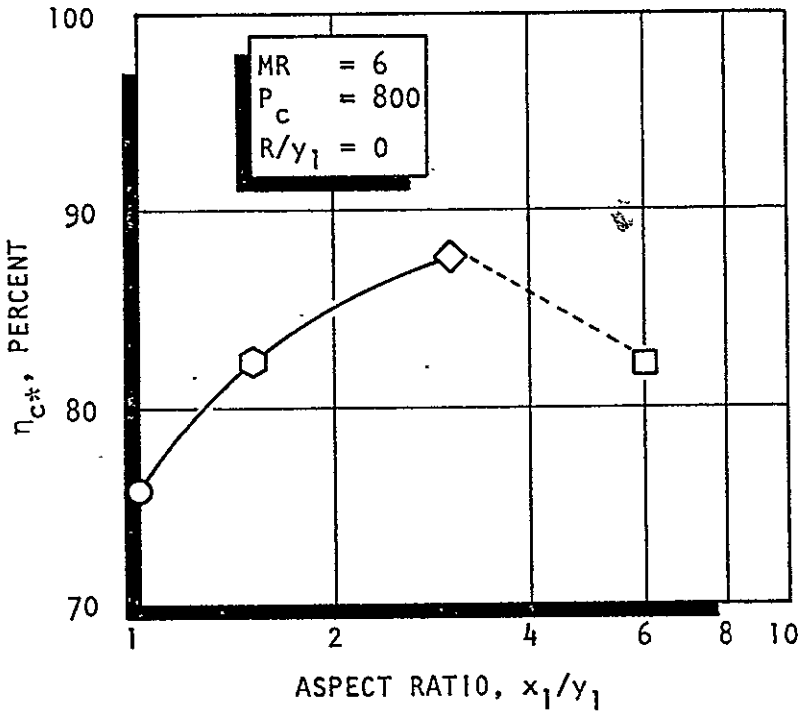

Figure 6-36. Variation of c* Efficiency With Aspect Ratio (baseline elements, nominal conditions)

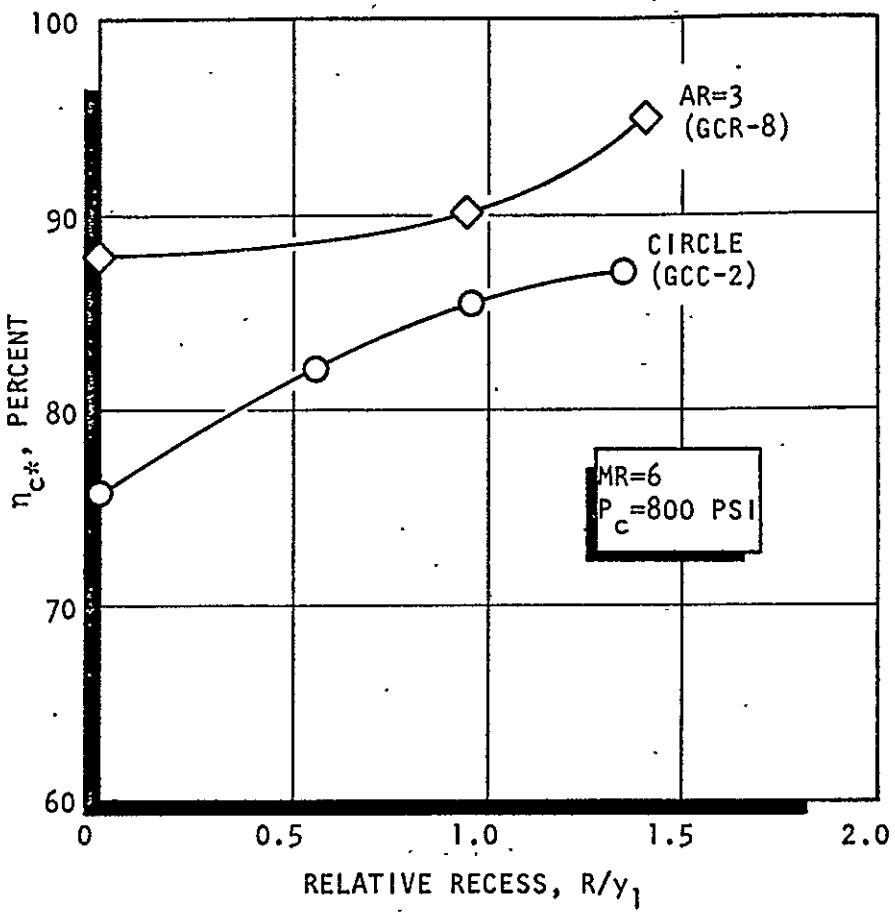

Figure 6-37. Characteristic Velocity Efficiency as a Function of Center-Post Recess (nominal conditions)

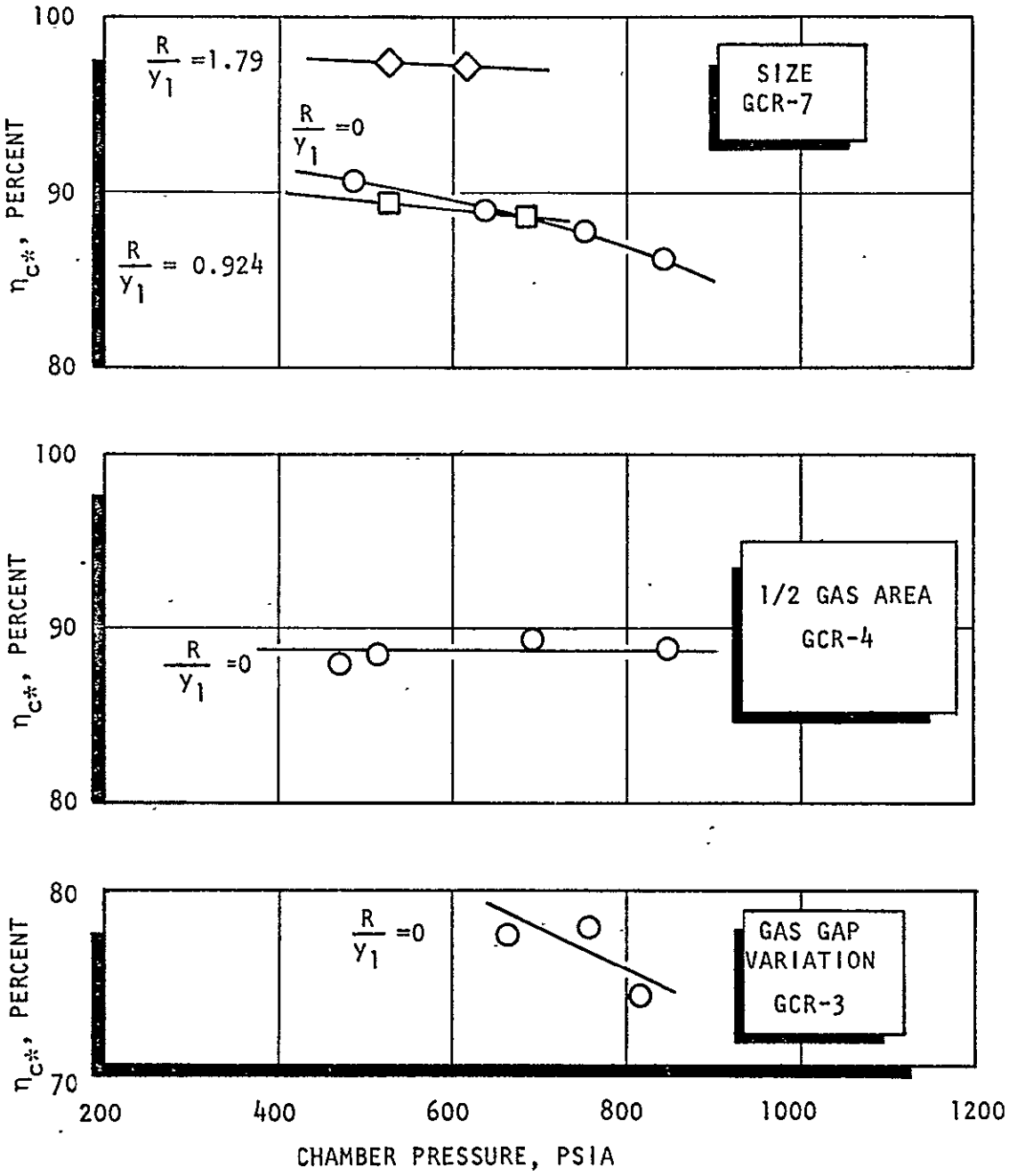

Figure 6-38. Variation About AR=3 Comparisons, c* Efficiency as a Function of Chamber Pressure

6.4 CORRELATION OF THE TEST RESULTS

This section contains a comparison of the gas/liquid cold flow and hot fire results. The approach to this comparison has been discussed, briefly, in section 6.1. Basically the cold-flow results have been transformed into mixing limited ($\eta_{c^*_{mix}}$) and vaporization limited ($\eta_{c^*_{vap}}$) c* efficiency values and these values employed as the primary basis of comparison with hot-fire c* efficiency trends. The methods employed to compute the values of $\eta_{c^*_{vap}}$ and $\eta_{c^*_{mix}}$ are summarized in Appendix B. The results of these computations are presented in Fig. 6-39 and 6-40.

The mixing limited c* efficiency, $\eta_{c^*_{mix}}$, is presented in Fig. 6-39 as a function of E_m for all of the injector elements of Phase III. It can be seen that one curve describes these data quite well. However, this curve is only valid for mixture ratio 6.0. Other mixture ratios will yield separate curves. This points to the fact that E_m and $\eta_{c^*_{mix}}$ are not uniquely related.

The vaporization limited efficiency results are presented in Fig. 6-40 wherein the value of $\eta_{c^*_{vap}}$ is shown as a function of the mass median liquid oxygen droplet diameter. The droplet distributiin function employed to compute these results was shown in Fig. 6-18.

Comparisons between cold flow and hot fire are made at the nominal conditions. A list of these conditions may be found in Table 6-4. The results of the calculations of mixing limited and vaporization limited efficiency are summarized in Table 6-6. For each element, the values of E_m, $\eta_{c^*_{mix}}$, $\overline{D}_{wax}$, $\overline{D}_{LOX}$, $\eta_{c^*_{vap}}$ and ($\eta_{c^*_{C.F.}}$) are presented.

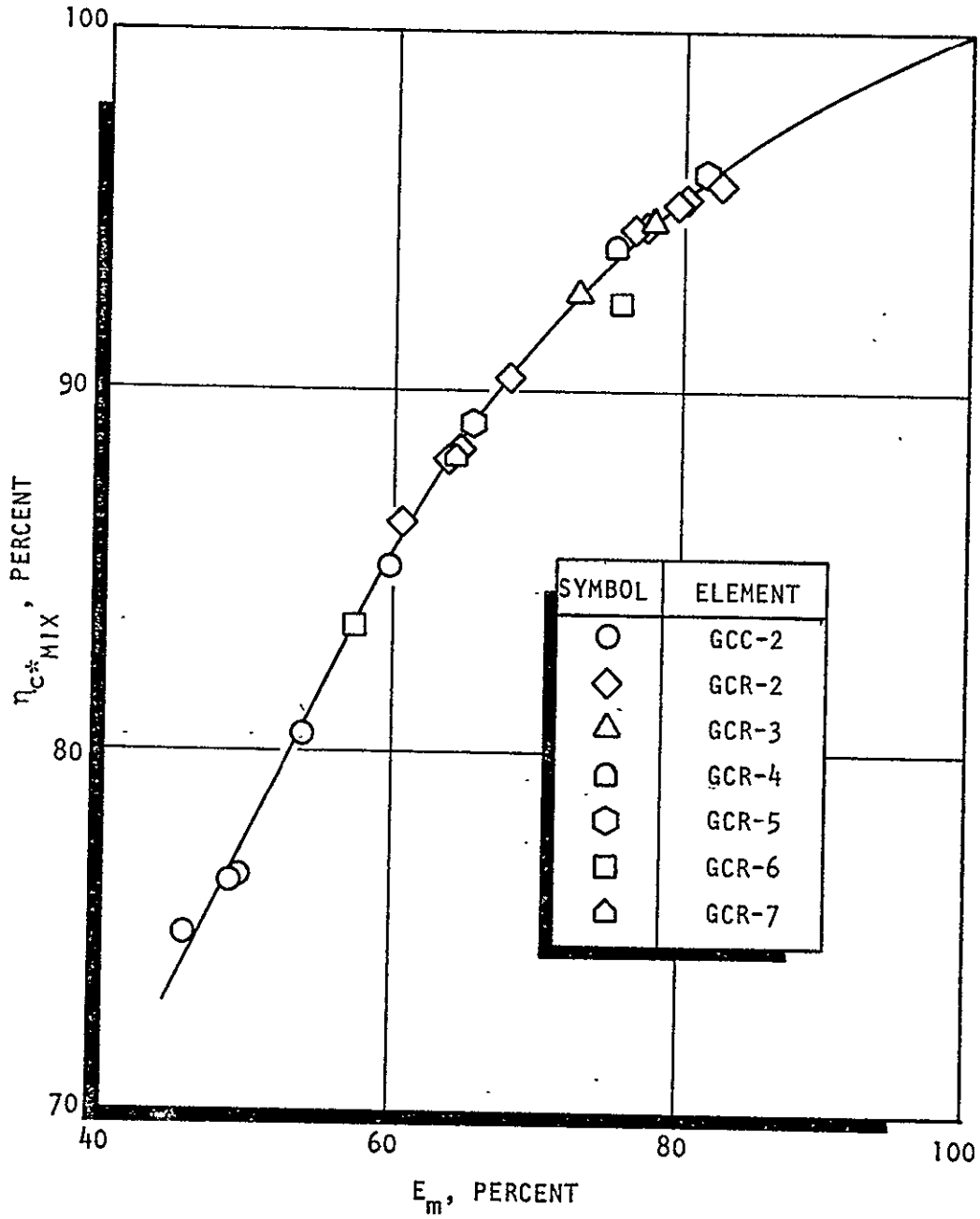

Figure 6-39. Mixing Limited c* Efficiency as a Function of E_m, for LOX/GH_2 at a Mixture Ratio 6.0:1 (all injector elements)

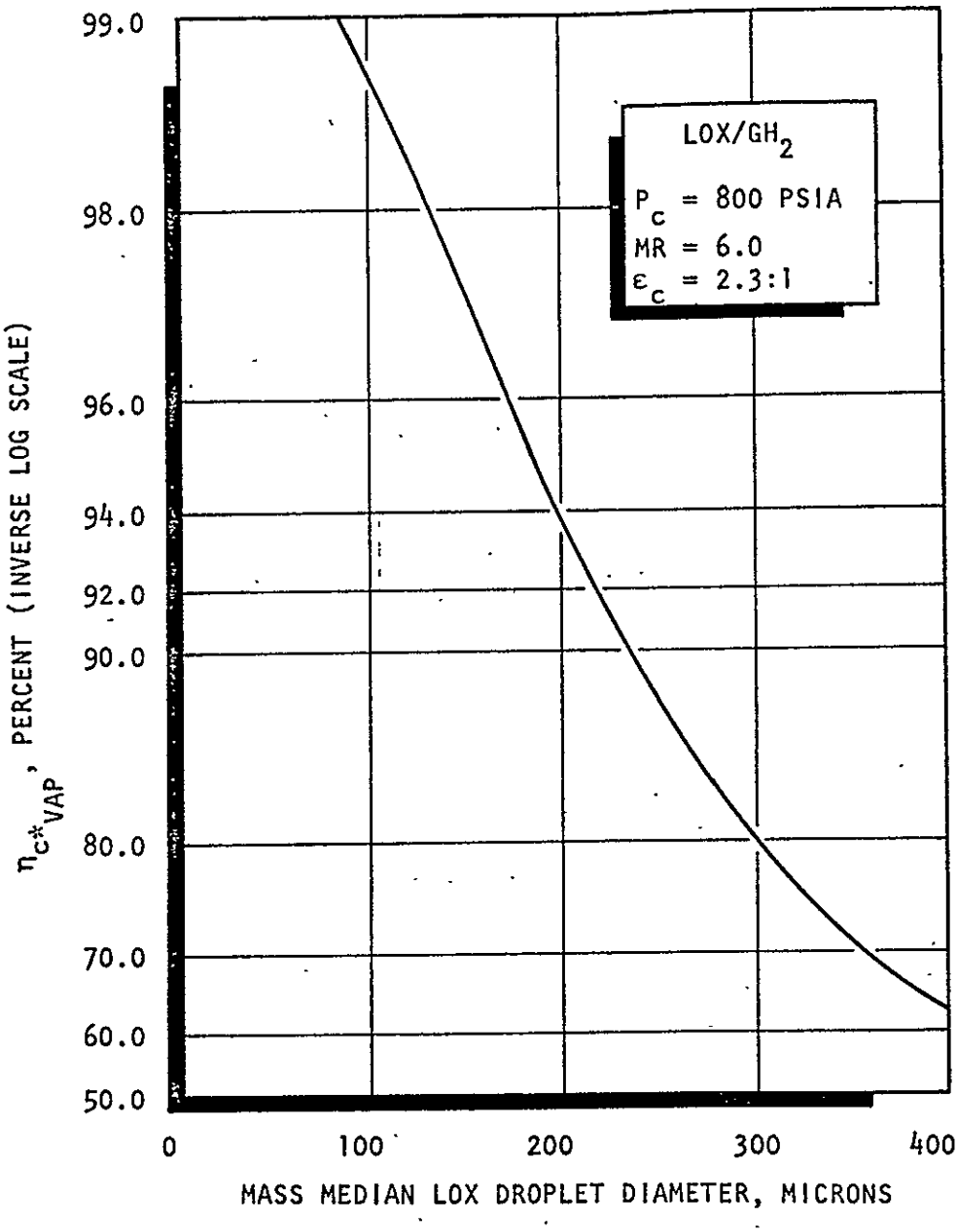

Figure 6-40. Vaporization Limited c* Efficiency for LOX/GH$_2$ at Mixture Ratio 6.0:1 for P_c = 800 psia and Contraction Ratio 2.3:1

TABLE 6-6. RESULTS OF MIXING-LIMITED AND VAPORIZATION-LIMITED C* EFFICIENCY CALCULATIONS BASED UPON COLD-FLOW DATA (NOMINAL CONDITIONS)

Element Code No.	Element Type	Relative Recess R/y_1	E_m, %	η_{c^*} mix	$\overline{D}_{wax}$ microns	$\overline{D}_{LOX}$ microns	η_{c^*} vap	η_{c^*} C.F.
GCC-2	Circle	0	47.0	75.1	395	150	97.3	73.1
		0.564	49.0	76.7	342	130	98.0	75.2
		0.954	52.8	79.8	310	118	98.4	78.5
		1.344	57.2	83.3	281	107	98.6	82.1
GCR-9	AR = 1.5	0	57.2	83.3	399	152	97.2	81.0
GCR-8	AR = 3	0	64.0	88.0	488	186	94.8	83.4
		0.564	67.5	90.2	413	157	96.9	87.4
		0.944	74.5	93.4	363	138	97.8	91.3
		1.411	81.0	95.6	314	120	98.3	94.0
GCR-10	AR = 6	0	65.8	89.2	428	163	96.6	86.2
GCR-7	Size	0	64.4	88.3	287	109	98.6	87.1
GCR-3	Gas gap	0	49.5	77.2	321	122	98.3	75.9

The conversion from wax droplet diameter to liquid oxygen droplet diameter was based upon a property correction for gas/liquid atomization developed by Ingebo. This correction has been employed for gas/liquid concentric tube results in a FLOX/methane injector study at Rocketdyne (Ref. 6-4). The value of the correction was computed with Eq. 6-7.

$$\frac{\overline{D}_{LOX}}{\overline{D}_{WAX}} = \frac{\left(\frac{\sigma\mu}{\rho}\right)_{LOX}}{\left(\frac{\sigma\mu}{\rho}\right)_{WAX}} = 0.381$$

where

$\sigma \equiv$ surface tension
$\mu \equiv$ viscosity
$\rho \equiv$ density

Comparisons between the cold-flow and hot-fire c* efficiencies are presented in Fig. 6-41 through 6-44 for the baseline elements and two of the variations about AR = 3. In each figure, curves for both the cold-flow c* efficiency ($\eta_{c^*_{C.F.}} = \eta_{c^*_{mix}} \times \eta_{c^*_{vap}}$) and the mixing limited c* efficiency, $\eta_{c^*_{mix}}$ are presented. The curves for $\eta_{c^*_{mix}}$ alone show the mixing limited c* performance and imply the assumption, $\eta_{c^*_{vap}}$ = 100 percent. Examination of Fig. 6-41 through 6-44 will show that the curves representing mixing limited performance are much more representative of the hot-fire results than the curves which include a vaporization limited component. This result is quite reasonable in light of the fact that no account of secondary droplet breakup has been taken in the calculation of the liquid oxygen droplet diameters.

In this thrust chamber (with a contraction ratio of 2.3:1) the combustion gas can be expected to reach a velocity of 1400 ft/sec in the chamber and 5000 ft/sec at the throat. These velocities are more than adequate to produce substantial secondary droplet breakup. Rocketdyne is presently initiating a program to investigate the effect of secondary atomization with G/L circular concentric tube injector elements.

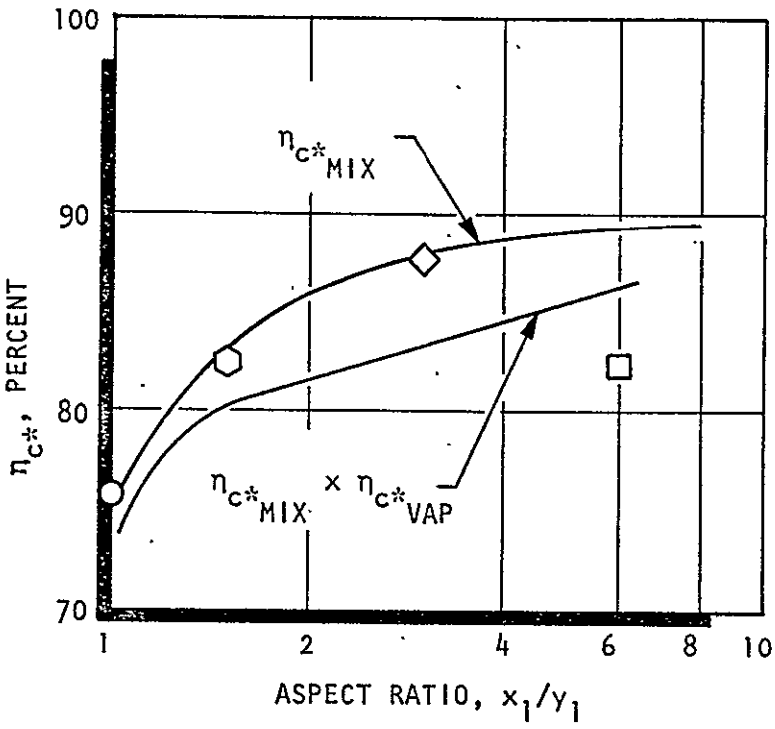

Figure 6-41. Comparison of Hot-Fire and Cold-Flow c* Efficiencies for the Baseline Elements at Zero Recess

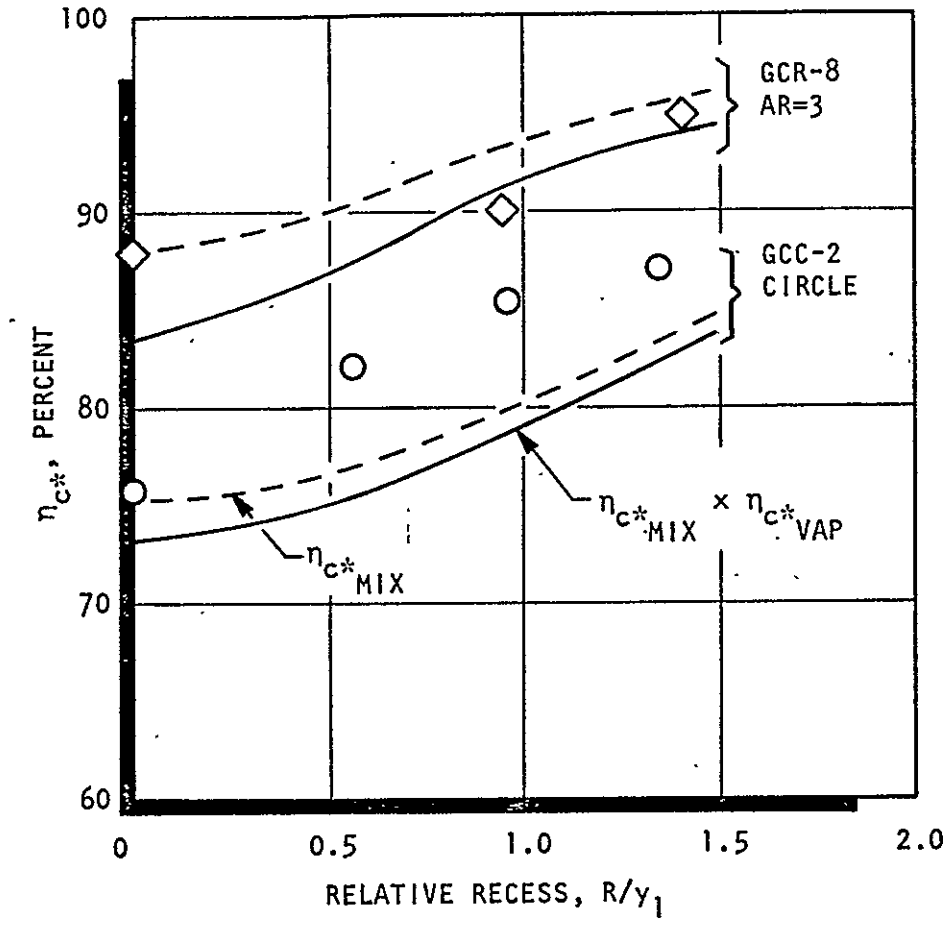

Figure 6-42. Comparison of Cold-Flow and Hot-Fire c* Efficiencies for the CCTE (GCC-2) and the RCTE (AR=3, GCR-8) Presented as a Function of Center-Post Recess

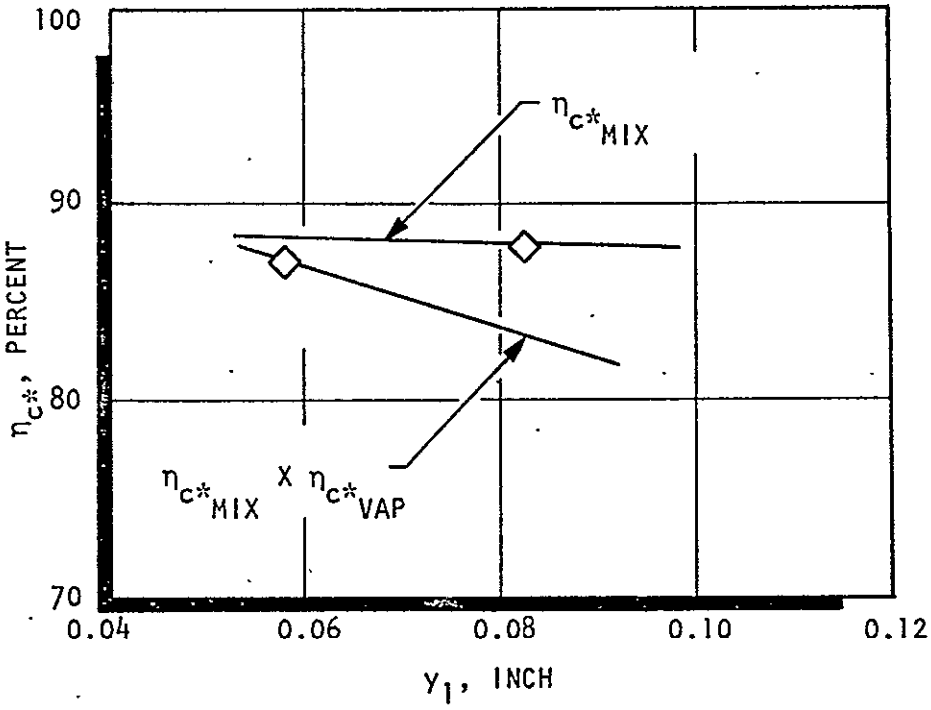

Figure 6-43. Comparison of Cold-Flow and Hot-Fire c* Efficiencies Showing the Effect of Element Size

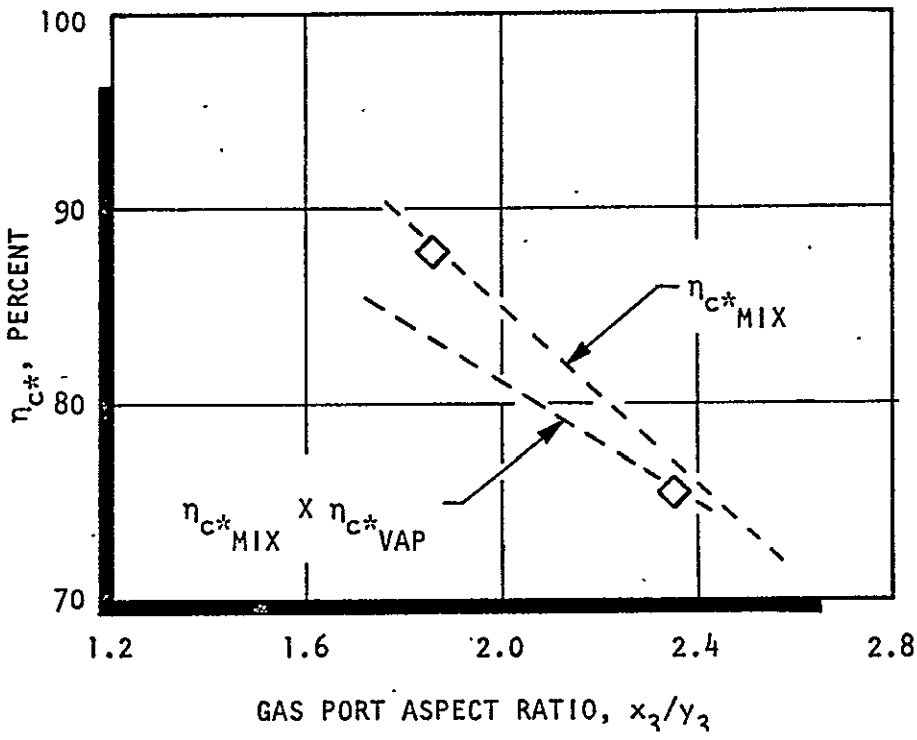

Figure 6-44. Comparison of Cold-Flow and Hot-Fire c* Efficiencies Showing the Effect of Gas Port Aspect Ratio, x_3/y_3

No attempt was made to correct for the influence of secondary breakup in this report due to the fact that there were no experimental data available for G/L secondary breakup at the time of publication. However, sufficient basic data have been presented in this document to allow corrections to be made at such time that these complementary data become available. However, the mixing limited c* results approximate the hot-fire data so well that, even with a more sophisticated droplet size correction, it appears that the values of η_{c^*vap} must approach 100 percent in most cases.

The nominal conditions-baseline element comparison presented in Fig. 6-41 shows that three of the four elements follow the mixing limited c* trend almost exactly. The highest aspect ratio element does not fall on this curve. One possible explanation for this deviation is the following. As the aspect ratio is increased, relative distortion of the flowfield increases (see Fig. 6-7). The aspect ratio 6:1 element is the only element for which the liquid component significantly "breaks through" the gas component to the outer portions of the flowfield (see Fig. 6-7). This could mean that a significant portion of the liquid oxygen may have impinged upon the chamber wall forming a liquid film that would significantly interfere with both the mixing and vaporization mechanisms. This effect would only be associated with extremely small diameter chambers, the higher aspect ratio elements would be oriented with respect to the chamber wall in such a manner that the gas (fuel) component would be next to the wall, not the liquid component.

A comparison of cold-flow and hot-fire c* efficiencies for the baseline CCTE and the AR = 3 RCTE is presented in Fig. 6-42 as a function of center-post recess. Here again, the mixing limited cold-flow curves are more representative of the hot-fire performance. The level and increase of performance with recess are quite closely approximated in the case of the RCTE. The performance of the CCTE increased to a greater degree than was estimated from cold flow.

Two of the variations about aspect ratio 3:1 are compared on the basis of c* efficiency in Fig. 6-43 and 6-44. In Fig. 6-43, the effect of element size clearly

demonstrates the "mixing limited" nature of the hot-fire results. Reference to Fig. 6-10 and 6-22a will recall that the cold-flow results showed no change in level of mixing with size. However, a significant reduction or primary dropsize was suggested as element size was reduced. The hot-fire results show no significant change in performance with size.

The effect of gas port aspect ratio is shown in Fig. 6-44. The trends suggested by cold-flow results are drawn as straight lines only to represent the change from one aspect ratio to the other, and are not representative of the true curves that should connect these two points (see Fig. 6-13). The change in level of performance, and indeed the actual values of performance, are represented by the mixing limited cold-flow results.

In summary, it may be concluded that the correlation between the mixing limited cold-flow c* efficiencies and the hot-fire performance values is excellent. It may be assumed, therefore, that the mixing trends suggested by the cold-flow data are truly representative of the processes encountered in hot fire and that the cold-flow design guidelines may be employed in the formulation of injector designs for hot fire.

Due to the mixing limited nature of the hot-fire results, the trends in concentric tube atomization characteristics have neither been confirmed nor denied. However, other studies (see Ref. 6-4) have clearly confirmed the validity of the cold -flow atomization representation.

7.0 APPLICATIONS OF THE RESULTS TO INJECTOR DESIGN

Detailed design criteria are presented in each of the three major sections of this report: Single Orifice Studies, Single Element Liquid/Liquid Studies, and Single Element Gas/Liquid Studies. It is not the intent of this section to reproduce all of these results from the standpoint of injector design. Rather, four of the more interesting aspects of the results have been selected for presentation to provide general guidelines for the application of noncircular technology. These examples include: computation of the orifice coefficient for a noncircular orifice (liquid propellants), design of rectangular unlike doublets for maximum mixing (liquid/liquid applications), design of unlike triplets for maximum mixing (liquid/liquid applications), and basis for the selection of rectangular concentric tube elements for gas/liquid injector applications.

7.1 COMPUTATION OF THE ORIFICE COEFFICIENT FOR A NONCIRCULAR ORIFICE (LIQUID PROPELLANTS)

Summaries of results of the orifice coefficient models that have been discussed and appear in Fig. 4-14 and 4-16. Predicted values of orifice coefficient are plotted as functions of orifice L/D, Reynolds, and the parameter $\sqrt{(L/D)/Re}$ in Fig. 4-14 for round-entrnace orifices and in Fig. 4-16 for sharp entrance orifices. The Reynolds No. is based on the hydraulic diameter, making these results applicable to orifices of arbitrary shape. The effect of cross velocity on orifice coefficient is shown in Fig. 4-18. Orifice coefficient, normalized with respect to its value at zero cross velocity, is plotted as a function of manifold velocity head divided by the static pressure drop across the orifice.

A typical design example is presented below to demonstrate the use of these curves. The problem is to determine the discharge coefficient for a given orifice under specific operating conditions. The parameters to be used for this example are listed below:

GIVEN:

Orifice Shape	square (sharp edged entrance)
Orifice Size	0.1" on a side

Orifice Area	0.01 inch^2
Hydraulic Diameter	0.1"
Flowrate	0.2 lb/sec
Fluid	Water
Manifold Velocity	20 ft/sec
L/D	21.5

FIND:

Orifice Coefficient

The first step in the procedure is to compute the Reynolds:

$$Re = \frac{V_o \, D_H}{12 \, \nu}$$

where

V_o = velocity through orifice, ft/sec

D_H = hydraulic diameter, inches

ν = kinematic viscosity, ft^2/sec

The velocity may be computed using the continuity equation:

$$V_o = \frac{\dot{w}}{\rho A} = \frac{0.2(144)}{62.4 \ (0.01)} = 46.2 \text{ ft/sec}$$

The Reynolds No. is now:

$$Re = \frac{46.2(0.1)}{12 \ (10^{-5})} = 3.85 \times 10^4$$

A discharge coefficient for zero cross velocity may now be estimated from Fig. 4-16 At Re = 38,500 and L/D = 21.5 - 1.5 (for entrance length), the value of C_D is approximately 0.71. This is the coefficient at zero cross velocity, or $C_{D_{V_c}} = 0$

To find the effect of cross velocity from Fig. 4-18, the static pressure drop across the orifice must be computed. This would actually be an iterative process except that cross velocity produces a second order effect. This makes the first calculation fairly accurate. To compute the ΔP, the value of C_D at zero cross velocity may be used as a first approximation:

$$\Delta P_s \simeq \frac{144\ \dot{w}^2}{C_D^2\ A^2} / \ 2g\rho$$

Substituting:

$$\Delta P_s \simeq \frac{(144)\ (0.2)^2}{(0.71)^2\ (0.01)^2} \ / \ 2(32.2)\ (62.4) = 28.5 \text{ psid}$$

Next, the velocity head in the manifold is computed:

$$\frac{\frac{1}{2}\ \rho V_c^{\ 2}}{(144)g} = \frac{1}{2}\ \frac{(62.4)\ (20)^2}{(144)\ (32.2)} = 2.69 \text{ psi}$$

To enter Fig. 4-16, the parameter $\frac{1}{2}\ \rho V_c^{\ 2}/\Delta P_s$ is calculated:

$$\frac{\frac{1}{2}\ \rho V_c^{\ 2}}{\Delta P} \simeq \frac{2.69}{28.5} = 0.094$$

From Fig. 4-16 at $\dfrac{\frac{1}{2}\ \rho V_c^{\ 2}}{\Delta P_s} = 0.094$:

$$\frac{C_D}{C_{D_{V_{c=0}}}} = 0.95$$

Finally, the value of C_D is computed (including the effect of cross velocity):

$$C_D = C_{D_{V_{c=0}}}\ \frac{C_D}{C_{V_{c=0}}} = 0.71\ (0.95) = 0.675$$

7.2 DESIGN OF RECTANGULAR UNLIKE DOUBLETS FOR MAXIMUM MIXING (LIQUID/LIQUID PROPELLANTS)

The design guidelines for optimum mixing are essentially identical for both circular and noncircular unlike doublets. That is:

$$\phi = 1$$

However, the noncircular orifices provide an additional degree of design flexibility

$$AR_o \Big/ \left(\frac{b_f}{b_o}\right)^3 = 8$$

The importance of this additional flexiblity is illustrated in the following discussion. The specification of a propellant combination and an operational mixture ratio, when combined with the criterion, $\phi = 1$, yields the following relationships:

- for circular orifices:

$$\left(\frac{d_f}{d_o}\right)_{opt} = \sqrt[3]{\frac{\rho_o/\rho_f}{MR^2}}$$

- for rectangular orifices:

$$\left(\frac{b_f}{b_o}\right)_{opt} = \sqrt[3]{\frac{\rho_o/\rho_f}{MR^2}}$$

For the circular orifice, this is the end. The mixing level associated with the particular orifice diameter ratio must be accepted. This limitation is due to the fact that the element area ratio is directly related to the orifice diameter ratio.

However, for the rectangular elements, the added flexibility provided by AR_o allows the maximum level of mixing to be achieved; this, added to $\emptyset = 1.0$, yields the set of design criteria for rectangular unlike doublets;

$$(AR_o)_{opt} = \left(\frac{b_o}{W}\right)_{opt} = 8\left(\frac{b_f}{b_o}\right)^3_{opt} = 8\,\frac{(\rho_o/\rho_f)}{MR^2}$$

Example:

- Assume the following injector design problem:

  Propellants NTO/50-50

  $\rho_o/\rho_f = 1.59$

  Mixture Ratio = 1.6

- The first step is to compute $(b_f/b_o)_{opt}$ such that $\emptyset = 1$:

$$\frac{b_f}{b_o} = \sqrt[3]{\frac{1.59}{(1.6)^2}} = 0.853$$

- The next step is to compute the optimum oxidizer orifice aspect ratio:

$$(AR_o)_{opt} = \left(\frac{b_o}{w}\right)_{opt} = 8\,(0.853)^3 = 5$$

- The fuel orifice aspect ratio is then computed to complete the design:

$$AR_f = \frac{b_f}{w} = \left(\frac{b_o}{w}\right)\frac{b_f}{bo} = (5)\,(0.853) = 4.27$$

- The expected level of mixing for this element would be:

  E_m = 87.5 percent (rounded entrance)
  E_m = 87.5 percent (sharp entrance)
  with $\dot{w} \simeq 0.18$ lb/sec

7.3 DESIGN OF UNLIKE-TRIPLET ELEMENTS FOR MAXIMUM MIXING (LIQUID/LIQUID PROPELLANTS)

The design guidelines for triplet elements having circular orifices are quite simple. Basically, the element design should be configured such that the following criteria are met:

$$\phi = 1.00 \qquad d_1/d_2 \geq 1.0$$

$$\phi \simeq 0.714 \qquad d_1/d_2 < 1.0$$

For a given propellant combination and specified mixture ratio, the value of ϕ may be computed with the following relationship:

GIVEN:

ρ_1 and ρ_2

and mixture ratio = $\dot{W}_2/\dot{W}_1$

$$\phi = \frac{1}{2}\frac{\rho_2}{\rho_1}\left(\frac{d_2}{d_1}\right)^3 \frac{1}{MR^2}$$

Since the value of ϕ is specified for optimum mixing, the following equation represents the design criteria for triplets:

$$\frac{d_1}{d_2} = \sqrt[3]{\frac{1}{2}\,\frac{\rho_2/\rho_1}{\phi\ MR^2}}$$

Once the value of d_1/d_2 (iteration may be required to fix the appropriate value of ϕ), has been established, the maximum level of mixing is determined.

Example:

- Assume the following injector design problem

  Propellants NTO/50-50

  $\rho_o/\rho_f = 1.59$

  Mixture Ratio = 1.6

  Oxidizer in Central Orifice (No. 2)

- To start, it will be assumed that $d_1/d_2 < 1$. The value of d_1/d_2 is then computed (such that $\phi = 0.714$):

$$\frac{d_1}{d_2} = \sqrt{\frac{1}{2} \frac{1.59}{(0.714)(1.6)^2}} = 0.758$$

- Indeed, the value of $d_1/d_2 < 1$, and this is, therefore, the correct value of d_1/d_2.

- For this design, the maximum level of mixing expected is:

  E_m = 93.2 percent (rounded inlet)

  with $\dot{W}_T$ = 0.08 lb/sec

7.4 BASIS FOR THE SELECTION OF RECTANGULAR CONCENTRIC TUBE ELEMENTS FOR GAS/LIQUID INJECTOR APPLICATIONS

The results that have been presented for the gas/liquid rectangular concentric tube injector elements suggest that the introduction of rectangular shape for injector design would be most beneficial for those applications in which high mixture ratio (MR > 4) and/or low gas momentum (fuel Δp < 50 to 100 psi) are imposed. Most typical gas/liquid injectors do operate with mixture ratios greater than 4. For these applications, the rectangular shape can be employed to significantly

improve mixing. However, care must be taken to ensure that the particular thrust chamber is not vaporization performance limited. (It has been shown that an increased aspect ratio produced an increased primary droplet diameter (Fig. 6-21). An aspect ratio of at least 6:1 must be employed to achieve dropsizes which are comparable to a circular element of equivalent injection areas.)

In general, no significant additional mixing advantage is achieved for aspect ratios greater than 3:1 for zero centerpost recess. However, higher aspect ratios appear to offer added mixing quality with recessed centerposts (Fig. 6-6).

Aspect ratios much greater than 6:1 are probably not practical from a fabrication standpoint. However, the higher aspect ratios ($\approx$ 6:1) are attractive as they provide the desirable mixing advantages and, at the same time, offer no apparent atomization penalty (Fig. 6-21).

The data obtained under this program suggest the general design guidelines presented in Table 7-1.

TABLE 7-1. SUGGESTED DESIGN GUIDELINES FOR APPLICATION OF RECTANGULAR CONCENTRIC TUBE INJECTOR ELEMENTS

Quantity	Target Valves
Range of Application	$\dot{W}_L/\dot{W}_G > 4.0$
Liquid Port Aspect Ratio	X_1/Y_1 3:1 (Mixing Limited) X_1/Y_1 6:1 (Mixing and Vaporization Limited)
Centerpost Recess	$R/Y_1 \simeq 1.0$
Gas Port Aspect Ratio	X_3/Y_3 2.1 For $X_1/Y_1 = 3.0$ X_3/Y_3 Unknown for $X_1/Y_1 = 6$

8.0 CONCLUDING REMARKS

Presented in this section is a brief list of those items which the author considers most important. It is strongly recommended that Zajac's atomization work (Ref. 8-1) be studied in conjunction with this report and that particular attention be given to his concluding remarks concerning the application of cold-flow atomization data to injector design.

8.1 SINGLE ORIFICES

1. The hydraulic diameter for a given orifice shape, as it influences the L/D and the Reynolds No., is the controlling variable for the determination of the effect of shape upon the value of the orifice coefficient.

2. The data suggest that noncircular shapes are less sensitive to "hydraulic flip" in the "short L/D regime" (e.g., $L/D \leq 6$, sharp edged inlets, where D is the hydraulic diameter). Further, it is concluded that it is the density of the environment, not the pressure, that most influences the stability of the orifice flow. (This is, of course, not true in those cases wherein cavitation is the destabilizing influence.)

8.2 LIQUID/LIQUID ELEMENTS

1. The additonal degree of freedom associated with rectangular orifices, aspect ratio, allows maximum levels of E_m to be realized for unlike doublets regardless of the propellant density ratio or mixture ratio. Going to more complex shapes does not appear to offer any significant additional advantage.

2. The primary dropsizes produced by unlike doublets with noncircular orifices appear to be somewhat smaller than those produced with circular orifices. This result is more than likely due to the greater degree of jet "development" produced by the noncircular shapes.

3. The single element (circular orifice) mixture ratio uniformity levels, E_m, produced by unlike triplets appear to be somewhat higher than those

produced by unlike doublets. However, the dropsizes produced by triplets are larger than those produced by unlike doublets (at least in the laminar flow regime).

4. Reynolds No., orifice entrance condition, and orifice L/D play an important role in the mixing and atomization processes.

8.3 GAS/LIQUID ELEMENT

1. Rectangular shape may be employed to significantly improve the mixture ratio uniformity of concentric tube injectors operating at mixture ratios in excess of 4:1 (most gas/liquid injectors operate in this range). Combined with centerpost recess, high levels of single-element mixture ratio uniformity can be realized ($E_m \approx 85$ percent with relatively low gas momentum, $\rho_g V_g^2 \approx 50$ psi).
2. The spray field produced by rectangular concentric tube elements can be "tailored" to provide mass and mixture ratio control near chamber walls. This allows for improved injector/chamber wall thermal compatibility and could reduce, or eliminate, the requirements for wall film coolant.

8.4 GENERAL CONCLUSIONS

1. Design criteria for the mixing characteristics developed with cold-flow techniques may be employed directly to injector design. On the other hand, the application of cold-flow atomization results to injector design is by no means straightforward. Considerations such as propellant property corrections, dependence upon complex vaporization models, secondary droplet breakup, and the influences of the properties of the environment make the direct interpretation of atomization data extremely complicated. However, the atomization trends suggested by cold-flow results do serve as highly valuable guidelines for the injector designer.
2. The objective of this program has been to study and characterize new and somewhat revolutionary injector element configurations. The approach that was adopted to accomplish this objective emobodied the favorable aspects

of both the "scientific method" and the practical realities of research and development in a highly cost conscious market place.

The study of noncircular elements was initiated with a preliminary analysis followed by cold-flow experimentation, on a single-element scale, to characterize the individual contributions of propellant mixing and atomization to the overall performance of the element.

It is already apparent that this approach has contributed insight into the characteristics and advantages of noncircular orifice injectors that would not have been obtained by a traditional cut-and-try, hot-firing approach.

To illustrate this, consider what information would have been available had this program been structured such that the method for element characterization was hot-fire experimentation. What would the conclusions be at this point in time?

Essentially, it would be known at best that certain noncircular elements provided a higher c* efficiency than their circular counterparts for a fixed set of operating conditions. However, there would be no indication of why the performance had improved and no guidance as to the inherent advantages and limitations of the noncircular orifice element.

However, results obtained under this study show the degree to which mixing and atomization contribute individually to overall performance and the relationships between these contributions and the operational parameters (i.e., flowrate per element and mixture ratio).

It must be concluded that the adoption of the approach that has been taken has provided extensive savings in cost and frustation, while providing the maximum amount of information for element characterization.

9.0 RECOMMENDATIONS FOR FUTURE WORK

9.1 LIQUID/LIQUID WORK

An evaluation of the mixing characteristics of rectangular unlike doublets with unequal facing widths (i.e., $w_o \neq w_f$) is strongly recommended. The addition flexibility of the parameter w_o/w_f, when added to the flexibility provided by ARo could, perhaps, greatly increase the maximum levels of single-element mixing available with unlike-doublet elements. This is an extremely valuable goal due to the fact that the simplicity of the unlike-double element makes it an attractive candidate for injector desing.

In conjunction with the mixing evaluation, a detailed study of reactive stream separation ("blowapart") should be conducted. If the unlike doublet is to be employed with hypergolic propellants, this problem must be addressed and definitive design guidelines for the avoidance of blowapart established.

9.2 GAS/LIQUID WORK

In the areas of gas/liquid rectangular and circular concentric tube mixing and atomization, further cold-flow experimentation is required with variation of area ratio. This will aid in generalizing the results that are presently restricted.

Further data are required concerning the effect of gas port aspect ratio, x_3/y_3, upon the mixing characteristics for rectangular concentric tube elements (RCTE). The results presented in this report show this to be a potentially valuable parameter for the optimization of mixing, and also for the control of spatial mixture ratio distribution produced by injector elements. The latter feature could have valuable application with regard to injector/thrust chamber compatibility.

The work with RCTE's should be carried to its natural conclusion; the design and hot-fire demonstration of large-scale injector designed for high mixture ratio (i.e., LOX/GH_2 at MR$\approx$6) and low gas injection momentum. This type of study could also include a variation of the orientation of the peripheral elements to evaluate the advantage of RCTE's for improved injector/chamber compatibility, and perhaps stability.

10.0. REFERENCES

1-1. Nurick, W. H. and R. M. McHale: Noncircular Orifice Holes and Advanced Fabrication Techniques for Liquid Rocket Injectors, Phase I Final Report, Contract NAS9-9528, NASA CR-10870, Rocketdyne Division Rockwell International, Canoga Park, California, 15 September 1970.

1-2. McHale, R. M.: Noncircular Orifice Holes and Advanced Fabrication Techniques for Liquid Rocket Injectors, Phase II Final Report, Contract NAS9-9528, NASA CR-108571, Rocketdyne, 22 February 1971.

1-3. McHale, R. M.: Noncircular Orifice Holes and Advanced Fabrication Techniques for Liquid Rocket Injectors, Phases III and IV Final Report, Contract NAS9-9528, Report R-9270, Rocketdyne, June 1973.

2-1. Rupe, J. H.: A Correlation Between the Dynamic Properties of a Pair of Impinging Streams and the Uniformity of Mixture Ratio Distribution in the Resulting Spray, Progress Report 20-209, JPL, Pasadena, California, 28 March 1956.

2-2. Burick, R. J.: Space Storable Propellant Performance Program Coaxial Injector Characterization, Contract NAS3-12051, NASA CR-120936, Rocketdyne October 1972.

2-3. Mehegan, P. F., et al.: Investigation of Gas-Augmented Injectors, Final Report, Contract NAS3-12001, NASA CR 72703, Rocketdyne, September 1970.

4-1. McHale, R. M.: Tables of Experimental Data for Contract NAS9-9528, Noncircular Orifice Study, Rocketdyne, June 1973.

4-2. Nurick, W. H. and R. M. McHale: Noncircular Orifice Holes and Advanced Fabrication Techniques for Liquid Rocket Injectors, Phase I Final Report, Contract NAS9-9528, NASA CR-10870, Rocketdyne, 15 September 1970.

4-3. Northop, R. P.: "Flow Stability in Small Orifices," Presented at the ARS on 30 November 1951 at the Annual Meeting of the ASME in Atlantic City, New Jersey.

4-4. Schlichting, H.: Boundary Layer Theory, 4th ed., McGraw-Hill Book Co., Inc., New York.

4-5. Rivas, M. A. and A. H. Shapiro: "On the Theory of Discharge Coefficients for Rounded-Entrance Flowmeters and Venturis," Transactions of ASME.

5-1. Dowbrowski, N. and W. Johns: "The Aerodynamic Instability and Disintegration of Viscous Liquid Sheets," Chem. Eng. Sci., Vol. 18, pp 203-214, 1963.

5-2. Hasson, P. and R. Peck: "Thickness Distribution in a Sheet Formed by Impinging Jets," AIChE Journal, Vol. 10, No. 5, pp 752-754, 1964.

5-3. Zajac, L.: Correlation of Injector Spray Dropsize Distribution and Injector Variables, Final Report, R-8455, Rocketdyne, December 1971.

5-4. Elverum, G. and T. Morey: "Criteria for Optimum Mixture Ratio Distribution Using Several Types of Impinging Stream Injector Elements," Memo No. 30-5, JPL, Pasadena, California, 25 February 1959.

5-5. Dickerson, R. et al.: Correlation of Spray Injector Parameters with Rocket Engine Performance, AFRPL-TR-68-147, Final Report, Rocketdyne, June 1968.

5-6. Falk, A. and C. Nagai: Space Storable Propellant Performance Study, Final Report, NASA-CR-72487, Rocketdyne, November 1968.

5-7. Nurick, W. and R. McHale: "Noncircular Orifice Holes and Advanced Fabrication Techniques for Liquid Rocket Injectors," Phase I Final Report, NASA-CR-108570, R-8224, Rocketdyne, November 1970.

5-8. McHale, R. M.: Tables of Exp. Data for Contract NAS9-9528, Noncircular Orifice Study, Rocketdyne, June 1973.

5-9. Nurick, W.: The Influence of Injector Cavitation on Mixing Uniformity, Company-Sponsored Study (S.A. 60274), in progress, Rocketdyne, 1973.

5-10. Nurick, W.: Reactive Stream Separation, Company-Sponsored Study (S.A. 60218), No report published.

5-11. Rupe, J.: The Liquid-Phase Mixing of a Pair of Impinging Streams, Progress Report No. 20-195, JPL, Pasadena, California, August 1953.

5-12. Rupe, J.: A Correlation Between the Dynamic Properties of a Pair of Impinging Streams and the Uniformity of Mixture Ratio Distribution in the Resulting Spray, Progress Report No. 20-209, JPL, Pasadena, California, March 1956.

5-13. Hoehn, F., J. Rupe, and J. Soher: Liquid-Phase Mixing of Bipropellant Doublets, Technical Dept. 32-1546, JPL, Pasadena, California, February 1972.

5-14. Hall, G.: "Analytical Determination of the Discharge Characteristics of Cylindrical Tube Orifices," Jr. Mech. Engr Sci., Vol. 5, No. 1, 1963.

5-15. Hasson, D. and J. Mizrah, "The Dropsize of Fan Spray Nozzles: Measurements by the Solidifying Wax Method Compared with Those Obtained by Other Sizing Techniques," Trans. Instin. Chem. Engrs, Vol. 39, pp 415-419, 1961.

5-16. Clayton, R.: Experimental Observations Relating the Inception of Liquid Rocket Engine Popping and Resonant Combustion to the Stagnation Dynamics of Injection Impingement, Technical Report 32-1479, JPL, Pasadena, California, December 1970.

6-1. Streeter, V. L.: Fluid Mechanics, 4th Ed., McGraw-Hill Book Co., New York, 1966.

6-2. McHale, R. M.: Tables of Experimental Data for Contract NAS9-9528, Noncircular Orifice Study, Rocketdyne, June 1973.

6-3. McHale, R. M.: Noncircular Orifice Holes and Advanced Fabrication Techniques for Liquid Rocket Injectors, Phases III and IV Final Report, Report No. R-9270, Rocketdyne, June 1973.

6-4. Burick, R. J.: Space Storable Propellant Performance Program Coaxial Injector Characterization, Contract NAS3-12051, NASA CR-120936, October 1972.

8-1. Zajac, L. J.: Correlation of Spray Dropsize Distribution and Injector Variables, Final Report, Contract NAS7-726, R-8455, Rocketdyne, 1972.

APPENDIX A

DETERMINATION OF OPTIMUM MIXING PARAMETER FOR NONCIRCULAR ELEMENTS

INTRODUCTION

Mixing characteristics of two impinging jets of dissimilar fluids were first studied by Rupe (Ref. A-1) in 1953. Rupe evaluated the effect of density, velocity, diameter, and impingement angle on the mixing uniformity, and found the resultant mixing characteristics strongly dependent upon these variables. In particular, Rupe has shown that a given unlike impinging doublet injector (circular orifice) produces optimum mixing uniformity when the product of density, velocity-squared, and the diameter for each of the jets are equal, and that this optimum level is a function of geometry. It is not clear from Rupe's work whether the variables, ρ, U, D, are all independent, composed of a dynamic pressure term (ρU^2) and a characteristic dimension, or a single variable $\rho U^2 D$. Over the past 15 years, Rupe's result has been routinely applied to design injectors without a clear understanding of the significance of the fluid dynamics defined by his relationship. From an applications standpoint this is understandable and presented no design problems for circular orifices. However, reformulation for noncircular design results in several possible forms of Rupe's criteria, depending upon the specification or grouping of the variables. Consequently, application of Rupe's criteria to noncircular orifice designs requires understanding of the mechanisms controlling mixing.

DISCUSSION

Based on Rupe's work, a dimensionless quantity that his experiments have shown important to mixing is:

$$\rho_1 U_1^2 D_1 / \rho_2 U_2^2 D_2 \qquad \text{(A-1)}$$

Inspection of the physical significance of the variables contained in Eq. A-1 for circular geometry shows that the variables can be reformulated in terms of dynamic pressure ($\emptyset$)

$$\emptyset(D_f/D_o) = 1.0 \tag{A-2}$$

or momentum ratio of the jets (M_f/M_o), and a diameter ratio:

$$M_f/M_1 \ (D_o/D_f) = 1.0 \tag{A-3}$$

It becomes obvious that neither of the above physical interpretations result in a meaningful dimensionless group since they still result in two physical dimensionless ratios.

Since for circular orifices the above equations are dependent, application of either definition (Eq. A-2 or A-3) will lead to the proper design values. However, if the criteria are extended to other orifice geometries wherein the equations become independent (e.g., noncircular orifices); then the physical significance of Eq. A-1 must be known to select the proper form. As an example, a set of rectangular orifices impinging at 60 degrees, having equal widths, result in the following equations which are equivalent to Eq. A-2 and A-3.

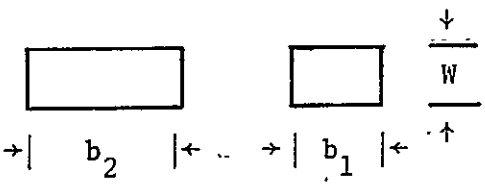

$$\emptyset(D_f/D_o)_{hydraulic} = (\rho_1 \ U_1^2/\rho_2 \ U_2^2) \ (D_f/D_o)_{hydraulic} \tag{A-4}$$

$$(M_f/M_o) \ (D_o/D_f)_{hydraulic} = (\rho_1 \ U_1^2 \ A_1/\rho_2 \ U_2^2 \ A_2) \ \left(\frac{D_o}{D_f}\right)_{hydraulic} \tag{A-5}$$

In this example, the hydraulic diameter ratio has been substituted for the geometric term. Note that these equations are independent and, therefore, physical significance of the original equations is not clear, it is possible that neither of these correlations will result in a meaningful description of the mixing process.

Equation A-1 can also be formulated in terms of the centerline momentum of the jets. It is easily shown that on the basis of centerline momentum, Eq. A-1 for circular orifices is:

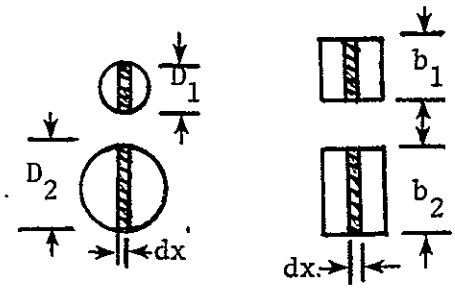

(a) circular jets (b) rectangular jets

$$\phi = \rho_1 U_1^2 D_1 \, dx / \rho_2 U_2^2 D_2 \, dx = \rho_1 U_1^2 D_1 / \rho_2 U_2^2 D_2 \qquad \text{(A-6)}$$

and for rectangular orifices is:

$$\phi = \rho_1 U_1^2 b_1 / \rho_2 U_2^2 b_2 \qquad \text{(A-7)}$$

During the conduct of the program, elements using differing shaped orifices were studied. These elements are listed in Table A-1. The specific designs are such that they are ideal for determining which, if any, of the above definitions of Eq. A-1 control mixing.

The experimental results are presented in Fig. A-1 in terms of all of the definitions. It is obvious that only the centerline momentum ratio results in all of the elements having optimum E_m at the same value of ϕ. In addition the optimum occurs at a value of ϕ equal to one, illustrating that the balance of centerline momenta results in optimum mixing uniformity.

APPENDIX A REFERENCES

A-1. Rupe, J. H.: A Correlation Between the Dynamic Properties of a Pair of Impinging Streams and the Uniformity of Mixture Ratio Distribution in the Resulting Spray, Progress Report No. 20-209, Jet Propulsion Laboratory, Pasadena, California, 28 March 1956.

TABLE A-1. RECTANGULAR/TRIANGULAR ELEMENT GEOMETRY-SHARP EDGE INLETS

Configuration	b_f/b_o	Oxidizer Aspect Ratio ($AR_o = b_o/w_o$)		
		0.54	0.90	1.97
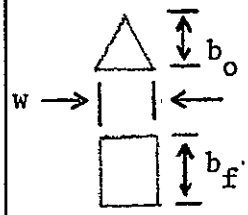	0.885	--	--	1.0 0.0532 0.164 0.0532
	0.935	AR_F* = 4.0 w = 0.026 b_o = 0.0532 b_f = 0.0266		--
	0.942	--	2.0 0.0751 0.0685 0.0376	--

*Nominal Values

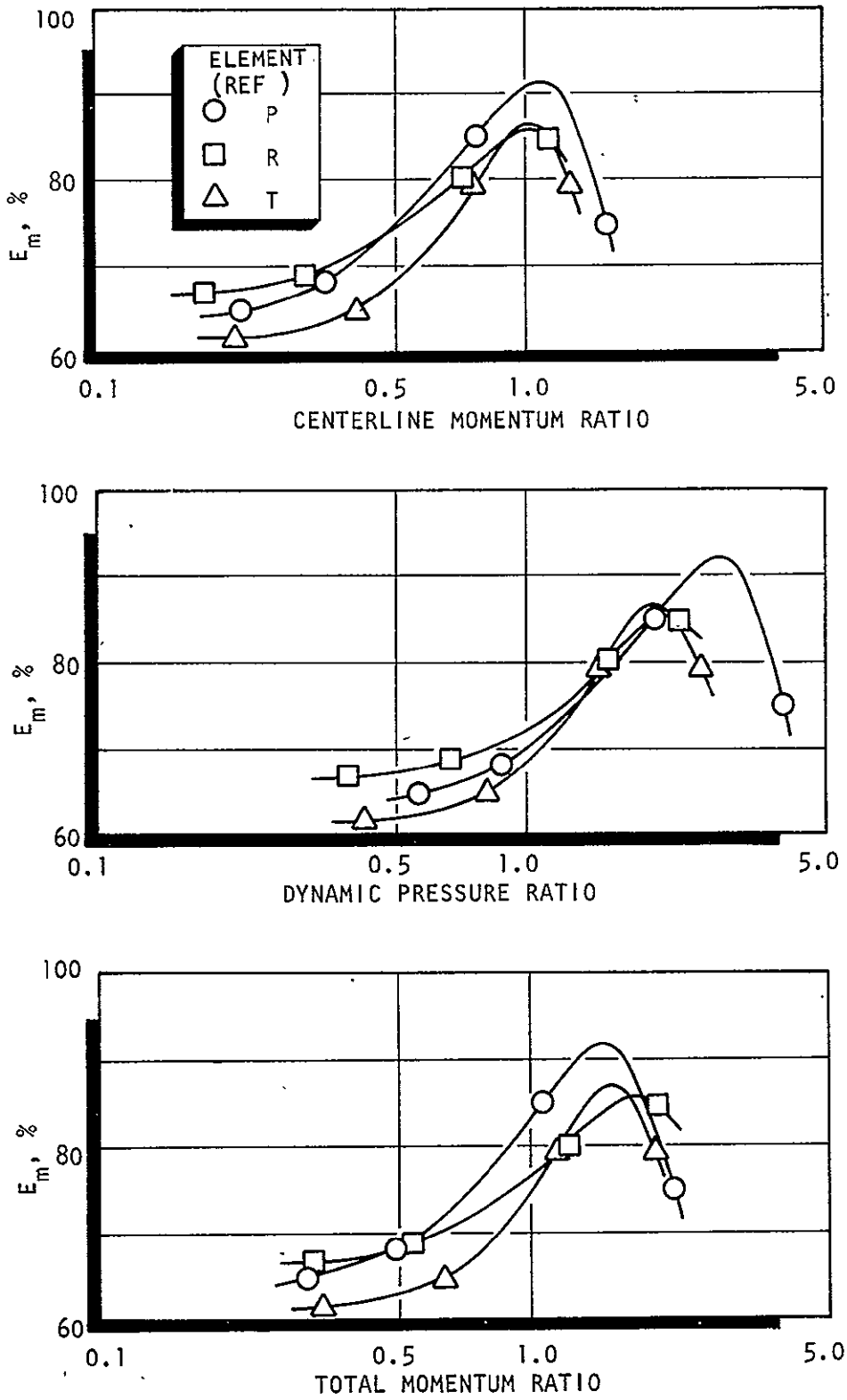

Figure A-1. Comparison of Three Possible Physical Interpretations of the Parameter, ϕ

APPENDIX B

COMBUSTION MODELS

VAPORIZATION LIMITED COMBUSTION

The vaporization limited combustion model formulation is based on the development of mathematical expressions for the various physical processes involved in the combustion of liquid droplet sprays in a bipropellant liquid rocket engine. The model considers propellants to be injected as sprays containing ranges of discrete droplet size groups, each possessing a given average diameter. The total spray mass is distributed among the various groups according to an experimental mass distribution function.

Of central importance in the model is the solution of the individual droplet burning rates, which are assumed to be limited by diffusion. Analysis of the dynamic behavior of single droplets is justified on the basis that the volumetric flowrate of liquid propellants into the downstream region is only about 1 to 2 percent of that of the combustion gases and, therefore, that the likelihood of droplet collisions or interference with one another is negligibly small. Under rocket conditions, in the uniform mixing zone, droplets are spaced on the order of 2 to 3 diameters apart, while the vapor film thickness is on the order of 5 to 15 percent of the droplet diameters. As a result, each droplet is considered to be immersed in an infinite combusiton gas medium.

The calculation of single droplet evaporation is based on a spherically symmetric model of simultaneous heat transfer to, and mass transfer from a liquid sphere.

The liquid droplet temperature is assumed to vary with time, but to be uniform through the drop. Forced convection and resultant nonspherical transfer processes are accounted for through empirical Nusselt number correlations for both heat and mass transfer.

In evaluating the convective contribution, relative gas-to-droplet velocity is required. Droplet velocities are obtained from a drag relationship for evaporating spheres. A composite form of the drag coefficient for accelerating spheres which accounts for droplet flattening is employed.

Compressible gas dynamics are accounted for with area changes corresponding to chamber geometry. The droplets are treated as point sources (or sinks) of fuel (mass), oxidizer (mass), momentum, and energy with local transport rates obtained by summing the contributions of all droplets at any given location in the chamber.

The gas-phase energy equation is simplified normally by the assumption that the composition and stagnation temperature are the equilibrium values for the gas-phase oxidizer, fuel mixture ratio, and the chamber pressure. Other gas properties (static temperature, density, etc.) are evaluated from the respective stagnation values by applying the local Mach number to the frozen isentropic expansion equations.

The model is solved in numerical form by high-speed digital computers. It requires input of the "upstream boundary condition," which completely describes the initial conditions of spray (dropsize distribution, drop velocities, and temperature) and gas (composition, flowrate, and pressure) at the location where computation is started. Chamber geometry must also be specified.

Solution proceeds in a stepwise manner moving downstream to the nozzle throat. At each step, interphase transport of mass, momentum, and energy is evaluated from the transport equations previously described with subsequent solution of gas-phase equation of state and continuity, momentum, and energy balances. This results in a description of droplet group diameters, velocities, and temperatures as well as gas composition, velocity, and pressure at the new location.

This "marching technique" proceeds into the nozzle up to the geometric throat, where it is necessary to satisfy the downstream boundary condition of sonic gas velocity. If the throat Mach number deviates from unity by more than a preselected tolerance, iteration is required whereby propellant flowrates are

adjusted and the entire calculation repeated. In practice, convergence of this iteration is rapid and a solution is readily obtained. The general validity of the analytical results is determined to a major extent by the accuracy of the input spray description. Vaporization rate limited c* efficiency is computed from the following equation:

$$\eta_{c^*,vap} = \left[\frac{\dot{w}_B}{\dot{w}_I}\right]\left[\frac{c^*_B}{c^*_I}\right] \qquad \text{(B-1)}$$

where

$\dot{w}_B$ = flowrate of burned gas at the geometric throat

$\dot{w}_I$ = injection flowrate of fuel plus oxidizer

c^*_B = theoretical c* corresponding to the composition of the burned gas at the geometric throat

c^*_I = theoretical c* corresponding to the injection mixture ratio of liquid fuel and oxidizer

MIXING LIMITED COMBUSTION

Over the past 15 years, mass and mixture ratio distribution uniformity ("mixing") has been extensively studied both analytically and experimentally. Experimental/analytical correlations demonstrate quantitatively that high combustion efficiency in rocket engine thrust chambers occurs only when the initial local mixture ratio distribution is at, or near, the target chamber mixture ratio. This implies that the injector should provide a spray field having a uniform mixture ratio over the entire flow cross section.

The sketch on the following page illustrates a typical curve of theoretical equilibrium c* as a function of propellant mixture ratio (oxidizer/fuel).

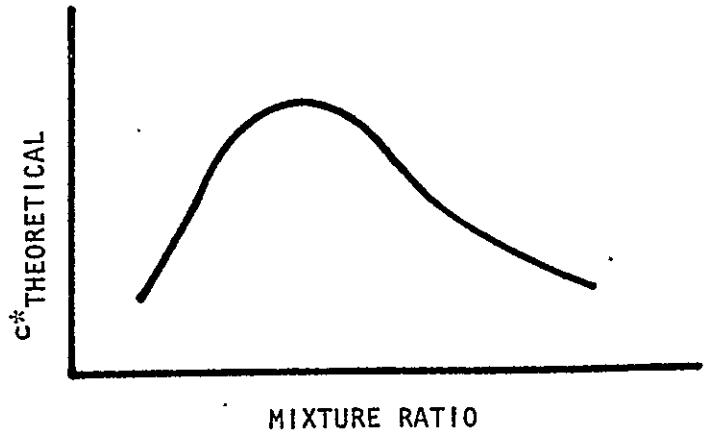

Normally the design operating point of overall injected mixture ratio falls close to the peak, and any maldistribution of propellant mixture ratio results in a loss in overall c*. An analytical model has been developed at Rocketdyne to relate these maldistributions to an attendant loss in c* efficiency. The development of this model is outlined in the following paragraphs.

Wrubel (Ref. B-1) describes an analysis of mixing losses whereby the flow is hypothetically subdivided into "i" stream tubes, each containing propellant at some mixture ratio that is uniform within that stream tube. No mass or energy is considered to cross stream boundaries. Propellant vaporization, mixing, and combustion are treated as being complete upstream of the start of nozzle convergence. Within the nozzle, the flow is handled as being one-dimensional and isentropic. At each axial station the static pressure is considered uniform for all stream tubes. In addition, boundary layer effects are neglected. The resulting equation relating the mixing limited c* efficiency to the local mass and mixture ratio distribution is:

$$\eta_{mix} = \sum_i \left(\frac{\dot{w}_i}{\dot{w}_T} \frac{c^*_i}{c^*_{theo}} \frac{A_{t,i}}{A^*_i} \right) \tag{B-2}$$

Here $A_{t,i}/A^*_i$ is the ratio of the cross-sectional area of the ith stream tube at the minimum chamber area to its area at the point it becomes sonic. For most

cases of interest the specific heat ratios γ_i, are all of similar value so the shifts in location of the sonic condition from the geometric throat will be small and the preceding equation is closely approximated by:

$$\eta_{mix} = \sum_i \frac{\dot{w}_i}{\dot{w}_T} \frac{c^*_i}{c^*_{theo}} \tag{B-3}$$

where the effective c* is simply a weighted average of the local c* for the individual stream tubes. For any given propellant mixture ratio distribution, Eq. B-3 provides a simple means of determining c* efficiency loss due to "mixing."

Most investigators agree that distributions developed by spray mixing near the injector will not be appreciably changed downstream by turbulent mixing of the gases. As a consequence, if the initial spray distribution formed by an injector can be experimentally determined, $(\eta_{c^*})_{mix}$ can be computed by using Eq. B-3.

Rupe (Ref. B-2) introduced a term, commonly known as E_m, which is an index of mixing uniformity:

$$E_m = 1 - \sum_i^N \frac{\dot{w}_i}{\dot{w}_T} \frac{(R - r_i)}{R} - \sum_i^N \frac{\dot{w}_i}{\dot{w}_T} \frac{(R - \bar{r}_i)}{R - 1} \tag{B-4}$$

where

E_m = mixing index

$\dot{w}_i/\dot{w}_T$ = mass fraction in the stream tube

R = ratio of total oxidizer mass to total oxidizer and fuel mass

r_i = ratio of oxidizer mass to total oxidizer and fuel mass in an individual stream tube for $r_i < R$

$\bar{r}_i$ = ratio of oxidizer mass to total oxidizer and fuel mass in an individual stream tube for $r_i > R$

The factor E_m, is not uniquely defined by $(\eta_{c*})_{mix}$. The correspondence is strongly affected by the propellant combination and the nominal mixture ratio. This term is employed to describe the average mixing uniformity of a given spray field.

APPENDIX B REFERENCES

B-1. Wrubel, J. R.: "Some Effects of Gas Stratification on Choked Nozzle Flows," AIAA Paper 64-266, 1964.

B-2. Rupe, H. J.: A Correlation Between the Dynamic Properties of a Pair of Impinging Streams and the Uniformity of Mixture-Ratio Distribution in the Resulting Spray, Progress Report No. 20-209, Jet Propulsion Laboratory, Pasadena, California, 28 March 1956.